UNIVERSITAT DE BARCELONA

# Luminescent gold(I) supramolecular assemblies on materials and biological chemistry

Andrea Pinto Martínez

# Luminescent gold(I) supramolecular assemblies on materials and biological chemistry

Andrea Pinto Martínez

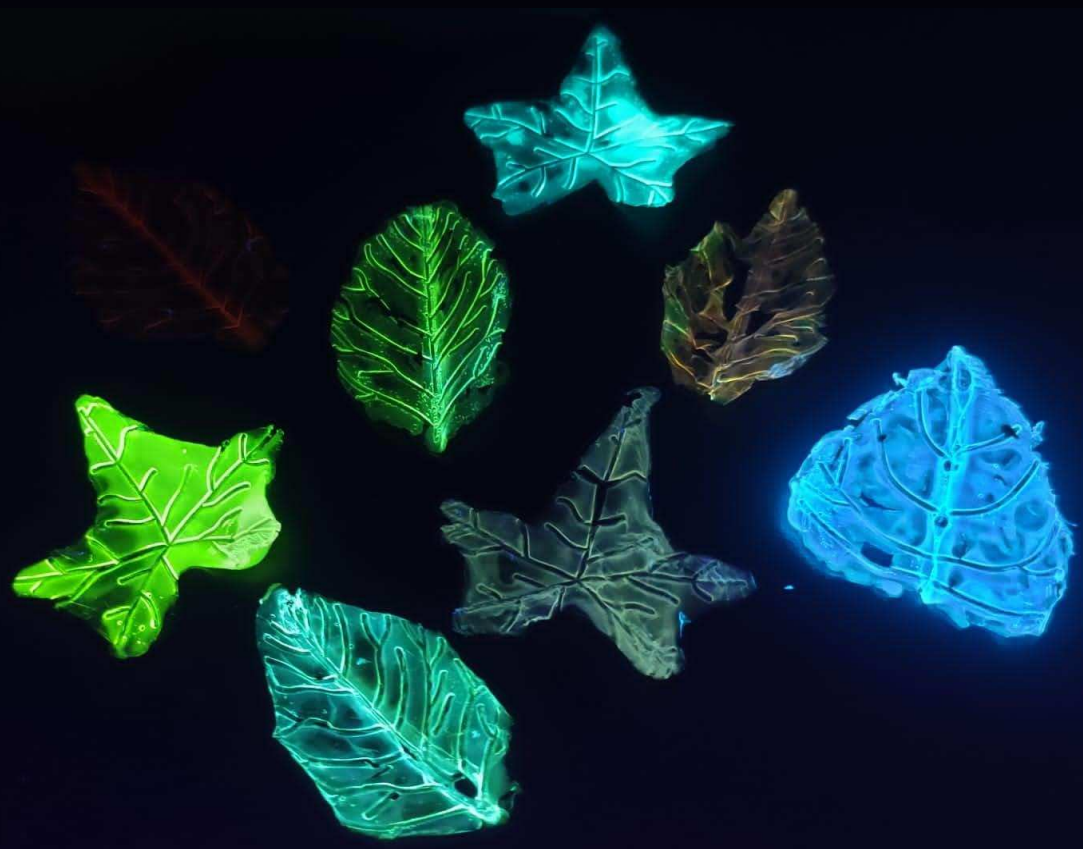



UNIVERSITAT DE BARCELONA

Document signat digitalment per: ANDREA PINTO I MARTINEZ

UNIVERSITAT DE BARCELONA

# Luminescent gold(I) supramolecular assemblies on materials and biological chemistry

Andrea Pinto Martínez

Document signat digitalment per: ANDREA PINTO I MARTINEZ

**UNIVERSITAT DE BARCELONA**

Facultat de Química

Departament de Química Inorgànica i Orgànica

Secció de Química Inorgànica

Institut de Nanociència i Nanotecnologia

Programa de Doctorat de

HDK11 Nanociència

# Luminescent gold(I) supramolecular assemblies on materials and biological chemistry

**Andrea Pinto Martínez**

Memòria presentada per optar al grau de Doctor per la Universitat de Barcelona

**Director: Prof. Laura Rodríguez Raurell**

**Tutor: Prof. Laura Rodríguez Raurell**

UNIVERSITAT DE BARCELONA

Document signat digitalment per: ANDREA PINTO I MARTINEZ

Oro parece, plata no es

Document signat digitalment per: ANDREA PINTO I MARTINEZ

# CONTENTS

Document signat digitalment per: ANDREA PINTO I MARTINEZ

Document signat digitalment per: ANDREA PINTO I MARTINEZ

# AGRAÏMENTS

Després de tots aquests anys per fi ha arribat el moment d'agrair. De fet, sou molta gent la que ha compartit tots els alts i baixos que té una tesi i no m'agradaria deixar-me ningú! (he hagut de fer un Excel perquè tinc la memòria d'un peix). Així que intentaré seguir més o menys un ordre cronològic.

Primer de tot i com no pot ser d'una altra manera, m'agradaria agrair a la Prof. Laura Rodríguez per acceptar a una altra hippie i que entra tard a treballar al seu grup. En tots aquests anys que hem compartit he crescut com a química i com a persona i tot això ha estat gràcies a tu. D'aquesta tesi doctoral no només m'emporto a una magnífica directora que dona la vida per a tu, també a una excel·lent persona! Això no és el final sinó el principi!

A la gent del grup, Dra. Inmaculada Angurell, Dr. Oriol Rossell i Dr. Miquel Seco ha estat un plaer formar part d'aquest grup d'investigació!

Al Dr. João Carlos Lima per sempre estar disposat a explicar els conceptes no sempre fàcils d'entendre de la fotofísica i per aguantar totes les bromes sobre els portuguesos! Muito obrigada!

A la gent d'un singular departament que sens dubte sempre recordaré! En particular agrair al Dr. Albert Figuerola per un gran ALBA compartit, pel congrés a Lisboa i en general per tots els riures que ens hem fet i al Dr. Arnald Grabulosa per totes les discussions polítiques i d'horaris! També m'agradaria agrair a la gent que sense ella no seriem res! A l'Anna Ruiz per aguantar totes les demandes i sempre estar disposada a petar una xerrada sobre la vida, a la Teresa i la Cristina per fer totes les gestions burocràtiques que sempre són odioses!

A tots els tècnics tant importants per a que puguem avançar en la investigació, en especial a la Laura Ortiz per la paciència i dedicació per trobar el pic molecular i al Dr. Francisco Cárdenas i Victor Meriel per sempre estar disponibles perquè en el grup puguem fer fòsfors!

A tota la gent del laboratori, els quals hem compartit moltes hores junts! Ara ve una gran llista de gent! Primer de tot m'agradaria agrair a la gent que va compartir els meus inicis en el grup, a l'Eli i a la Raquel, les quals em van fer disfrutar les hores en el laboratori i van omplir d'alegria tot el laboratori. Com no, al meu company etern, al

geni del mal, a tu Fran que sempre has estat allà per tot! Per ensenyar-me la bricomania del laboratori, per tots els riures de par de lerdos que ens hem fet, sempre seràs el meu company! A la Noora i el Richard per un magnífic any compartit! A la gent que ha passat pel laboratori durant tots aquests anys i que sempre tindré un bon record, a la Giulia per ensenyar com es fa una columna di la mamma, a la sempre estilosa Camille, a la meva minionsita Ingrid, a l'Ona i a l'Eli, gràcies a totes! A la meva persona dramàtica preferida, a tu Ari (o Ariazna jejeje), sé que vols un paràgraf sencer per a tu però necessitaria pàgines senceres per agrair i per expressar el que ha significat compartir totes les vivències amb tu! Gràcies per sempre estar allà donant suport a cada ratllada, per tots els teus comentaris espontanis, els teus acudits (sempre dolents jajaja), totes les birres compartides, en general, gràcies per sempre estar allà! A l'altra persona formadora del trio lalala, a la meva xiqueta de la Terra Alta, a tu Rosa fill meu, gràcies per la teva passió per la química i la cristal·lografia (jellyfish!), pels bailoteos al teu laboratori a les tantes de la tarda, els teus cants a lo Aretha, la llista seria interminable i tot es resumeix en gràcies per existir i haver compartit aquests anys amb mi! A una increïble nova incorporació del laboratori, a mi mujercita de la química, a tu Araceli, gràcies per compartir la passió per les coses luminescents, els submarinos (que espero que facis molts més), per la teva generositat i per totes les hores que hem compartit, sé que ha sigut breu però espero que en un futur puguem compartir més hores de treball juntes! A una persona que va venir per fer una estada d'uns pocs mesos però que ja la podem considerar com del grup, a ti Valentina, gracias por tus estoy matta! y por ser mi compañera de conciertos - quiero perderme por el caminoooo, todo suena mejor, si suena contigooo! Al nostre mexicà del grup, Guillermo, gracias por la chamarra (no por el mescal ni el tequila) y por compartir la pasión por las canciones de Paquita! A la Dana té gana per les magdalenes i pels cotilleos del departament! Al David per sempre pillar-nos fent el tonto pel departament i respondre amb un somriure. A la gent que ha passat pel departament i que sempre tindré un bon record, a una conformant del grup Fardatxo, a la nostra noia del triangle, Lidia, gràcies per totes les vivències que hem compartit! A la noieta de Cervere, Marione, per un dels millors congressos viscuts, tots els riures que ens vam fer a l'ALBA i per un viatge a Euskadi brutal! A un ponzoñoso del Poble9 que no sap que el Clot és el millor barri, a tu Guillem per totes les converses que vam viure a la sala d'aparells i per compartir el drama que és estar moltes hores al fluorímetre. A la Laia, Jan Romanov, Berta, Pau, Beltzane, Marta, Vero, Raúl, Saskia, i Júlia pel temps compartit!

Als de Coimbra, Fani (la xiqueta de la terreta), Dani (Voxero), Roberto (el cavaller), Aingeru (el guapo) i Dani (acho), un grup brutal que només en un mes ja vaig considerar com una família en una ciutat plena de cuestas i feta pols del tercer mundo. Gràcies per totes les nits de karaoke, pel quim dos ossos, pels cubates del tropical, per les tostas del Luna, per totes les canecas (mais uma!) i per tots els llocs que ens vau descobrir (està en català perquè sé que ho entendreu jeje).

A mis rubias de conocimiento, Toni, Gabri i Jakub, por compartir todos los dramas del máster que nos han hecho aún más fuertes!

A tota la gent que va compartir en el seu moment la carrera i que segueix sent una part molt important de la meva vida, Terri, Jordi, Manrico, El Marc, Broto, Elfa, Marta Ble, Helena, Emma, Albertillo, Berni, i Amor de persona a tots vosaltres gràcies per tot, trobo molt a faltar els nostres migdies jugant al UNO i cridant com a locos!

A una nova gent que vaig descobrir aprenent euskera, a la Adela, Mauro, Montse i Aina, gràcies per totes les birres compartides després de classe, els pintxos del Euskal Etxea i la gran nit del Cangrejo!

A qui ha estat gairebé tota la meva vida i que m'ha vist des de la meva època més pavoncia (o inclús abans) fins ara! Glòria, Judit, Soto i Mireia, amb vosaltres he crescut com a persona, espero que puguem compartir moltes més etapes de la vida juntes!

A una família que s'ha creat al carrer Sòcrates! Al meu maridito, Álex (més conegut com Alexa Towers) a tu t'he d'agrair la vida sencera! Tot va començar amb una proposta de viure junts i s'ha convertit en tota una aventura de locos! I give you cocinanteo, coreografias de Poti, subidas en el sofà por indignación, noches de Rupaul i eurovision, dies de garrapata, de marujeo per sant Andreu and it's everything! També vull agrair a l'Andrea pels matins de charlamenta i a la Carras per ser la meva filla i passar juntes un confinament!

Finalment i per ser últims no són els menys importants (tot el contrari), a la meva família, al meu pare, la meva mare, el meu germà i la meva gossa, moltes gràcies perquè sense vosaltres no seria la mateixa persona!

En general, a tots, moltes gràcies, me dais la vida!

# RESUMEN DE LA TESIS

Durante los últimos años, el grupo de investigación donde se ha realizado esta Tesis Doctoral ha sido pionero en el desarrollo de diferentes complejos de oro(I) y los ensamblajes supramoleculares resultantes con una amplia variedad de aplicaciones. El punto de partida de este intensivo desarrollo de ensamblajes supramoleculares se sitúa en el estudio de un sistema de oro(I)-alquinilo con fosfinas solubles en agua, el cual, dio lugar a la formación de un hidrogel con propiedades luminiscentes. Este ejemplo fue el precedente de un exhaustivo estudio de los procesos de agregación de los complejos de oro(I), donde modificaciones en el cromóforo o la incorporación de carga en el sistema dio lugar a un amplio abanico de morfologías (bastoncillos, vesículas, cuadrados, estrellas…) con diferentes propiedades luminiscentes. Teniendo en cuenta este precedente, la Tesis Doctoral que se presenta se centra en utilizar la química supramolecular de los complejos de oro(I) con el objetivo de modular sus propiedades luminiscentes, dando un paso más en la metodología establecida en el grupo de investigación. Se pretende diseñar e investigar nuevos compuestos y ensamblajes de oro(I) con propiedades mejoradas y aptos para ser estudiados en diferentes tipos de aplicaciones, desde materiales luminiscentes, reconocimiento molecular o aplicaciones biológicas.

Los complejos sintetizados han sido diseñados racionalmente, donde las diferentes partes de la estructura molecular fueron seleccionadas para una aplicación determinada. Los compuestos de oro(I) presentan una coordinación lineal. La primera posición de coordinación estará ocupada por el anteriormente dicho grupo alquinilo-cromóforo, responsable, en parte, de las propiedades luminiscentes observadas. Para la segunda posición de coordinación se han escogido mayoritariamente fosfinas, ya que son ligandos que pueden modular la solubilidad en diferentes disolventes, así como la nuclearidad de los compuestos resultantes. Los carbenos también han sido utilizados con el objetivo de introducir planaridad en el compuesto final.

Se han utilizado una gran variedad de técnicas para evidenciar la correcta formación de los compuestos orgánicos y organometálicos sintetizados (RMN multinuclear y multidimensional, IR, ESI y difracción de rayos X). Las estructuras supramoleculares obtenidas han sido debidamente analizadas por DLS, SEM, UV-vis, luminiscencia y SAXS.

# ABSTRACT

During the last years, the research group where this Doctoral Thesis has been carried out has been pioneer in the development of different gold(I) complexes and resulting supramolecular assemblies with a wide variety of applications. The starting point of this intensive study is found in the finding of a gold(I)-alkynyl system containing a water-soluble phosphane, which gave rise to the formation of a hydrogel. This example was the precedent for an exhaustive study of the aggregation processes of gold(I) complexes, where modifications in the chromophore or the incorporation of charge in the system gave rise to a wide variety of morphologies (rods, vesicles, square, stars ...) with different luminescent properties. Taking into account this precedent, this Doctoral Thesis focuses on using the supramolecular chemistry of gold(I) complexes in order to modulate their luminescent properties, going one step further in the methodology established by the group. We have designed and investigated new gold(I) compounds and assemblies that present improved properties and are suitable to be studied in different types of applications, ranging from luminescent materials, molecular recognition or biological applications. These complexes have been rationally designed, where the different parts of the molecular structure were selected for a specific goal. Gold(I) complexes present a linear coordination. In our compounds, the first coordination position is occupied by an alkynyl-chromophore, responsible, in part, of the resulting luminescent properties. The second coordination position is occupied, in general, by phosphanes, since they can modulate the solubility in different solvents and the nuclearity of the resulting compounds. Carbenes have also been used in order to introduce planarity in the final compound.

A great variety of techniques have been used to check the correct formation of organic and organometallic compounds (NMR, IR, ESI, and X-ray diffraction). The supramolecular structures obtained have been duly analyzed by DLS, SEM, UV-vis, luminescence and SAXS.

# PREFACE

The research reported in this Thesis was developed in the Supra and Nanostructured Systems group (SuNS) at the Departament de Quimica Inorgànica i Orgànica, Secció de Química Inorgànica de la Universitat de Barcelona. It was financially supported by a PhD fellowship from Generalitat de Catalunya (Ajuts per la contractació de personal investigafor novell (FI-DGR)) and by Ministerio de Ciencia e Innovación of Spain (AEI/FEDER, UE Projects CTQ2016-76120-P and PID2019-104121GB-100).

The results of this research has been disseminated in several international conferences:

- Pinto, A., Zonta, C., Licini, G., Rodríguez, L. III International Symposium on Nanoparticles/Nanomaterials and Applications, ISN2A 2018 (Lisbon, Portugal): Shotgun and poster communication entitled "Tripodal Supramolecular Gold(I) derivatives with tunable luminescent properties".
- Pinto, A., Rodríguez, L. 10a Trobada de Joves Investigadors dels Països Catalans (Barcelona, Spain): Oral presentation entirled "Sistemes Supramoleculars d'or(I). Estudi de les Potencials Aplicacions i Morfologies".
- Pinto, A. Dalmases, M., Aguiló, E., Figuerola, A., Rodríguez, L. XXXVI GEQO Congress Organometallic Group (Zaragoza, Spain): Poster communication entitled "Aggregation studies of hybrid systems containing gold(I) complexes and gold nanoparticles".
- Pinto, A. Dalmases, M., Aguiló, E., Figuerola, A., Rodríguez, L. XXXVII-Bienal Quimica (Donostia, Spain): Poster communication entitled "Preparation and antitumoral activity of Au based inorganic-organometallic nanocomposites".
- Pinto, A., Lima, J.C., Rodríguez, L. XXXVII Reunión del Grupo Especializado de Química Organometálica (Alcalá de Henares, Spain): Shotgun communication entitled "Aggregation studies of gold(I) complexes with biological activity".
- Pinto, A., Echeverri, M., Gómez-Lor, B., Rodríguez, L. 3rd HC3A Meeting (Toulouse, France): Oral communication entitled "Luminescent Au(I) benzothiadiazole-based derivatives".

- Pinto, A., Cunha, C., Pina, J., Seixas de Melo, J.S., Lima, J.C., Ridríguez, L. III Workshop on Chemistry of Group 11 Elements (Lisbon, Portugal): Oral communication entitled "Photophysical effect of the coordination of gold(I) to coumarin chromophore".
- Pinto, A., Roma-Rodriges, C., Lima, J.C., Fernandes, A.R., Rodríguez, L. 1st SupraMat Network (online congress): Shotgun communication entitled "Effect of the aggregation on the biological activity of gold(I) complexes".

Additionally, the research reported in Chapters **2**, **3** and **6** has already been published in:

- M. Dalmases, A. Pinto, P. Lippmann, Ingo Ott, L. Rodríguez, A. Figuerola. "Preparation and Antitumoral Activity of Au-Based Inorganic-Organometallic Nanocomposites". Frontiers in Chemistry **2019**, 7, 60.
- Q Sun, G Aragay, A Pinto, E Aguiló, L Rodríguez, P Ballester. "Influence of the Attachment of a Gold(I) Phosphine Moiety at the Upper Rim of a Calix[4]pyrrole on the Binding of Tetraalkylammonium Chloride Salts". Chemistry–A European Journal, **2020**, 26, 2020.
- A Pinto, G Spigolon, R Gavara, C Zonta, G Licini, L Rodriguez. "Tripodal gold(I) polypyridyl complexes and their $Cu^{+}$ and $Zn^{2+}$ heterometallic derivatives. Effects on luminescence". Dalton Trans, **2020**, 49, 14613.
- A. Pinto, C. Cunha, G. Aullón, J. C. Lima, L. Rodríguez, J. Seixas de Melo. "Comprehensive investigation of the photophysical properties of alkynylcoumarin gold(I) complexes". J. Phys. Chem. jp-2021-079855. Accepted.

and research reported in Chapters **4**, **5**, **7**, **8** and **9** will be published soon:

- A. Pinto, C. Roma-Rodrigues, J. Ward, R. Puttreddy, K. Rissanen, P. Baptista, A. Fernandes, J. C. Lima, L. Rodríguez. "Aggregation versus biological activity in gold(I) complexes. An unesplored concept". Inorg. Chem. ic-2021-02359y.R1. Submitted.
- A. Pinto, M. Echeverri, B. Gómez-Lor, L. Rodríguez. "How to achieve near unity fluorescence quantum yields of gold(I) benzothiadiazole-based derivative". Inorg. Chem. Front. QI-RES-07-2021-000849. Submitted.

# ABBREVIATIONS

| | |
|---|---|
| DMSO | Dimethyl sulfoxide |
| THF | Tetrahydrofuran |
| IR | Infrared |
| NMR | Nuclear magnetic resonance |
| ES | Electrospray |
| SEM | Scanning electron microscope |
| t | triplet |
| d | doublet |
| s | singlet |
| m | multiplet |
| ISC | Intersystem crossing |
| SOC-ISC | Spin-orbit coupling intersystem crossing |
| ACQ | Aggregation caused quenching |
| AIE | Aggregation induced emission |
| RTP | Room temperature phosphorescent |
| PMMA | Polymethyl methacrylate |
| PS | Polystyrene |
| PVA | Polyvinyl acetate |
| PTA | 1,3,5-triaza-7-phosphatricyclo[1.3.1.13.7]decane |
| DAPTA | 3,7-diacetyl-,3,7-triaza-5-phosphabicyclo[3.3.1]nonane |
| SAXS | Small angle X-ray scattering |
| DLS | Dynamic light scattering |
| XRD | X-ray diffraction |
| TPA | Tris(2-pyridymethyl)amine |
| Acac | Acetylacetonate |
| DFT | Density functional theory |
| MTOACl | Methyltrioctylammonium chloride |
| TBACl | Tetrabutylammonium chloride |
| ITC | Isothermal titration calorimetry |
| HOMO | Highest occupied molecular orbital |
| LUMO | Lowest unoccupied molecular orbital |

| | |
|---|---|
| BTD | Benzothiadiazole |
| DMF | N,N-Dimethylformamide |
| CT | Charge tranfer |
| ICT | Internal charge transfer |
| PEG | Poly(ehyleneglycol) |
| CAC | Critical aggregation concentration |
| ICP | Inductible coupled plasma |

# CHAPTER 1

## Introduction

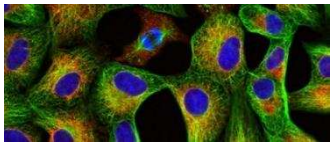

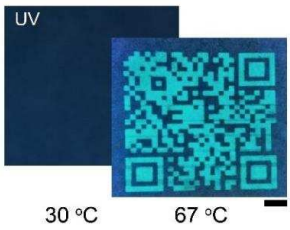


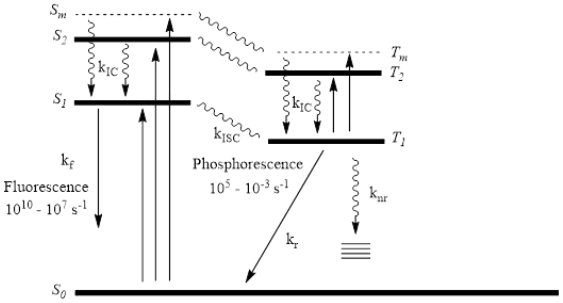

# 1. INTRODUCTION

## 1.1. Luminescent Materials and Supramolecular Chemistry

The development of new luminescent materials is a highly relevant research field and has attracted great interest due to the huge amount of applications in many different areas such as organic light-emitting diode (OLED), bioimaging or sensors.[1,2] There are several approaches to build luminescent materials that include different research fields. Among them, (supra)molecular chemistry is a challenging area and consist of the careful design of the chemical structure of the molecules in order to achieve the desired photophysical properties together with their possible assemblies.

Hence, in order to design the molecules and understand the processes involved in their emission pathways, it is necessary to clarify some fundamental bases on this topic. Photophysics is the research field that refers to several electronic internal processes induced by the absorption of light that do not lead to overall changes in the chemical structure of the molecule. In order to discuss the photophysical processes, it is useful to describe the Jablonski diagram, which illustrates the different possible electronic and vibrational transitions (Figure 1.1).

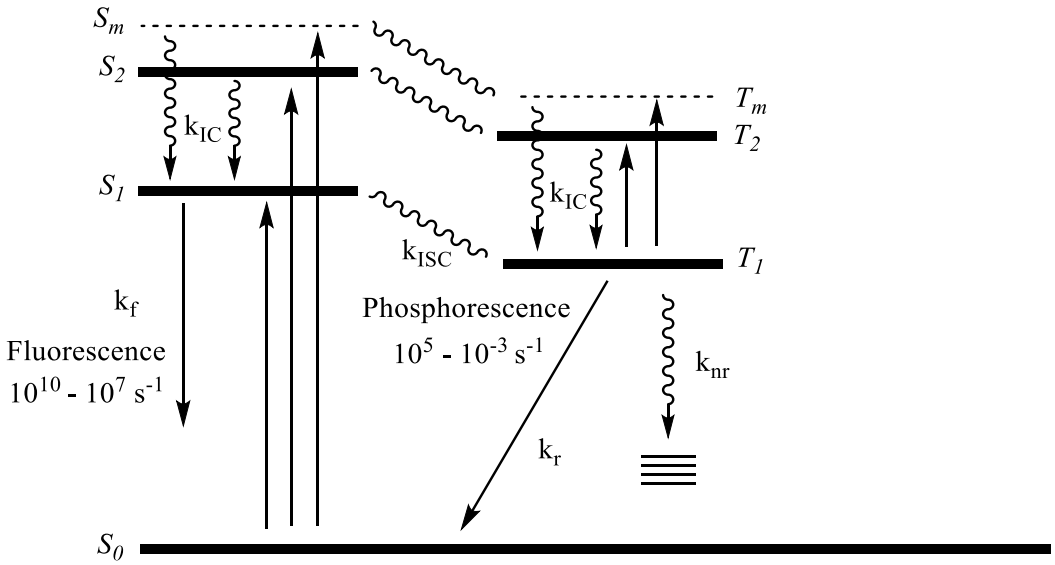


**Figure 1.1.** Simplified Jablonski diagram illustrating the main photophysical processes.

Absorption occurs when a molecule receives a photon of the light promoting the excitation of an electron from its ground state to a higher energy excited state. The molecule relaxes through internal conversion (IC) to the lowest excited state and then can undergo one of three different possible processes: 1) vibrational relaxation, which is a non-radiative pathway where the relaxation to the ground state is mediated by collisions between the molecules and its surrounding environment; 2) emission of a photon, which is a radiative pathway known as fluorescence. This transition consists of a decay from the $S_1$ state to the $S_0$, and since it is an allowed transition (both states have the same spin multiplicity), this process is fast and occurs in the picoseconds to nanoseconds time scale; 3) the electrons can undergo intersystem crossing (ISC) to the triplet excited state ($T_1$), through a change in the spin multiplicity. The decay of the $T_1$ state to the $S_0$ is a spin forbidden pathway, so the photoluminescence that results from this transition occurs on a much slower time scale, (microseconds to up to seconds) and is called phosphorescence. Although the intersystem crossing is an improbable pathway for some molecules due to its a forbidden nature, it is possible to favour it through different experimental conditions. A usual method is the introduction of heavy atoms, such as a transition metal or halogens, in the chemical structure, close to the chromophoric unit. In this way, the intersystem crossing is more efficient due to spin-orbital interaction, a relativistic effect that is higher in atoms with large nuclei. This mechanism is known as a spin-orbit coupling intersystem crossing (SOC-ISC).[3,4] Alternative methods have also been studied in recent years to promote the intersystem crossing, such as using a spinconverter,[5] introduction of carbonyl groups,[6] radical-enhanced ISC[7] and twist-induced ISC.[8]

The processes described until now are related to an individual molecule, but, intermolecular interactions between two or more molecules can also affect the photophysical properties of the compounds. The resulting supramolecular structures can be controlled by the introduction of specific functional groups that can promote non-covalent interactions such as hydrogen bonding, π-π stacking or Van der Waal forces. In this way, Supramolecular Chemistry has provided an unusual "bottom-up" approach to design sub-nanoscale small molecules to form well-defined nano- or microscale supramolecular architectures and consequently become one of the promising methods for being used in nanoscience and nanotechnology.[9-11]

Over the past few decades, Supramolecular Chemistry has expanded its applications in different fields and has continued to build larger and more complex architectures such

as macromolecules and multimetallic helicates,[12] rotaxanes,[13] metal-organic frameworks (MOFs), coordination polymers, clusters, etc.[14] Such studies help and guide to design and construct complex synthetic molecular machines, which led to the recent Nobel Prize in Chemistry (2016) being awarded to Sauvage, Sroddart and Feringa for their pioneering work. Since then, significant contributions to the field of self-assembly have facilitated the understanding of the principles behind intermolecular interactions and guided the development of new targeting and functional materials.

Supramolecular Chemistry provides the possibility to design molecules with interactive properties with a large variety of potential intermolecular interactions. This principle offers endless of possibilities for the construction of a variety of supramolecular structures with tunable specific properties and functionalities on demand. In particular, Supramolecular Chemistry can be an effective tool to manufacture luminescent materials, which is of special interest due to their optical properties that can be modulated by the reversible non-covalent nature of the supramolecular system. Supramolecular structures may present some properties totally different from those of the small molecules, which increase the interest of researchers in this field for the design and development of novel materials based on self-assembled units.

A nice example of how molecular assemblies can show totally different properties from isolated molecules is the inconsistency found in some cases between a molecular behaviour and their aggregated form. For instance, luminophores with planar and strong intermolecular interactions frequently show bright emission in the monomeric state but weakened or even quenched emission in the aggregated state (phenomenon known as aggregation caused quenching, ACQ) (Figure 1.2a). In contrast, some propeller shaped molecules show no emission in their dilute solution but much enhanced emission in their aggregated form (phenomenon known as aggregation induced emission, AIE) (Figure 1.2b).

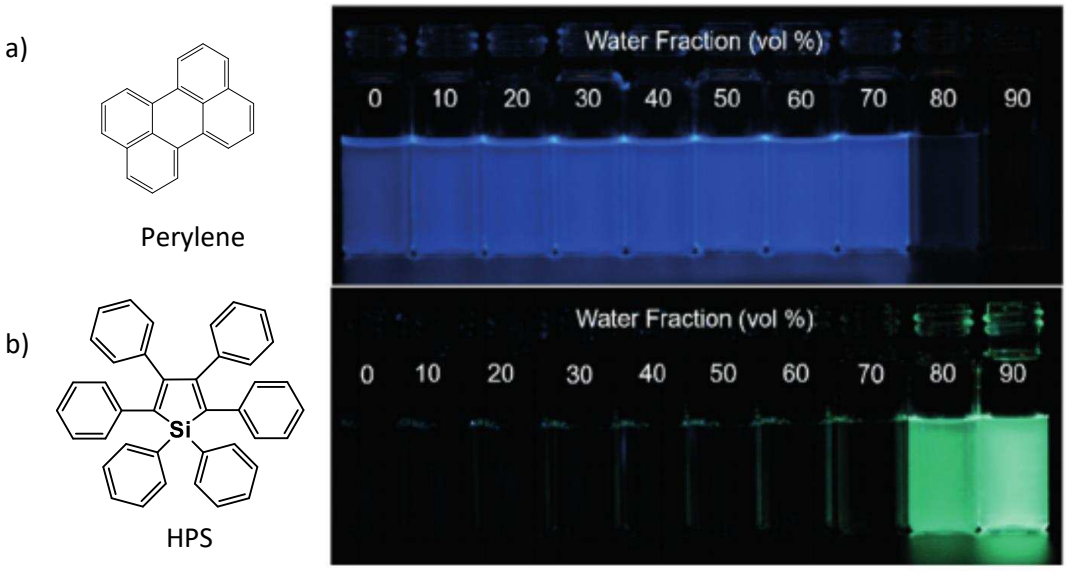


**Figure 1.2.** Molecular structures and photographs of a) perylene and b) hexaphenylsilole (HPS) solutions with different poor solvent fractions taken under ultraviolet light irradiation. Adapted with permission from.[15] Copyright 2020 John Wiley and Sons.

Based on the intrinsic dynamic and reversible property of non-covalent interactions that are involved in the processes of aggregation, self-assembly provides the luminophores a control in the conformation and the possibility to switch and respond to external stimuli. These stimuli can be classified by their nature as physical (light, temperature, mechanical, electrical, magnetic), chemical (molecules such as solvents, guests, cations, or anions), or biological (enzymes, receptors). Some examples are summarized below.

## 1.2. Mechanochromic effect

Mechanochromism is a change in the luminescence, usually in the colour of the resulting emission, of a material induced by the application of a mechanical stimulus such as pressure. The ability to selectively detect the mechanical stress is a useful tool for technological applications. The change in the luminescent properties induced for a mechanical stress is almost exclusively originated from variations on the molecular structure, conformational rearrangements, and/or changes of intermolecular interactions. These principles can be applied in small molecules that show mechanochromism, as well as in polymeric materials. In the case of the small

molecules, the mechanochromic effect is usually associated with mechanically induced rearrangement of the molecules and a transition from the crystalline to the amorphous state. The photophysical properties of organic and organometallic compounds that contain conjugated π-system are highly sensitive to intermolecular distance and the geometric orientation (Figure 1.3).[16- 19]

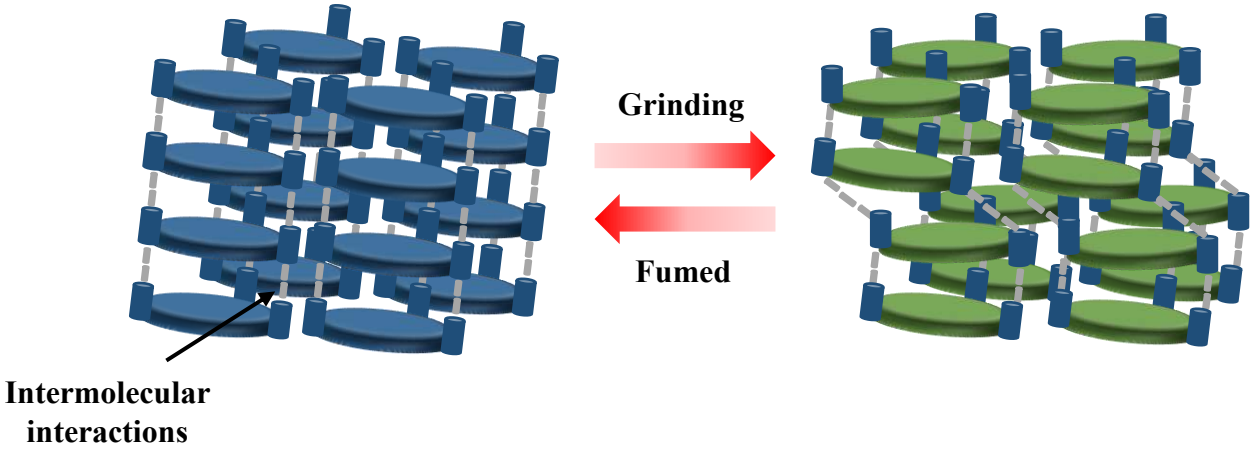


**Figure 1.3.** Schematic representation of the assembled structures of a compound when a mechanical stress is applied.

Some requirements must be accomplished in order to obtain mechanochromic materials: 1) the molecules should form at least two different stable states with different molecular assemblies; 2) the arrangement of the different molecular assemblies must be different enough in order to impact in their photophysical properties; 3) the molecular packing must be possible to modify by application of mechanical force.

The emerging knowledge in this field over the years allows to draw several strategies to design luminescent mechanochromic materials. Some of the approaches to create metastable states are the establishment of a competitive effect between different intermolecular interactions,[20] interfere with the formation of thermodynamically stable assemblies[21] or the incorporation an AIE-active moiety in the chemical structure which have potential to be transformed to more closely packed assembly when a mechanically stimulation is applied.[22]

In this respect, the influence of the AIE research in the field of mechanochromic fluorescent materials has gained great importance, since it enables an early-stage detection of the damage of the materials.[23] The dispersion of these compounds in polymer matrixes can amplify these changes due to the variations in the interactions

between the interphase and the supramolecular conformation. Notably, this incorporation may be done by the dispersion of chromophoric probes within polymers or by a covalent bonding of the chromophoric units with the macromolecular chains.[24]

## 1.3. Solvatochromic effect

Solvatochromism is a term to describe the changes in the photophysical properties of a chemical substance by variation of the solvent. An interaction between the solute and the solvent is involved in this process and two different situations may happen: 1) the dipole moment of the molecule increases upon excitation and, therefore, a higher dipolar moment or polarizable solvent will stabilize more the excited state than the ground state. In this case, the separation between the ground and the excited states decreases and a red shift is observed when the polarity of the solvent increases (positive solvatochromism); 2) the dipole moment of the molecule decreases in the excited state compared to the ground state in polar solvents and, consequently, the ground state is stabilized. In this case, there is an increase of the separation between the ground state and the excited state, and a blue shift is observed when the polarity of the solvent increases (negative solvatochromism).

Fluorophores with a π-extended structures that present π-π* transitions, display commonly larger dipole moment in the excited state than in the ground state and situation 1 will be the most common. In contrast, molecules with a n-π* transitions, which is undergone from one of the electrons located at a lone-pair, in an n orbital of the heteroatom of the molecular structure, to a π*orbital of the molecular system, involve a reduction of the dipole moment of the molecule and situation 2 will be the most common.[25]

The interaction of the chemical substance with the solvent can promote variations in the position, intensity and shape of the absorption or emission bands. Generally speaking, the emission spectra of the fluorophores is more affected by the solvent than absorption since fluorescence lifetimes are usually much longer than the time required for solvent relaxation.[26] Inspection of Figure 1.4 can make more easily to understand why absorption spectra are less sensitive to the effect of the solvent. When the excited state of a molecule is created, this is surrounded by solvent molecules and during this time the solvent molecules present rotational reorientation in order to stabilize it. This process is called solvent relaxation, which depends on the solvent, and occurs in about

$10^{-10}$ s. Absorption process occurs in about $10^{-15}$ s, a time too short for the motion of the molecule or solvent. In contrast, fluorescence lifetimes ($10^{-9}$ s) are usually much longer than the time required for solvent relaxation. Solvent relaxation stabilizes the energy of the excited state of the molecules in polar solvents (for those cases that there is a larger dipole moment in the excited state than in the ground state, usually π- π* transition). When the excited molecule returns to the ground state, the electronic configuration of the solvent molecules does not have time to be reorganized in the time scale of the fluorescence and the energy of this ground state presents high energy than the equilibrium ground state.[26,27]

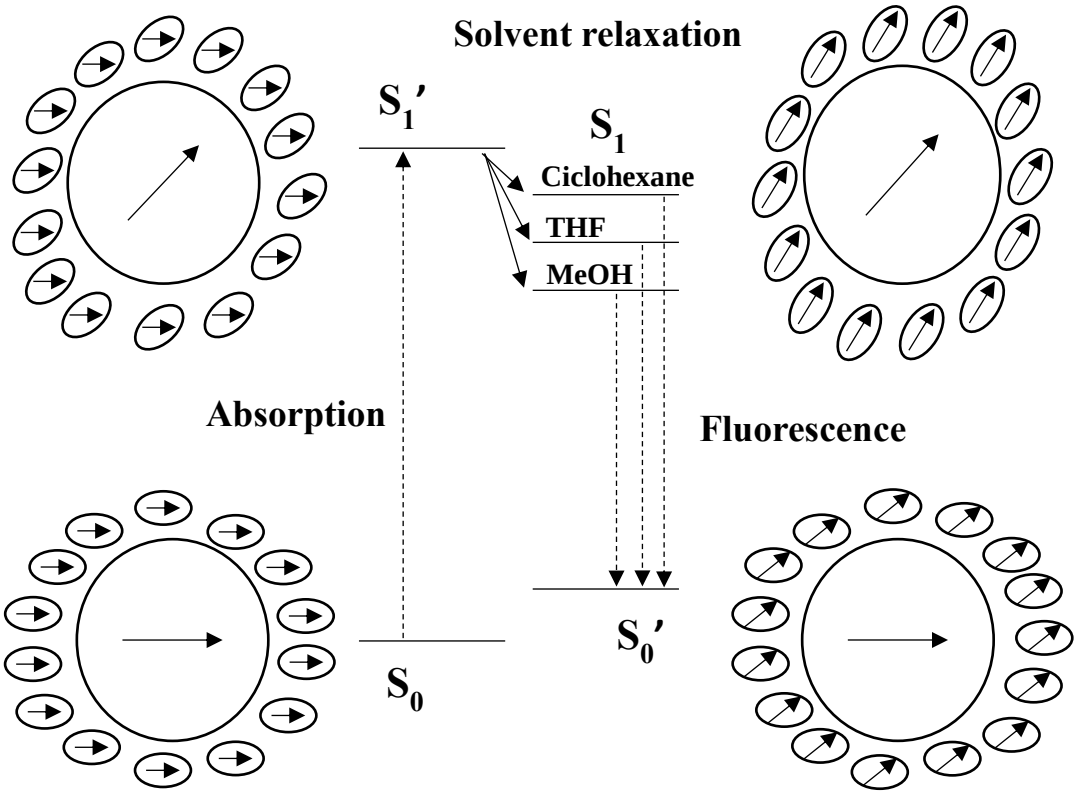


**Figure 1.4.** Solvent effects on electronic state energies. $S_0$ is the ground state, $S_1$ in the excited state, dashed line: radiative process, solid lines: non-radiative processes.

Several methods are used to analyse the solvatochromic effects. For example, Lippert-Mataga plots[28] are used to determine the magnitude of the Stokes' shift (difference between the ground and excited state energies) in terms of changes in the molecular dipole moment. It is assumed that the polarity of the solvent is the only parameter under consideration, but this becomes an oversimplification. To overcome this problem, a

multiparametric Kamlet-Taft method[29] has been introduced and consists of considering four single empirical parameters, and each one considers a particular aspect of the solvent such as the polarizability, solvent ability to act as a hydrogen-bond donor or the ability of bulk solvents to behave as a hydrogen-bond acceptors. These two methods are described in more detail in Chapter 5.

Due to all these aspects, a chemical substance with solvatochromic effect must present specific characteristics which make its intermolecular interactions sensitive to small changes in the environment. Compounds that present a charge-transfer transition have found to be highly dependent on the environment. Commonly, these types of compounds are composed by a donor (D) and acceptor (A) chromophores connected by a bridge. In their excitation process, the changes in the charge distribution led to a large dipole moment which strongly modify the interactions with the environment.[30]

Although solvatochromism has been mostly used to rationalize the solvent effect on the reaction rates or retention times in chromatography,[31,32] recently, it has been used as imaging tool of live cells and tissues since any biomolecular interaction or change in biomolecular organization results in a modification in their environment and, as a consequence, in their photophysical properties.[33]

## 1.4. Host-guest and metal coordination interactions

Molecular recognition represents one of the bases of the supramolecular chemistry where the formation of supramolecules is based on the principles of molecular complementary. The molecules that act as receptors are called hosts and those that are recognized are known as guest. Host-guest systems play a significant role in the development of advanced supramolecular materials and even in biological processes due to their good selectivity, high efficiency, and responsiveness. Typically, a host-guest system is forming an adduct complex through various non-covalent interactions with excellent selectivity because of the size of the cavity.[34] Since the discovering and the synthesis of the crown ethers in 1960 by Pederson, which was used as the host molecule to selectively bind alkali metals, an increasing number of new compounds for molecular recognition has been developed. The most important building blocks for supramolecular assemblies based on host-guest found in the literature are macrocyclic hosts, including crown ethers[35,36], cyclodextrins (CDs),[37] calixarenes,[38] curcubit[n]urils (CB[n]s),[39-41] and pillararenes.[42,43]

The incorporation of these recognizing units into a fluorescent system allows to create functional smart materials with tunable photophysical properties.[44] One approach is the incorporation of crown ether elements into AIE systems, which allows the manipulation of the assembly and control the morphologies of the materials with reversibility (Figure 1.5).[45] In the particular case exemplified in Figure 1.5, benzo-15-crown-5 macrocycles were functionalized on the four arms of tetraphenylethene (TPE) molecules to afford a supramolecular fluorescent probe for $K^+$ with the crown ether moieties serving as recognizing unit. When the $K^+$ is coordinated to the crown ether, induce a crosslink among the monomers, which is accompanied by the enhancement of the fluorescence originated from the AIE effect.

Most of the molecular recognition processes reported in the literature are mainly in solution and are useful for the development of basic research and molecular design. In contrast, for emerging technologies and practical applications it is usually necessary that this process takes place in a different media, such as surfaces, where the environmental effects and perturbations should be considered. This is important since most of the molecular recognition in practical situations occurs at an interface as can be seen for example in cell membranes, DNA complexes and device surfaces.[46]

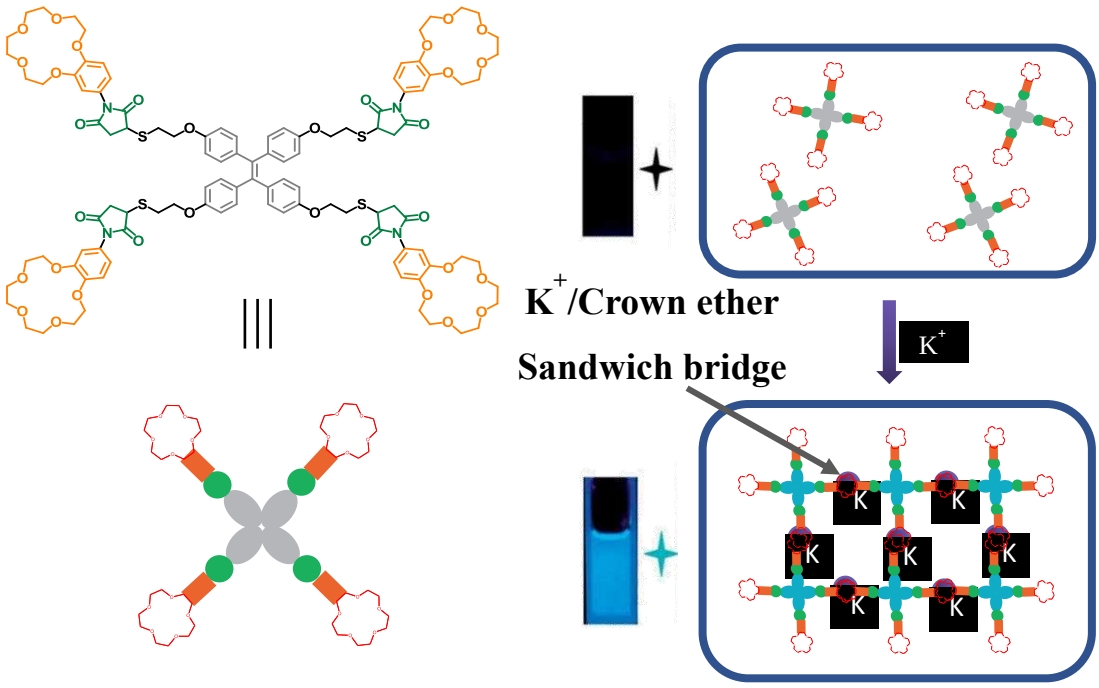


**Figure 1.5.** Schematic illustration of a molecule with AIE induced by recognition between the crown ether moieties and $K^+$ ions.

Another approach for the design of a supramolecule is the metal coordination, which provides strength, well-defined geometry and reversibility and represents a powerful tool for the assembly of supramolecular species with controllable architectures.[47,48] The assembly by the coordination of a metal requires the use of preformed building blocks that contains one or several binding sites. The binding sites can be Lewis basic groups, which are suitably placed in the molecule in order to promote the self-assembly. The final properties can be introduced by the incorporation of the appropriate functional groups in its structure, which can be for example luminescence, magnetism, or chirality.

## 1.5. Matrices

In terms of device fabrication or processing applications, such as sensors, solid-state lighting or organic light emitting diodes, the incorporation of the molecules within matrices or formation of thin films can make this process much easier. In addition, for luminescent materials, the non-radiative pathways can be minimized. The non-radiative losses can be classified in intramolecular and in external losses to the environment. In this way, the collisions with quenching sites are mitigated with the incorporation of the fluorophores in matrices by the suppression of vibrational and diffusional motions. A wide variety of matrices used for luminescent purposes exists in the literature, such as silica glasses,[49] hydrogen bonded polymer matrices,[50] graphene quantum dots[51] or zeolites.[52]

This strategy has been used more recently to achieve room temperature phosphorescence (RTP).[53] However, systems with bright RTP are challenging to obtain, since the vibration and diffusion in amorphous matrix favor the vibrational loss of triplet excitons, causing frequently significant quenching in their phosphorescence.[54] To address this issue, the inclusion of luminescent molecules within a carefully chosen matrix is extremely important in order to mitigate the vibrational triplet decay. Well-known candidates are poly(methyl)methacrylate (PMMA), polyvinyl acetate (PVA) and polystyrene (PS), which provides rigidity of the final sample and can also introduce new non-covalent intermolecular interactions between the matrix and the fluorophore that help to suppress non-radiative pahways (Figure 1.6).[55]

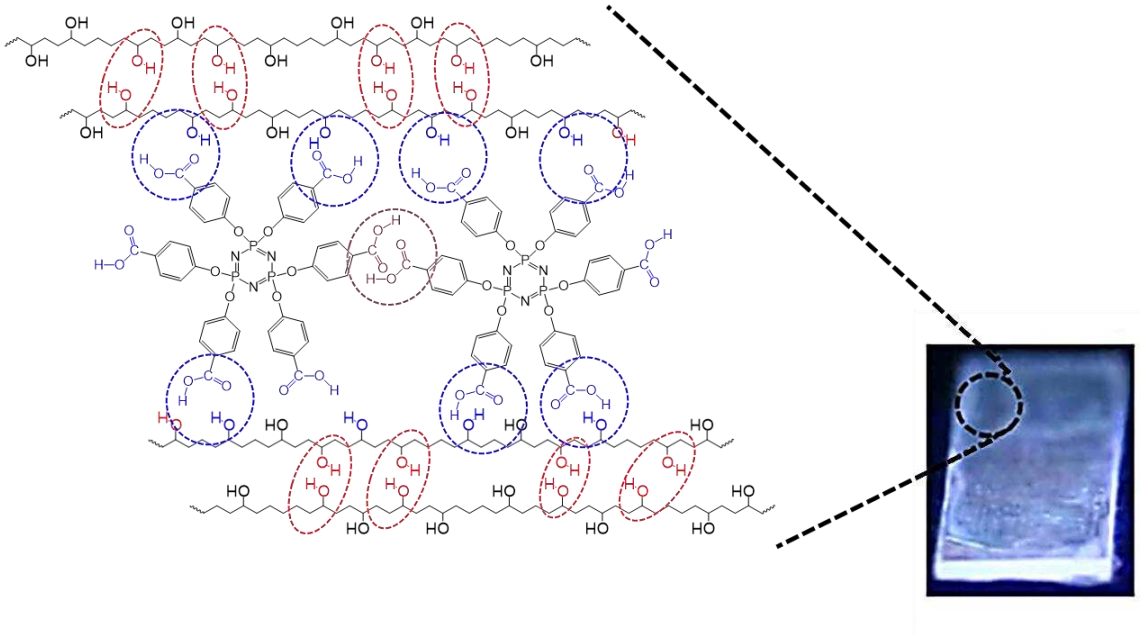

**Figure 1.6.** Example of the inclusion of a phosphorescent molecule into a polymeric matrix.

## 1.6. Incorporation of gold(I) atoms

Gold(I) is a closed shell cation with an electronic configuration of $5d^{10}6s^{0}$, which justifies the relative stability of gold(I) compounds. Unlike the expected repulsion between two metal cations, an important number of examples of metal atoms containing $d^{10}\cdots d^{10}$ interactions are known.[56] In the particular case of gold(I), these interactions have been observed in crystal structures with distances between the two gold centers ranging 2.7 and 3.5 Å, being below the sum of two van der Waals radii (3.8 Å). In 1990, Schmidbaur defined these interactions as "the unprecedented affinity between gold *atoms even with "closed-shell" electronic configurations and equivalent electrical* charges" and give the name of aurophilic attraction.[57] Aurophilicity has become a very interesting topic because it plays an important role in the resulting emissive properties and assemblies of gold(I) complexes. The strength of Au(I)···Au(I) interactions have been theoretically calculated and are in the range 29-46 kJ $mol^{-1}$, which are comparable with hydrogen bond.[58] Hence, apart from the well-known weak interactions of the organic molecules, gold(I) complexes can establish metal···metal interactions, which can be not only observed in solid state, but can be also maintained in solution, since the formation of supramolecular assemblies has been detected.[59-61]

The luminescence of gold(I) complexes can be originated from the fluorophore but also it can be strongly affected by the presence of Au(I)···Au(I) interactions in the complexes. When the luminescence comes from the fluorophore, it can be produced by transitions among π orbitals from the organic part or by transitions involving the metal center, where a charge transfer is involved (π- π* transitions). The incorporation of gold(I) can promote the observation of phosphorescence emission due to the heavy-atom effect, which opens access to the low-lying emissive triplet state through the intersystem crossing (ISC). However, in complexes containing an extended aromatic system, emission from the singlet may compete with ISC, which results in the generation of either dual singlet/triplet emission[62,63] or only singlet emission from an organic chromophore.[64] In this way, the photophysical behavior is strongly driven by the nature of the ligand and the coordination-sphere geometry, namely by the distance between the metal and the organic chromophore, which is a crucial parameter for an effective spin-orbit coupling. For those transitions where the ligand is not involved (metal centered transitions), also the geometry around the metal center strongly affects the resulting photophysical properties. For instance, phosphorescence is generally not observed for isolated linear molecules, since it is a forbidden transition (takes place with a change in the symmetry between the HOMO and LUMO, Laporte rules) and thus, the resulting phosphorescence is not observed. In contrast, in three coordinated species, the transition is orbitally forbidden, and phosphorescence can take place[65]. In general, it can be assumed that having a trigonal-planar geometry leads to a higher probability of having a metal-centered phosphorescent emission. Nevertheless, it is not a necessary condition since a moderate deviation from linearity produces a shortening of the HOMO-LUMO gap (Figure 1.7).[66] Thus, it can be assumed that a deviation from the linearity on gold(I) complexes would contribute to a shortening of the HOMO-LUMO gap, and therefore to a higher probability of having phosphorescence emission. This can be achieved by the introducing of bulky ligands or by the establishment of strong gold(I)-gold(I) interactions that will distort the linearity of these complexes.[67]

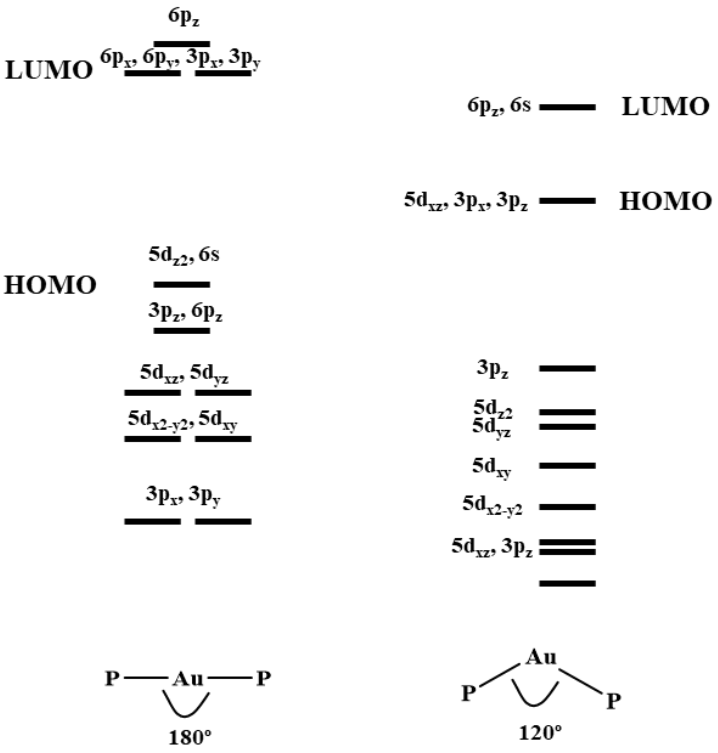


**Figure 1.7.** Molecular orbital diagram for $[AuP_2]^+$ type complexes showing the decrease on the HOMO-LUMO gap in non-linear Au systems.[67]

Although a deviation of the linearity produced by the establishment of gold(I)-gold(I) interactions led to a shortening of the HOMO-LUMO gap, the interaction between the two metals by themselves lead also to the same phenomenon. This is due to an overlap of the orbitals of the gold(I) atom, where the degree of shortening is dependent on the number of interacting gold atoms (Figure 1.8).[67]

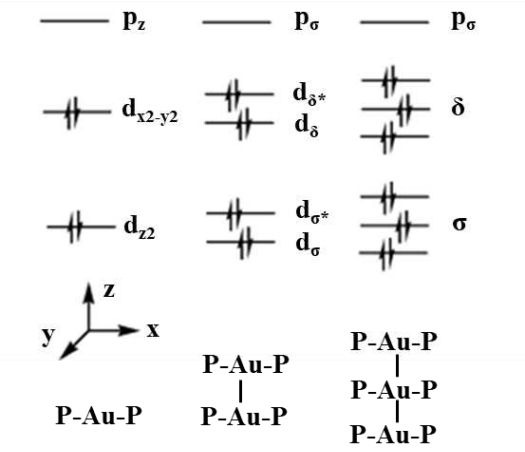


**Figure 1.8.** Qualitative molecular orbital diagram of $[AuP_2]^+$.[67]

## 1.7. Objectives of the present work

During the last years, the Supra and Nanostructured research group at the Universitat de Barcelona (where this thesis has been carried out), has been pioneer in the development of different gold(I) complexes and resulting supramolecular assemblies with a wide variety of applications. It begins with the synthesis of alkynyl gold(I) derivatives containing water soluble phosphanes (PTA = 1,3,5-triaza-7-phosphatricyclo[1.3.1.13.7]decane and DAPTA = 3,7-diacetyl-,3,7-triaza-5-phosphabicyclo[3.3.1]nonane), which were found to form luminescent organometallic hydrogels (Figure 1.9).[68,69] This aggregation was unexpected since this kind of compounds do not contain any common ligand well-known to induce gelation. The process was observed to be favoured by the establishment of aurophilic interactions, hydrogen bonds and π-π stacking.[70] This work was the starting point of an intensive study of the supramolecular assemblies where modifications on the chromophore unit or the incorporation of a charge in the chemical structure gave rise to different types of morphologies (rods, vesicles, squares, stars…) that display different luminescent properties.[71,72]

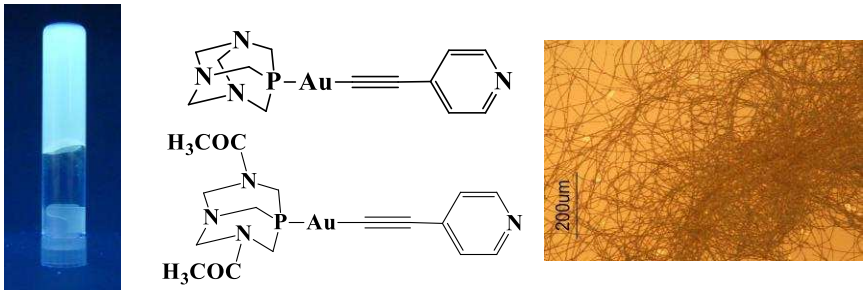


**Figure 1.9.** Luminescent hydrogel under UV-light (left); chemical structure of gold(I) derivatives (middle); optical microscope image of the fibres that form the hydrogel.

Taking all this into consideration, this work aims to use the supramolecular chemistry of gold(I) complexes in order to modulate the luminescent properties going one step further on the methodology established by the group. The design and investigation of new supramolecular gold(I) compounds and assemblies with improved luminescent properties has been performed and studied in different type of applications, going from luminescent materials, molecular recognition or biology. Such complexes were

rationally designed, where the different parts of the molecules were selected in function of the desired goal.

The particular objectives of this Doctoral Thesis are summarized below, together with the chapter where they are described.

In **Chapter 2**, the tris(2-pyridymethyl)amine (TPA) metalloligand, has been used to synthesize gold(I) complexes containing three different monophosphanes and a triphosphane. The free coordination positions available in the TPA ligand have been explored in order to obtain heterometallic structures with tunable photophysical properties.

In **Chapter 3**, a gold(I) derivative from the calix[4]pyrrole (macrocycle), known for their ability to bind halides, has been synthesized and used to perform molecular recognition studies of halides followed by UV-vis, emission and NMR spectroscopies.

In **Chapter 4**, coumarins have been chosen as fluorescent groups to coordinate to the gold(I) atom, due to their well-known tunable photochemical and photophysical properties depending on their substituents. The effect of the electrondonating/electronwithdrawing substituents at the coumarin rings on the photophysical properties has been analysed. Additionally, the potential use of the gold(I) complexes synthesized as photosensitizers for the generation of singlet oxygen has been also investigated.

In **Chapter 5**, new gold(I) complexes containing benzothiadiazole (BTD) core have been synthesized. They contain flexible long alkyl chain in order to promote the alignment of the molecules. The steric hindrance and the planarity of the second coordination position of the gold(I) have been studied with incorporation of different types of phosphane and carbenes. The solvatochromic and mechanochromic properties together with the incorporation of the compounds synthesized in polymer matrixes have been explored. The induction of the aggregation together with the incorporation of the gold(I) complexes synthesized in polymer matrices allows us to achieve near unity fluorescence quantum yields.

In **Chapter 6**, gold nanoparticles have been made interact with those systems that were previously found to form hydrogels[68,69] in order to induce new metallophilic interactions between organometallic molecules and nanoparticles. We have studied

how these metallophilic contacts can modulate the resulting assemblies in the new hybrid materials. Additionally, the biological activity of the resulting hybrid systems has been studied and compared with the isolated gold(I) and gold(0) precursors.

In **Chapter 7**, gold(I) complexes previously studied in the group[73] with important activity against cancer cells, were used to perform a careful analysis of the state of the gold(I) complex before entering the cells. A detailed and complete analysis of their aggregation process has been performed in order to correlate it with their biological properties. Moreover, since the gold(I) complex containing tris(1-naphthyl)phosphane showed a great selectivity for one cancer cell line (A2780 ovarian cells), a new family of compounds containing a naphthyl group has been synthesized for being tested in the biological assays.

In **Chapter 8**, an amphiphilic moiety has been introduced in a pyridine type ligand incorporated in the chemical structure of the complexes. Although the pyridine ligands are widely used in coordination chemistry, gold(I) pyridine complexes are limited and can be a hidden potential. The incorporation of a luminescent chromophore in the second position (coumarin, used in **Chapter 4**, and aniline, used in **Chapter 7**) has been used for the synthesis of gold(I) complexes. Since the introduction of an amphiphilic moiety is a well-known ligand to induce self-assembly, aggregation studies and potential applications have been also explored.

In **Chapter 9**, gold(I) complexes containing TPE core have been designed and synthesized in order to analyse the resulting AIE behaviour. The effect of the steric hindrance at the second coordination position of the gold(I) has been studied by the incorporation of different types of phosphanes suitable to promote the aggregation. The changes on the resulting luminescence induced by the aggregation have been explored.

In general, phosphanes have been chosen to occupy the second coordination position of the gold(I) atoms, due to their ability to modulate the solubility of the gold(I) derivatives in a wide range of solvents and also their nuclearity. In particular, PTA and DAPTA are the most used due to their ability to increase the solubility of the resulting compounds in aqueous media. There has been an increasing efforts in industry and academia to replace chemical processes in traditional organic solvents with an alternative solvent like water (green solvent). The development of water soluble compounds has become extremely relevant since water is the biologically most relevant

solvent. Carbenes were also used in **Chapter 5**, in order to improve the planarity of the compounds and favour intermolecular contacts.

A wide variety of characterization techniques have been used to evidence the correct formation of the organic and organometallic compounds (NMR, IR, ESI and X-Ray Diffraction). Their resulting supramolecular assemblies have been carefully analysed through DLS, optical microscope, SEM, UV-vis absorption, emission and SAXS.

SAXS was performed at the NCD-SWEET beamline at the ALBA Synchrotron thanks to two consecutive funded projects and it is a useful tool to characterize the aggregates in their early stages.

A complete photophysical characterization has been performed through UV-vis, emission, quantum yields and lifetimes. Some of them in our research group but those more specialized were used thanks to the facilities of Univ. NOVA de Lisboa and Coimbra Laser lab collaboration project.

## 1.8. References


1. Bauri, K., Saha, B., Banerjee, A. and De, P. Polym. Chem. **2020**, 11, 7293–7315.
2. Liu, J., Yang, Z., Ye, B., Zhao, Z., Ruan, Y., Guo, T., Yu, X., Chen, G. and Xu, S. J. Mater. Chem. C, **2019**, 7, 4934–4955.
3. Demchenko, A. P. Introduction to fluorescence sensing. **2015**, Springer International Publishing, ISBN: 978-3-319-79318-4.
4. Valeur, B. and Berberan-Santos, M. N. Molecular Fluorescence: Principles and Applications. **2012**, Wiley-VCH Verlag GmbH & Co, ISBN: 9783527650002.
5. Zhao, J., Xu, K., Yang, W., Wang, Z. and Zhong, F. Chem. Soc. Rev. **2015**, 44, 8904–8939.
6. Rajagopal, S. K., Mallia, A. R. and Hariharan, M. Phys. Chem. Chem. Phys. **2017**, 19, 28225–28231.
7. Wang, Z. Gao, Y., Hussain, M., Kundu, S., Rane, V., Hayvali, M., Yildiz, E. A., Zhao, J., Yaglioglu, H. G., Das, R., Luo, L. and Li J. Chem. Eur. J. **2018**, 24, 18663–18675.
8. Nagarajan, K., Mallia, A. R., Muraleedharan, K. and Hariharan, M. Chem. Sci. **2017**, 8, 1776–1782.
9. Edwards-Gayle, C. J. C. and Hamley, I. W. Org. Biomol. Chem. **2017**, 15, 5867–5876.
10. Coleman, A. C., Beierle, J. M., Stuart, M. C. A, Maciá, B., Caroli, G., Mika, J. T., van Dijken, D. J., Chen, J., Browne, W. R. and Feringa, B. L. L. Nat. Nanotechnol. **2011**, 6, 547–552.
11. Zhang, Q., Qu, D. H., Tian, H. and Feringa, B. L. Matter, **2020**, 3, 355–370.
12. Yashima, E., Ousaka, N., Taura, D., Shimonura, K., Ikai, T. and Maeda, K. Chem. Rev. **2016**, 116, 13752–13990.
13. Erbas-Cakmak, S., Leigh, D. A., McTernan, C. T. and Nussbaumer, A. L. Chem. Rev. **2015**, 115, 10081–10206.
14. Tranchemontagne, D. J., Tranchemontagne, J. L., O'keeffe, M. and Yaghi, O.

M. Chem. Soc. Rev. **2009**, 38, 1257–1283.

15. Zhao, Z., Zhang, H., Lam, J. W. Y. and Tang, B. Z. Angew. Chemie - Int. Ed. **2020**, 59, 9888–9907.

16. Sagara, Y. and Kato, T. Nat. Chem. **2009**, 1, 605–610.

17. Hong, Y., Lam, J. W. Y. and Tang, B. Z. Chem. Soc. Rev. **2011**, 40, 5361–5388.

18. Chi, Z., Zhang, X., Xu, B., Zhou, X., Ma, C., Zhang, Y., Liu, S. and Xu, J. Chem. Soc. Rev. **2012**, 41, 3878–3896.

19. Sagara, Y., Yamane, S., Mitani, M., Weder, C. and Kato, T. Adv. Mater. **2016**, 28, 1073–1095.

20. Yuan, M. S., Wang, D. E., Xue, P., Wang, W., Wang, J. C., Tu, Q., Liu, Z., Liu, Y., Zhang, Y. and Wang, J. Chem. Mater. **2014**, 26, 2467–2477.

21. Sagara, Y. and Kato, T. Angew. Chem. In. Ed. **2008**, 120, 5253–5256.

22. Yoon, S. J., Chung, J. W., Gierschner, J., Kim, K. S., Choi, M. G., Kim, D. and Park, S. Y. J. Am. Chem. Soc. **2010**, 132, 13675–13683.

23. Pucci, A. Sensors, **2019**, 19, 4969–4987.

24. Pucci, A., Bizzarri, R. and Ruggeri, G. Soft Matter, **2011**, 7, 3689–3700.

25. Pimentel, G. C. J. Am. Chem. Soc. **1957**, 79, 3323–3326.

26. Lakowicz J.R. Principles of Fluorescence Spectroscopy. **2006**. Springer Boston, MA. ISBN: 978-0-387-46312-4.

27. Reichardt, C. Chem. Rev. **1994**, 94, 2319–2358.

28. Mataga, N., Kaifu, Y. and Koizumi, M. Communication, **1955**, 28, 690–691.

29. Yokoyama, T., Taft, R. W. and Kamlet, M. J. J. Am. Chem. Soc. **1974**, 98, 3233–3237.

30. Marini, A., Muñoz-Losa, A., Biancardi, A. and Mennucci, B. J. Phys. Chem. B, **2010**, 114, 17128–17135.

31. Nunes, R., Nunes, N., Elvas-Leitão, R. and Martins, F. J. Mol. Liq. **2018**, 266, 259–268.

32. Spange, S., Lungwitz, R. and Schade, A. J. Mol. Liq. **2014**, 192, 137–143.

33. Klymchenko, A. S. Acc. Chem. Res. **2017**, 50, 366–375.

34. Liu, Z., Nalluri, S. K. M. and Fraser Stoddart, J. Chem. Soc. Rev. **2017**, 46, 2459–2478.

35. Gokel, G. W., Leevy, W. M. and Weber, M. E. Chem. Rev. **2004**, 104, 2723–2750.

36. Leininger, S., Olenyuk, B. and Stang, P. J. Chem. Rev. **2000**, 100, 853–907.

37. Harada, A. **2001**, 34, 456–464.

38. Sansone, F., Baldini, L., Casnati, A. and Ungaro, R. New J. Chem. **2010**, 34, 2715–2728.

39. Lagona, J., Mukhopadhyay, P., Chakrabarti, S. and Isaacs, L. Angew. Chemie - Int. Ed. **2005**, 44, 4844–4870.

40. Lee, J. W., Samal, S., Selvapalam, N., Kim, H. J. and Kim, K. Acc. Chem. Res. **2003**, 36, 621–630.

41. Kim, K. Chem. Soc. Rev. **2002**, 31, 96–107.

42. Strutt, N. L., Zhang, H., Schneebeli, S. T. and Stoddart, J. F. Acc. Chem. Res. **2014**, 47, 2631–2642.

43. Cragg, P. J. and Sharma, K. Chem. Soc. Rev. **2012**, 41, 597–607.

44. Wang, H., Ji, X., Li, Z. and Huang, F. Adv. Mater. **2017**, 29, 1606117–16061139.

45. Lou, X. Y. and Yang, Y. W. Adv. Opt. Mater. **2018**, 6, 1–25.

46. Ariga, K., Ito, H., Hill, J. P. and Tsukube, H. Chem. Soc. Rev. **2012**, 41, 5800–5835.

47. Chakrabarty, R., Mukherjee, P. S. and Stang, P. J. Chem. Rev. **2011**, 111, 6810–6918.

48. Percástegui, E. G., Ronson, T. K. and Nitschke, J. Chem. Rev. **2020**, 120, 13480–13544.

49. Levy, D. and Avnir, D. J. Photochem. Photobiol. A Chem. **1991**, 57, 41–63.

50. Al-Attar, H. A. and Monkman, A. P. Adv. Funct. Mater. **2012**, 22, 3824–3832.

51. Mueller, M. L., Yan, X., McGuire, J. A. and Li, L. S. Nano Lett. **2010**, 10, 2679–2682.

52. Márquez, F., Zicovich-Wilson, C. M., Corma, A., Palomares, E. and García, H. J. Phys. Chem. B, **2001**, 105, 9973–9979.

53. Liu, Y., Zhan, G., Liu, Z. W., Bian, Z. Q. and Huang, C. H. Chinese Chem. Lett. **2016**, 27, 1231–1240.

54. Huang, Q., Gao, H., Yang, S., Ding, D., Lin, Z. and Ling, Q. Nano Res. **2020**, 13, 1035–1043.

55. Gan, N., Shi, H., An, Z. and Huang, W. Adv. Funct. Mater. **2018**, 28, 1–24.

56. Sculfort, S. and Braunstein, P. Chem. Soc. Rev. **2011**, 40, 2741–2760.

57. Schmidbaur, H. Gold Bull. **1990**, 23, 11–21.

58. Pyykkö, P. Chem. Rev. **1997**, 97, 597–636.

59. Lima, J. C. and Rodríguez, L. Inorganics, **2015**, 3, 1–18.

60. Rodríguez, L., Ferrer, M., Crehuet, R., Anglada, J. and Lima, J. C. Inorg. Chem. **2012**, 51, 7636–7641.

61. Romo-Islas, G. and Gavara, R. Inorganics, **2021**, 9, 1–36.

62. Li, X. L., Zhang, K. J., Li, J. J., Cheng, X. X. and Chen, Z. N. Eur. J. Inorg. Chem. 2010, 3449–3457.

63. Aguiló, E., Moro, A. J., Outis, M., Pina, J., Sarmento, D., Seixas de Melo, J. S., Rodríguez, L., and Lima, J. C. Inorg. Chem. **2018**, 57, 13423–13430.

64. Yao, X. X., Guo, Y. M., Chen, J., Huang, M. M., Shi, Y. and Li, X., L. J. Organomet. Chem. **2017**, 834, 58–63.

65. Visbal, R., López-De-Luzuriaga, J. M., Laguna, A. and Gimeno, M. C. Dalton Trans. **2014**, 43, 328–334.

66. Assefa, Z., Staples, R. J. and Fackler, J. P. Inorg. Chem. **1994**, 33, 2790–2798.

67. Laguna, A. Modern Supramolecular Gold Chemistry: Gold-Metal Interactions

and Applications. Wiley-VCH, **2008**, 978-3-527-32029-5.

68. Gavara, R., Llorca, J., Lima, J. C. and Rodríguez, L. Chem. Commun. **2013**, 49, 72–74.

69. Aguiló, E., Gavara, R., Lima, J. C., Llorca, J. and Rodríguez, L. J. Mater. Chem. C, **2013**, 1, 5538–5547.

70. Gavara, R., Aguiló, E., Guerra, C. F., Rodríguez, L. and Lima, J. C. Inorg. Chem. **2015**, 54, 5195–5203.

71. Aguiló, E., Gavara, R., Baucells, C., Guitart, M., Lima, J. C., Llorca, J. and Rodríguez, L. Dalton. Trans. **2016**, 45, 7328–7339.

72. Giestas, L., Gavara, R., Aguiló, E., Svahn, N., Lima, J. C. and Rodríguez, L. Supramol. Chem. **2018**, 30, 278–285.

73. Svahn, N., Moro, A. J., Roma-Rodrigues, C., Puttreddy, R., Rissanen, K., Baptista, P. V., Fernandes, A. R., Lima, J. C. and Rodríguez, L. Chem. - A Eur. J. **2018**, 24, 14654–14667.

# CHAPTER 2

## Tripodal gold(I) complexes vs $Cu^{+}$ and $Zn^{2+}$ heterometallic derivatives.

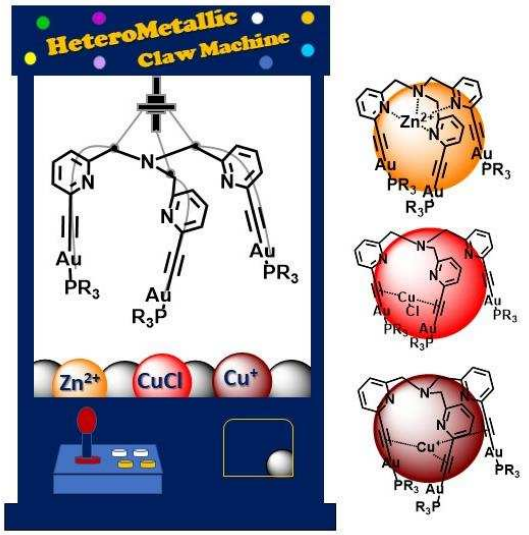


Part of this Chapter has been published in A. Pinto, G. Spigolon, R. Gavara, C. Zonta, G. Licini, L. Rodriguez. Dalton Transactions, **2020**, **49**, 14613-14625.

# 2. TRIPODAL GOLD(I) COMPLEXES vs $Cu^{2+}$ AND $Zn^{2+}$ HETEROMETALLIC DERIVATIVES

## 2.1. Introduction

Materials that alter their physical properties under the influence of the external environmental changes are of significant interest in the recent years due to the wide range of applications in sophisticated technologies and daily life such as memory devices, printing technologies, or surfaces.[1-3] In particular, the construction of multicolour photoluminescence materials that can be tuned in a simple manner are of great interest.[4,5] Controlling the multicolour states has been carried out through dynamic chemistry, for example, dynamic coordination between a metal and a ligand as an effective way to obtain multiple colour states.

In terms of the election of the ligands, their electronic and steric characteristics, as well as the number of donor atoms are key factors. Multidentate ligands containing two or more pyridine donor units play a significant role in modern coordination. Tris(2-pyridymethyl)amine (TPA) that possesses three pyridyl moieties connected to a central N atom, and its derivatives (Figure 2.1) are an important class. These ligands can interact with a wide variety of metal ions and its coordination chemistry has been extensively studied.[6–17]

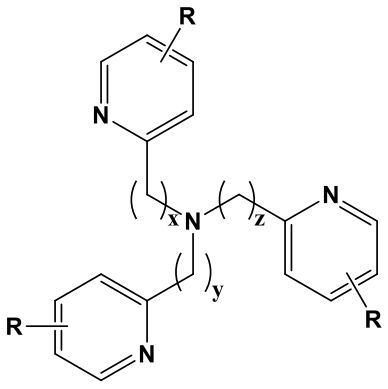


**Figure 2.1.** General structure of tris(pyridylmethyl)amine (TPA) tripodal ligands.

For example, TPA derivatives, whose pyridyl group facilitates the coordination to second- or third-row transitional metals with different coordination geometries, have been extensively used as enzyme models,[18,19] in catalytic applications range from oxidations using,[20–22] oxygen binding and activation,[23–26] water oxidation,[27] esters hydrolysis,[28–31] hydrogen production,[32] nitrene transfer,[33] and atom-transfer radical addition and polymerization[34–39] and as a spin-crossover species.[40,41]

The functionalization of TPA backbone has been obtained originally by introduction of the desired functional group before the formation of the skeleton.[37] The addition of a terminal alkynyl moiety by the use of cross-coupling reactions allows the coordination of closed-shell metals, like gold(I), that can introduce additional arrangements and luminescent properties by the establishment of metallophilic interactions.[42] The luminescent properties of gold(I) complexes depends on many factors, such as the number of interacting metals present in the complex and their proximity. Additionally, gold(I) atoms are well known to facilitate a triplet excited state emission due to the heavy atom effect.[43] More precisely, heterometallic complexes built by interactions between gold(I) and another closed-shell metal ions, such as Cu(I),[44] Ag(I),[45] Tl(I),[46] Pb(II),[47] Hg(II),[48] Bi(III)[49] or Sn(II)[50] have been also studied due to a direct correlation between the presence of these interactions and the resulting photophysical properties. Among them, the interactions between Au(I) and Cu(I) atoms are not much represented. There are different strategies that allow this kind of interactions, but, in most cases, the metallophillic Au(I)···Cu(I) contact takes place by the imposition given by specific bridging ligands.[51,52] Another strategy is the use of alkynyl ligands that leads σ-bonding coordination to Au(I) centres and π-bonding coordination to Cu(I) centres giving rise to Au(I)···Cu(I) interactions. This coordination mode of alkynyl ligand provides additional opportunities for fine tuning of the photophysical characteristics of the resulting complexes.[53,54]

On the other hand, tertiary phosphanes are common soft donor ligands that have been extensively used to prepare gold(I) complexes. These ligands are very interesting since are able to modulate important parameters such as: 1) the solubility; 2) the nuclearity and, 3) the bulkiness of the resulting complexes.[55]

In this context, in this chapter we describe the synthesis of different tripodal gold(I) alkynyl complexes derived from the TPA ligand and containing three different monophosphanes and also a triphosphane. The potential coordination positions

(pyridyl, ethynyl and metal···metal) available at TPA ligand have been explored in order to obtain heterometallic structures with tunable photophysical properties.

## 2.2. Results and Discussion

### 2.2.1. Synthesis and Characterization

The synthesis of tris((6-ethylpyridin-2-yl)methyl)amine (**2.L**) was carried out at the laboratory of Prof. Giulia Licini at the Università di Padova. The synthesis of the tripodal gold(I) complexes $N[Au(C{\equiv}Cpy)(PTA)]_3$ (**2.1**) and $N[Au(C{\equiv}Cpy)(DAPTA)]_3$ (**2.2**) were obtained by the deprotonation of the terminal protons of the alkynyl groups in **2.L** and subsequent reaction with the previously synthesized $[AuCl(PR_3)]$ ($PR_3$ = PTA, DAPTA) precursors in 1:3 stoichiometry (see Scheme 2.1).

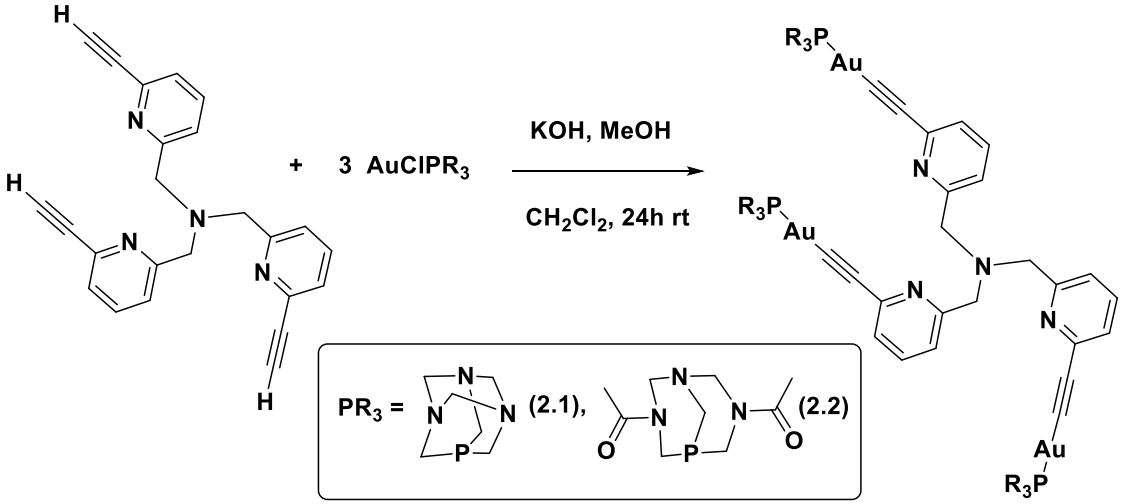


**Scheme 2.1.** Synthesis of complexes **2.1** and **2.2**.

This synthetic procedure was not successful in the case of **2.3** (containing triphenylphosphane, $PPh_3$), and the reaction should be performed by the previous substitution of chloride ligand by the acetylacetonate (synthesis of $[Au(acac)PPh_3]$ complex) that reacts with the terminal protons of the tripodal ligand producing the coordination of the gold metal atom to the alkynyl moiety and acetylacetone as volatile subproduct (Scheme 2.2).

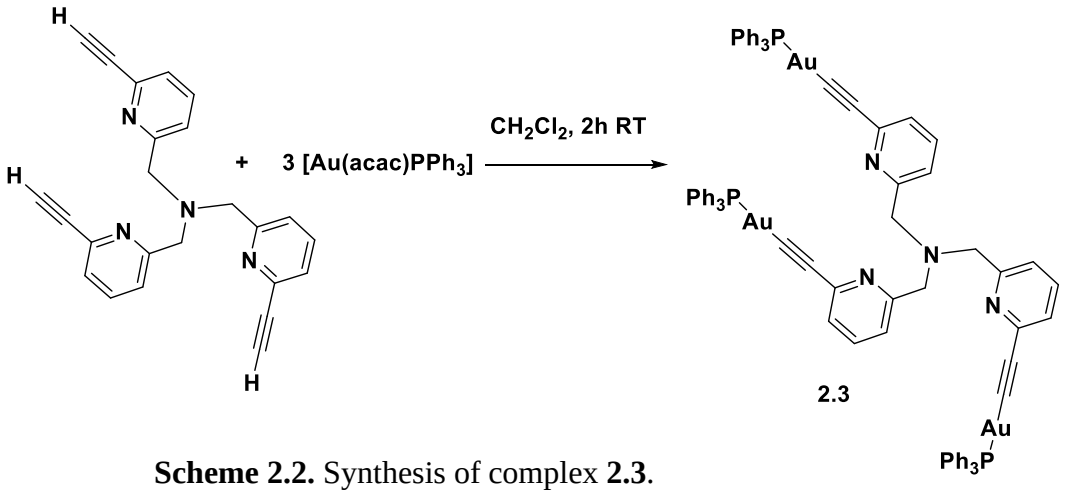


**Scheme 2.2.** Synthesis of complex **2.3**.

All complexes were obtained as yellow solids stable to air and moisture in moderate yields. Their spectroscopic data support the proposed stoichiometry. $^{1}H$ NMR spectra display the typical pattern of the PTA, DAPTA and $PPh_3$ phosphanes, the protons of the pyridyl moiety and the disappearance of the terminal alkynyl proton (Figure 2.2). $^{31}P\{^{1}H\}$ NMR spectra show only one signal at ca. -52 (**2.1**), 3 (**2.2**) and 29 ppm (**2.3**), which confirms the equivalence of the phosphorous atoms in the molecule and their coordination to the gold centers. IR spectra show the corresponding vibration bands of the C≡C fragment at ca. 2100 $cm^{-1}$, together with the disappearance of the signal of the terminal proton, the presence of C-P and C=C vibrations of the phosphanes and the C=O strong band in the case of **2.2**. The final evidence of the formation of the complexes was given by the recorded molecular peak by ESI(+) spectrometry at m/z 1422.274 for **2.1** ($[M + H^{+}]^{+}$), 557.098 ($[M+3H^{+} + MeOH]^{3+}$) for **2.2** and 1737.300 ($[M + H^{+}]^{+}$) in the case of **2.3**.

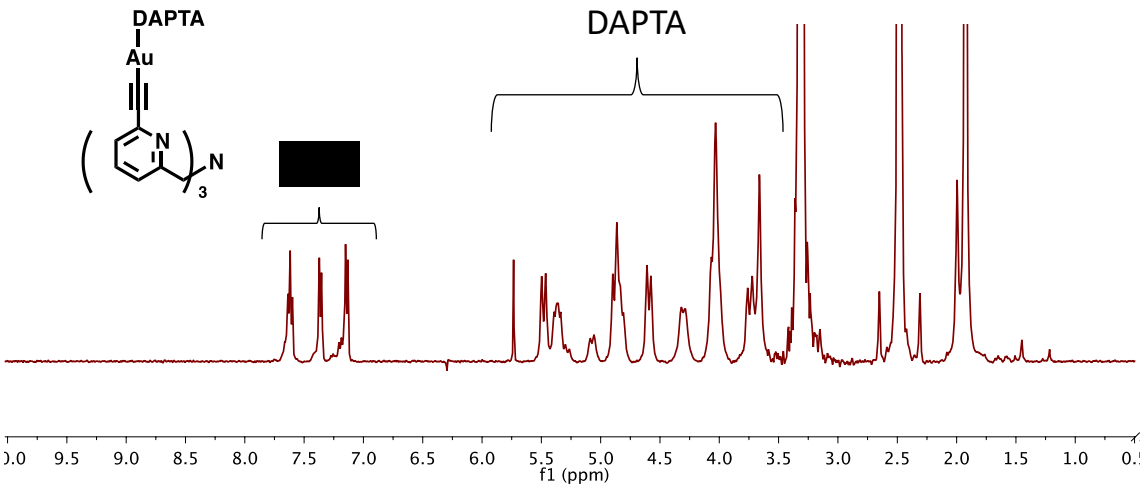


**Figure 2.2.** $^{1}H$ NMR spectrum of **2.2** in DMSO-$d_6$.

The reaction of **2.L** with the trinuclear gold(I) source (triphos)$(AuCl)_3$ (triphos = 1,1,1-tris(diphenylphosphinomethyl)ethane) in 1:1 ratio was also assayed to obtain a cage complex following the same conditions previously detailed for **2.1** and **2.2** (Scheme 2.3). The correct formation of the cage-like compound **2.4** was evidenced by the molecular peak at m/z 1592.290 ($[M+NH_4]^+$) and the expected bands at IR and $^1H$ and $^{31}P$ NMR peaks.

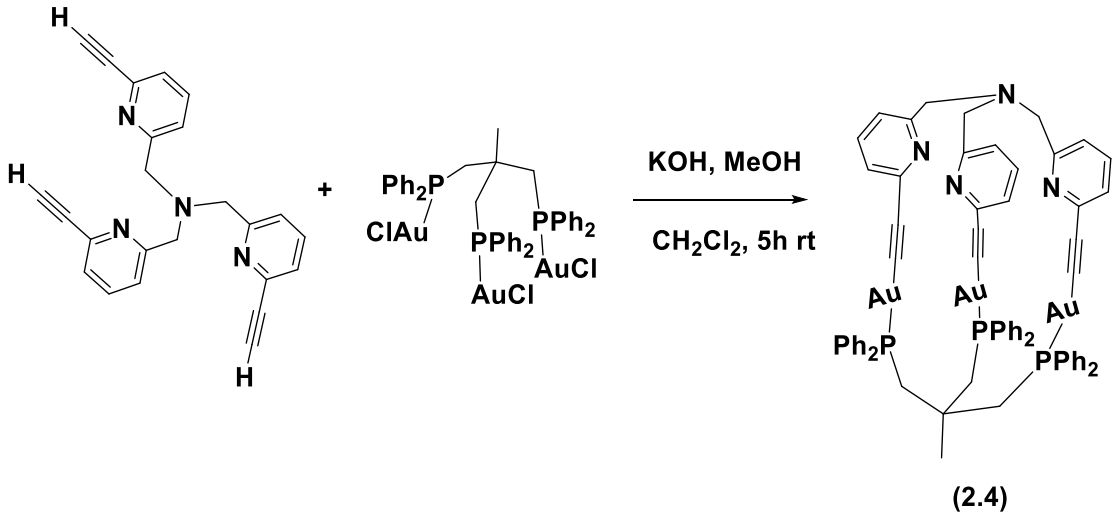


**Scheme 2.3.** Synthesis of complex **2.4**.

### 2.2.2. Photophysical characterization

Absorption and emission spectra of all complexes were recorded in dimethyl sulfoxide (DMSO) at $10^{-5}$ M concentration and the results are summarized in Table 2.1.

**Table 2.1.** Absorption and emission data of the homometallic gold(I) complexes **2.1**-**4** and the ligand precursor, **2.L** in DMSO. $\lambda_{exc}$ = 350 nm.

| **Compound** | Absorption $\lambda_{max}$ (nm) ($\varepsilon$ ($10^3$ $M^{-1}$ $cm^{-1}$)) | Emission $\lambda_{max}$ (nm) | Emission $\lambda_{max}$ (nm) solid |
|---|---|---|---|
| **2.L** | 283 (5.2) | 440 | - |
| **2.1** | 268 (2.9), 306 (42.4) | 472 | 531 |
| **2.2** | 275 (29.7), 305 (31.2) | 473 | 530 |
| **2.3** | 278 (15.4), 300 (22.3) | 441 | - |
| **2.4** | 278 (15.4), 300 (6.2) | 440 | - |

All gold(I) complexes display two absorption bands centered at ca. 270 nm and ca. 300 nm (Figure 2.3). These bands are assigned to an intraligand [$\pi \rightarrow \pi^{*}$ (C≡C or C≡C-Py) transition. An increase of the baseline in the absorption spectra due to the presence of small aggregates is observed in the case of **2.4**, in agreement with the lower solubility observed for this complex.

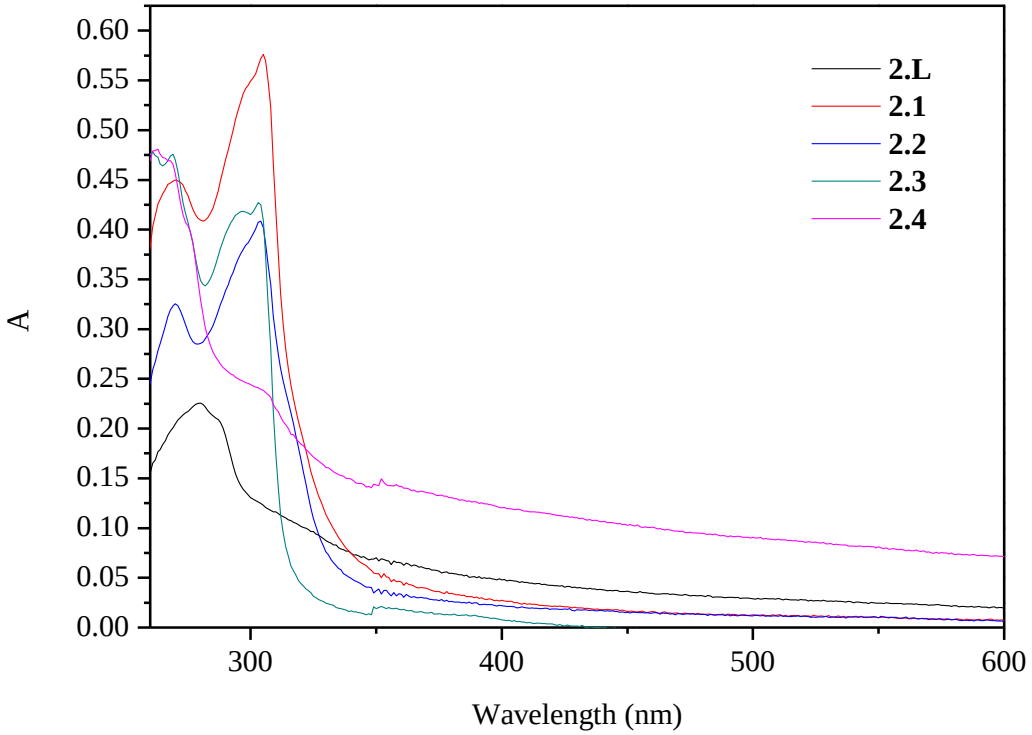


**Figure 2.3**. Absorption spectra in DMSO of compounds **2.L** and **2.1-4** at ca. $1 \cdot 10^{-5}$ M

Absorption bands become broader when the complexes are dissolved in a "bad" solvent, such as acetonitrile, together with an increase of the baseline (scattering) as previously observed for complex **2.4** in DMSO. UV-vis absorption and emission spectra at different DMSO-water contents mixtures were recorded in order to analyze in more detail the formation of aggregates (Figure 2.4). The absorption bands at 270 nm and 308 nm become red-shifted, less intense and broader with increasing the water contents (considered as "bad" solvent), due to the aggregates' formation.[56]

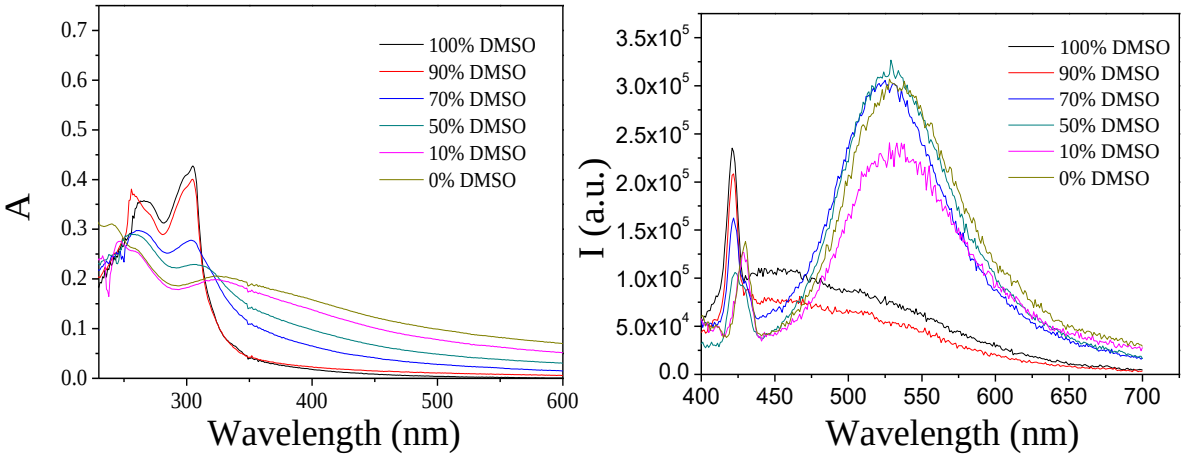


**Figure 2.4**. Absorption (left) and emission (rigth) spectra of **2.1** at different DMSO-water content.

Only a significant emission was recorded in DMSO solution for **2.L** upon excitation of the samples at 350 nm. Gold(I) complexes display a very weak emission probably due to non-radiative decays from previously populated triplet state. Nevertheless, when the aggregation takes place (higher water contents in DMSO/ water mixtures, see Figure 2.4), a broad emission bands appears at ca. 530 nm for **2.1** and **2.2** while the corresponding emission band of complex **2.3** is found at higher energy (ca. 480 nm). No significant emission was recorded for cage-like complex **2.4** in solution. Thus, we can rationalize that the aggregation process induces an enhanced emission due to the possibility conferred by the open conformation of the tripodal complexes that can favor the contact between the different arms, and as consequence, the approach/contact between the gold(I) atoms and the possible establishment of other weak interactions such as π–π stacking. The emission band is assigned to triplet metal-centered $^{3}$MM or $^{3}$MMLCT transitions, according to the literature.[43,57] Only significant emission could be recorded for **2.1** and **2.2** in solid state with maxima that fits perfectly with the recorded for aggregated samples in solution.

### 2.2.3. Tuning luminescence by the formation of heterometallic complexes.

The luminescence profile of the gold(I) complexes often depends dramatically on the presence of metal···metal interactions (metallophilicity). In this way, a modification of the conformation of the complex resulting from the coordination of a second metal

center may change the resulting luminescence. With this goal in mind, the homometallic gold(I) compounds were made react with different metal salts to analyze the possible tuning of the luminescence of **2.1-4** gold(I) complexes.

The TPA ligand (**2.L**) presents two kinds of binding units (the pyridyl and the alkynyl moieties) suitable to interact with the metal salts. Hence, $Zn^{2+}$ and $Cu^{+}$ salts have been chosen due to the well-known coordination of $Zn^{2+}$ to the nitrogen atoms of the pyridyl moiety[58–60] and the coordination of $Cu^{+}$ to the alkynyl group.[61–65]

A preliminary analysis of the possible formation of heterometallic complexes was performed by absorption and emission titrations. In this way, we could also identify the stoichiometry of the resulting heterometallic complexes. Increasing amounts of the metal salt were added into a solution of the complexes **2.1-3** and the absorption and emission spectra were recorded after each addition. The very low solubility of **2.4** precluded to carry out this type of studies. A decrease on the absorption band is observed in the case of complexes **2.1** and **2.2**, when larger amounts of the $Zn^{2+}$ salt (due to a decrease of the baseline due to the solubilization of the aggregates) while a blue shift together with a decrease of the baseline is observed in the presence of $Cu^{+}$ salts. On the other hand, the presence of both $Zn^{2+}$ and $Cu^{+}$ metal salts induce the formation of a lower energy absorption band together with an isosbestic point at ca. 310 nm in the case of complex **2.3**. The different behavior is attributed to the different solubility of the homometallic complexes in the solvent used for the titrations. Complexes **2.1** and **2.2** are initially in the aggregated form, while complex **2.3** is in the monomeric form. The addition of different amounts of $Zn^{2+}$ and $Cu^{+}$ salts to a $1 \cdot 10^{-5}$ M solution of all gold complexes leads to a quenching of the emission band in all cases being indicative of the interaction of these ions with the gold complex (Figure 2.5). In this way, the stoichiometry of the heterometallic complexes was found to be 1:1 in all cases, according to the plot of the emission maxima versus the number of equivalents of the metal salt added.

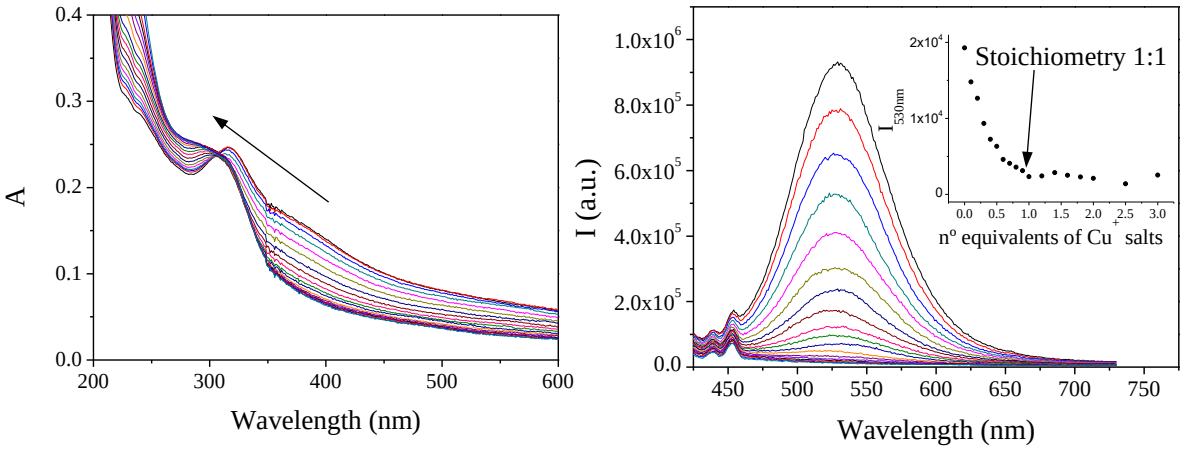


**Figure 2.5.** Absorption (left) and emission (right, $\lambda_{exc}$ = 350nm) titrations of **2.1** with increasing amounts of CuCl. Inset: Plot of the variation of emission maximum against number of equivalents of $Cu^+$ salt.

Heterometallic complexes (Au/$Cu^+$ and Au/$Zn^{2+}$) were isolated by the reaction of the $Cu^+$ ($Cl^-$ and $BF_4^-$) and $Zn^{2+}$ ($NO_3^-$) salts to independent solutions of the gold(I) complexes (Scheme 2.4). An alternative method was required in the case of the heterometallic complexes derived from **2.4** (**2.4a-c**) complexes. The observed lower solubility in common solvents and the closed conformation of the complex seems to avoid the interaction with corresponding second metal cation once the cage is formed. The reaction was then performed in a one-pot synthesis by the addition of the corresponding $Cu^+$ and $Zn^{2+}$ salts in the same reaction mixture containing the precursors for the synthesis of **2.4**.

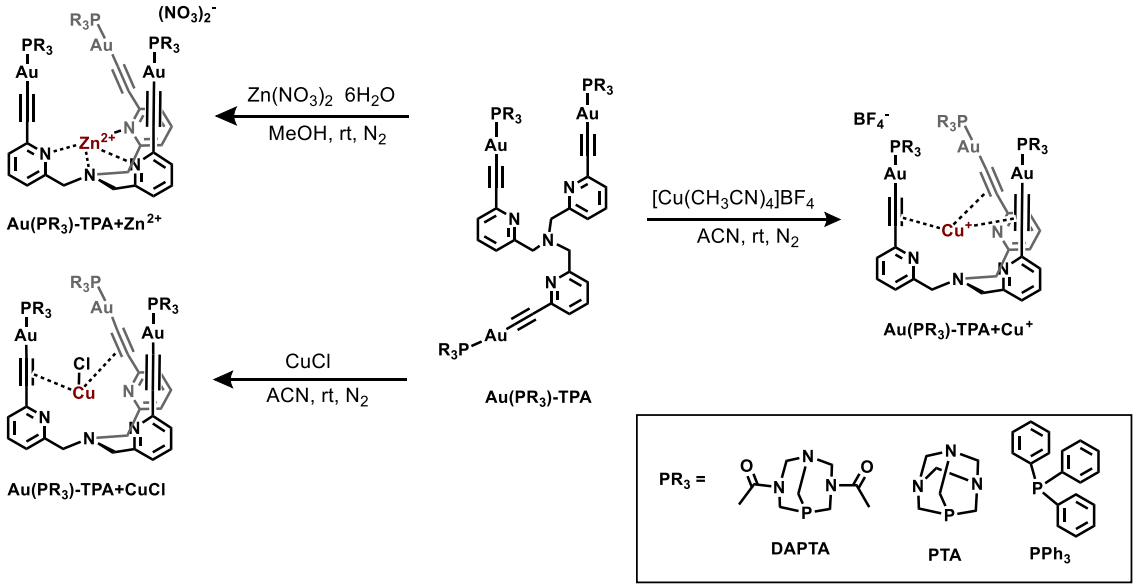


**Scheme 2.4.** Synthesis of $Zn^{2+}$- and $Cu^+$- heterometallic complexes obtained from **2.1**-**3**.

Characterization of the heterometallic complexes by NMR, IR and mass spectrometry indicates their correct formation. $^{1}H$ NMR spectra evidences different coordination motifs for $Zn^{2+}$ and $Cu^{+}$ complexes (Figure 2.6). With comparison with the homometallic gold(I) complex, the NMR spectra of $Zn^{2+}$-complexes display a shift and broadening of the methylene proton resonances in the complex. Different shifts are observed for the pyridyl protons, being upfield shifted for a proton (closer to the central methylene group) and downfield shifted for b and c protons, as previously observed for other Zn-TPA complexes reported in the literature.[66,67] On the other hand, the global downfield shift of all the pyridyl protons recorded for $Cu^{+}$-heterometallic systems, indicates that the copper coordination occurs in the vicinity and that a different coordination motif is expected in comparison with $Zn^{2+}$-derivatives.

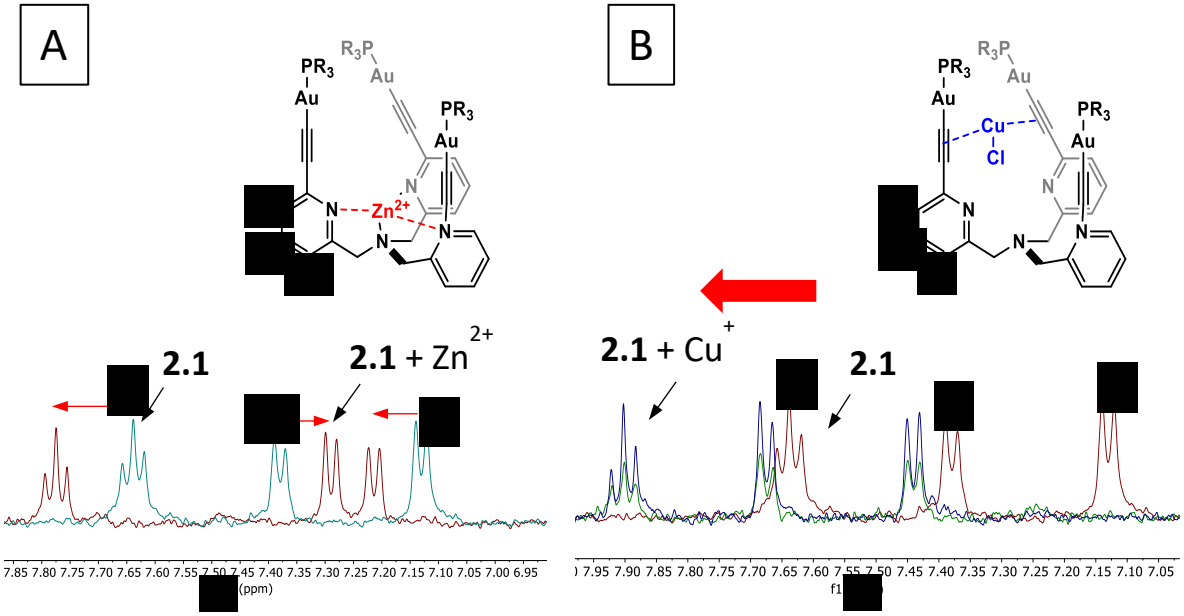


**Figure 2.6.** (**A**) $^{1}H$ NMR of compound **2.1** (green line) and with the addition of $Zn^{2+}$ (red line) and (**B**) $^{1}H$ NMR of compound **2.1** (red line) and with the addition of CuCl and $Cu(CH_3CN)_4(BF_4)$ (green and blue line).

$^{31}P$ NMR spectra of all the heterometallic complexes display only one pic, being an evidence of the equivalence of the phosphorous environment in the complexes, without a significant shift of the signal with the incorporation of the second metal salt. IR spectroscopy indicates that the alkynyl moiety is involved in the coordination of $Cu^{+}$ (Figure 2.7). In addition, a different coordination mode between the two copper salts used in this work can be identified. In the case of CuCl there are two different stretching frequencies, one corresponding to one free arm (identical to homometallic gold(I)

complex) while the other two are expected to coordinate to $Cu^{+}$ as suggested by the presence of a new vibration band ca. 50 $cm^{-1}$ shifted to lower wavenumbers. This coordination is in agreement with the literature[39,68] where the chloride anion is expected to be coordinated to $Cu^{+}$. However, two different stretching frequencies were recorded in the case of $[Cu(NCMe)_4]BF_4$, but both shifted in relation of homometallic compound (Figure 2.7). This is possibly due to an asymmetric coordination of $Cu^{+}$ to the three arms of the tripodal complex. Mass spectra confirms the presence of chloride in the structure and supports the different coordination of the two salts, due to the presence of the Cl in the molecular peak of the **xb** series (x = **2.1**, **2.2**, **2.4**).

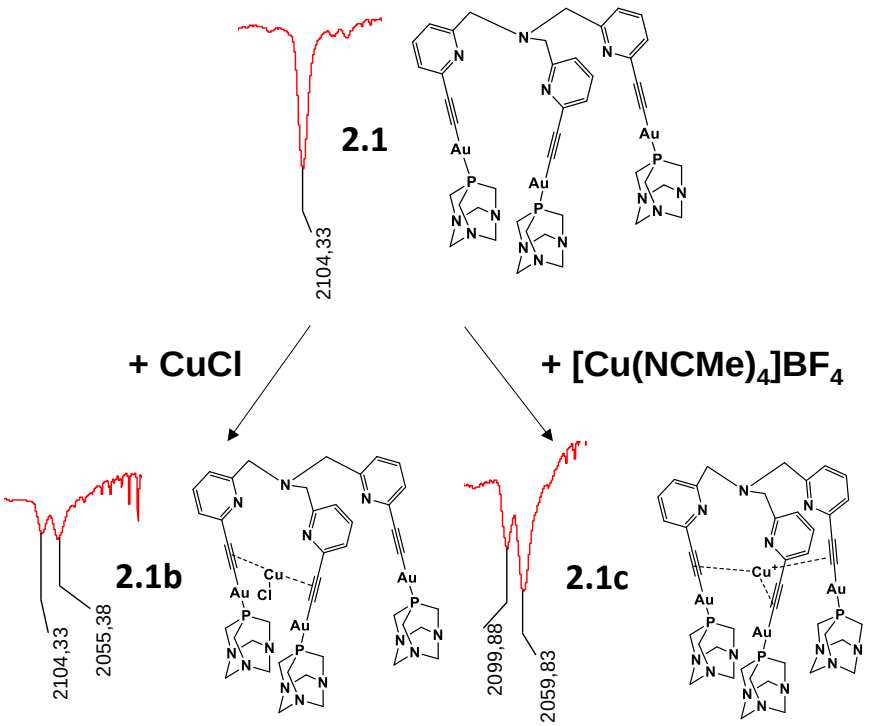


**Figure 2.7.** IR spectra of **2.1** and respective $Cu^{+}$ derivatives of **2.1b** and **2.1c**.

The photophysical properties were studied in solution and in solid state for all the synthesized heterometallic complexes and the results are summarized in Table 2.2. Significant differences between $Zn^{2+}$ and $Cu^{+}$ heterometallic derivatives were observed in the absorption spectra. In the case of $Zn^{2+}$ derivatives, the vibronic resolution is maintained while $Cu^{+}$ derivatives become broader, probably due to a decrease of the vibration freedom of the alkynyl moieties blocked by the coordination of the $Cu^{+}$ cation.

**Table 2.2.** Absorption and emission data of heterometallic gold(I) complexes **2.1-4a-c** . $\lambda_{exc}$ = 350 nm.

| **Compound** | Absorption $\lambda_{max}$ (nm) ($\varepsilon$ ($10^3$ $M^{-1}$ $cm^{-1}$)) | Emission $\lambda_{max}$ (nm) | Emission $\lambda_{max}$ (nm) solid |
|---|---|---|---|
| **2.1a** | 272 (40.0), 315 (41.7) | - | 577 |
| **2.1b** | 288 (34.9) | - | 600 |
| **2.1c** | 283 (34.9), 316 (32.4) | - | 650 |
| **2.2a** | 273 (32.9), 306 (39.2) | - | 571 |
| **2.2b** | 280 (23.7), 320 (20.9) | - | 610 |
| **2.2c** | 284 (37.6), 317 (35.8) | - | 662 |
| **2.3a** | 270(15.2), 311(2.1) | 442 | - |
| **2.3b** | 270(16.0), 308(9.1) | 442 | - |
| **2.3c** | 270(14.8),319(6.6) | 442 | - |
| **2.4a** | 273 (38.2), 304 (38.0) | 442, 589 | 579 |
| **2.4b** | 273(38.1), 304(36.4) | 442 | 626 |
| **2.4c** | 272(71.2), 305(63.7) | 442, 649 | 620 |

The emission spectra of the heterometallic complexes were recorded both in solution and in the solid state. The emission spectra in the solid state evidenced the different coordination of zinc and copper heterometallic complexes. A gradual red shift by the addition of the different metal salts can be observed when going from Au/Zn to Au/CuCl and Au/Cu compounds exemplified in the Figure 2.8 for series **2.2**. This change in the luminescence properties of compound **2.2** (similar behavior was observed for **2.1**) is due to the different coordination of the metal and the expected modification in the aurophilic interactions that in solid state must take place together with additional Cu···Au interactions. When the zinc is coordinated to the pyridyl moieties, the three arms of the tripodal unit are expected to approach to each other and thus, gold atoms must be closer, being able to establish Au···Au contacts, as supported by DFT calculations (see below). On the other hand, two of the three gold atoms become closer when CuCl coordinates to the alkynyl group, and the aurophilic interactions are expected to be more effective. Finally, an approximation of the three gold atoms, increasing aurophilic/metallophilic interactions must be produced when

$[Cu(NCMe)_4]BF_4$ coordinates to all alkynyl moieties. Moreover, it can be observed that in the case of **2.4**, the addition of a metal salt gives rise to an emission in the solid state (remember that **2.4** does not present luminescent properties in the solid state). These statements are supported by the literature.[53,69,70] Unfortunately, several attempts to grow single crystals suitable for X-ray diffraction failed, mainly due to the low solubility of the complexes in common and volatile solvents and preclude to confirm these coordination modes.

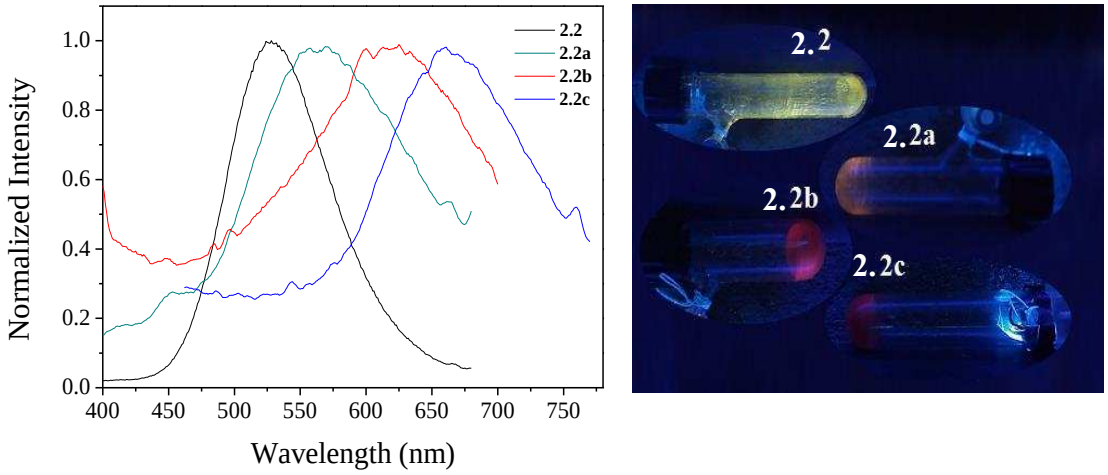


**Figure 2.8.** Normalized emission spectra in solid state of compounds **2.2**, **2.2a**, **2.2b** and **2.2c** (left); image of the solids observed under UV light (right).

### 2.2.4. Theoretical Calculations

DFT calculations were performed in collaboration with Dr. Cristiano Zonta, from Licini's group at Università di Padova, in order to have more evidence of the different coordination observed for $Zn^{2+}$ and $Cu^{+}$ in the heterometallic complexes and the observed changes in their photophysical properties. The different coordination modes calculated for series **2.1** complexes is depicted in Figure 2.9. DFT calculations do not predict aurophilic interactions for **2.1** with Au···Au distances of 5.5 Å. The coordination of $Zn^{2+}$ is expected to be produced through the pyridine moieties of TPA ligands, in agreement with NMR and IR data, allowing the three gold atoms to be closer with a distance of 3.9 Å that is equivalent for the three gold atoms. The $Cu^{+}$ heterometallic complexes were also minimized considering the two expected coordination modes (chloride coordination and $Cu^{+}$ coordination to two alkynyl moieties and $BF_4^{-}$ free counterion with $Cu^{+}$ coordination to three alkynyl moieties). In

the case of CuCl two gold arms gets closer and the chloride does not allow the coordination with the third arm. The distances between the two gold(I) atoms are higher than 4 Å, but short Cu···Au distances were observed. The use of $[Cu(NCMe)_4]BF_4$ favors the approach of the tripodal form of TPA where four short metal···metal (Au···Au and Cu···Au) interactions were observed.

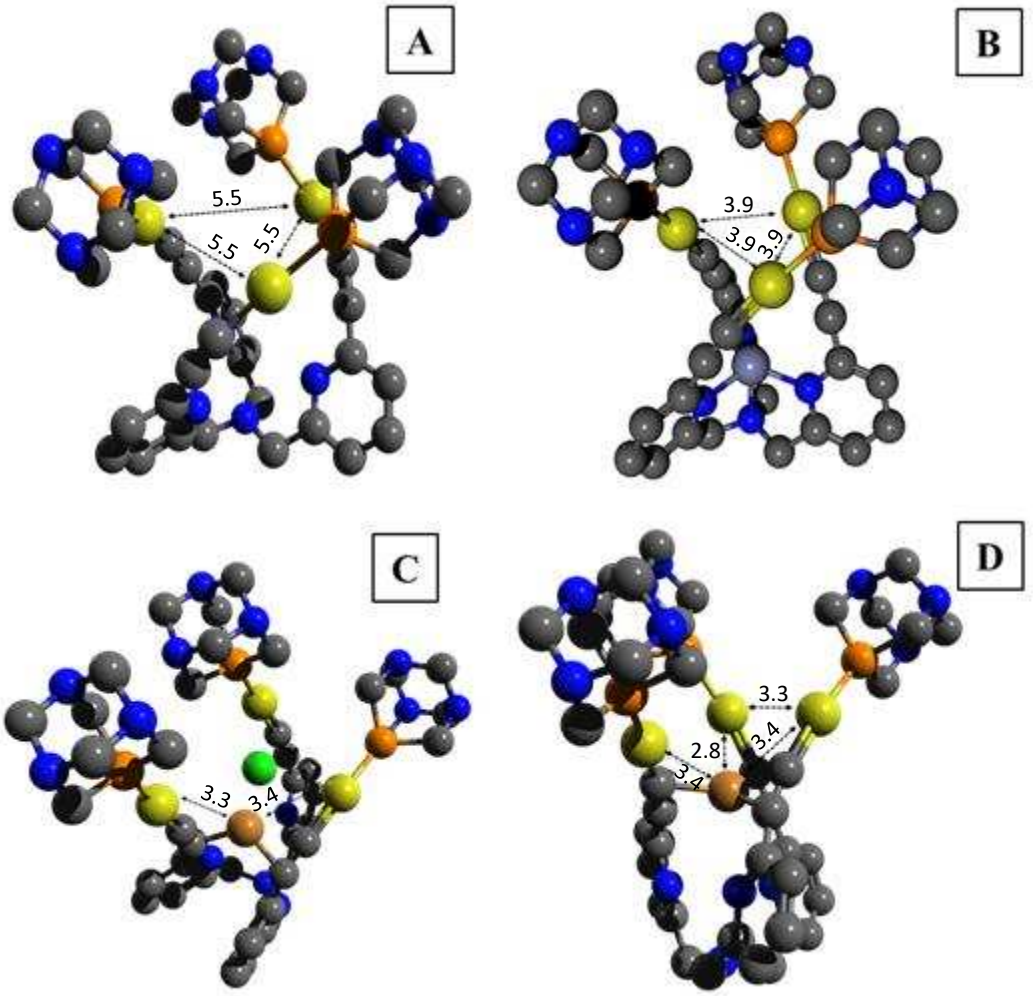


**Figure 2.9.** DFT structures for **2.1** (A) and the Zn structure, **2.1a** (B), CuCl, **2.1b** (C) and $CuBF_4$, **2.1c** (D). Intermetallic distances are indicated. Density functional theory (DFT) calculations were carried out by the use of the PBE0 functional. In the DFT energy calculations the def2-TZVPP basis set was used (including the def2-TZVPP pseudopotential for Au) and 6-31G(d,p) for all the other atoms.

The most important data is that the intermetallic distances obtained by DFT calculations (**2.1** > **2.1a** > **2.1b** > **2.1c**) are in agreement with the recorded emission red-shift when going from the homometallic gold complex to the zinc and copper heterometallic derivatives.

## 2.3. Conclusions

The synthesis of four different gold(I) complexes with open structure (**2.1-3**) and cage-like structure (**2.4**) can be successfully accomplished following different experimental procedures depending on important parameters such as: 1) the solubility of the phosphane and resulting complex in organic and in polar media; 2) open or closed geometry (and consequently, steric hindrance).

The formation of aggregates induces an enhancement of the emission where Au···Au interactions plays an important role in the resulting photophysical properties (mainly emission wavelength). Clear evidence of the aggregation process was observed in the increase of the baseline and the broadening of the absorption spectra.

The formation of heterometallic complexes using different salts ($Zn^{2+}$ and $Cu^{+}$) was accomplished with 1:1 stoichiometry predicted through absorption and emission titrations.

A detailed analysis of NMR, IR and emission spectroscopy evidenced the different coordination sites for the second metal added. These different coordination modes result in the capacity to tune the emission in the solid state making a red-shift in the order Au < Au/Zn < Au/Cu-Cl < Au/Cu-$BF_4$.

DFT calculations confirms the different positions adopted by the second metal and predict the intermetallic distances that are responsible for the red shift observed in the emission in solid state.

## 2.4. Experimental Section

### 2.4.1. General procedures

All manipulations have been performed under prepurified $N_2$ using standard Schlenk techniques. All solvents have been distilled from appropriated drying agents. Commercial reagents 1,3,5-triaza-7-phosphatricyclo[3.3.1.13.7]decane (PTA, Aldrich 97%), 3,7-diacetyl-1,3,7-triaza-5- phosphabicyclo[3.3.1]nonane (DAPTA, Aldrich 97%), copper (I) chloride (Aldrich, 99%), zinc nitrate hexahydrate (Aldrich, 98%). Literature methods have been used to prepare [AuCl($PR_3$)] ($PR_3$ = PTA,[71] DAPTA,[72] $PPh_3$,[73] [Au($PPh_3$)(acac)],[74] tetrakis(acetonitrile)copper(I) tetrafluoroborate.[75] Tris((6-ethylpyridin-2-yl)methyl)amine (**L**) was provided by Prof. Giulia Licini group, from Università di Padova, Italy.

### 2.4.2. Physical measurements

Infrared spectra have been recorded on a FT-IR 520 Nicolet Spectrophotometer. $^{1}H$ NMR (δ(TMS) = 0.0 ppm), $^{31}P\{^{1}H\}$ NMR (δ(85% $H_3PO_4$) = 0.0 ppm) spectra have been obtained on a Varian Mercury 400 and Bruker 400 (Universitat de Barcelona). ElectroSpray-Mass spectra (+) has been recorded on a Fisons VG Quatro spectrometer (Universitat de Barcelona). MALDI-TOF spectra (+) has been recorded on an Applied Biosystems 4700 Proteomics Analyzer. Absorption spectra have been recorded on a Varian Cary 100 Bio UV- spectrophotometer and emission spectra on a Horiba-Jobin-Yvon SPEX Nanolog spectrofluorimeter (Universitat de Barcelona).

### 2.4.3. Computational details

Theoretical calculations have been done in Dipartimento di Scienze Chimiche from Università di Padova by Dr. Cristiano Zonta. All compounds were minimized with the Gaussian16 program package.[76] at the DFT level of theory with a hybrid density functional PBE0.[77] The basis set consisted of a quasi-relativistic effective core potential basis set def2-TZVPPD for gold atoms and 6-31G(d,p) for all atoms.[78] Frequencies were calculated to verify the minima.

### 2.4.4. Synthesis and Characterization

**Synthesis N[Au(C≡C-Py)(PTA)]$_3$ (2.1)**

KOH (22 mg, 0.39 mmol) was added to a solution of tris((6-ethynylpyridine-2-yl)methyl)amine (35 mg, 0.096 mmol) in methanol (15 mL). After 30 min of stirring, a solution of [AuCl(PTA)] (122 mg, 0.31 mmol) in dichloromethane (15 mL) was

added. After 24 hours of stirring at room temperature, the solution was concentrated to ca. 15 mL and ether was added to precipitate a yellow solid. The product was isolated by filtration and dried under vacuum. Yield 63 % (86 mg).

$^{31}P\{^{1}H\}$ NMR (DMSO-$d_6$, ppm): -52.4. $^{1}H$ NMR (DMSO-$d_6$, ppm): 4.33 (s, 18H, N-$CH_2$-P), 4.36 (d, J = 12.4 Hz, 9H, N-$CH_2$-N), 4.52 (d, J = 12.4 Hz, 9H, N-$CH_2$-N), 7.13 (d, J = 7.6Hz, 3H, $H_{Py}$), 7.38 (d, J = 7.6Hz, 3H, $H_{Py}$), 7.64 (t, J = 8Hz, 3H, $H_{Py}$). IR (KBr, $cm^{-1}$): ν(C≡C): 2103; ν($CH_2$-P): 1450; ν(C-N): 1270. ESI-MS (+) m/z: 1422.274 ($[M+H]^{+}$, calc: 1422.263). Anal. Found (calcd for $C_{42}H_{51}Au_3N_{13}P_3 \cdot 4\ CH_2Cl_2$): C 31.36 (31.37); H 3.22 (3.38); N 10.28 (10.34).

**Synthesis N[Au(C≡C-Py)(DAPTA)]$_3$ (2.2)**

KOH (14 mg, 0.24 mmol) was added to a solution of tris((6-ethynylpyridine-2-yl)methyl)amine (20 mg, 0.056 mmol) in methanol (15 mL). After 30 min of stirring, a solution of [AuCl(DAPTA)] (80 mg, 0.17 mmol) in dichloromethane (15 mL) was added. After 24 hours of stirring at room temperature, the solution was concentrated to ca. 15 mL and ether was added to precipitate a yellow solid. The product was isolated by filtration and dried under vacuum. Yield: 40 % (37 mg).

$^{31}P\{^{1}H\}$ NMR (DMSO-$d_6$, ppm): 3.01. $^{1}H$ NMR (DMSO-$d_6$, ppm): 1.95 (s, 18H, COMe), 3.69 (s, 3H, N-$CH_2$-P), 3.96 (s, 6H, N-$CH_2$-P), 4.08 (d, J = 13.2 Hz, 3H, N-$CH_2$-N), 4.24 (m, 3H, N-$CH_2$-P), 4.62 (d, J = 12.8 Hz, 3H, N-$CH_2$-N), 4.80 (m, 3H, N-$CH_2$-P), 4.91 (d, J = 14.4 Hz, 3H, N-$CH_2$-N), 5.33 (m, 3H, N-$CH_2$-P), 5.51 (d, J = 13.2 Hz, 3H, N-$CH_2$-N), 7.17 (d, J = 7.6 Hz, 3H, HPy), 7.41 (d, J = 7.6 Hz, 3H, HPy), 7.66 (t, J = 7.6 Hz, 3H, HPy). IR (KBr, $cm^{-1}$): ν(C≡C): 2106; ν(C=O): 1636; ν(CH2-P): 1442; ν(C-N): 1234. ESI-MS (+) m/z: 557.098 (($[M+3H + CH_3OH]^{3+}$, calc: 557.457). Anal. Found (calcd for $C_{51}H_{63}Au_3N_{13}O_6P_3 \cdot 5CH_2Cl_2$): C 32.23 (32.61); H 3.45 (3.57); N 8.93 (8.83).

**Synthesis N[Au(C≡C-Py)($PPh_3$)]$_3$ (2.3)**

A dichloromethane solution (4 mL) of [Au(acac)$PPh_3$] (55 mg, 0.10 mmol) was added dropwise to a dichloromethane solution (6 mL) of tris((6-ethynylpyridine-2-yl)methyl)amine (19 mg, 0.03 mmol). After 2 h of stirring at room temperature, the solution was concentrated under vacuum to a final volume of 3 ml and hexane was slowly added. During all the manipulations, the solution was protected from the light

in order to avoid decomposition. The white suspension was separated from brown solid and it was dried under vacuum to give a yellow solid. Yield: 60% (31 mg).

$^{31}P\{^{1}H\}$ NMR ($CDCl_3$, ppm): 29.1. $^{1}H$ NMR ($CDCl_3$, ppm): 7.67 (9H, dd, J = 12.0, 7.6 Hz,), 7.49 (45H, m), 3.83 (6H, s). IR (KBr, $cm^{-1}$): ν(C≡C): 2112. ESI-MS (+) m/z: 1737.300 ($[M+H]^{+}$, calc: 1737.302). Anal. Found (calcd for $C_{78}H_{60}Au_3N_4P_3 \cdot 3\,CH_2Cl_2$): C 48.28 (48.84); H 3.06 (3.34); N 2.60 (2.81).

**Synthesis of [N[Au(C≡C-Py)]$_3$(triphos)] (2.4)**

KOH (46 mg, 0.82 mmol) was added to a solution of tris((6-ethynylpyridine-2-yl)methyl)amine (76 mg, 0.21 mmol) in methanol (20 mL). After 30 min of stirring, a solution of [$(AuCl)_3$(triphos)] (278 mg, 0.21 mmol) in dichloromethane (20 mL) was added. After 5 hours of stirring at room temperature, the solution was concentrated to ca. 20 mL and hexane was added to precipitate an orange solid. The product was isolated by filtration and dried under vacuum. Yield: 54 % (178 mg).

$^{31}P\{^{1}H\}$ NMR ($CDCl_3$, ppm): 16.9. $^{1}H$ NMR ($CDCl_3$, ppm): 0.88 (s, 3H, $CH_3$-C-), 3.37 (d, J = 11.6 Hz, 6H, C-$CH_2$-P), 7.48 (m, 18H, P-Ph), 7.79 (m, 12H, P-Ph). IR (KBr, $cm^{-1}$): ν(C≡C): 2113; ν($PPh_2$): 1435, 1098. ESI-MS (+) m/z: 1592.29 ($[M+NH_4]^{+}$, calc: 1592.29). Anal. Found (calcd for $C_{65}H_{54}Au_3N_4P_3 \cdot 5\,CH_2Cl_2$): C 41.84 (42.05); H 3.24 (3.23); N 2.69 (2.80).

**Synthesis of [N[Au(C≡C-Py)(PTA)]$_3$Zn]$(NO_3)_2$ (2.1a)**

Solid $Zn(NO_3)_2$ (2.8 mg, $9.42 \cdot 10^{-3}$ mmol) was added to a solution of **2.1** (5 mg, $3.51 \cdot 10^{-3}$ mmol) in MeOH (10 mL). The solution was stirred for 2h at room temperature and then evaporated to dryness under vacuum to yield an orange solid that was washed with methanol. Yield: 65% (5 mg).

$^{31}P\{^{1}H\}$ NMR (DMSO-$d_6$ ppm): -52.2. $^{1}H$ NMR (DMSO $d_6$ ppm): 4.33 (s, 18H, N-$CH_2$-P), 4.36 (d, J = 12.4 Hz, 9H, N-$CH_2$-N), 4.52 (d, J = 12.4 Hz, 9H, N-$CH_2$-N), 7.13 (d, J = 7.6 Hz, 3H, $H_{Py}$), 7.38 (d, J = 7.6 Hz, 3H, $H_{Py}$), 7.64 (t, J = 8 Hz, 3H, $H_{Py}$). IR (KBr, $cm^{-1}$): ν(C≡C): 2104; ν($CH_2$-P): 1450; ν($NO^{3-}$): 1383; ν(C-N): 1270. MALDI-TOF m/z: 1565.1 ($[[M + H_2O]+NO_3]^{+}$, calc.: 1565.1). Anal. Found (calcd for $C_{42}H_{51}Au_3N_{15}O_6P_3Zn \cdot 5H_2O$): C 30.05 (29.65); H 3.16 (3.61); N 12.35 (12.35).

**Synthesis of [N[Au(C≡C-Py)(PTA)]$_3$CuCl] (2.1b)**

Solid CuCl (0.51 mg, 0.005 mmol) was added to a solution of **2.1** (5 mg, 0.004 mmol) in $CH_3CN$ (10 mL). The solution was stirred during 2h at room temperature and then evaporated to dryness under vacuum to yield an orange solid that was washed with acetonitrile. Yield: 80% (5 mg).

$^{31}P\{^{1}H\}$ NMR (DMSO-$d_6$ ppm): -52.2. $^{1}H$ NMR (DMSO-$d_6$ ppm): 4.33 (s, 18H, N-$CH_2$-P), 4.36 (d, J = 12.4 Hz, 9H, N-$CH_2$-N), 4.52 (d, J = 12.4 Hz, 9H, N-$CH_2$-N), 7.44 (d, J = 8 Hz, 3H, $H_{Py}$), 7.67 (d, J = 8 Hz, 3H, $H_{Py}$), 7.90 (t, J = 7.6 Hz, 3H, $H_{Py}$). IR (KBr, $cm^{-1}$): ν(C≡C): 2104, 2055; ν($CH_2$-P): 1450; ν(C-N): 1270. MALDI-TOF m/z: 1561.1 ([[M + H]+$CH_3CN$]$^{+}$, calc.: 1561.1). Anal. Found (calcd for $C_{42}H_{51}Au_3ClCuN_{13}P_3 \cdot 4\ CH_2Cl_2$): C 29.47 (29.70); H 2.97 (3.20); N 9.56 (9.79).

**Synthesis of [N[Au(C≡C-Py)(PTA)]$_3$Cu]$BF_4$ (2.1c)**

Similar procedure was used in the synthesis of **2.1c** with respect to **2.1b** but using $[Cu(NCMe)_4]BF_4$ instead of CuCl. Yield: 75% (5 mg).

$^{31}P\{^{1}H\}$ NMR (DMSO-$d_6$ ppm): -52.2. $^{1}H$ NMR (DMSO-$d_6$ ppm): 4.33 (s, 18H, N-$CH_2$-P), 4.36 (d, J = 12.4 Hz, 9H, N-$CH_2$-N), 4.52 (d, J = 12.4 Hz, 9H, N-$CH_2$-N), 7.44 (d, J = 8 Hz, 3H, $H_{Py}$), 7.67 (d, J = 8 Hz, 3H, $H_{Py}$), 7.90 (t, J = 7.6 Hz, 3H, $H_{Py}$). IR (KBr, $cm^{-1}$): ν(C≡C): 2099, 2059; ν($CH_2$-P): 1450; ν(C-N): 1270. MALDI-TOF m/z: 1592.9 ([M + DMSO]$^{+}$, calc.: 1562.2). Anal. Found (calcd for $C_{42}H_{51}Au_3BCuF_4N_{13}P_3 \cdot 3\ CH_2Cl_2$): C 29.88 (29.59); H 3.10 (3.14); N 9.60 (9.90).

**Synthesis of [N[Au(C≡C-Py)(DAPTA)]$_3$Zn]$(NO_3)_2$ (2.2a)**

Solid $Zn(NO_3)_2 \cdot 6H_2O$ (1.3 mg, $4.37 \cdot 10^{-3}$ mmol) was added to a solution of **2.2** (4 mg, $2.44 \cdot 10^{-3}$ mmol) in MeOH (10 mL). The solution was stirred for 2h at room temperature and then evaporated to dryness under vacuum to yield a yellow solid that was washed with methanol. Yield: 55% (3 mg).

$^{31}P\{^{1}H\}$ NMR (DMSO-$d_6$ ppm): 3.01. $^{1}H$ NMR (DMSO-$d_6$ ppm): 1.95 (s, 18H, COMe), 3.70 (d, J = 15.6 Hz, 3H, N-$CH_2$-P), 3.99 (s, 6H, N-$CH_2$-P), 4.10 (d, J = 14 Hz, 3H, N-$CH_2$-N), 4.27 (s, 3H, N-$CH_2$-P), 4.61 (d, J = 13.2 Hz, 3H, N-$CH_2$-N), 4.79 (m, 3H, N-$CH_2$-P), 4.91 (d, J = 14 Hz, 3H, N-$CH_2$-N), 5.36 (d, J = 13.6 Hz, 3H, N-$CH_2$-P), 5.51 (d, J = 14 Hz, 3H, N-$CH_2$-N), 7.28 (d, J = 8 Hz, 3H, $H_{Py}$), 7.40 (d, J = 7.6 Hz, 3H,

$H_{Py}$), 7.73 (t, J = 7.6 Hz, 3H, $H_{Py}$). IR (KBr, $cm^{-1}$): ν(C≡C): 2103; ν(C=O): 1636; ν($CH_2$-P): 1440; ν($NO^{3-}$)1383; ν(C-N): 1232. MALDI-TOF m/z: 926.2 ([M + $CH_2Cl_2$ + $2H_2O$ + $CH_3OH$]$^{2+}$, calc.: 926.6). Anal. Found (calcd for $C_{51}H_{63}Au_3N_{15}O_{12}P_3Zn\cdot 5\ H_2O$): C 31.57 (31.95); H 4.01 (3.84); N 10.62 (10.96).

**Synthesis of [N[Au(C≡C-Py)(DAPTA)]$_3$CuCl] (2.2b)**

Solid CuCl (0.43 mg, $4.34\cdot 10^{-3}$ mmol) was added to a solution of **2.2** (5.3 mg, $3.24\cdot 10^{-3}$ mmol) in $CH_3CN$ (10 mL). The solution was stirred for 2h at room temperature and then evaporated to dryness under vacuum to yield an orange solid that was washed with acetonitrile. Yield: 85% (5 mg).

$^{31}P\{^{1}H\}$ NMR (DMSO-$d_6$ ppm): 3.01. $^{1}H$ NMR (DMSO-$d_6$ ppm): 1.97 (s, 18H, COMe), 3.71 (d, J = 14 Hz, 3H, N-$CH_2$-P), 3.97 (s, 6H, N-$CH_2$-P), 4.10 (d, J = 13.6 Hz, 3H, N-$CH_2$-N), 4.24 (d, J = 12.4 Hz, 3H, N.$CH_2$-P), 4.34 (s, 6H, N-$CH_2$-Py), 4.62 (d, J = 13.6 Hz, 3H, N-$CH_2$-N), 4.81 (m, 3H, N-$CH_2$-P), 4.92 (d, J = 14 Hz, 3H, N-$CH_2$-N), 5.34 (m, 3H, N-$CH_2$-P), 5.52 (d, J = 13.2 Hz, 3H, N-$CH_2$-N), 7.44 (d, J = 7.6 Hz, 3H, $H_{Py}$), 7.67 (d, J = 7.2 Hz, 3H, $H_{Py}$), 7.90 (t, J = 7.6 Hz 3H, $H_{Py}$). IR (KBr, $cm^{-1}$): ν(C≡C): 2103, 2060; ν(C=O): 1628; ν($CH_2$-P): 1444; ν(C-N): 1232. MALDI-TOF m/z: 1790.9 ([M + H + $3H_2O$]$^{+}$, calc.: 1790.3). Anal. Found (calcd for $C_{51}H_{63}Au_3ClCuN_{13}O_6P_3\cdot 3\ CH_2Cl_2\cdot 2\ H_2O$): C 31.65 (31.99); H 3.47 (3.63); N 8.65 (8.98).

**Synthesis of [N[Au(C≡C-Py)(DAPTA)]$_3$Cu][$BF_4$] (2.2c)**

Similar procedure was used in the synthesis of **2.2c** with respect to **2.2b** but using $[Cu(NCMe)_4]BF_4$ instead of CuCl. Yield: 74% (5 mg).

$^{31}P\{^{1}H\}$ NMR (DMSO-$d_6$ ppm): 3.01. $^{1}H$ NMR (DMSO-$d_6$ ppm): 1.97 (s, 18H, COMe), 3.70 (d, J = 15.2 Hz, 3H, N-$CH_2$-P), 3.96 (s, 6H, N-$CH_2$-P), 4.10 (d, J = 14 Hz, 3H, N-$CH_2$-N), 4.24 (d, J = 14 Hz, 3H, N-$CH_2$-P), 4.34 (s, 6H, N-$CH_2$-Py), 4.62 (d, J = 14 Hz, 3H, N-$CH_2$-N), 4.79 (m, 3H, N-$CH_2$-P), 4.92 (d, J = 13.6 Hz, 3H, N-$CH_2$-N), 5.33 (m, 3H, N-$CH_2$-P), 5.53 (d, J = 13.2 Hz, 3H, N-$CH_2$-N), 7.44 (d, J = 7.6 Hz, 3H, $H_{Py}$), 7.67 (d, J = 7.6 Hz, 3H, $H_{Py}$), 7.90 (t, J = 7.6 Hz, 3H, $H_{Py}$). IR (KBr, $cm^{-1}$): ν(C≡C): 2098, 2055; ν(C=O): 1637; ν($CH_2$-P): 1439; ν(C-N): 1232. Anal. Found (calcd for $C_{51}H_{63}Au_3BCuF_4N_{13}O_6P_3\cdot 2CH_2Cl_2\cdot H_2O$): C 32.02 (32.21); H 3.26 (3.52); N 9.12 (9.21).

**Synthesis of [N[Au(C≡C-Py)(PPh$_3$)]$_3$Zn](NO$_3$)$_2$ (2.3a)**

Solid $Zn(NO_3)_2 \cdot 6H_2O$ (1.71 mg, $5.76 \cdot 10^{-3}$ mmol) was added to a solution of **3** (5.0 mg, $2.88 \cdot 10^{-3}$ mmol) in MeOH (10 mL). The solution was stirred for 2h at room temperature and then evaporated to dryness under vacuum to yield a yellow solid that was washed with methanol. Yield: 55% (3 mg).

$^{31}P\{^{1}H\}$ NMR ($CD_3CN$ ppm): 33.0. $^{1}H$ NMR ($CD_3CN$ ppm): 3.75 (s, 6H, $CH_2$), 7.42 (d, J = 8Hz, 3H, Py), 7.62 (m, 45H, $PPh_3$), 7.78 (d, J = 8 Hz, 3H, Py), 7.94 (t, J = 8 Hz, 3H, Py). IR (KBr, $cm^{-1}$): ν(C≡C): 2103; ν(C=O): 1636; ν($CH_2$-P): 1440; ν($NO^{3-}$)1383; ν(C-N): 1232. Anal. Found (calcd for $C_{78}H_{60}Au_3N_6O_6P_3Zn \cdot 5H_2O$): C 46.70 (46.46); H 3.75 (3.50); N 4.25 (4.17).

**Synthesis of [N[Au(C≡C-Py)(PPh$_3$)]$_3$CuCl] (2.3b)**

Solid CuCl (0.34 mg, $3.45 \cdot 10^{-3}$ mmol) was added to a solution of **2.3** (6 mg, $3.45 \cdot 10^{-3}$ mmol) in $CH_3CN$ (10 mL). The solution was stirred during 2h at room temperature and then evaporated to dryness under vacuum to yield an orange solid that was washed with acetonitrile. Yield: 50% (3 mg).

$^{31}P\{^{1}H\}$ NMR ($CD_3CN$ ppm): 33.0. $^{1}H$ NMR ($CD_3CN$ ppm): 3.27 (s, 6H, $CH_2$), 7.29 (d, J = 7.6 Hz, 3H, Py), 7.49 (m, 45H, $PPh_3$), 7.64 (d, J = 6.8 Hz, 3H, Py), 7.76 (t, J = 8 Hz, 3H, Py). IR (KBr, $cm^{-1}$): ν(C≡C): 2100, 2080; ν($CH_2$-P): 1453; ν(C-N): 1265. Anal. Found (calcd for $C_{78}H_{60}Au_3CuClN_4P_3 \cdot 3\ CH_2Cl_2$): C 46.73 (46.53); H 3.33 (3.18); N 2.86 (2.68).

**Synthesis of [N[Au(C≡C-Py)(PPh$_3$)]$_3$Cu]BF$_4$ (2.3c)**

Similar procedure was used in the synthesis of **2.3c** with respect to **2.3b** but using $[Cu(NCMe)_4]BF_4$ instead of CuCl. Yield: 75% (3 mg).

$^{31}P\{^{1}H\}$ NMR ($CD_3CN$ ppm): 33.0. $^{1}H$ NMR ($CD_3CN$ ppm): 4.23 (s, 6H, $CH_2$), 7.30 (d, J = 7.6 Hz, 3H, Py), 7.39 (d, J = 7.6 Hz, 3H, Py), 7.52 (m, 45H, $PPh_3$), 7.74 (t, J = 7.6 Hz, 3H, Py). IR (KBr, $cm^{-1}$): ν(C≡C): 2099, 2059; ν($CH_2$-P): 1450; ν(C-N): 1270. Anal. Found (calcd for $C_{78}H_{60}Au_3CuBF_4N_4P_3 \cdot 4\ CH_2Cl_2$): C 44.34 (44.22); H 3.45 (3.08); N 2.7 (2.52).

**Synthesis of $[N[Au(C\equiv C\text{-}Py)]_3(triphos)Zn](NO_3)_2$ (2.4a)**

KOH (16.1 mg, 0.3 mmol) was added to a solution of tris((6-ethynylpyridine-2-yl)methyl)amine (20 mg, 0.055 mmol) in methanol (15 mL). After 30 min of stirring a solution of $(AuCl)_3$(triphos) (75 mg, 0.057 mmol) and $Zn(NO_3)_2\cdot 6H_2O$ (33 mg, 0.11 mmol) in a mixture of methanol/dichloromethane (1:2) (15 mL) was added. After 5 hours of stirring at room temperature the solution was concentrated to ca. 15 mL and hexane was added to precipitate an orange solid. The product was isolated by filtration and dried under vacuum. Yield 85% (82 mg).

$^{31}P\{^{1}H\}$ NMR (DMSO-$d_6$, ppm): 17.4. $^{1}H$ NMR (DMSO-$d_6$, ppm): 7.1-7.9 (m, 3H, P-Ph). IR (KBr, $cm^{-1}$): ν(C≡C): 2108; ν($PPh_2$): 1432, 1094**.** MALDI-TOF m/z: 819.0 ($M^{2+}$, calc.: 819.0). Anal. Found (calcd for $C_{65}H_{54}Au_3N_6O_6P_3Zn\cdot 5\ H_2O$): C 41.85 (42.10); H 3.26 (3.48); N 4.32 (4.53).

**Synthesis of $[N[Au(C\equiv C\text{-}Py)]_3(triphos)CuCl]$ (2.4b)**

KOH (11.1 mg, 0.2 mmol) was added to a solution of tris((6-ethynylpyridine-2-yl)methyl)amine (19.5 mg, 0.054 mmol) in methanol (15 mL). After 30 min of stirring, a solution of $(AuCl)_3$(triphos) (73.6 mg, 0.056 mmol) and CuCl (5.9 mg, 0.059 mmol) in a mixture of acetonitrile/dichloromethane (1:2) (15 mL) was added. After 5 hours of stirring at room temperature the solution was concentrated to ca. 15 mL and hexane was added to precipitate an orange solid. The product was isolated by filtration and dried under vacuum. Yield 75 % (68 mg).

$^{31}P\{^{1}H\}$ NMR (DMSO-$d_6$, ppm): 17.4. $^{1}H$ NMR (DMSO-$d_6$, ppm): 7.1-7.9 (m, 3H, P-Ph). IR (KBr, $cm^{-1}$): ν(C≡C): 2108, 1957; ν($PPh_2$): 1432, 1098. MALDI-TOF m/z: 1673.1 ($[M + H]^{+}$, calc.: 1673.1). Anal. Found (calcd for $C_{65}H_{54}Au_3CuClN_4P_3\cdot 3\ CH_2Cl_2\cdot 2\ H_2O$): C 41.75 (41.57); H 3.26 (3.28); N 2.69 (2.85).

**Synthesis of $[N[Au(C\equiv C\text{-}Py)]_3(triphos)Cu]BF_4$ (2.4c)**

Similar procedure was used in the synthesis of **2.4c** with respect to **2.4b** but using $[Cu(NCMe)_4]BF_4$ instead of CuCl. Yield 80 % (74 mg).

$^{31}P\{^{1}H\}$ NMR (DMSO-$d_6$, ppm): 17.4. $^{1}H$ NMR (DMSO-$d_6$, ppm): 7.1-7.9 (m, 3H, P-Ph). IR (KBr, $cm^{-1}$): ν(C≡C): 2113, 1957; ν($PPh_2$): 1436, 1098. MALDI-TOF m/z: 1637.0 ($M^{+}$, calc.: 1637.2). Anal. Found (calcd for $C_{65}H_{54}Au_3CuBF_4N_4P_3\cdot 2\ CH_2Cl_2$): C 42.1 (42.46); H 3.36 (3.08); N 3.1 (2.96).

## 2.5. References


1. Pietschnig, R. Smart inorganic polymers: synthesis, properties, and emerging applications in materials and life science. Wiley-VCH, **2019**, ISBN: 9783527819140.
2. Oliveira, J., Correia, V., Castro, H., Martins, P. and Lanceros-Mendez, S. Addit. Manuf. **2018**, 21, 269–283.
3. Guo, F. and Guo, Z. RSC Adv. **2016**, 6, 36623–36641.
4. Hou, X., Ke, C., Bruns, C. J., McGonigal, P. R., Pettman, R. B. and Stoddart, F. Nat. Commun. **2015**, 6, 1–9.
5. Ji, X., Shi, B, Wang, H., Xia, D., Jie, K., Wu, Z. L. and Huang, F. Adv. Mater. **2015**, 27, 8062–8066.
6. Canary, J. W., Allen, C. S., Castagnetto, J. M. and Wang, Y. J. Am. Chem. Soc. **1995**, 117, 8484–8485.
7. Zahn, S., Das, D. and Canary, J. W. Inorg. Chem. **2006**, 45, 6056–6063.
8. Badetti, E., Wurst, K., Licini, G. and Zonta, C. Chem. - A Eur. J. **2016**, 22, 6515–6518.
9. Berardozzi, R., Badetti, E., Carmo dos Santos, N. A., Wurst, K., Licini, G., Pescitelli, G., Zonta, C. and Di Bari, L. Chem. Commun. **2016**, 52, 8428–8431.
10. Canary, J. W., Mortezaei, S. and Liang, J. Chem. Commun. **2010**, 46, 5850–5860.
11. Mortezaei, S., Catarineu, N. R. and Canary, J. W. J. Am. Chem. Soc. **2012**, 134, 8054–8057.
12. You, L., Berman, J. S. and Anslyn, E. V. Nat. Chem. **2011**, 3, 943–948.
13. You, L., Pescitelli, G., Anslyn, E. V. and Di Bari, L. J. Am. Chem. Soc. **2012**, 134, 7117–7125.
14. Joyce, L. A., Maynor, M. S., Dragna, J. M., da Cruz, G. M., Lynch, V. M., Canary, J. W. and Anslyn, E. V. J. Am. Chem. Soc. **2011**, 133, 13746–13752.

15. Zhou, Y., Ren, Y., Zhang, L., You, L., Yuan, Y. and Anslyn, E. V. Tetrahedron **2015**, 71, 3515–3521.

16. Lin, C. Y., Giuliano, M. W., Ellis, B. D., Miller, S. J. and Anslyn, E. V. Chem. Sci. **2016**, 7, 4085–4090.

17. Scaramuzzo, F. A., Licini, G. and Zonta, C. Chem. - A Eur. J. **2013**, 19, 16809–16813.

18. Chufán, E. E., Mondal, B., Gandhi, T., Kim, E., Rubie, N. D., Moënne-Loccoz, P. and Karlin, K. Inorg. Chem. **2007**, 46, 6382–6394.

19. Vardhaman, A. K., Barman, P., Kumar, S., Sastri, C. V., Kumar, D. and Visser, S. P. Angew. Chemie - Int. Ed. **2013**, 52, 12288–12292.

20. Chen, K., Costas, M., Kim, J., Tipton, A. K. and Que, L. J. Am. Chem. Soc. **2002**, 124, 3026–3035.

21. Borrell, M. and Costas, M. J. Am. Chem. Soc. **2017**, 139, 12821–12829.

22. Yamaguchi, M., Kousaka, H., Izawa, S., Ichii, Y., Kumano, T., Masui, D. and Yamagishi, T. Inorg. Chem. **2006**, 45, 8342–8354.

23. Hitomi, Y., Ando, A., Matsui, H, Ito, T., Tanaka, T., Ogo, S. and Funabiki, T. Inorg. Chem. **2005**, 44, 3473–3478.

24. Chishiro, T., Shimazaki, Y., Tani, F., Tachi, Y., Naruta, Y., Karasawa, S., Hayami, S. and Maeda, Y. Angew. Chem. Int. Ed. **2003**, 115, 2894–2897.

25. Maiti, D., Woertink, J. S., Ghiladi, R. A., Solomon, E. I. and Karlin, K. D. Inorg. Chem. **2009**, 48, 8342–8356.

26. Yatabe, T., Kikkawa, M., Matsumoto, T., Nakai, H., Kaneko, K. and Ogo, S. Dalton Trans. **2014**, 43, 3063–3071.

27. Fillol, J. L., Codolà, Z., Garcia-Bosch, I., Gómez, L., Pla, J. J. and Costas, M. Nat. Chem. **2011**, 3, 807–813.

28. Humphreys, K. J., Karlin, K. D. and Rokita, S. E. J. Am. Chem. Soc. **2002**, 124, 6009–6019.

29. Mancin, F. and Tecilla, P. New J. Chem. **2007**, 31, 800–817.

30. Zhu, L., dos Santos, O., Koo, C. W., Rybstein, M., Pape, L. and Canary, J. W.. Inorg. Chem. **2003**, 42, 7912–7920.

31. Feng, G., Mareque-Rivas, J. C., Torres Martín De Rosales, R. and Williams, N. H. J. Am. Chem. Soc. **2005**, 127, 13470–13471.

32. Natali, M., Badetti, E., Deponti, E., Gamberoni, M., Scaramuzzo, F. A., Sartorel, A. and Zonta, C. Dalton Trans. **2016**, 45, 14764–14773.

33. Huang, M., Yang, T., Paretsky, J. D., Berry, J. F. and Schomaker, J. M. J. Am. Chem. Soc. **2017**, 139, 17376–17386 .

34. Pintauer, T. and Matyjaszewski, K. Coord. Chem. Rev. **2005**, 249, 1155–1184.

35. Tsarevsky, N. V., Braunecker, W. A., Vacca, A., Gans, P. and Matyjaszewski, K. Macromol. Symp. **2007**, 248, 60–70.

36. Matyjaszewski, K. Macromolecules, **2012**, 45, 4015–4039.

37. Carmo dos Santos, N. A., Lorandi, F., Badetti, E., Wurst, K., Isse, A. A., Gennaro, A., Licini, G. and Zonta, C. Polymer. **2017**, 128, 169–176.

38. Ribelli, T. G., Fantin, M., Daran, J. C., Auf¡gustine, K. F., Poli, R. and Matyjaszewski, K. J. Am. Chem. Soc. **2018**, 140, 1525–1534.

39. Enciso, A. E., Lorandi, F., Mehmood, A., Fantin, M., Szczepaniak, G., Janesko, B. G. and Matyjaszewski, K. Angew. Chem. Int. Ed. **2020**, 132, 15020–15030.

40. Min, K. S., Dipasquale, A., Rheingold, A. L. and Miller, J. S. Inorg. Chem. **2007**,46 1048–1050.

41. García-López, V., Waerenborgh, J. C., Vieira, B. J. C., Clemente-León, M. and Coronado, E. Dalton Trans. **2018**, 47, 9156–9163.

42. Lima, J. C. and Rodríguez, L. Chem. Soc. Rev. **2011**, 40, 5442–5456.

43. Aguiló, E., Moro, A. J., Outis, M., Pina, J., Sarmento, D., Seixas de Melo, J. S., Rodríguez, L. and Lima, J.C. Inorg. Chem. **2018**, 57, 13423–13430.

44. Catalano, V. J., López-De-Luzuriaga, J. M., Monge, M., Olmos, M. E. and Pascual, D. Dalton Trans. **2014**, 43, 16486–16497.

45. Fernández, E. J., López de Luzuriaga, J. M., Monge, M., Rodríguez, M. A., Crespo, O., Concepción Gimeno, M., Laguna, A. and Jones, P. G. Chem. - A Eur. J. **2000**, 6, 636–644.

46. Catalano, V. J., Bennett, B. L., Kar, H. M. and Noll, B. C. J. Am. Chem. Soc. **1999**, 121, 10235–10236.

47. López-de-Luzuriaga, J. M., Monge, M., Moreno, S., Olmos, M. E. and Rodríguez-Castillo, M. Angew. Chemie - Int. Ed. **2021**, 60, 640–644.

48. Hupf, E., Kather, R., Vogt, M., Lork, E., Mebs, S. and Beckmann, J. Inorg. Chem. **2016**, 55, 11513–11521.

49. Fernández, E. J., Laguna, A., López de Luzuriaga, J. M., Monge, M., Nema, M., Olmos, M. E., Pérez, J. and Silvestru, C. Chem. Commun. **2007**, 28, 571–573.

50. Cabeza, J. A., Fernández-Colinas, J. M., García-Álvarez, P. and Polo, D. Inorg. Chem. **2012**, 51, 3896–3903.

51. Chen, K., Strasser, C. E., Schmitt, J. C., Shearer, J. and Catalano, V. J. Inorg. Chem. **2012**, 51, 1207–1209.

52. Catalano, V. J., Moore, A. L., Shearer, J. and Kim, J. Inorg. Chem. **2009**, 48, 11362–11375.

53. Shakirova, J. R., Grachova, E. V., Gurzhity, V. V., Thangaraj, S. K., Janis, J., Melkinov, A. S., Karttunen, A. J., Tunik, S. P. and Koshevoy, I. O. Angew. Chem. In. Ed. **2018**, 130, 14350–14354.

54. Ibáñez, S. and Peris, E. Chem. - A Eur. J. **2019**, 25, 8254–8258.

55. Svahn, N., Moro, A. J., Roma Rodrigues, C., Puttreddy, R., Rissanen, K., Baptista, P. V., Fernandes, A. R., Lima, J. C. and Rodríguez, L. Chem. - A Eur. J. **2018**, 24, 14654–14667.

56. Pinto, A., Svahn, N., Lima, J. C. and Rodríguez, L. Dalton Trans. **2017**, 46, 11125–11139.

57. Gavara, R., Lima, J. C. and Rodríguez, L. Photochem. Photobiol. Sci. **2016**, 15, 635–643.

58. Camara, V., Masciocchi, N., Gil-Rubio, J. and Vicente, J. Chem. - A Eur. J. **2014**, 20, 1389–1402.

59. Cámara, V., Barquero, N., Bautista, D., Gil-Rubio, J. and Vicente, J. Inorg. Chem. **2015**, 54, 6147–6156.

60. Aguiló, E., Moro, A. J., Gavara, R., Alfonso, I., Pérez, Y., Zaccaria, F., Fonseca Guerra, C., Malfois, M., Baucells, C., Ferrer, M., Lima, J. C. and Rodríguez, L. Inorg. Chem. **2018**, 57, 1017–1028.

61. Blanco, M. C., Cámara, J., Concepción Gimeno, M., Jones, P. G., Laguna, A., López de Luzuriaga, J. M., Olmos, M. E. and Villacampa, M. D. Organometallics **2012**, 31, 2597–2605.

62. Manbeck, G. F., Brennessel, W. W., Stockland, R. A. and Eisenberg, R. J. Am. Chem. Soc. **2010**, 132, 12307–12318.

63. De La Riva, H., Niewhuyzen, M., Fierro, C. M., Raithby, P. R., Male, L. and Lagunas, M. C. Inorg. Chem. **2006**, 45, 1418–1420.

64. Dau, T. M., Shakirova, J. R., Doménech, A., Jänis, J., Haukka, M., Grachova, E. V., Pakkanen, T. A., Tunik, S. P. and Koshevoy, I. O. Eur. J. Inorg. Chem. **2013**, 4976–4983.

65. Shakirova, J. R., Grachova, E. V., Melnikov, A. S., Gurzhiy, V. V., Tunik, S. P., Haukka, M., Pakkanen, T. A. and Koshevoy, I. O. Organometallics, **2013**, 32, 4061–4069.

66. Liang, J., Zhang, J., Zhu, L., Duarandin, A., Young, V. G., Geacintov, N. and Canary, J. W. Inorg. Chem. **2009**, 48, 11196–11208.

67. Zahn, S. and Canary, J. W. J. Am. Chem. Soc. **2002**, 124, 9204–9211.

68. Belyaev, A., Dau, T. M., Jänis, J., Grachova, E. V., Tunik, S., P. and Koshevoy, I. O. Organometallics **2016**, 35, 3763–3774.

69. Hau, F. K. W., He, X., Lam, W. H. and Yam, V. W. W. Chem. Commun. **2011**, 47, 8778–8780.

70. Rodríguez, L., Lodeiro, C., Lima, J. C. and Crehuet, R. Inorg. Chem. **2008**, 47, 4952–4962.

71. Assefa, Z., McBurnett, B. G., Staples, R. J. and Fackler, J. P. Inorg. Chem. **1995**, 34, 75–83.

72. Vergara, E., Miranda, S., Mohr, F., Cerrada, E., Tiekink, E. R. T., Romero, P., Mendía, A. and Laguna, M. Eur. J. Inorg. Chem. **2007**, 2926–2933.

73. Kowala, C. and Swan, J. M. Aust. J. Chem. **1966**, 19, 547–554.

74. Adrian, M. S. and Fackler, J. P. Inorg. Synth,. **1998**, 32, 172–177.

75. G. J. Kubas, B. Monzyk and A. L. Crumbliss, Inorg. Synth., 1979, **19**, 90–92.

76. M. J. Frisch, G. W. Trucks, H. B. Schlegel, G. E. Scuseria, M. A. Robb, J. R. Cheeseman, G. Scalmani, V. Barone, G. A. Petersson, H. Nakatsuji, X. Li, M. Caricato, A. V. Marenich, J. Bloino, B. G. Janesko, R. Gomperts, B. Mennucci, H. P. Hratchian, J. V. Ortiz, A. F. Izmaylov, J. L. Sonnenberg, D. Williams-Young, F. Ding, F. Lipparini, F. Egidi, J. Goings, B. Peng, A. Petrone, T. Henderson, D. Ranasinghe, V. G. Zakrzewski, J. Gao, N. Rega, G. Zheng, W. Liang, M. Hada, M. Ehara, K. Toyota, R. Fukuda, J. Hasegawa, M. Ishida, T. Nakajima, Y. Honda, O. Kitao, H. Nakai, T. Vreven, K. Throssell, J. A. Montgomery, Jr., J. E. Peralta, F. Ogliaro, M. J. Bearpark, J. J. Heyd, E. N. Brothers, K. N. Kudin, V. N. Staroverov, T. A. Keith, R. Kobayashi, J. Normand, K. Raghavachari, A. P. Rendell, J. C. Burant, S. S. Iyengar, J. Tomasi, M. Cossi, J. M. Millam, M. Klene, C. Adamo, R. Cammi, J. W. Ochterski, R. L. Martin, K. Morokuma, O. Farkas, J. B. Foresman, and D. J. Fox, Gaussian, Inc., Wallingford CT, **2016**.

77. Perdew, J. P., Burke, K. and Ernzerhof, M. Phys. Rev. Lett. **1996**, 77, 3865–3868.

78. Chernyshev, A. N., Chernysheva, M. V., Hirva, P., Kukushkin, V. Y. and Haukka, M. Dalton Trans. **2015**, 44, 14523–14531.

# CHAPTER 3

## Influence of the Attachment of Gold(I) at the Upper Rim of a Calix[4]pyrrole on the Binding of Tetraalkylammonium Chloride Salts

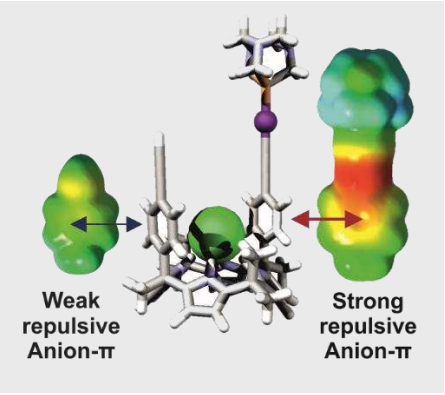


Part of this Chapter has been published in Q. Sun, G. Aragay, A. Pinto, E. Aguiló, L. Rodríguez, P. Ballester. Chemistry–A European Journal, **2020**, 26, 2020

# 3. INFLUENCE OF THE ATTACHMENT OF GOLD(I) AT THE UPPER RIM OF A CALIX[4]PYRROLE ON THE BINDING OF TETRAALKYLAMMONIUM CHLORIDE SALTS

## 3.1. Introduction

Since the "lock-and-key" concept formulated more than a century ago by Emil Fisher, the understanding of the molecular interactions, enzyme reactivity and material properties have continued to attract the attention of researchers. This concept has inspired synthetic chemists in the design of synthetic receptors and catalysts. Building blocks that present a rigid 3-D structure play an important role in the field of molecular receptors. Regarding this, a wide range of macrocycles possessing the required architectures and synthetic tailorability exists. These macrocycles include calixarenes,[1] crown ethers,[2] cyclodextrins,[3] cryptands[4] and cucurbiturils[5] among others. Their facile synthesis, distinct conformational preferences, π-electron rich cavities, separate ion-binding site and ease of functionalization give a great opportunity for the development of new receptors.

In particular, containers based on the calix[4]pyrrole macrocycle are further very attractive as they are relatively easy to modify and helpful in ion transportation, recognition and extraction of species.[6–8] Calix[4]pyrrole consists of four pyrrole units linked through their 2 and 5 position via four tetrasubstituted $sp^3$ hybridized meso carbon atoms.[9,10] Functional groups can be introduced at the upper or lower rims of these units (Figure 3.1). The introduction of functional groups can tune the size of the inner space of the resulting cavity and their solubility in non-polar or aqueous solvents.

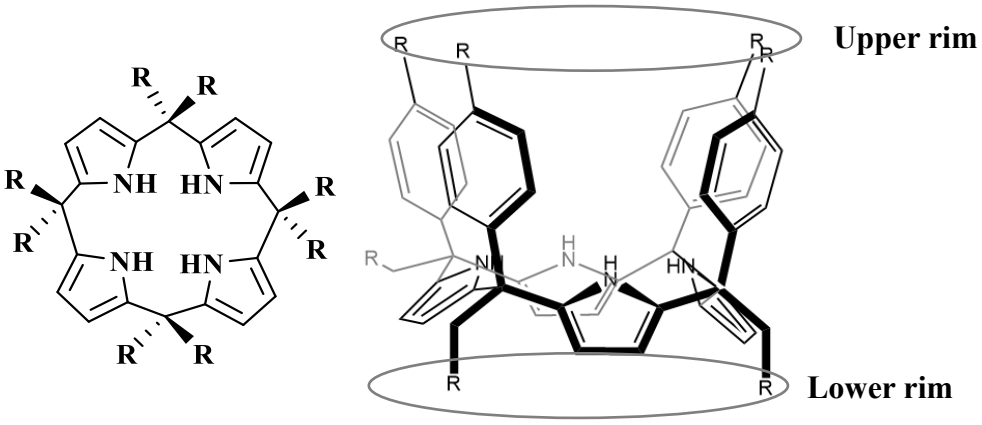


**Figure 3.1.** General structure of calix[4]pyrrole (left) and representation of upper rim and lower rim of the cavity of the calix[4]pyrrole.

Calix[4]pyrroles have an advantage as synthetic receptors owing to different conformational isomeric forms, which allow different uses and applications. For instance, the calix[4]pyrroles can adopt different conformers, including the cone, partial cone, 1,2-alternate and 1,3-alternate (Figure 3.2).

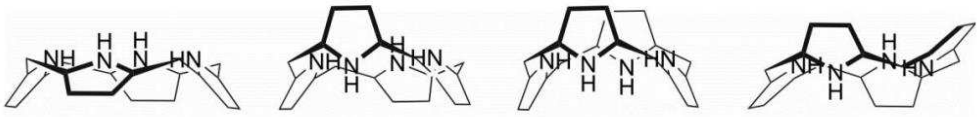

**(1)** **(2)** **(3)** **(4)**

**Figure 3.2.** Schematic representation of the different isomeric forms that adopt calix[4]pyrrole: cone (1), partial cone (2), 1,3-alternate (3) and 1,2-alternate (4).

In cone conformation, the calix[4]pyrrole displays a polar aromatic cavity ideal for the binding of spherical anions where the anion establishes four simultaneous hydrogen bonds with the pyrrole NHs (Figure 3.3).

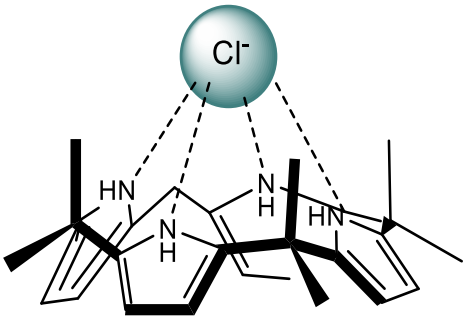


**Figure 3.3.** Schematic representation of a binding sites between a chloride anion and a calix[4] pyrrole.

Calix[4]pyrroles usually act as heteroditopic receptors for ion-pairs, especially in non-polar organic solvents like chloroform or dichloromethane, where the cation, usually prefers to bind opposite to the anion.[11–13] In contrast, in more polar organic solvents, like acetone or acetonitrile, the influence of the cation in the binding process is reduced.[14]

In this way, the confinement of guests in containers based on the calix[4]pyrrole affects not only their isomeric conformation but also their chemical-physical properties. Among all the techniques that can be used to observe and monitor the host-guest interaction, fluorescence spectroscopy is the best non-invasive spectral modality. Whereas, for example, absorbance measurements can at best determine concentrations down to ~ 0.1 μM, fluorescence can accurately measure concentrations one million times smaller. Numerous reports have been published in which calixarene-based smart fluorogenic materials have been used. The introduction of fluorescent properties mainly was done by the covalent bonding of a fluorophore unit, like pyrene.[15] Another strategy is the introduction of a metal in the chemical structure, like gold(I) atom. This metal can provide intrinsic luminescent properties to the receptor and their complexes. In addition, this type of substituents will endow to the receptor with the possibility to be involved in weak aurophilic interactions (Au(I)···Au(I)).[16,17]

Herein, the synthesis of a gold(I) calix[4]pyrrole derivative is reported in order to incorporate luminescent properties on the resulting compound. A description of the binding properties with chloride (as an anion involved in many biological processes) in different solvents has been tested. Several spectroscopic techniques have been used in

order to fully characterize the binding process and DFT calculations have confirmed the obtained experimental results.

## 3.2. Results and Discussion

### 3.2.1. Synthesis and characterization

The synthesis of the gold(I) calix[4]pyrrole **3.1** (Figure 3.4) was carried out with slight modifications of a previously reported method.[18] The correct formation of the compound was checked by comparison of the corresponding $^{1}H$ and $^{31}P$ NMR spectra with the reported data. Photophysical characterization was performed in order to corroborate the purity of the compound. In contrast with what happens in the organic calix[4]pyrrole, the gold(I) complex presents luminescent properties and phosphorescent emission when the oxygen is removed and at low temperature (77 K). This is a nice example on how a heavy-atom favours spin-orbital coupling effects being able to induce luminescence of non-emissive chromophores.

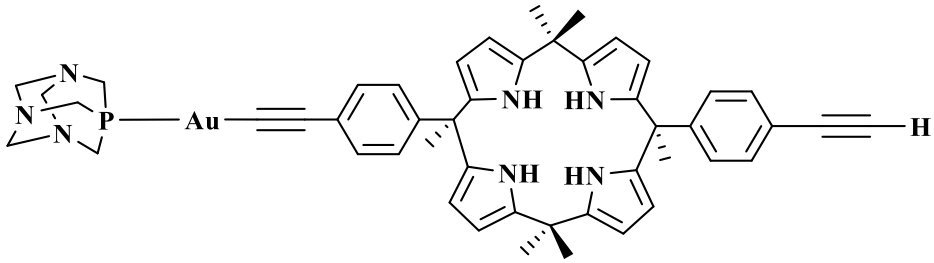


**3.1**

**Figure 3.4.** Gold(I) calix[4]pyrrole complex (**3.1**).

### 3.2.2. Molecular recognition

The gold(I) complex **3.1** was tested for molecular recognition of chloride since calix[4]pyrroles are well-known hosts used in the molecular recognition of mono-atomic spherical anions such as bromide, chloride or fluorine. The incorporation of a heavy atom in the chemical structure allows the possibility of following the host guest interaction by spectrofluorometric methods. The non-covalent interactions between the anion and the receptor may induce changes in the resulting luminescent properties.

3.2.2.1. UV-vis spectroscopy binding studies

The interaction between the parent bis-ary-ethynyl calix[4]pyrrole receptor (**3.L**) with TBACl and MTOACl was firstly studied using UV-vis spectroscopy. A $2 \cdot 10^{-5}$ M dichloromethane solution of MTOACl or TBACl containing also the receptor was progressively added to an independent solution of the receptor and UV-vis spectrum of the resulting mixture was acquired after each addition. The absorption spectra of the titration with MTOACl salt displays two absorption bands suggesting the co-existence of two species (Figure 3.5). Since calix[4]pyrroles can act as heteroditopic receptor in non-polar solvents, the anionic chloride complex [Cl⊂**3.L**]$^-$ and the ion-paired counterpart Cl⊂**3.L**·MTOA were considered during the mathematical analysis of the UV-vis titration data using HypSpec software.[19] The values obtained for [Cl⊂**3.L**]$^-$ and Cl⊂**3.L**·MTOA were K[Cl⊂**3.L**]$^-$ = $6.3 \cdot 10^4$ $M^{-1}$ and K(Cl⊂**3.L**·MTOA) = $6.3 \cdot 10^8$ $M^{-2}$. If the Cl⊂**3.L**·MTOA complex is considered to present a 1:1 stoichiometry, its binding constant can be estimated as K(Cl⊂**3.L**·MTOA) = $(6.3 \cdot 10^8\ M^{-2})^{1/2} = 2.5 \cdot 10^4$ $M^{-1}$. The titration of **3.L** with incremental amounts of TBACl leads to a diminution of this absorbance band but even after the addition of 32 equivalents of the salt, the saturation point was not reached. Probably, at this concentration the extent at which the complex is formed is low and the absorbance changes may be ascribed to an increase of the dielectric constant of the media.

The interaction between the receptor **3.1** with TBACl and MTOACl salts in dichloromethane solution has been followed by recording the absorption and emission spectra after each addition taking advantage of the emissive properties of the gold(I) complex. It is worth to say that non-significant changes have been observed in the emission spectra. A decrease of the absorbance and an increase of a tail at ca. 310 nm upon the addition of both salts was observed in the absorption spectra (Figure 3.5). Changes of the absorbance did not reach saturation as previously observed for **3.L**. Based on these results, UV-vis is not a suitable technique to study the binding of the chloride to the gold(I) receptor **3.1**.

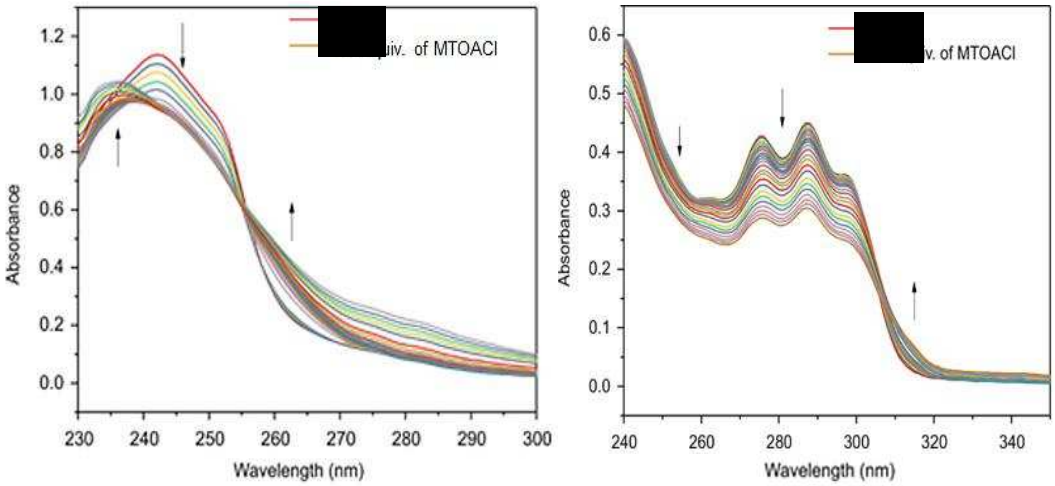


**Figure 3.5.** UV-vis spectra acquired for the titration of **3.L** (left) or **3.1** (right) with MTOACl in dichloromethane solutions.

3.2.2.2. NMR binding studies

The concentration used in UV-vis experiments was unsuitable for the measurement of equilibrium constant. For this reason, NMR spectroscopy was used. Firstly, the interaction between the parent bis-ary-ethynyl calix[4]pyrrole receptor (**3.L**) with TBACl and MTOACl was assayed. The $^{1}$H NMR spectrum of **3.L** in $CD_2Cl_2$ showed sharp and well-resolved proton signals in agreement with a $C_{2v}$ symmetry (Figure 3.6a). The incremental addition of TBACl to the host (**3.L**) solution induces chemical shift changes in some of the proton signals of **3.L** (Figure 3.6, top). In this case, where the peaks are assigned to the host in the complex and those to the free host are fused, the host-guest complexation experienced a very fast exchange rate compared to the NMR time scale.[20] The NH proton signal of **3.L** moved downfield ($\Delta\delta$ ~ 3.0 ppm), what suggests its involvement in hydrogen bonding interactions with the chloride. Protons of the β-pyrrole moiety ($b^1$ and $b^2$) moved upfield and downfield respectively, which indicates that the binding with the chloride is concomitant, and their interaction induces a change in the receptor's conformation from alternate to cone (Figure 3.6). The methylene protons alpha to the nitrogen atom of the TBA cation moved slightly downfield at increasing concentration. This behaviour indicates that TBA cation is involved in the complex, forming ion-paired complex, Cl⊂**3.L**·TBACl, where the TBA cation is expected to bind opposite to the anion in the electron-rich aromatic cavity. The NMR concentration (~ $10^{-3}$ M) suitable to reach a saturation of the equimolar complex (1:1) and the fittings of the β-pyrrole protons signals using HypSec program allows the obtention of a value for the binding constant for the ion-paired complex Cl⊂**3.L**·TBACl, K (Cl⊂**3.L**·TBACl) = 2.7·$10^2$ $M^{-1}$.

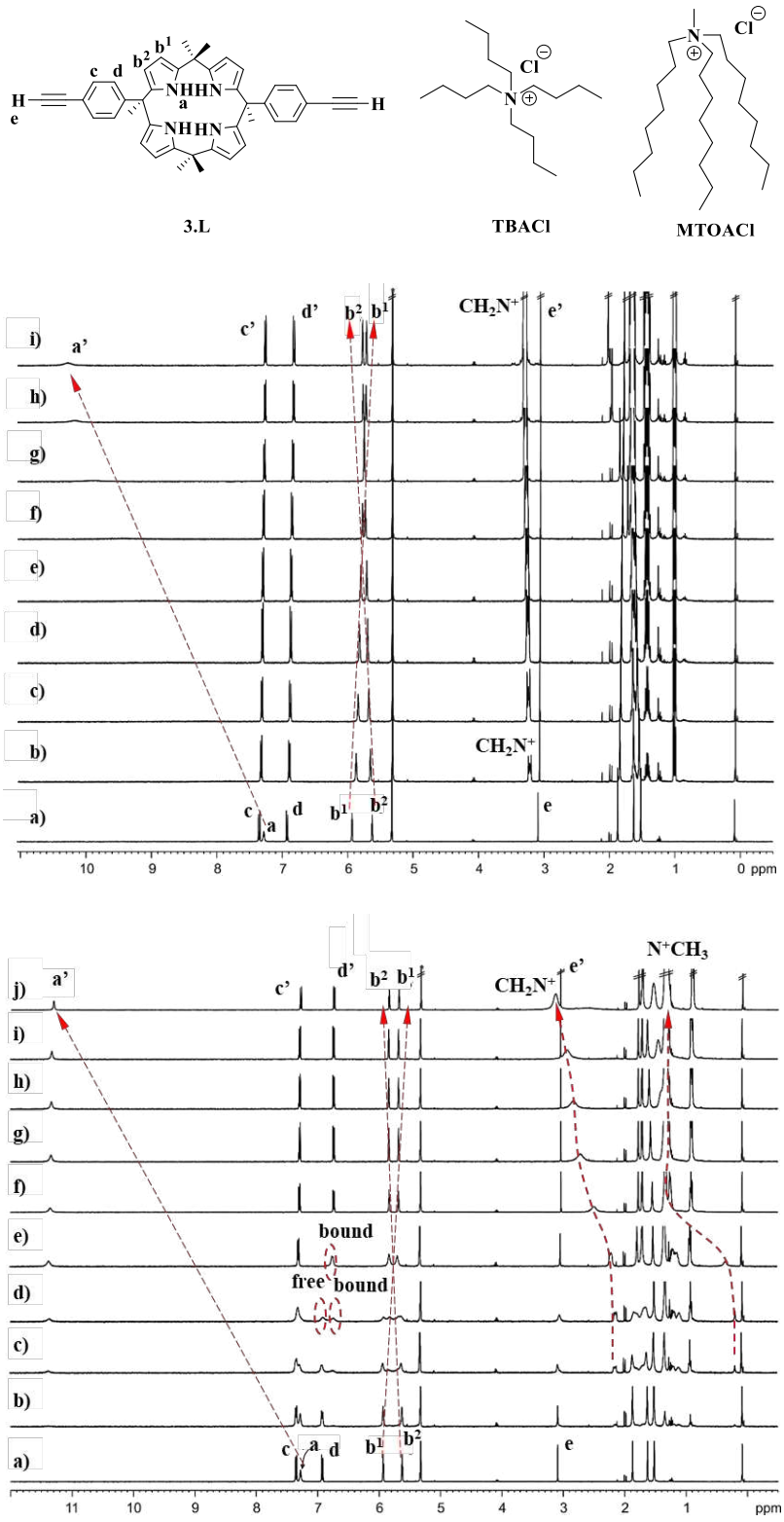


**Figure 3.6.** Top panel) $^{1}$H NMR spectra acquired during the titration of **3.L** ($10^{-3}$ M) with incremental amounts of TBACl in $CD_2Cl_2$ solution: a) 0; b) 0.5; c) 1; d) 1.5; e) 2; g) 3; g) 5; h) 8 and i) 10 equiv. Bottom panel) $^{1}$H NMR spectra acquired during the titration of **3.L** ($10^{-3}$ M) with incremental amounts of MTOACl in $CD_2Cl_2$ solution: a) 0; b) 0.1; c) 0.3; d) 0.5; e) 1; g) 1.5; g) 2; h) 2.5; i) 3 and j) 5 equivalents.

The analogous $^1$H NMR titration of **3.L** with MTOACl was performed and provided significant different results (Figure 3.6). The addition of 0.5 equivalents produced a broadening of the calix[4]pyrrole receptor, as well as the appearance of two separated signals (one related to the free host and the other related to the bound host-guest complex). Only the signals related to the bound receptor can be detected after the addition of 1 equivalent of MTOACl and further additions induce the sharpening of the signals of **3.L** without any chemical shift. In this case, where the signals of the host and the host-guest complex can be differentiated in the NMR spectra, the host-guest complexation equilibrium between **3.L** and MTOACl has a slow/intermediate exchange rate compared to the NMR time scale. The methyl group, alpha to the nitrogen atom of the MTOA cation, moved downfield ($\Delta\delta \sim 0.19$ ppm), while the methylene groups alpha to the nitrogen atom moved in a lesser extent. This can be rationalized owing to the deeper inclusion of the methyl group in the aromatic cavity defined by the pyrrole rings of **3.L**.

The increase in the affinity constant for Cl⊂**3.L**·MTOA complex (K(Cl⊂**3.L**·MTOA) = $2.5 \cdot 10^4$ $M^{-1}$, determined in section 3.2.2.1. UV-vis spectroscopy binding studies) compared to that of the Cl⊂**3.L**·TBACl counterpart (K (Cl⊂**3.L**·TBACl) = $2.7 \cdot 10^2$ $M^{-1}$) supports that **3.L** is acting as a heteroditopic receptor in dichloromethane solution. In addition, since the proton signals of MTOA cation experienced noticeable chemical shift changes, while TBA cation did not, the inclusion of the MTOA cation has a better inclusion than TBA in the aromatic cavity opposed to the bound chloride and is responsible of the observed selectivity.

Having clarified the binding properties of **3.L** towards MTOACl and TBACl in dichloromethane solutions, we can analyse the influence of the attachment of gold(I) in the chemical structure. The interaction of gold(I) complex **3.1** with MTOACl and TBACl using NMR spectroscopy was studied. Gold(I) complex **3.1** has a reduced solubility in dichloromethane and its NMR spectrum showed four aromatic proton signals in agreement with a $C_s$ symmetry. The aromatic protons can be divided in two different group of signals: 1) the aromatic protons from the ethynyl substituted meso-phenyl group that display two doublets at $\delta = 7.34$ and 6.92 ppm; 2) the aromatic protons of the meso-phenyl bearing the gold(I) appear slightly upfield shifted at $\delta =$ 7.19 and 6.81 ppm (Figure 3.7). The four chemically non-equivalent β-pyrrole proton ($Hb^1$-$Hb^4$) produced only two separate signals. The addition of incremental amounts of

each salt to separate dichloromethane solutions of **3.1** produced changes in the NMR that are similar to those described by the parent ligand **3.L**, meaning that it also acts as a heteroditopic receptor. Noteworthy, the appearance of unexpected second set of signals for the gold(I) receptor during the NMR titration, that became visible when we added salt over the equimolar point (blue arrows in Figure 3.7), makes us surmised that the ion-paired complex of **3.1** could be present in solution as a mixture of two conformers of the bound receptor.

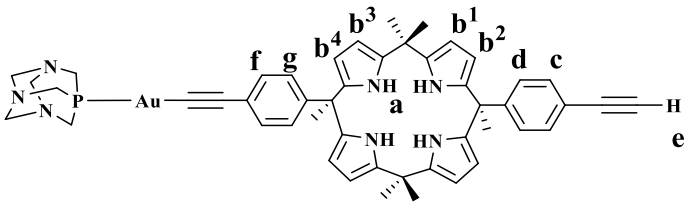


**3.1**

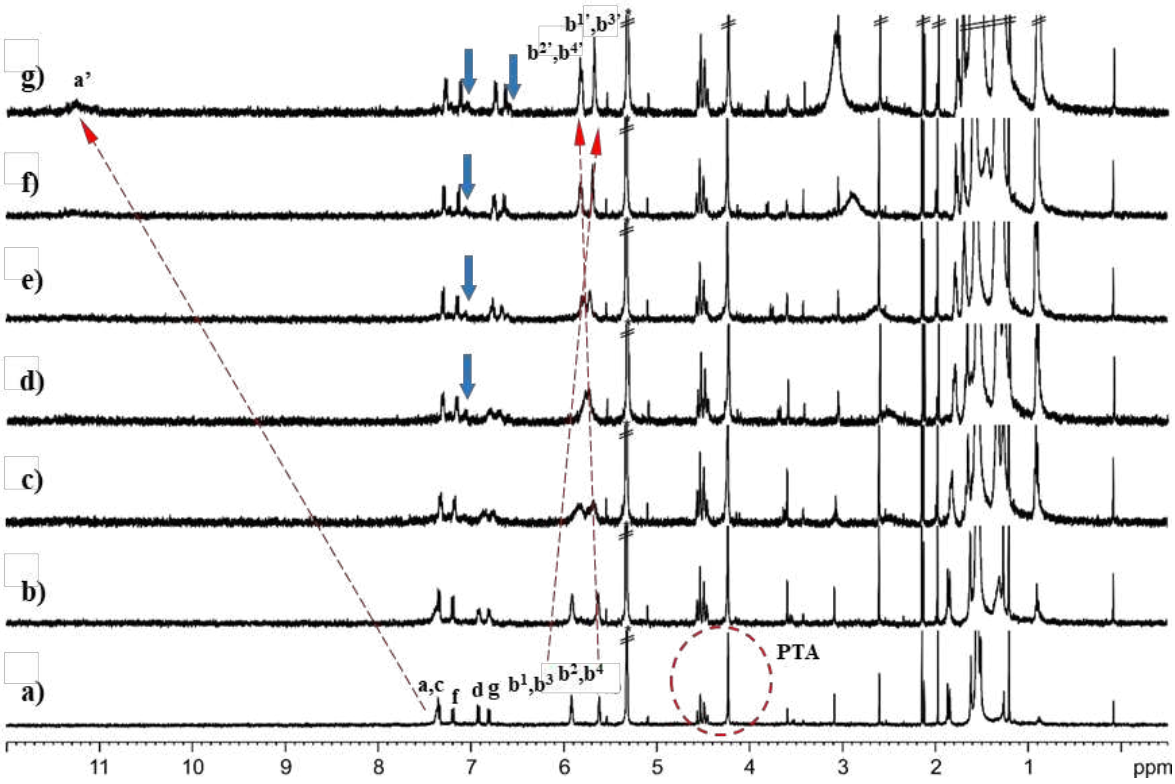


**Figure 3.7.** $^{1}$H NMR spectra acquired during the titration of **3.1** ($10^{-3}$ M) with incremental amounts of MTOACl in $CD_2Cl_2$ solution: a) 0; b) 0.5; c) 1; d) 1.5; e) 2; f) 3 and g) 5 equivalents.

Additional titration experiments in acetone solution were performed in order to gain further evidences of the presence of the mixture of the two conformers of **3.1** in solution. In acetone solution, the ion-pairing is expected to be weaker, and this might facilitate the assignment of the adduct of **3.1** and the salt. The gold(I) complex **3.1** was titrated with incremental amounts of both salts, TBACl and MTOACl, in separate NMR tubes. The result of the two titrations with the two salts are quite similar, in accordance with the more polar environment provided by the acetone that minimizes the ion-pairing, and therefore, **3.1** behaves as a monotopic receptor (Figure 3.8). In both cases, the chloride binding saturates after the addition of 1 equivalent, where the addition of more equivalents of the salt only induces small changes. As well as in the titrations with dichloromethane, a second set of signals was observed.

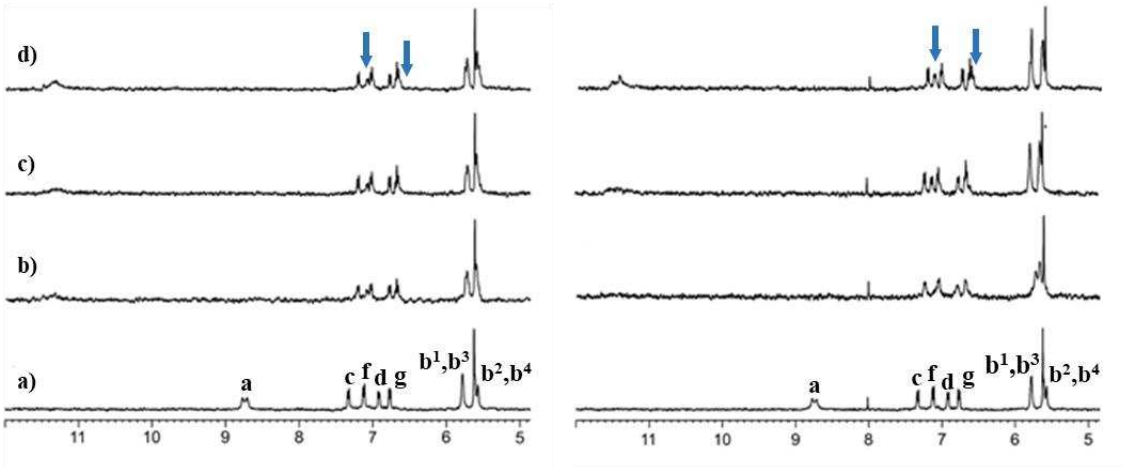


**Figure 3.8.** Left panel) $^{1}$H NMR (400 MHz, $d_6$-acetone, 298 K) spectra of the titration of **3.1** ($10^{-3}$ M) and TBACl: a) 0; b) 0.5; c) 1.0 and d) 2.0 equiv. Right panel) $^{1}$H NMR (400 MHz, $d_6$-acetone, 298 K) spectra of the titration of **3.1** ($10^{-3}$ M) and MTOACl: a) 0; b) 0.5; c) 1.0 and d) 2.0 equivalent.

The higher solubility of the gold(I) complex **3.1** in acetone allows to perform DOSY experiments that helps in the assignment of the second set of the signals that appears upon addition of chloride salt. It was observed that these signals are independent and this confirms that the gold(I) receptor present two different conformations in solution (Figure 3.9).

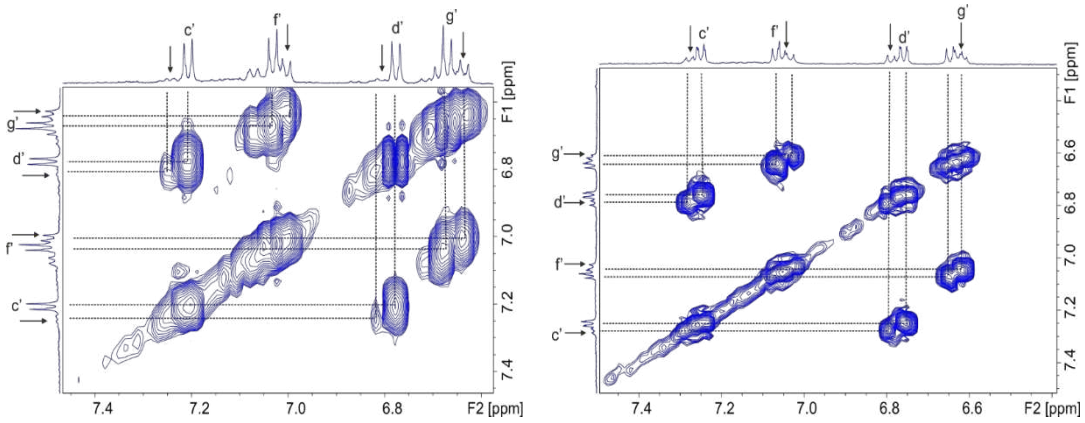


**Figure 3.9.** Left panel) Selected region of the COSY NMR (500 MHz, acetone- $d_6$, 298 K) spectrum of TBACl and **3.1** (ca. 3:1 ratio). Right panel) Selected region of the COSY NMR (500 MHz with cyroprobe, acetone-$d_6$, 298 K) spectrum of the MTOACl and **3.1** (ca. 3:1 ratio).

3.2.2.3. Isothermal Titration Calorimetry (ITC) experiments in acetone

Isothermal titration calorimetry (ITC) is a physical technique that measures directly the heat discharged or consumed where two molecules are in contact according to the basic principle of thermodynamics. The amount of heat discharged or consumed upon the host-guest interaction is defined as follows:[21]

$$Q = V_o \Delta H_b [H]_t \left\{ \frac{K_a[G]}{1 + K_a[G]} \right\}$$

Where Q is heat evolved/absorbed; $V_o$ is sample cell volume; $\Delta H_b$ is enthalpy of binding per mole of guest; $[H]_t$ corresponds to the total concentration of the host in the sample cell; $K_a$ is binding constant; [G] is concentration of free guest. Thereby, ITC allows to determine the entire thermodynamic parameters of the molecular binding that includes the binding constant ($K_a$), enthalpy ($\Delta H$), entropy ($\Delta S$), and the reaction stoichiometry (n).

In this way, isothermal titration calorimetry (ITC) experiments have been performed to characterize thermodynamically the binding processes in acetone of the receptors under study. Moreover, this technique let us obtain a more accurate value for the binding constant of host-guest complexes with the receptor **3.1**, that was not possible to measure so rigorously with the other techniques.

In all cases, the resulting exothermic binding isotherms showed a single sigmoidal behavior with the inflexion point centered at 1:1, host-guest, ratio (Figure 3.10). The curvature of the titration depends on the binding affinity, therefore, it is expected that receptor **3.1** has a lower binding constant value than the receptor **3.L**.

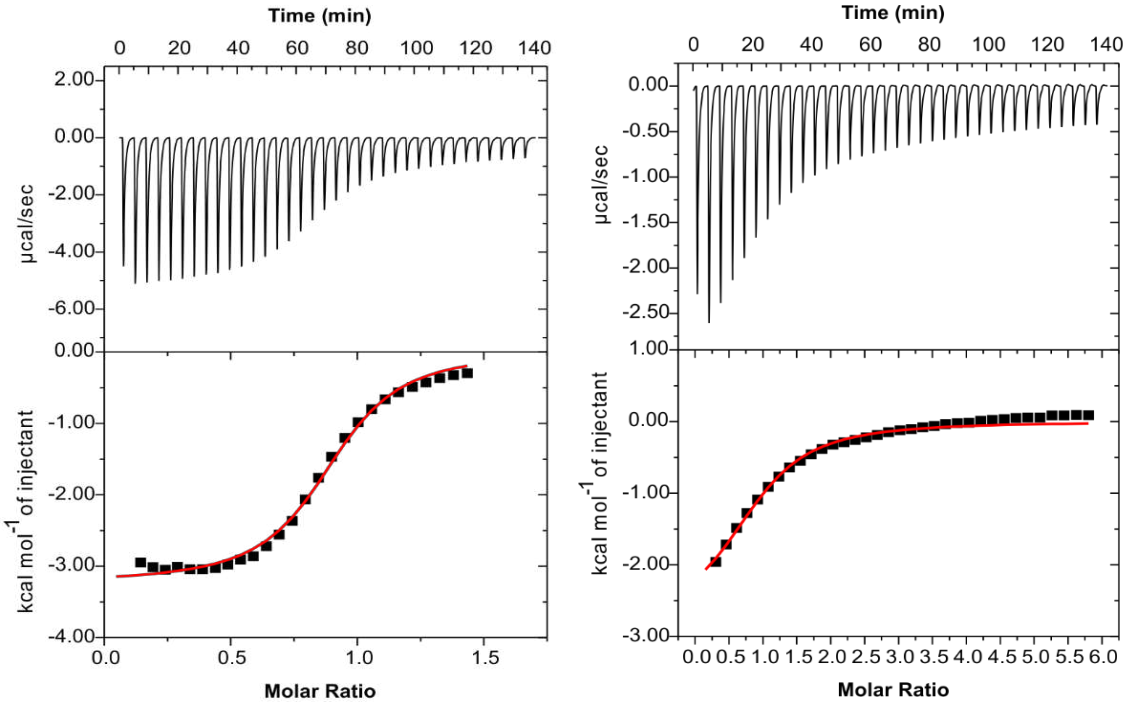


**Figure 3.10.** Top) Raw data for the ITC titrations of **3.L** (left) and **3.1** (right) with TBACl. Bottom) Normalized integration of heat vs TBACl/**3.L** and TBACl/**3.1** molar ratio, the fit of the extended binding isotherm (red line) also the experimental data is also shown.

The fittings of the corresponding isotherms using a simple 1:1 binding model give the thermodynamic parameters ($K_a$ and $\Delta H$) and are summarized in Table 3.1.

**Table 3.1.** Apparent binding constants ($K_a$, $M^{-1}$), enthalpies ($\Delta H$, Kcal $mol^{-1}$), free energies ($\Delta G$, Kcal $mol^{-1}$) and entropy ($\Delta S$, Kcal $mol^{-1}$ $K^{-1}$) of the binding equilibria of **3.L** and **3.1** with TAACl salts (TAA = $TBA^+$ or $MTOA^+$) in acetone at 295 K using direct ITC titrations.

| **Receptor** | **3.1** | | **3.L** | |
|---|---|---|---|---|
| **Salt** | **TBACl** | **MTOACl** | **TBACl** | **MTOACl** |
| $K_a$ x $10^{-4}$ | 1.0 | 2.4 | 4.8 | 7.1 |
| $\Delta H$ | -3.6 | -2.1 | -3.0 | -3.4 |
| $\Delta G$ | -5.5 | -6.0 | -6.3 | -6.5 |
| $\Delta S$ | 0.011 | 0.010 | 0.006 | 0.013 |

The values of the binding constant for the anionic complexes in acetone show differences between the two salts used. These values should be identical, since it is expected that the salt used as chloride precursor was completely dissociated. However, these results derive from not fully dissociation of ion-pairs in acetone solution.

The obtention of an accurate value for the apparent binding constant of the two receptors with chloride, can be used to study the effect of the incorporation of gold(I) atom into the chemical structure. The values obtained for the gold(I) complex are lower than the obtained for the ligand, indicating a repulsive effect between the chloride and the receptor **3.1** (see 3.2.3. Theoretical calculations). Finally, the binding of chloride in both receptors is both enthalpy and entropy driven. The entropic term indicates the importance of the solvation and desolvation processes that take place in polar solvent (acetone) for the binding of chloride through hydrogen-bonding interactions.

### 3.2.3. Theoretical calculations

The results above show that the gold(I) receptor presents two conformers in solution when it is interacting with the chloride anion and presents lower affinity for the binding process than its organic precursor. DFT calculations were performed in order to determine the modification of the electrostatic surface potential (ESP) at the center of the aromatic ring provoked by the substitution of the terminal alkynyl hydrogen atom by a gold(I) atom trying to rationalize the experimental results. For the sake of simplifying, the ESP have been computed for 1-ethynyl-4-methyl benzene and [2-[4-

(methyl)phenyl]ethynyl](1,3,5-triaza-7-phosphaadamantene)Au(I), as model systems of the two different aromatic walls of the receptors used in this chapter.

As shown in Figure 3.11, the incorporation of gold(I) atom in the chemical structure doubles the ESP value at the center of the aryl ring. Therefore, the aryl group becomes more electron rich and gold(I) complex prone a more repulsive anion-π interaction. This result can be used to explain the lower affinity of the gold(I) complex used as a receptor for chloride. Additionally, the existence of two conformers in solution during the NMR titrations can be ascribed to the existence of stronger repulsive chloride-π interactions. These energetic repulsions might induce the bound receptor to adopt a conformation different from the cone.

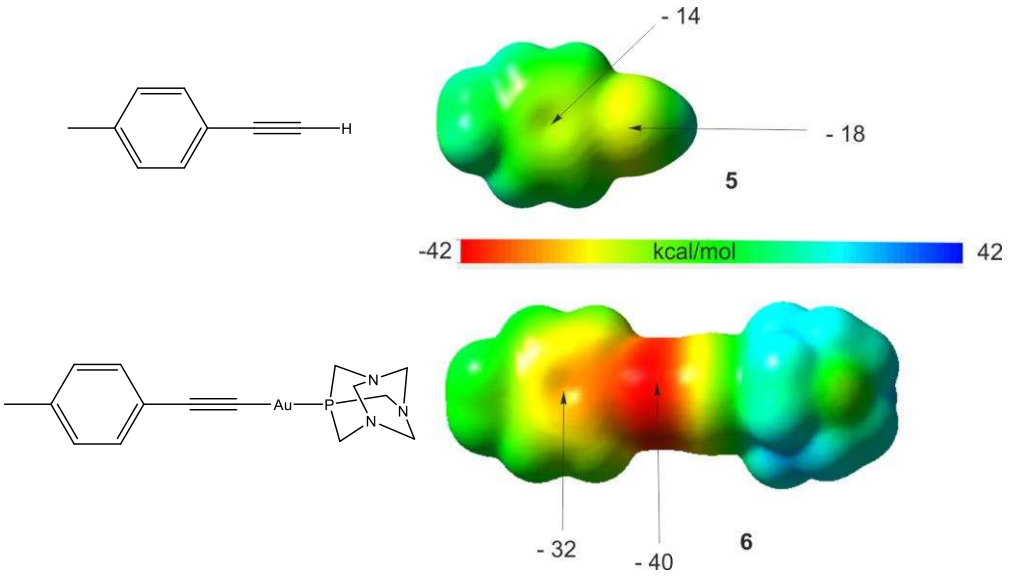


**Figure 3.11.** Calculated ESP values for the model systems 1-ethynyl-4-methyl benzene and [2-[4-(methyl)phenyl]ethynyl](1,3,5-triaza-7-phosphaadamantene)Au(I). ESP cubes mapped at electron density value of 0.0004 a.u.

In order to assign the relative the energies and structures to the different binding modes hypothesized for the [Cl⊂**3.1**]$^-$ complex, DFT calculations at bp86-D3 def2-SVP level of theory and continuum solvent model using GAUSSIAN 09 have been performed. Figure 3.12 depicts the energy-minimized structures in which the receptor adopts cone and half-cone conformations. The calculations show that the cone conformation is 2.2 kcal mol$^{-1}$ more stable than the half-cone conformation. So, we postulate that the two different signals observed during the NMR titrations performed in dichloromethane-$d_2$

and acetone-$d_6$ correspond to these two conformations, being the cone conformation favoured and present largely in solution.

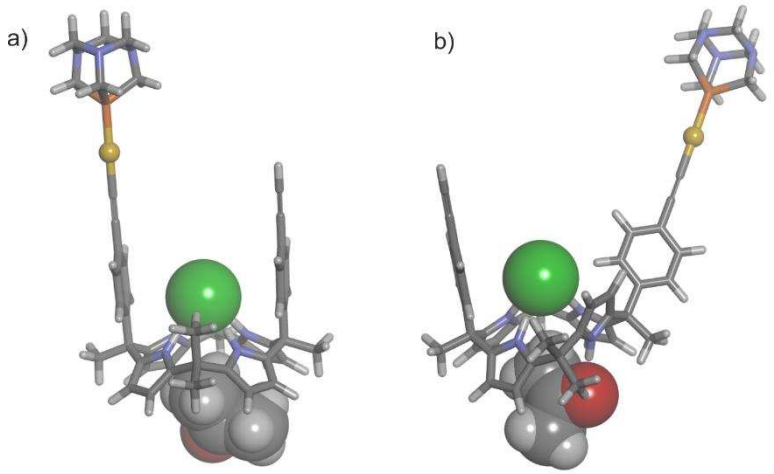


**Figure 3.12.** Energy minimized structures bp86-D3 def2-SVP of [Cl⊂**3.1**]⁻: a) receptor in cone conformation; b) receptor in half-cone conformation. The receptor is shown in ball and stick representation. The chloride and the implicit acetone as CPK models. The gold atom is displayed as scaled ball and stick. The calculation assigns an energy advantage of 2.2 kcal/mol to the complex with the receptor in cone conformation.

## 3.3. Conclusions

The synthesis of a mono gold(I) calix[4]pyrrole has been optimized being necessary a column chromatography purification of the starting materials. The incorporation of a gold(I) atom in the chemical structure provides luminescence properties in the resulting compound. Despite this, the photophysical properties do not allow to study the host-guest interactions between the gold(I) derivative and chloride.

NMR experiments in dichloromethane show that the parent ligand **3.L** and mono-gold(I) derivative **3.1** act as heteroditopic receptors in the binding of tetraalkylammonium chloride salts producing 1:1 ion-paired complex. The receptors show high selectivity and affinity for the binding of methyltrioctyl ammonium chloride (MTOACl) compared to tetrabutyl ammonium chloride (TBACl) due to the better fit of the methyl group of the MTOA cation in the cavity opposed to the anion binding site. Moreover, the existence of a mixture of two conformers has been detected in the

NMR titrations of gold(I) complex as host. This can be rationalized by DFT calculations that show that there is an increase in the negative ESP value at the centre of the phenyl ring that is responsible for this deleterious effect. Compounds **3.L** and **3.1** mainly function as homotopic receptors for chloride in acetone solution.

ITC experiments allow us to determine accurately the apparent binding constants values for gold(I) complexes and demonstrate that the cation effect of the salts is markedly reduced in this solvent. Also, the difference in energy between [Cl⊂**3.L**] and [Cl⊂**3.1**] is in range 0.8-0.5 kcal $mol^{-1}$ in favour of the later and in agreement with the DFT calculations.

## 3.4. Experimental section

The synthesis of 10α,20α-bis(4-[ethynylphenyl])calix[4]pyrrole was carried out by Dr.. Qingqing Sun from Institut Català d'Investigació Química (ICIQ), Tarragona.

**Synthesis of [Au{10α,20α-bis(4-[ethynylphenyl])calix[4]pyrrole}-(PTA)] (1).**

A solution of [AuCl(PTA)] (32 mg, 0.08 mmol) in $CH_2Cl_2$ (5 mL) was added to a solution of KOH (5 mg, 0.089 mmol) and 10α,20α-bis(4-[ethynylphenyl])calix[4]pirrole (50 mg, 0.083 mmol) in a mixture of MeOH (10 mL) and DCM (4 mL). After 2 hours of stirring at room temperature, the resulting pale yellow solution was concentrated to ca. 10 mL, and n-hexane (10 mL) was added to precipitate a pale yellow solid. The filtered solid was recrystallized in $CH_2Cl_2$/hexane solution and isolated by filtration. Yield: 60 % (45 mg).

$^1$H NMR (400 MHz, $(CD_3)_2CO$): 8.77 (br, 2H, N-H), 8.71 (br, 2H, N-H), 7.33 (d, 2H, J = 8.4 Hz), 7.12 (d, 2H, J = 8.4 Hz), 6.92 (d, 2H, J = 8.4 Hz), 6.77 (d, 2H, J = 8.4 Hz), 5.78 (m, 4H), 5.60 (s, 2H), 5.56 (s, 2H), 4.65-4.48 (d, 3H, J = 12.8 Hz, N-$CH_2$-N), 4.50-4.45 (d, 3H, J = 12.8 Hz, N-$CH_2$-N ), 4.36 (s, 6H, P-$CH_2$-N), 3.58 (s, 1H, C≡C-H), 1.87 (s, 3H, $CH_3$), 1.83 (s, 3H, $CH_3$), 1.65 (s, 6H, $CH_3$), 1.48 (s, 6H, $CH_3$). $^{31}P\{^1H\}$ NMR (162 MHz, $(CD_3)_2CO$, 298 K, δ ppm): -47.0 ppm. ES-MS (+) m/z: 954.40 ($[M + H]^+$, calc.: 954.40). IR (KBr, $cm^{-1}$): 3413 ν(N-H), 3105 ν(C≡C-H), 2092 ν(C≡C), 1637 ν(C=O), 1590 ν(C=N).

### 3.4.1. NMR binding studies

NMR titrations were performed at the Institut Català d'Investigació Química (ICIQ). A $10^{-3}$ M solution of the host was prepared in the corresponding deuterated solvent (dichloromethane-$d_2$, acetone-$d_6$). Subsequently, 0.5 mL of the solution was transferred to an NMR tube. The remaining solution was used to prepare the titrant solution (TBACl and MTOACl) at 20-30 fold higher concentration. Thus, the concentration of the host was maintained constant during the titration. The host solution was titrated by the addition of incremental amounts of the salt solution and recording an $^1$H NMR spectrum after each addition.

### 3.4.2. UV-vis titrations

UV-vis titrations were performed by preparing a dichloromethane solution of the host ($10^{-5}$ M). The same host solution was used to prepare MTOACl or TBACl solutions ($3 \cdot 10^{-3}$ M). Thus, the concentration of the host was maintained constant through each addition during the titration. The host solution was titrated by the addition of incremental amounts of the salt solution and recording a UV-vis spectrum after each addition.

### 3.4.3. ITC experiments

ITC experiments were performed by Dr. Qinqing Sun from ICIQ using a MicroCal VP-ITC MicroCalorimeter with the VP Viewer 2000 software. Dichloromethane titrations of host with MTOACl were carried out at 288 K by adding small aliquots (8 μL, 16 s) of a $2.8 \cdot 10^{-3}$ M solution of MTOACl into a $3.5 \cdot 10^{-4}$ solution of host. The association constants and the thermodynamic parameters of the binding processes were derived using the "one set of sites" model included in the Microcal software. Acetone ITC experiments with MTOACl and TBACl were performed at 288 K by injecting small aliquots (8 μL, 16 s) of $5.4 \cdot 10^{-3}$ M acetone solution of the salt using computer controlled micro syringe into a $3 \cdot 10^{-4}$ M solution of the host in the same solvent.

The association constants and the thermodynamic parameters of the binding processes were obtained from the fit of the titration data to a simple 1:1 binding model using HypΔH software.

### 3.4.4. Theoretical calculations.

The theoretical calculations were carried out by Prof. Pau Bsllester from ICIQ. The energy structures were obtained using DFT-dispersion method BP86-D3-def2-SVP level of theory and a continuum solvent model.

## 3.5. References


1. Español, E. S. and Villamil, M. M. Biomolecules **2019**, 9, 90–105.
2. Gokel, G. W., Leevy, W. M. and Weber, M. E. Chem. Rev. **2004**, 104, 2723–2750.
3. Lai, W. F., Rogach, A. L. and Wong, W. T. Chem. Soc. Rev. **2017**, 46, 6379–6419.
4. Kang, S. O., Llinares, J. M., Day, V. W. and Bowman-James, K. Chem. Soc. Rev. **2010**, 39, 3980–4003.
5. Murray, J., Kim, K., Ogoshi, T., Yao, W. and Gibb, B. C. Chem. Soc. Rev. **2017**, 46, 2479–2496.
6. Veauthier, J. M., Cho, W. S., Lynch, V. M. and Sessler, J. L. Inorg. Chem. **2004**, 43, 1220–1228.
7. Makwana, B. A., Vyas, D. J., Bhatt, K. D., Darji, S. and Jain, V. K. Appl. Nanosci. **2016**, 6, 555–566.
8. Sun, Q., Escobar, L. and Ballester, P. Angew. Chem. Int. Ed. **2021**, 133, 10447–10453.
9. Gale, P. A., Sessler, J. L. and Lynch, V. J. Am. Chem. Soc. **1996**, 732, 5140–5141.
10. Gale, P. A. and Sessler, J. L. Chem. Commun. **1998**, 1–8.
11. Romero, J. R., Aragay, G. and Ballester, P. Chem. Sci. **2016**, 8, 491–498.
12. Kim, S. K. and Sessler, J. L. Acc. Chem. Res. **2014**, 47, 2525–2536.
13. Park, I. W., Yoo, J., Adhikari, S., Park, J. S., Sessler, J. L. and Lee, C. H. Chem. - A Eur. J. **2012**, 18, 15073–15078.
14. Escobar, L. and Ballester, P. Chem. Rev. **2021**, 121, 2445–2514.
15. Kim, J. S. and Quang, D. T. Chem. Rev. **2015**, 107, 3780–3799.
16. Wan, S. and Lu, W. Angew. Chemie - Int. Ed. **2017**, 56, 1784–1788.
17. Lima, J. C. and Rodríguez, L. Chem. Soc. Rev. **2011**, 40, 5442–5456.

18. Aguiló, E. Estructuras supramoleculares de oro(I) con propiedades luminescentes. Estudios de agregación y aplicaciones. 2017. Tesis Doctoral Universitat de Barcelona.

19. Gans, P., Sabatini, A. and Vacca, A. Talanta 1996, **43**, 1739–1753 (1996).

20. Hirose, K. A practical guide for the determination of binding constants. J. Incl. Phenom. **2001**, 39, 193–209.

21. Srivastava, V. K. and Yadav, R. Isothermal titration calorimetry. Data Processing Handbook for Complex Biological Data Sources. Elsevier Inc., **2019**. doi:10.1016/B978-0-12-816548-5.00009-5.

# CHAPTER 4

## The role of gold on the luminescent properties of coumarin derivatives

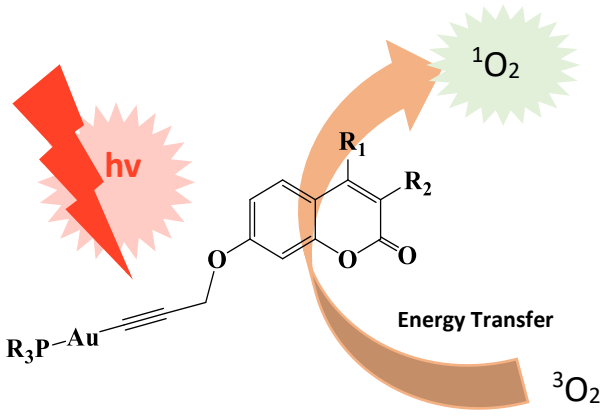


Part of this Chapter has been published in A. Pinto, C. Cunha, G. Aullón, J. C. Lima, L. Rodríguez, S. J. Seixas de Melo. J. Phys. Chem. **2021**, jp-2021-079855.R2. Accepted.

# 4. THE ROLE OF GOLD ON THE LUMINESCENT PROPERTIES OF COUMARIN DERIVATIVES

## 4.1. Introduction

Luminescent supramolecular materials have attracted considerable attention for being environmentally safer and are easier to modulate compared to the pure inorganic materials.[1] Currently, these compounds can be applied in electronic displays, luminescent switches, sensors and optical devices.[2]

In this field, phosphorescent compounds have become especially important for a variety of applications in different fields such as photodynamic therapy,[3] bioimaging,[4] optical limiting,[5] photon upconversion,[6] light-emitting diodes (OLEDs)[7] and oxygen sensing.[8] In particular, singlet oxygen production stays at the forefront of research due to its reactivity as a synthetic reagent,[9,10] as an intermediate in oxygenation reactions of polymers[11,12] or as a reactive oxygen species (ROS) for biological purposes.[13,14]

Unlike other molecules, oxygen's electronic ground state has a triplet spin, $O_2(X^3\sum_g^-)$. The two lowest energy excited electronic states of oxygen are the singlet states ($O_2(a^1\Delta_g)$ and $O_2(b^1\sum_g^+)$). In solution, $O_2(b^1\sum_g^+)$ generally decays to the $O_2(a^1\Delta_g)$ state before having time to react with another molecule.[15] Singlet oxygen can be formed, for example, by energy transfer from a photoexcited dye. This can be detected because singlet oxygen returns to its triplet ground state and, consequently, it emits phosphorescence at 1270 nm (Figure 4.1).

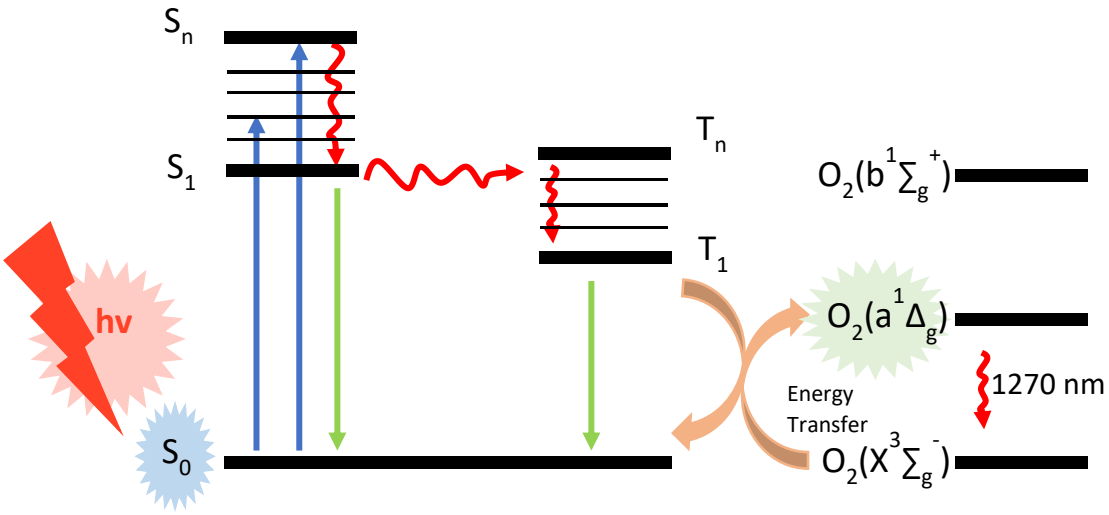


**Figure 4.1.** Diagram illustrating the formation of singlet oxygen.

Thus, the presence of a molecule (photosensitizer) that has populated its lowest energy triplet state is needed since the mechanism of producing singlet oxygen goes through an energy transfer from a triplet excited state. For this reason, an effective intersystem crossing is necessary and this may be favoured through different ways such as: host-guest interactions, halogen bonding,[16,17] hydrogen bonding,[18] aromatic carbonyl group[19,20] or charge transfer states.[21] But one of the most common and effective methods is the introduction of a heavy atom, such as a transition metal in the chemical structure of the photosensitizer due to its high spin orbit coupling. Among all the metals used in the literature for singlet oxygen production, gold(I) is scarcely explored and only few examples have been reported in the literature in this field.[22–24]

Coumarin derivatives are well-known for their photochemical and photophysical properties.[25] The spectroscopic properties of coumarin can easily be tuned by the introduction of substituents at different positions of the coumarin skeleton.[26,27] This allows to obtain compounds that strongly differ in their spectral and emissive abilities. Recently, coumarin derivatives have been received much attention due to their relative ease synthetic modification and excellent photophysical stability including high fluorescence quantum yields.[28] Currently, a variety of coumarin derivatives have been extensively studied in the research fields of organic optoelectric materials such as laser dyes[29,30] or aggregation induced emission (AIE) emitters.[31,32]

Thereby, coumarin derivatives can provide great possibilities of molecular design for the synthesis of gold(I) complexes. A few years ago, a series of new coumarin gold(I) coumarin complexes were reported in our group.[33] These complexes were found to favour the coumarin phosphorescent emission when the gold(I) atom was coordinated to the coumarin chromophore through an alkynyl moiety. Taking this into consideration, in this chapter, the synthesis and comprehensive photophysical characterization of different coumarin gold(I) derivatives was undertaken (Figure 4.2). The effect of the presence of different electrondonating/electronwithdrawing substituents at the coumarin ring on the resulting photophysical properties has been analysed. Additionally, the potential use of these complexes as photosensitizers for the generation of singlet oxygen was also investigated.

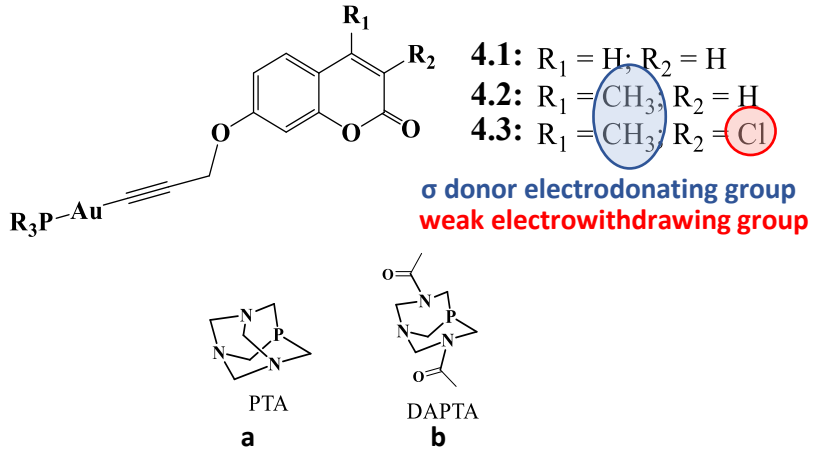


**Figure 4.2.** General structure of gold(I) derivatives synthesized in this chapter.

## 4.2. Results and Discussion

### 4.2.1. Synthesis and Characterization

The synthesis of the organic alkynyl ligands is the first step for the obtention of the gold(I) coumarin derivatives. The propargylation of coumarin derivatives have been prepared following the method previously reported by us (Scheme 4.1).[33] Commercially available hydroxycoumarins **4.L1-3** were made react with propargyl bromide in deoxygenated acetone in the presence of $K_2CO_3$. The propynyloxycoumarins **4.1-3** were obtained after 18-36 h of stirring under reflux and after purification by column chromatography in good yields (ca. 75%).

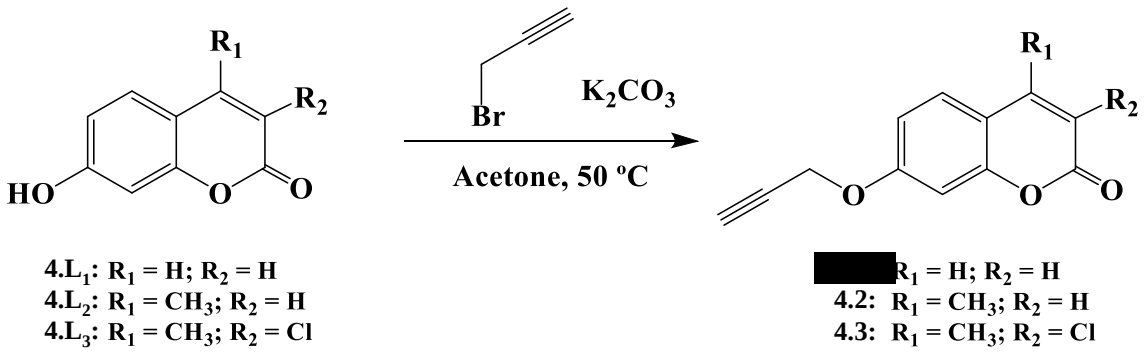


**Scheme 4.1.** Synthesis of propynyloxycoumarin ligands.

The compounds **4.1** and **4.2** were previously described[33] and their correct formation was corroborated by comparison of the previous spectroscopic data. Compound **4.3** has been characterized by $^{1}H$ NMR, IR and mass spectrometry showing the signals of the protons of the coumarin and the propargyl groups in the NMR spectrum and the typical vibrations of both carbonyl and terminal alkynyl groups in the same molecule in the corresponding IR.

Gold(I) coumarin derivatives **4.1-3a** (containing PTA phosphane) and **4.1-3b** (containing DAPTA phosphane) were obtained by deprotonation of the terminal alkynyl proton of **4.1-3** with a KOH solution in methanol and by the subsequent addition of a stoichiometric amount of [AuCl($PR_3$)] ($PR_3$ = PTA or DAPTA) complexes dissolved in dichloromethane (Scheme 4.2). Compounds **4.1a-b** and **4.2a-b** were previously described[33] and the recorded spectroscopic data indicates their correct formation in pure form.

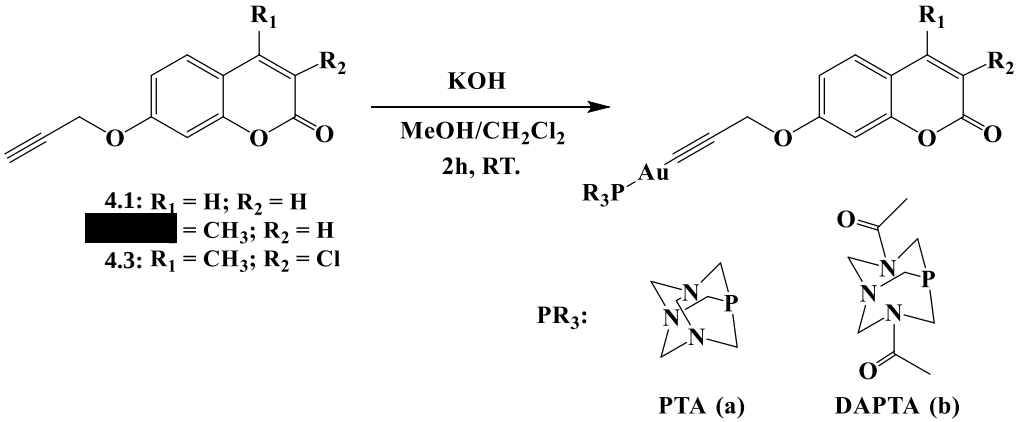


**Scheme 4.2.** Synthesis of the propynyloxycoumarin phosphane gold(I) complexes **4.1-3a** and **4.1-3b**.

The complexes **4.3a-b** were characterized by $^{1}H$ and $^{31}P$ NMR and IR spectroscopy and ESI(+) mass spectrometry. The correct formation of the complexes was evidenced by the disappearance of the terminal alkynyl proton clearly observed in the corresponding IR and $^{1}H$ NMR spectra. The protons of the phosphanes follow the typical patterns of PTA and DAPTA (Figure 4.3). $^{31}P\{^{1}H\}$ NMR spectra show also a single peak ca. 10 ppm downfield shifted with respect to the [AuCl($PR_3$)] precursors, as observed for other similar compounds.[33–38] The molecular peaks have been obtained by ESI (+) mass spectrometry for all the [M + $H^+$] monoprotonated species.

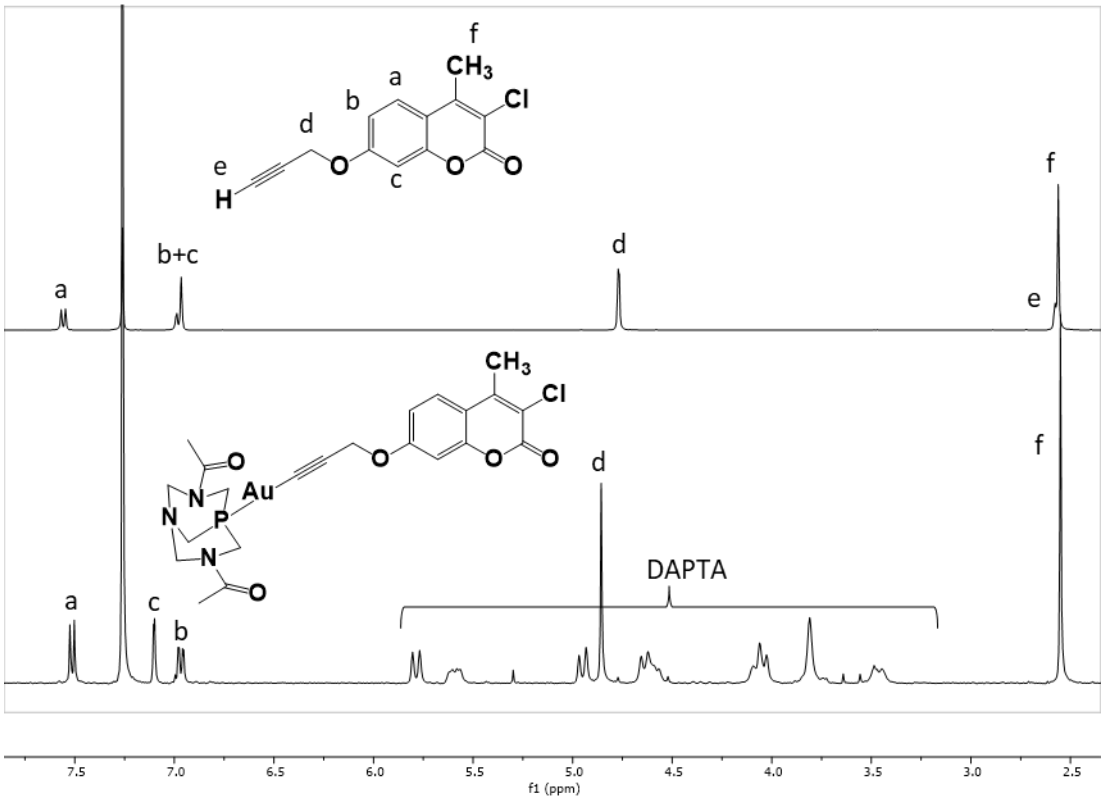


**Figure 4.3**. $^{1}H$ NMR spectra of **4.3** and **4.3b** in $CDCl_3$.

### 4.2.2. Photophysical Characterization

Absorption, fluorescence emission and excitation spectra of all the studied gold(I) complexes (**4.1a-b**, **4.2a-b** and **4.3a-b**) and the different propynyloxycoumarin (**4.1-3**) precursors were recorded in acetonitrile at room temperature (293 K) and are displayed in Figure 4.4. Phosphorescence emission was recorded in 2-methyltetrahydrofuran at low temperature, 77K (Figure 4.4). The absorption, fluorescence and phosphorescence

emission data, Stokes' shift and transient absorption ($T_1 \rightarrow T_n$) for all complexes are summarized in Table 4.1.

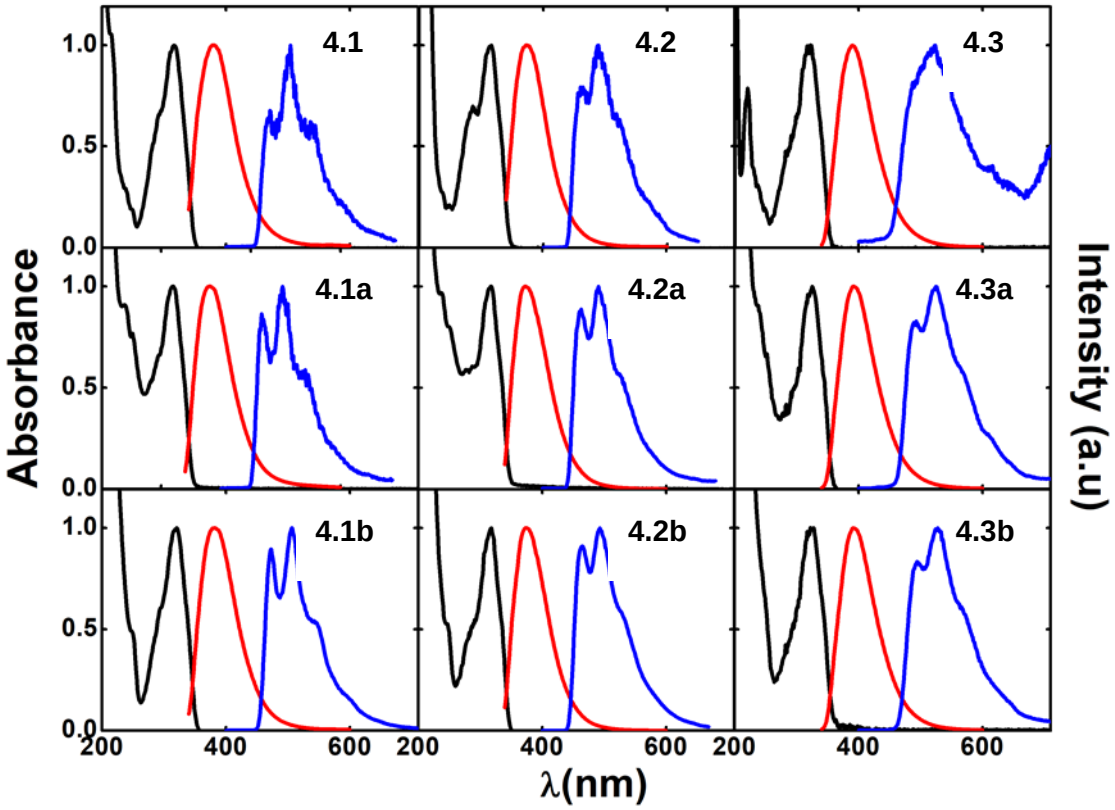


**Figure 4.4.** Normalized absorption (black line), fluorescence emission (red line) spectra in acetonitrile, at $1.3 \cdot 10^{-5}$ M concentration, and at 293K, and phosphorescence emission (blue line) spectra in 2-MeTHF, at 77K, of alkynylcoumarin phosphane gold(I) complexes and alkynyl coumarin precursors (**4.1-3**).

**Table 4.1**. Absorption, emission and phosphorescent maxima, Stokes' shift and transient $\boldsymbol{T_1 \rightarrow T_n}$ maxima of alkynylcoumarin phosphane gold(I) complexes (**4.1a-b**, **4.2a-b** and **4.3a-b**) and propynyloxycoumarin precursors (**4.1-3**).

| Compound | $\lambda_{abs,}$ (nm) | $^{Fluo}_{max}(S_1 \rightarrow S_0)$ (nm) | $^{Phosp}_{max}(T_1 \rightarrow S_0)$ (nm) | $\Delta_{ss}$ ($cm^{-1}$) | $^{abs}_{max}(T_1 \rightarrow T_n)$ (nm) |
|---|---|---|---|---|---|
| **4.1** | 316 | 381 | 504 | 5399 | - |
| **4.1a** | 320 | 381 | 503 | 5003 | 480 |
| **4.1b** | 321 | 381 | 507 | 4906 | 480 |
| **4.2** | 316 | 374 | 489 | 4908 | - |
| **4.2a** | 318 | 373 | 491 | 4637 | 480 |
| **4.2b** | 318 | 374 | 493 | 4709 | 480 |
| **4.3** | 323 | 390 | 524 | 5319 | - |
| **4.3a** | 325 | 393 | 525 | 5324 | 480 |
| **4.3b** | 328 | 392 | 528 | 4978 | 480 |

Absorption and emission spectra of gold(I) complexes are identical to those of their propynyloxycoumarin precursors **4.1-3** as previously observed for **4.1a-b** and **4.2a-b** in methanol.[33] This indicates that the spectral properties are essentially dependent on the propynyloxycoumarin ligand. The absorption spectra display a π-π* intraligand transition band at ca. 315-330 nm related to the coumarin unit.[39–43] The coumarin fluorescence emission is observed at ca. 375-395 nm and the phosphorescence vibronically structured band at ca. 490-530 nm is only observed at low temperature (77 K). The small Stokes' shift in all the compounds supports the fluorescence origin of the emission.

A general trend can be deduced comparing the absorption and emission maxima of the compounds. There is a red-shift in the order **4.2, 4.2a-b** < **4.1, 4.1a-b** < **4.3, 4.3a-b** where the presence of an electrondonating group (**4.2** derivatives) induces a blue-shift of the bands. On the contrary, the introduction of an electronwithdrawing group, such as the chlorine in **4.3**, induces a red-shift of the band, modifying the transition energy.

Ns-transient absorption (ns-TA) spectra were recorded in order to get further information of the triplet excited state population at room temperature, since phosphorescence was only detected at low temperature. The transient triplet-triplet

absorption spectra of the compounds were recorded in acetonitrile solutions at 293 K by using the laser flash photolysis equipment upon excitation of the samples at 266 nm of degassed acetonitrile solutions and are depicted in Figure 4.5. It can be recorded a broad triplet-triplet absorption band with a maximum that is basically constant for all the gold(I) compounds (ca. 480 nm). Thus, this means that the triplet state of all compounds is populated at room temperature and that it is essentially localized at the coumarin unit.

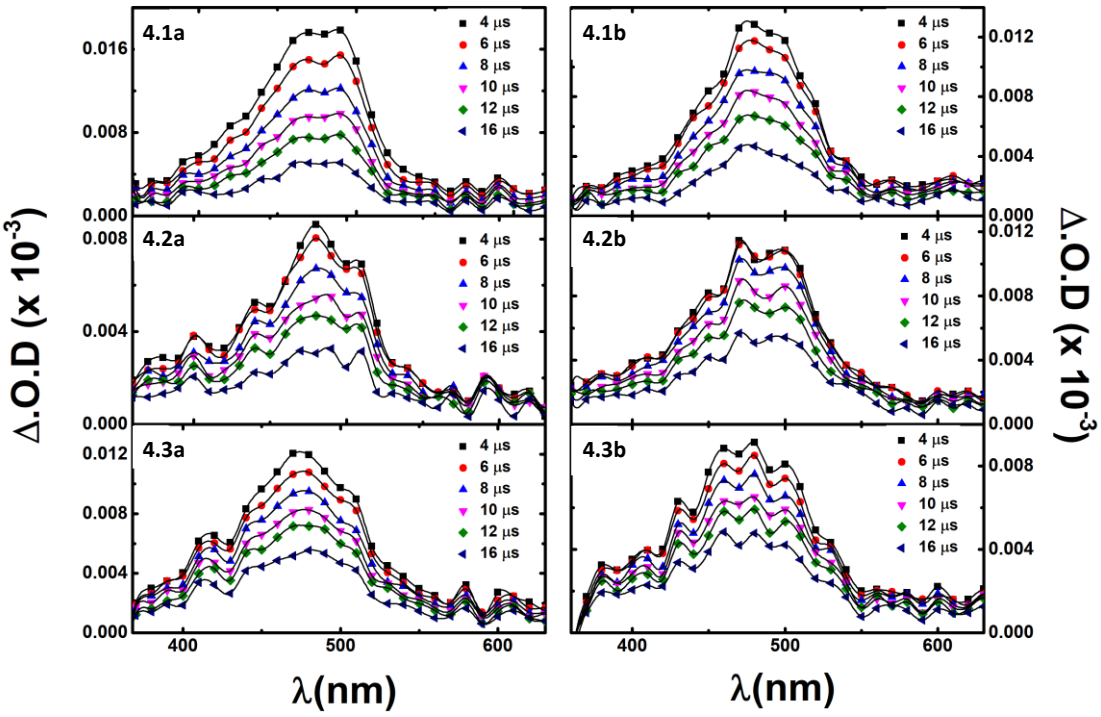


**Figure 4.5.** Transient triplet-triplet absorption spectra at selected time delays (right inset), time evolution of the transients for acetonitrile solutions of the corresponding gold(I) complexes (**4.1a-b**, **4.2a-b**, **4.3a-b**), at T=293 K. All spectra obtained with $N_2$ saturated solutions.

Fluorescence, phosphorescence, singlet oxygen sensitization quantum yields and lifetimes were measured, and the corresponding rate constants were calculated and summarized in Table 4.2. Fluorescence quantum yields do not change in the absence of oxygen, confirming the assignment of a singlet to singlet transition. A general trend can be deduced comparing the fluorescence and phosphorescence quantum yields at low temperature (77 K). Phosphorescence quantum yields increase when gold(I) is

incorporated in the chemical structure. This is a clear indication that gold promotes the intersystem crossing due to the heavy atom effect (increase of spin-orbit coupling, SOC). An exception is the case of gold(I) complexes **4.3a-b**, whose phosphorescent quantum yields are barely affected in comparison with their organic precursor **4.3**. Additionally, the sum of the fluorescent and phosphorescence quantum yields is relatively high (always above 67%) and in the cases of **4.2b** and **4.3** are equal to 1.

.

**Table 4.2**. Photophysical properties including quantum yield (fluorescence, $\phi_F$, phosphorescence, $\phi_{Ph}$, singlet oxy crossing, $\phi_T$, and internal conversion, $\phi_{IC}$), lifetimes ($\tau_F$, $\tau_{Ph}$ and $\tau_T$) and rate constant ($k_F$, $k_{NR}$, $k_Q$, $k_{IC}$ and $k_{ISC}$) ob ($N_2$ sat.) acetonitrile solutions at 293K and 77K for the investigated compounds

| Compound | $\phi_F$ (with $O_2$) 293K | $\phi_F$ ($N_2$ sat.) 293K | $\phi_F$ 77K | $\phi_{Ph}$ 77K | $\phi_F + \phi_{Ph}$ 77K | $\tau_F$ (ns) 293K | $\tau_{Ph}$ (s) 77K | $\tau_T$ (μs) 293K | $\phi_\Delta$ | $\phi_T$ | $\phi_{IC}$ |
|---|---|---|---|---|---|---|---|---|---|---|---|
| **4.1** | 0.008 | 0.011 | 0.621 | 0.048 | 0.669 | 0.012 | 0.77 | - | - | - | - |
| **4.1a** | 0.01 | 0.011 | 0.578 | 0.134 | 0.712 | 0.032 | 0.68 | 40 | 0.04 | 0.05 | 0.94 |
| **4.1b** | 0.011 | 0.012 | 0.558 | 0.133 | 0.691 | 0.038 | 0.65 | 10 | 0.04 | 0.35 | 0.64 |
| **4.2** | 0.013 | 0.016 | 0.677 | 0.198 | 0.875 | 0.035 | 1.06 | - | - | - | - |
| **4.2a** | 0.024 | 0.025 | 0.406 | 0.347 | 0.753 | 0.084 | 0.84 | 26 | 0.06 | 0.31 | 0.67 |
| **4.2b** | 0.03 | 0.032 | 0.539 | 0.461 | 1 | 0.078 | 0.74 | 15 | 0.07 | 0.24 | 0.73 |
| **4.3** | 0.613 | 0.666 | 0.975 | 0.05 | 1 | 2.15 | 0.224 | - | - | - | - |
| **4.3a** | 0.658 | 0.711 | 0.628 | 0.058 | 0.686 | 2.36 | 0.145 | 34 | 0.12 | 0.11 | 0.23 |
| **4.3b** | 0.665 | 0.728 | 0.52 | 0.048 | 0.568 | 2.5 | 0.154 | 37 | 0.18 | 0.24 | 0.10 |

$$\phi_{IC} = 1-(\phi_F + \phi_T); k_F = \frac{\phi_F}{\tau_F}; k_{NR} = \frac{(1-\phi_F)}{\tau_F}; k_{IC} = \frac{1-\phi_T-\phi_F}{\tau_F}; k_{ISC} = \frac{\phi_T}{\tau_F}$$

Fluorescence is a radiative pathway that competes with the following internal factors: the non-radiative internal conversion to the ground state and the intersystem crossing to the triplet state (Figure 4.6).

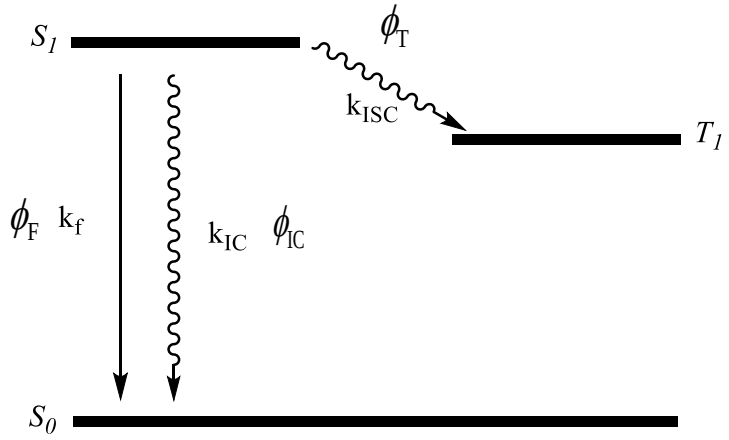


**Figure 4.6.** Simplified diagram of the deactivation processes from the excited states.

The values of the radiative ($k_F$), internal conversion ($k_{IC}$), and the intersystem crossing ($k_{ISC}$) rate constants were calculated for all the compounds. In general, $k_F$ remains constant for all the compounds with values ranging from 0.3-0.7 $ns^{-1}$. The internal conversion, which is radiationless decay pathway is dominant for **4.1**, **4.1a-b** and **4.2**, **4.2a-b**. Chlorine derivatives (**4.3**, **4.3a-b**) are an exception where the internal conversion rate constant and the intersystem crossing constant is much lower than for all the others compounds in agreement with the highest recorded values of the fluorescence quantum yields.

The triplet quantum yields population ($\phi_T$) of gold(I) complexes are in the range of 0.05-0.35% which are moderate. Interestingly, the incorporation of a methyl group at the 4 position of the coumarin (**4.2a-b**) favour the intersystem crossing as previously observed in the group.[33] Additionally, the phosphane plays an important role in compounds **4.1a-b**, being the complex containing DAPTA (**4.1b**), the gold(I) complex that presents the highest $\phi_T$.

### 4.2.3. Singlet oxygen production

Singlet oxygen, $^1O_2$, is usually formed when the excitation energy is transferred from the triplet of a molecule acting as sensitizer to the triplet ground state of the oxygen. The molecule used as photosensitizer should exhibit the following properties: (a) high

absorption coefficient in the spectral region of the excitation wavelength; (b) a well-defined triplet state with appropriate energy, $E_T \geq 95$ kJmol$^{-1}$, to allow the efficient energy transfer to the oxygen ground state; (c) high quantum yield of the triplet state, $\phi_T \geq 0.4$; (d) long triplet state lifetime, $\tau_T > 1$ µs, since the efficiency of the photosensitizer is dependent on the photophysical properties of its lowest excited triplet state; and (e) high photo-stability.[44]

Since the gold(I) compounds under study present moderate triplet quantum yields ($\phi_T$), considering an efficient energy transfer process is feasible. For this reason, $^1O_2$ quantum yields, $\phi_\Delta$, were determined by direct measurement of the phosphorescence at 1270 nm using 1H-phenal-1-one as standard reference. The $\phi_\Delta$ values (4-18%) obtained are moderate compared with other gold(I) complexes found in the literature.[22,23] Interestingly, it can be observed that the phosphane plays a direct role in this process since an increase of the singlet oxygen quantum yields is observed in the cases of compounds **4.2b** and **4.3b**. The compounds containing an electronwithdrawing group, **4.3a-b**, present the highest singlet oxygen quantum yields. Although these compounds do not present the highest values of triplet quantum yields, they have the highest triplet lifetimes and the ability to produce singlet oxygen depends largely on the production of a long-lived triplet state.[45–48]

Rate constants for the energy transfer from the gold(I) complexes to the molecular oxygen were obtained from equation 1,

$$k_Q = \left(\frac{1}{\tau_T} - \frac{1}{\tau_T^0}\right) \cdot \frac{1}{[Q]} \quad (1)\cdot$$

where $\tau_T^0$ is the triplet lifetime in the absence of oxygen and the $\tau_T$ in the presence of oxygen and [Q] is the concentration of the quencher (oxygen).

The values of the rate constants, $k_Q$ are displayed in Table 4.2 and are in the order of $10^{10}$ s$^{-1}$, which are slightly higher than the pure controlled diffusion reaction rates in this solvent ($k_{diff} = 1.9 \cdot 10^{10}$ Lmol$^{-1}$s$^{-1}$). This indicates that the process is not purely diffusional and an interaction between the ground states of the molecular oxygen and the gold(I) complexes, which increases the rate of the energy transfer process, cannot be discarded.

### 4.2.4. Theoretical studies

Theoretical studies were performed in collaboration with Prof. Gabriel Aullón from the Universitat de Barcelona in order to understand better the obtained photophysical results. The different molecular geometries were optimized by DFT calculations, and the main expected transitions have been analysed. Absorption spectra for the alkynyl coumarins precursors and gold(I) complexes reproduce the same trends than the experimental data. These studies let us identify that the observed shift of absorption maxima in the order **4.2, 4.2a-b** < **4.1, 4.1a-b** < **4.3, 4.3a-b** is due to the modification in the HOMO-LUMO energy gap which is affected with the substituents located at the 3 and 4 position at the coumarin ring (Figure 4.7).

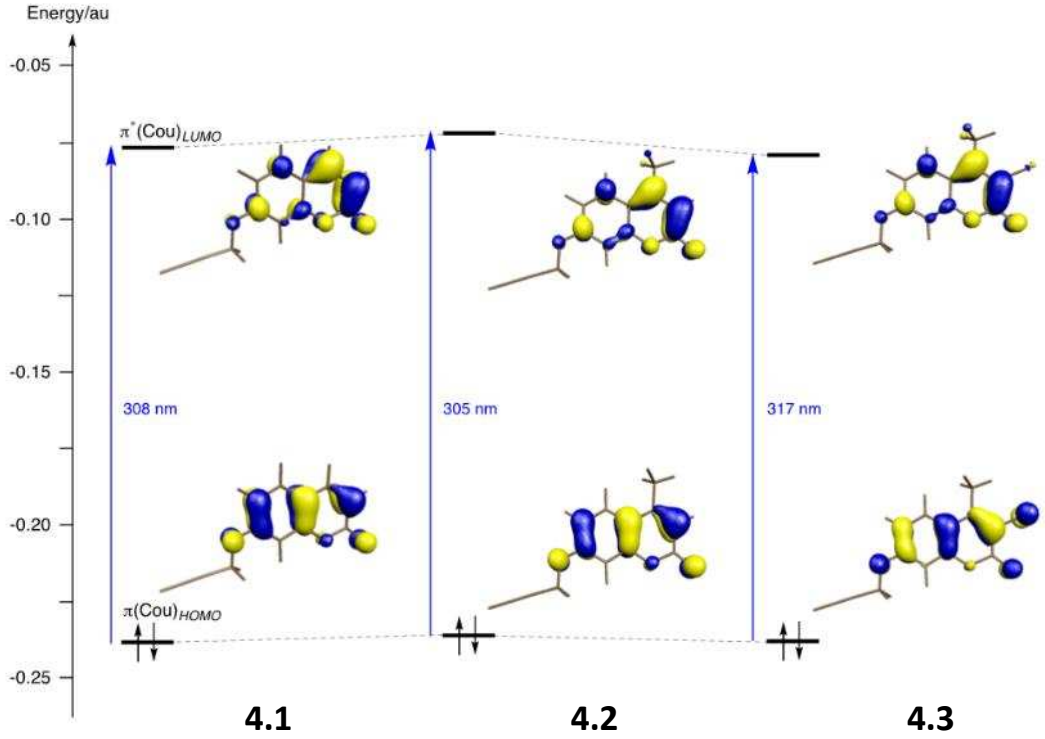


**Figure 4.7**. Schematic representation of main expected transition in the absorption spectra of organic coumarins (**4.1-3**).

The phosphorescent properties and the probability of the intersystem crossing of the coumarin derivatives is determined not only from the nature of the excited singlet and triplet states but also by the energy gap between them. In this way, the geometries for the first singlet and triplet states were optimized. The $S_1$-$T_1$ energy gaps and the bent angles were also calculated. The energy of the triplet state and the energy gap obtained is practically independent of the coordination of gold(I) in the chemical structure, and there is only small variation between each family of coumarins (Table 4.3).

**Table 4.3**. Calculated energies for lowest singlet and triplet state $S_1$ and $T_1$, (in eV, and nm in parenthesis) from the ground state $S_0$ for the coumarin derivatives in acetonitrile solution. $S_1$-$T_1$ energy gap and bent angles ($\theta C^4 \cdot O^1$) are also shown.

| Compound | $S_1$ | $T_1$ | $S_1$-$T_1$ Energy gap | ($\theta C^4 \cdot O^1$) |
|---|---|---|---|---|
| **4.1** | 4.02 (308) | 2.62 (473) | 1.24 | 179.9 |
| **4.1a** | 3.89 (318) | 2.61 (475) | 1.13 | 180.0 |
| **4.1b** | 3.98 (312) | 2.61 (475) | 1.22 | 179.8 |
| **4.2** | 4.07 (305) | 2.70 (459) | 1.2 | 179.7 |
| **4.2a** | 4.00 (310) | 2.69 (461) | 1.15 | 179.2 |
| **4.2b** | 4.03 (308) | 2.69 (460) | 1.18 | 179.7 |
| **4.3** | 3.91 (317) | 2.53 (489) | 1.17 | 165.7 |
| **4.3a** | 3.82 (325) | 2.53 (491) | 1.1 | 165.1 |
| **4.3b** | 3.87 (320) | 2.53 (490) | 1.15 | 165.1 |

A detailed analysis of the optimized geometries of all the compounds has been carried out in order to understand the absence of phosphorescence in the family of compounds **4.3**. Although in all cases the atoms remain in more or less planar environment ($\theta C^4 \cdot O^1$) in Table 4.3, a significant deformation of the lactone rings is observed in the compounds of series **4.3**, being practically planar in the families **4.1** and **4.2**. So, a major structural arrangement is needed to involve triplet states in the family of compounds **4.3**, even though a low gap is calculated, and therefore only fluorescence is observed.

## 4.3. Conclusions

Three series of gold(I) complexes containing different substituents in the chemical structure of propargyloxycoumarin chromophores were successfully synthesized and a comprehensive and in depth photophysical characterization was performed. The photophysical properties of the gold(I) complexes are mainly due to the propargyloxycoumari ligands since they present a similar profile. The experimental data together with the theoretical calculations show that the excited state is mainly located in the ligand. Internal conversion dominates the deactivation of the excited states of gold(I) complexes **4.1a-b** and **4.2a-b**, whereas the dominance of the radiative fluorescence decay is observed for the compounds that contain the electronwitdrawing group, **4.3a-b**. Finally, the gold(I) compounds sensitize singlet oxygen with the highest $\phi_\Delta$ values of 12% and 18% obtained for the chloro derivatives (**4.3a-b**).

## 4.4. Experimental Section

### 4.4.1. General procedures

All manipulations have been performed under pre-purified $N_2$ using standard Schlenk techniques. All solvents have been distilled from appropriated drying agents. Commercial reagents 1,3,5-triaza-7-phosphatricyclo[3.3.1.13.7]decane (PTA, Aldrich 97%), 3,7-diacetyl-1,3,7-triaza-5- phosphabicyclo[3.3.1]nonane (DAPTA, Aldrich 97%). Deoxygenation was done by bubbling the solutions with a stream of argon or nitrogen during approximately 20 min. All measured solutions were freshly prepared (within the day) unless noted otherwise. Literature methods have been used to prepare [AuCl($PR_3$)] ($PR_3$ = PTA,[49] DAPTA[50]), **4.1**[33], **4.1a-b**[33], **4.2**[33], **4.2a-b**.[33]

### 4.4.2. Physical Measurements

Infrared spectra have been recorded on a FT-IR 520 Nicolet Spectrophotometer. $^1$H NMR ($\delta$(TMS) = 0.0 ppm), $^{31}$P NMR ($\delta$(85% $H_3PO_4$) = 0.0 ppm) spectra have been obtained on a Varian Mercury 400 and Bruker 400 (Universitat de Barcelona). Electrospray-Mass spectra (+) have been recorded on a Fisons VG Quatro spectrometer (Universitat de Barcelona). Absorption spectra were obtained in a 5 mm or 10 mm quartz cuvette in acetonitrile on a Cary 5000 UV-Vis-NIR or Shimadzu UV-2450 spectrophotometer. The emission spectra of the compounds in solution were obtained in fluorescence quartz cuvette of 5 mm or 10 mm path length, using a Horiba-Jobin-Yvon Fluorolog 3.22 or Fluoromax spectrometers. Phosphorescence spectra and decays were obtained with the D1934 unit of Fluoromax 3.22 spectrometer. All the fluorescence and phosphorescence spectra were corrected for the wavelength response of the system with the appropriate correction files obtained for the instrument.

-Fluorescence Quantum Yields determination

Emission quantum yields of the compounds were determined with Hamamatsu Quantaurus QY absolute photoluminescence quantum yields spectrometer model C11437 (integration sphere) at the Departamento de Quimica from Universidade de Coimbra during a short stage period.

-Lifetimes measurements

Fluorescence lifetimes have been recorded at the Departamento de Quimica from Universidade de Coimbra.

Fluorescence lifetimes were measured by using a home-built picosecond time-correlated single photon counting (TCSPC) apparatus.[51] It consists of a IBH PicoLED (with excitation at 275 nm) as excitation source light, a double substractive Oriel Cornestone 260 monochromator and Hamamatsu microchannel plate photomultiplier (R3809U-50). The signal acquisition and data processing are performed with Becker & Hickl SPC-630-TCSPC module. The fluorescence decays and the intrumental response functions (IRF) were collected using 1024 channels in time scales varyig from 3.26 to 6.4 ps/channel scale, until 2000-5000 counts at maximum were reached. The full width at half-maximum (fwhm) f the IRF was 0.95-1.10 ns. Deconvolution of the fluorescence decay curves was performed using the modulation function methods as implemented by Stricker et al. in the SAND[52] which allows a value of ca. 10% of the fwhm (9 ps) as the time resolution of the equipment with this escitation source.

- Laser Flash Photolysis Experiments.

Transient absorption spectra were measured using flash photolysis setup composed of a LKS 60 ns lased photolysis spectrometer at the Departamento de Quimica from Universidade de Coimbra. Applied Photophyics with a Brilliant Q-Switch Nd YAG laser from Quantel using the fourth harmonics ($\lambda_{ex}$ = 266 nm, laser pulse half width equal to 6 ns). Transient absorption spectra were obtained by monitoring the optical density change at 5-10 nm intervals at least 10 decays at each wavelength.

- Singlet Oxygen Yields

Room-temperature singlet oxygen phosphorescence was detected at 1270 nm with a Hoiba-Jobin-Yvon SPEX Fluorog 3.22 using the Hamamatsu R5509-42 photomultiplier previously reported at the Departamento de Quimica from Universidade de Coimbra. The use of a Schott RG 1000 filter was essential to eliminate from the infrared signal all the first harmonic contribution of sensitizer emission in the region below 850 nm. The singlet oxygen formation quantum yield was then determined by direct measurement of the phosphorescence at 1270 nm following irradiation of the aerated solution in acetonitrile of the samples. 1H-phenal-1-one in acetonitrile ($\phi_\Delta$ = 0.98) was used as standard reference,[53] applying eq. (2).

$$\phi_\Delta = \phi_\Delta^{ref} \frac{Emission_{1270\,nm}}{Emission_{1270\,nm}^{ref}} \qquad (2)$$

with $\phi_\Delta^{ref}$ the singlet oxygen formation quantum yield of the reference compound.

### 4.4.3. Synthesis and Characterization

**Synthesis of 3-chloro-4-methyl-7-(prop-2-in-1-yloxy)-1-benzopyran-2-one (4.3)**

Solid 3-chloro-4-methyl-7-hydroxy-1-benzopyran-2-one (0.20 g, 0.95 mmol) and $K_2CO_3$ (0.164 g, 1.2 mmol) were dissolved in deoxygenated acetone (50 mL). After 5 min of stirring, propargyl bromide (132 µL, 1.2 mmol) was added dropwise and the solution of the reaction was concentrated to dryness, extracted with ethyl acetate-water, and purified by silica chromatography using dichloromethane-ethyl acetate, 9:1, as an eluent to obtain a white solid in 75% yield (277 mg).

$^1$H NMR ($CDCl_3$, ppm): 7.56 (d, J = 8.4 Hz, 1H, O–C–CH–CH), 6.98 (d, J = 8.4 Hz, 1H, O–C–CH–CH), 6.96 (s, 1H, CO–CH–C), 4.77 (d, J = 2 Hz, 2H, $CH_2$), 2.58 (t, J = 2.4 Hz, 1H, C≡CH), 2.56 (s, 3H, $CH_3$). IR (KBr, $cm^{-1}$): 2100 (C≡C), 1670 (C=O). ESI-MS (+) m/z: 249.03 ($[M+H]^+$, calc: 249.02).

**Synthesis of [Au{3-chloro-4-methyl-7-(prop-2-in-1-yloxy)-1-benzopyran-2-one}-(PTA)] (4.3a)**

A Solution of KOH (10.4 mg, 0.18 mmol) in methanol (2 mL) was added to a solution of 3-chloro-4-methyl-7-(prop-2-in-1-yloxy)-1-benzopyran-2-one (25 mg, 0.11 mmol) in methanol (5 mL). After 30 min of stirring a dichloromethane solution (5 mL) of [AuCl(PTA)] ( 41.5 mg, 0.11 mmol) was added and the solution was maintained at room temperature protected from the light with aluminium foil. After 1h of stirring, the solution was concentrated to ca. 2 mL and hexane (5 mL) was added to precipitate an orange pale solid which was filtered and obtained in 47% yield (30mg).

$^1$H NMR ($CD_3CN$, ppm): 7.67 (d, J = 8.8 Hz, 1H, O–C–CH–CH), 6.99 (d, J = 8.8 Hz, 1H, O–C–CH–CH), 6.93 (s, 1H, CO–CH–C), 4.81 (s, 2H, $CH_2$), 4.52-4.36 (AB q, J = 13 Hz, 6H, N-$CH_2$-N), 4.19 (s, 6H, N-$CH_2$-P), 2.54 (s, 3H, $CH_3$). $^{31}P\{^1H\}$ NMR ($CD_3CN$, ppm): -49.9. IR (KBr, $cm^{-1}$): 2100 (C≡C), 1670 (C=O). ESI-MS (+) m/z: 602.0667 ($[M+H]^+$, calc: 602.0596).

**Synthesis of [Au{3-chloro-4-methyl-7-(prop-2-in-1-yloxy)-1-benzopyran-2-one}-(DAPTA)] (4.3b)**

Details of synthesis of **4.3a** were also applied to the preparation of this compound but using DAPTA instead of PTA phosphane. A pale orange solid was obtained in 69% yield (50 mg).

$^{1}$H NMR ($CDCl_3$, ppm): 7.51 (d, J = 8.8 Hz, 1H, O–C–CH–CH), 7.10 (s, 1H, CO–CH–C), 6.96 (dd, J = 8.8 Hz, 1H, O–C–CH–CH), 5.78 (d, J = 14 Hz, 1H, N-$CH_2$-N), 5.58 (m, 1H, N-$CH_2$-P), 4.95 (d, J = 14 Hz, 1H, N-$CH_2$-N), 4.86 (s, 2H, $CH_2$), 4.66-4.56 (m, 2H, N-$CH_2$-N + N-$CH_2$-P), 4.09-4.03 (m, 2H, N-$CH_2$-N + N-$CH_2$-P), 3.81 (s, 2H, N-$CH_2$-P), 3.46 (d, J = 16 Hz, 1H, N-$CH_2$-P), 2.55 (s, 3H, $CH_3$), 2.10 (s, 6H, N-CO-$CH_3$). $^{31}$P{$^{1}$H} NMR ($CDCl_3$, ppm): - 22.4. IR (KBr, $cm^{-1}$): 2110 (C≡C), 1622 (C=O). ESI-MS (+) m/z: 674.0877 ($[M+H]^+$, calc: 674.0803).

## 4.5. References


1. Klauk, H. Organic Electronics: Materials, Manufacturing, and Application. Wiley-VCH, **2006**, ISBN: 978-3-527-31264-1.

2. Li, Z., Hu, X., Liu, G., Tian, L., Gao, H., Dong, X., Gao, T., Cao, M., Lee, C. S., Wang, P. and Wang, Y. J. Phys. Chem. C **2021**, 125, 1980–1989.

3. Collins, H. A., Khurana, M., Moriyama, E. H., Mariampillai, A., Dahlstedt, E., Balaz, M., Kuimova, M. K., Drobizhev, M., Yang, V. X. D., Phillips, D., Rebane, A., Wilson, B. C. and Anderson, H .L. Nat. Photonics **2008**, 2, 420–424.

4. Zhang, S., Hosaka, M., Yoshihara, T., Negishi, K., Iida, Y., Tobita, S. and Takeuchi, T. Cancer Res. **2010**, 70, 4490–4498.

5. Zhou, G., Wong, W. Y., Poon, S. Y., Ye, C. and Lin, Z. Adv. Funct. Mater. **2009**, 19, 531–544.

6. Baluschev, S., Miteva, T., Yakutkin, V., Nelles, G., Yasuda, A. and Wegner, G. Phys. Rev. Lett. **2006**, 97, 7–9.

7. Reineke, S., Lindler, F., Schwartz, G., Seidler, N., Walzer, K., Lüssem, B. and Leo, K. Nature **2009**, 459, 234–238.

8. Mills, A., Lepre, A., Theobald, B. R. C., Slade, E. and Murrer, B. A. Anal. Chem. **1997**, 69, 2842–2847.

9. Clennan, E. L. and Pace, A. Tetrahedron **2005**, 61, 6665–6691.

10. Matsumoto, M. Synthesis with Singlet Oxygen. In Singlet O2; Frimer, A. A., Ed.; CRC Press: Boca Raton, FL, **1985**.

11. Scurlock, R. D., Wang, B., Ogilby, P. R., Sheats, J. R. and Clough, R. L. J. Am. Chem. Soc. **1995**, 117, 10194–10202.

12. Gonçalves, E. S. and Ogilby, P. R. Langmuir **2008**, 24, 9056–9065.

13. Redmond, R. W. and Kochevar, I. E. Photochem. Photobiol. **2006**, 82, 1178.

14. Davies, M. J. Biochem. Biophys. Res. Commun. **2003**, 305, 761–770.

15. Halliwell, B. and Gutteridge, J. M. C. Biochem. J. **1984**, 219, 1–14.

16. Bolton, O., Lee, D., Jung, J. and Kim, J. Chem. Mater. **2014**, 26, 6644–6649.

17. Sun, X., Zhang, B., Li, X., Trindle, C. O. and Zhang, G. J. Phys. Chem. A **2016**, 120, 5791–5797.

18. Zhang, T., Wang, C. and Ma, X. Ind. Eng. Chem. Res. **2019**, 58, 7778–7785.

19. Zhao, C., Jin, Y., Wang J., Cao, X., Ma, X. and Tian, H. Chem. Commun. **2019**, 55, 5355–5358.

20. Yang, Z., Mao, Z., Zhang, X., Ou, D., Mu, Y., Zhang, Y., Zhao, C., Liu, S. Chi, Z., Xu, J., Wu, Y. C., Lu, P. Y., Lien, A. and Bryce, M. R. Angew. Chem. Int. Ed. **2016**, 128, 2221–2225.

21. Kuno, S., Akeno, H., Ohtani, H. and Yuasa, H. Phys. Chem. Chem. Phys. **2015**, 17, 15989–15995.

22. Goswami, S., Winkel, R. W. and Schanze, K. S. Inorg. Chem. **2015**, 54, 10007–10014.

23. Üçüncü, M., Karakus, E., Demirci, E. K., Sayar, M., Dartar, S. and Emrullahoglu, M. Org. Lett. **2017**, 19, 2522–2525.

24. Longevial, J. F., Cheikh, K., Aggad, D., Lebrun, A., van der Lee, A., Tielens, F., Clément, S., Morère, A., Garcia, M., Gary-Bobo, M. and Richeter, S. Chem. - A Eur. J. **2017**, 23, 14017–14026.

25. Wang, Z. S., Hara, K., Dan-oh, Y., Kasada, C., Shinpo, A., Suga, S., Arakawa, H. and Sugihara, H. J. Phys. Chem. B **2005**, 109, 3907–3914.

26. Donovalová, J., Cigán, M., Stankovicová, H., Gaspar, J., Danko, M., Gáplovský, A. and Hrdlovic, P. Molecules **2012**, 17, 3259–3276 .

27. Abid-Jarraya, N., Khemakhem, K., Turki-Guermazi, H., Abid, S., Saffon, N. and Fery-Forgues, S. Dyes. Pigment. **2016**, 132, 177–184.

28. Cui, R. R., Lv, Y. C., Zhao, Y. S., Zhao, N. and Li, N. Mater. Chem. Front. **2018**, 2, 910–916.

29. Jones, G., Jackson, W. R., Choi, C. Y. and Bergmark, W. R. J. Phys. Chem. **1985**, 89, 294–300.

30. Reactions, E. and Wepster, M. Ii, J. Am. Chem. Soc. **1973**, 833, 4699–4700.

31. Zhang, P., Liu, W., Niu, G., Xiao, H., Wang, M., Ge, J., Wu, J., Zhang, H., Li, Y. and Wang, P. J. Org. Chem. **2017**, 82, 3456–3462.

32. Bu, F., Duan, R., Xie, Y., Yi, Y., Peng, Q., Hu, R., Qin, A., Zhao, Z. and Tang, B. Z.. Angew. Chem. Int. Ed. **2015**, 54, 14492–14497.

33. Arcau, J., Andermark, V., Aguiló, E., Gandioso, A., Moro, A., Cetina, M., Lima, J. C., Rissanen, K., Ott, I. and Rodríguez, L. Dalton Trans. **2014**, 43, 4426–4436.

34. García-Moreno, E., Gascón, S., Rodriguez-Yoldi, M. J., Cerrada, E. and Laguna, M. S. Organometallics **2013**, 32, 3710–3720.

35. Moro, A. J., Rome, B., Aguiló, E., Arcau, J., Puttreddy, R., Rissanen, K., Lima, J. C. and Rodríguez, L. Org. Biomol. Chem. **2015**, 13, 2026–2033.

36. Gavara, R., Aguiló, E., Schur, J., Llorca, J., Ott, I. and Rodríguez, L. Inorg. Chim. Acta **2016**, 446, 189–197.

37. Andermark, V., Göke, K., Kokoschka, M., Abu el Maaty, M. A., Lum, C. T., Zou, T., Sun, R. W. Y., Aguiló, E., Oehninger, L., Rodríguez, L., Bunjes, H., Wölfl, S., Che, C. M. and Ott, I. J. Inorg. Biochem. **2016**, 160, 140–148.

38. Aguiló, E., Moro, A. J., Gavara, R., Alfonso, I., Pérez, Y., Zaccaria, F., Guerra, C. F., Malfois, M., Baucells, C., Ferrer, M., Lima, J. C. and Rodríguez, L. Inorg. Chem. **2018**, 57, 1017–1028.

39. Seixas De Melo, J. S., Cabral, C., Lima, J. C. and Maçanita, A. L. J. Phys. Chem. A **2011**, 115, 8392–8398.

40. Oliveira, E., Capelo, J. L., Lima, J. C. and Lodeiro, C. Amino Acids **2012**, 43, 1779–1790.

41. Heldt, J. R., Heldt, J., Stoń, M. and Diehl, H. A. Spectrochim. Acta Part A Mol. Biomol. Spectrosc. **1995**, 51, 1549–1563.

42. Ferrer, M., Gutiérrez, A., Rodríguez, L., Rossell, O., Lima, J. C., Font-Bardia, M. and Solans, X. Eur. J. Inorg. Chem. **2008**, 3, 2899–2909.

43. Seixas De Melo, J. and Fernandes, P. F. J. Mol. Struct. **2001**, 565–566, 69–78.

44. Quina, F. H. and Silva, G. T. M. J. Photochem. Photobiol. **2021**, 7, 100042.

45. Abdel-Shafi, A. A., Beer, P. D., Mortimer, R. J. and Wilkinson, F. Helv. Chim. Acta **2001**, 84, 2784–2795.

46. Girardot, C., Lemercier, G., Mulatier, J. C., Andraud, C., Chauvin, J. and Baldeck, P. L. Tetrahedron Lett. **2008**,49, 1753–1758.

47. El-Sayed, Y. S. and El-Daly, S. A. Chinese J. Chem. **2010**, 28, 363–370.

48. Yu, Z., Wu, Y., Peng, Q., Sun, C., Chen, J., Yao, J. and Fu, H. Chem. - A Eur. J. **2016**, 22, 4717–4722.

49. Assefa, Z., McBurnett, B. G., Staples, R. J. and Fackler, J. P. Inorg. Chem. **1995**, 34, 75–83.

50. Vergara, E., Miranda, S., Mohr, F., Cerrada, E., Tiekink, E. R. T., Romero, P., Mendía, A. and Laguna, M. Eur. J. Inorg. Chem. **2007**, 2926–2933.

51. Pina, J., Seixas de Melo, J., Burrows, H. D., Maçanita, A. L., Galbrecht, F., Bünnagel, T. and Scherf, U. Macromolecules **2009**, 42, 1710–1719.

52. Striker, G., Subramaniam, V., Seidel, C. A. M. and Volkmer, A. J. Phys. Chem. B **1999**, 103, 8612–8617.

53. Kristiansen, M., Scurlock, R. D., Iu, K. and Ogilby, P. R. J. Phys. Chem. **1991**, 95 5190–5197.

# CHAPTER 5

## Solvatochromic and mechanochromic BTD-gold(I) complexes

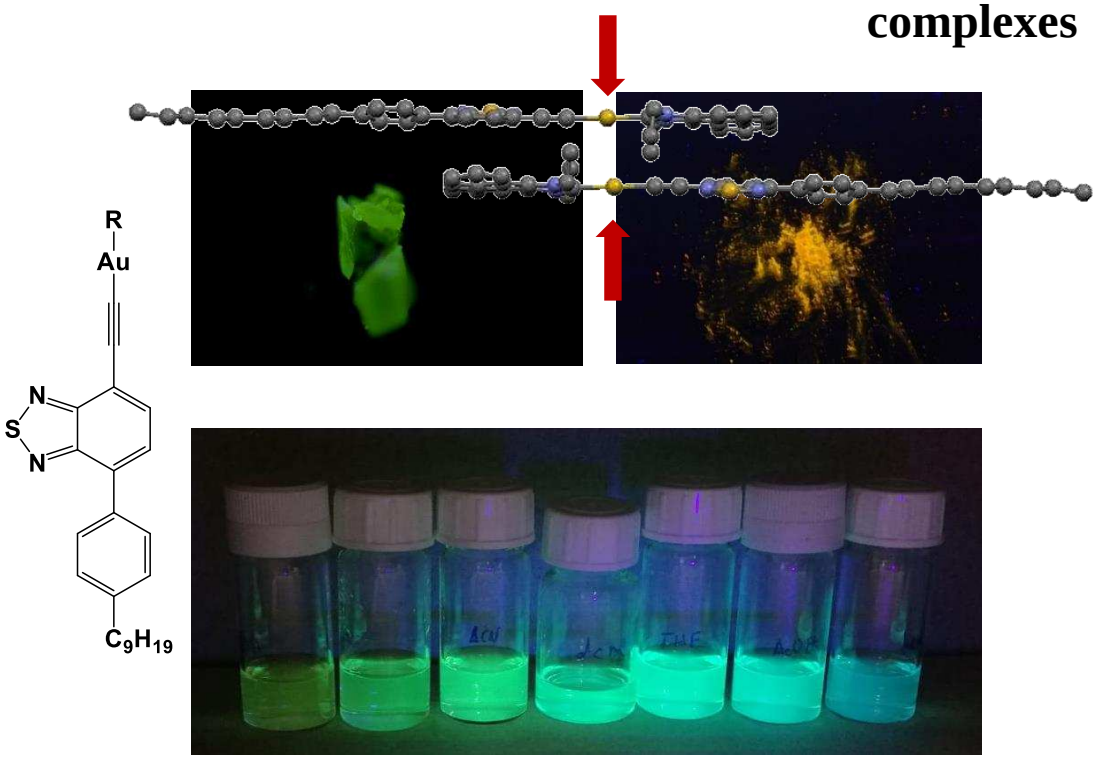


Part of this Chapter has been submitted in A. Pinto, M. Echeverri, B. Gómez-Lor., L. Rodríguez. Inorg. Chem. Front. QI-RES-07-2021-000849.

# 5. SOLVATOCHROMIC AND MECHANOCROMIC BTD-GOLD(I) COMPLEXES

## 5.1. Introduction

Organic electronics is an area of materials science dealing with electrically conductive polymers and conductive small molecules. In this kind of materials, the behavior of a single electron depends on the energy of the highest occupied molecular orbital (HOMO) and the lowest unoccupied molecular orbital (LUMO). The design of molecules with tunable HOMO and LUMO levels allows to achieve a control over the properties of the materials. The molecules with low HOMO/LUMO gap are of particular interest due to their ability to easily donate or accept an electron, which is the basic process in all organic electronic devices. There are two basic strategies to endow a low HOMO/LUMO gap: 1) by extending π-conjugation in the molecule and 2) by construction of covalent π-electron donor (D) and π-electron acceptor (A) compounds. On the basis of the second strategy, the intensity and position of the intramolecular charge transfer band of the donor-acceptor system depends on the nature of the linker between the two units and the substituents influencing the donor or acceptor character.

In the last few years, benzothiadiazole (BTD) unit (Figure 5.1), which is an electron acceptor fluorophore,[1] has emerged as a promising molecular design motif for various applications such as organic field-effect transistors,[2,3] light emitting diodes,[4] photovoltaics,[5] redox switchable donor-acceptor systems[6] or fluorescent probes,[7] among others.

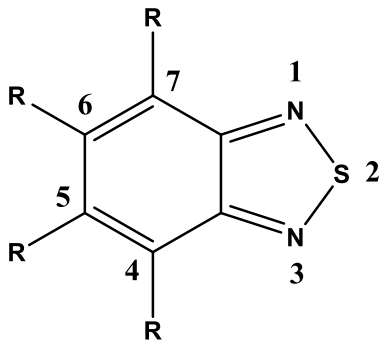


**Figure 5.1.** General chemical structure of the 2,1,3-Benzothiadiazole (BTD) unit.

In particular, BTD derivatives present desirable characteristics for organic light technology, such as: 1) the strong electron withdrawing properties that can be used for electron carriers; 2) high fluorescence quantum efficiencies;[1] 3) in general, well-ordered crystal structures due to their highly polarized properties, which engage a variety of supramolecular interactions such as hydrogen bonding, chalcogen S···N bonding orπ–π interactions;[7–9] 4) its electron deficiency moiety presents n-type semiconducting properties, which can be used as units of electron acceptors for conducting materials.[10]

The development of synthetic methods and research on the properties of purely organic BTD derivatives has been stimulated in the last years. However, the use of metals for the construction of new BTD-derivatives has received much less attention. The presence of two $sp^2$ nitrogen atoms on the thiadiazole ring to the BTD unit can act as a coordinating motif for transition metals.[11] On the other hand, the introduction of coordinating substituents on the benzene ring allows also the possibility of introducing a metal in the chemical structure. Interestingly, the combination of BTD ligand and a metal may induce new properties or modify some characteristics of the ligand.

On the other hand, organometallic architectures containing metal-acetylide motifs have received much attention due to strong interactions between the metal and the π-system of the ligand. Heavy atoms, such as gold(I), can improve the efficiency of the light emitting diodes by favouring an emissive triplet state through the promotion of the intersystem crossing (ISC) transition. Furthermore, as it has been stated in previous Chapters of this Thesis, gold(I) complexes are able to establish Au(I)···Au(I) interactions that play an important role on the resulting luminescent properties. Although gold(I) complexes generally display phosphorescence owing to the large spin-orbit coupling (SOC) constant ($\xi_{Au}$ ~ 5100 $cm^{-1}$), ligand-centered fluorescence has also been reported in a number of gold(I) complexes. Indeed, the few examples of gold(I) complexes containing BTD units that are reported in the literature display radiative fluorescence emission.[12,13]

The introduction of molecules in a thin film have emerged as a potential tool for their deposition on a substrate, since the emission in solid state of the compounds is crucial for practical device applications. Also, the introduction of the compounds in a polymeric matrix can enhance some of the properties of the compounds. Generally speaking, the luminescence of π-conjugated compounds is quenched in solid state due to a promotion of the non-radiative pathway.[14] Hence, the polymer allows the dispersion of the compounds and also ensure a rigid environment in order to reduce vibrational movements

since it presents long and intertwined chains. Recently, we observed in our group that the inclusion of gold(I) compounds in polymer matrixes such as PMMA or Zeonex improves the phosphorescence emission quantum yields of these compounds.[15,16]

In this context, we have designed in this chapter gold(I) complexes containing a BTD core with terminal Au-$PR_3$ or Au-carbene groups that contain flexible chain in order to favour the alignment and intermolecular contacts of the molecules. The effect of the steric hindrance and the planarity of the complexes on the resulting photophysical properties has been evaluated by the incorporation of two different types of ligands coordinated at the terminal position of the gold(I) atom: phosphanes and carbenes. Specifically, the resulting solvatochromic and mechanochromic properties and the inclusion of the molecules in polymeric matrixes have been explored.

## 5.2. Results and discussion

### 5.2.1. Synthesis and characterization

5.2.1.1. Synthesis of imidazolium salts

Three different imidazolium salts that differ in the aromaticity of the backbones were synthesized (Figure 5.2). **Im1** and **Im2** were synthesized by slight modifications of a previously reported experimental method (Scheme 5.1).[17,18] Briefly, the commercially available imidazole and benzimidazole were reacted with ethyl iodide in acetonitrile yielding the imidazolium salts **Im1** and **Im2** in good yields. **Im3** was synthesized by slight modifications of a previously reported experimental method (Scheme 5.2)[19] that requires four synthetic steps. The commercially available 9,10-phenanthrenequinone was initially reacted with formaldehyde and ammonium acetate in acetic acid to give rise the 1H-phenanthro[9,10-d]imidazole. Subsequent deprotonation of the NH proton by the addition of a strong base yields the ionic compound that was isolated by the addition of diethyl ether. Then, the alkylation of the deprotonated imidazole with ethyl iodide at 130ºC in DMF yields 1-ethylphenanthro[9,10-d]imidazole. Finally, a second alkylation with ethyl iodide provides the imidazolium salt **Im3**.

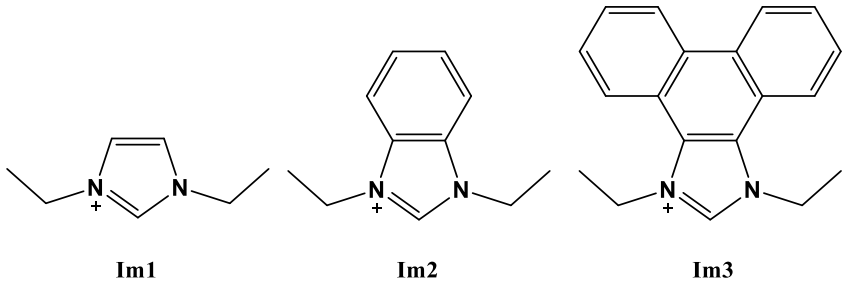


**Figure 5.2.** Imidazolium salts used in this work.

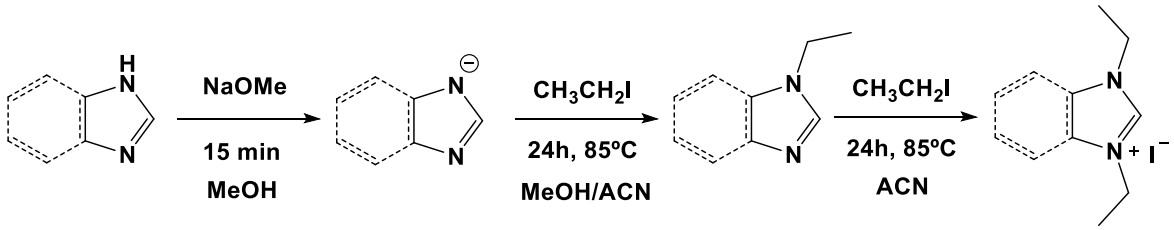


**Scheme 5.1.** Synthesis of the imidazolium salts **Im1** and **Im2**.

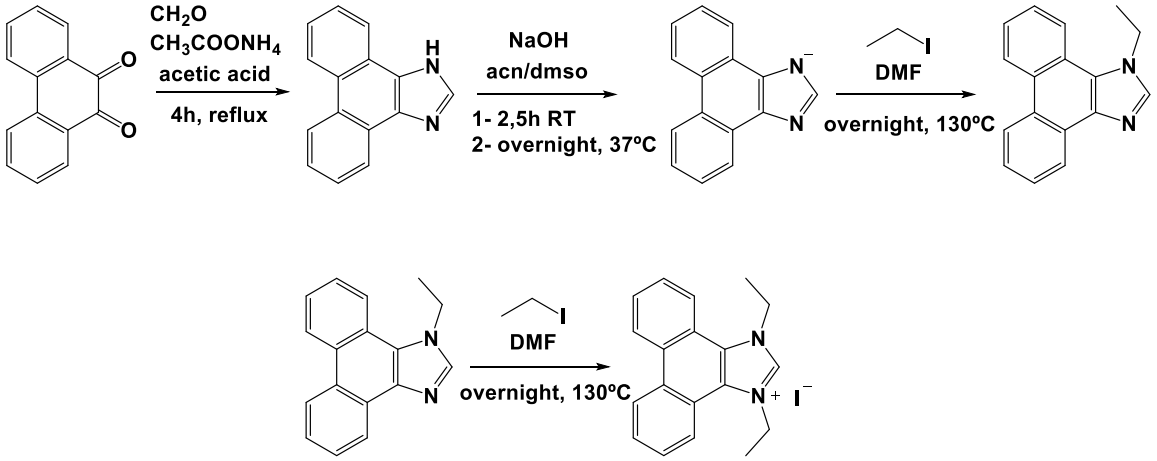


**Scheme 5.2.** Synthesis of the imidazolium salt **Im3**.

5.2.1.2. Synthesis of gold(I) benzothiadiazole-based derivatives containing phosphanes

The synthesis of gold(I) complexes was performed through two subsequent steps. The first step was the reaction of the previously synthesized 4-ethynyl-7-(4-nonylphenyl)benzo[c][1,2,5]thiadiazole, **5.L** with AuCl(tht) to yield [Au(4-ethynyl-7-(4-nonylphenyl)benzo[c][1,2,5]thiadiazole)]$_n$ (**5.1**). This polymer was isolated and made then react with one equivalent of the corresponding phosphane, $PR_3$, to afford the desired products [Au(4-ethynyl-7-(4-nonylphenyl)benzo[c][1,2,5]thiadiazole)($PR_3$)] ($PR_3$ = triethylphosphane (**5.2**), triphenylphosphane (**5.3**) and tri-1-naphthylphosphane (**5.4**)) in yields above than 70% (Scheme 5.3).

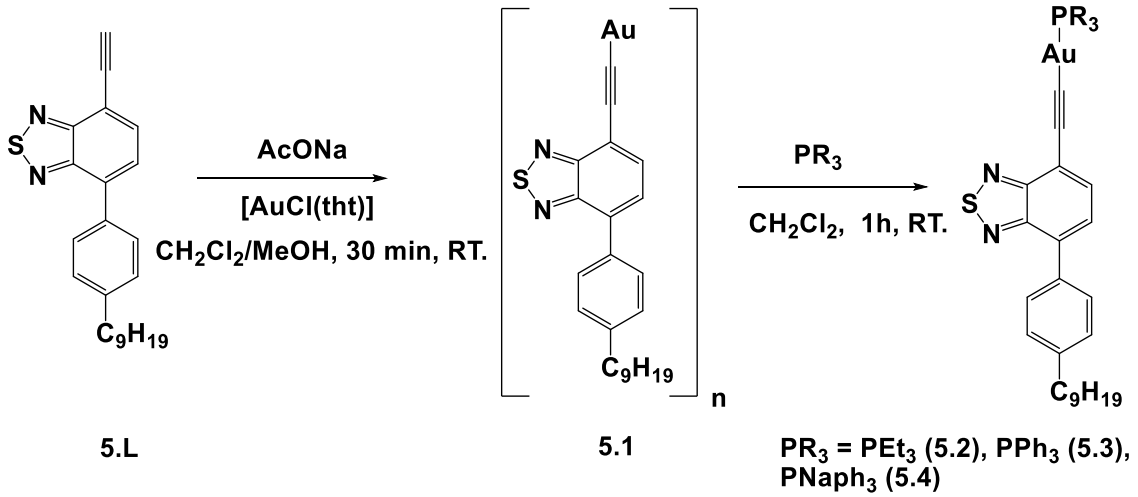


**Scheme 5.3.** Synthesis of the gold(I) benzothiadiazole-based derivatives.

All complexes were characterized by $^{1}H$ and $^{31}P$ NMR and IR spectroscopy as well as by HRESI-MS (+) in the case of **5.2** and **5.3** and MALDI-TOF in the case of **5.4**. The $^{1}H$ NMR spectra display the expected proton patterns of **5.L** as well as the protons related to the phosphane. The disappearance of the terminal alkynyl proton is a clear indication of the formation of the complexes. $^{31}P\{^{1}H\}$ NMR spectra display in all cases only one peak, that is ca. 50 ppm downfield shifted with respect to the free phosphane upon coordination to the metal.[20,21] The characteristic vibration of υ(C≡C) around 2100 $cm^{-1}$ is approximately 100 $cm^{-1}$ shifted to longer wavenumbers with respect to the same vibration in the polymer (**5.1**), as previously observed in other gold(I) derivatives.[20,21] Mass spectra was a final evidence of the correct formation of the complexes and display the monoprotonated species $[M + H]^{+}$ in all cases.

5.2.1.3. Synthesis of gold(I) benzothiadiazole-based derivatives containing carbenes

Three different gold(I) benzothiadiazole derivatives were synthesized by a previously established method (Schemes 5.4 and 5.5).[22] The gold(I) chloride imidazole complexes were obtained by treating the imidazole salt with $Ag_2O$ followed by a ligand exchange reaction with [AuCl(tht)]. Then, the labile chloride ligand was replaced by the benzothiadiazole that was previously deprotonated.

All complexes were characterized by $^{1}$H NMR and IR spectroscopy as well as by ESI-MS (+) spectrometry. $^{1}$H NMR spectra display the proton pattern of **5.L** as well as the protons related to the imidazole. Also, the disappearance of the N-C**H**-N proton of the imidazole part is a good indication that the metal is coordinated. Mass spectra shows the monoprotonated species $[M + H]^{+}$ for **5.5**, **5.6** and **5.7**.

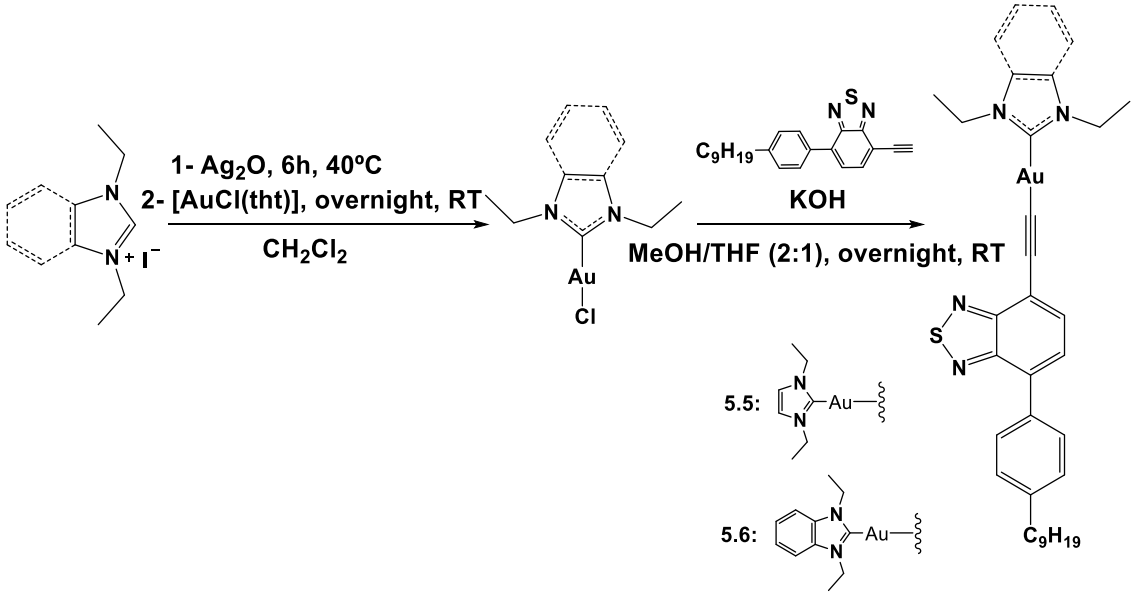


**Scheme 5.4.** Synthesis of gold(I) benzothiadiazole-based derivatives **5.5** and **5.6**.

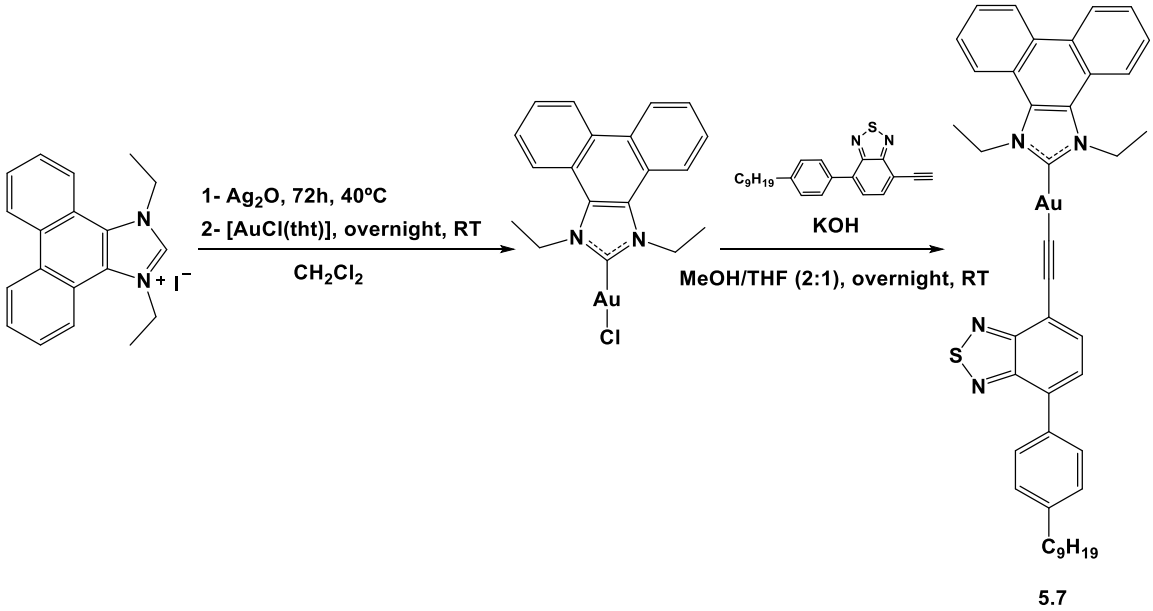


**Scheme 5.5.** Synthesis of gold(I) benzothiadiazole-based derivative **5.7**.

### 5.2.2. X-ray crystal structure determination

Single crystals suitable for X-ray diffraction were successfully grown from dichloromethane/hexane solutions of the complexes **5.3**, **5.4**, **5.6** and **5.7**. They crystalize in the P-1 space group of the triclinic system. Selected bond length and angles are summarized in Table 5.1.

**Table 5.1.** Selected bond lengths (Å) and angles (deg) for the X-ray crystal structures of **5.3**, **5.4**, **5.6** and **5.7**.

| Compound | Distance (Å) | Angle (º) |
|---|---|---|
| **5.3** | Au-P: 2.275<br>Au-C1: 1.996<br>Au···Au: 9.286 | C-Au-P: 176.66 |
| **5.4** | Au-P: 2.282<br>Au-C1: 2.018<br>Au ··Au: 13.704 | C-Au-P: 175.92 |
| **5.6** | Au-C(Im2): 2.009<br>Au-C: 1.979<br>Au···Au: 5.630 | C-Au-C: 176.06 |
| **5.7** | Au-C(Im3): 2.018<br>Au-C: 1.980<br>Au ··Au: 3.360 | C-Au-C: 178.06 |

The X-ray crystal structure of **5.3** consists of two molecules in the asymmetric unit in parallel disposition but slightly shifted in the parallel plane with C-H···π(C≡C) weak contacts. In contrast, **5.4**, **5.6** and **5.7** crystallize with a single molecule in the unit cell (Figure 5.3). A linear geometry is observed for all complexes around the metal atom with a P-Au-C angle of 176º and a C(Im)-Au-C angle of 177º. For those compounds that contain phosphanes, the P-Au and Au-C distances are in agreement with those previously reported for other $PR_3$-(I)-acetylide complexes.[23–25] The bond distances between the gold(I) centre and the C of the imidazole or the alkynyl are around 2.0 Å in the case of carbene complexes, similarly to other compounds with an alkynyl and an imidazole attached to the gold.[26,27] The complexes display intermolecular N-H···$C_{sp}$, C-H···π, and S···H short contacts in the 3D crystal packing.

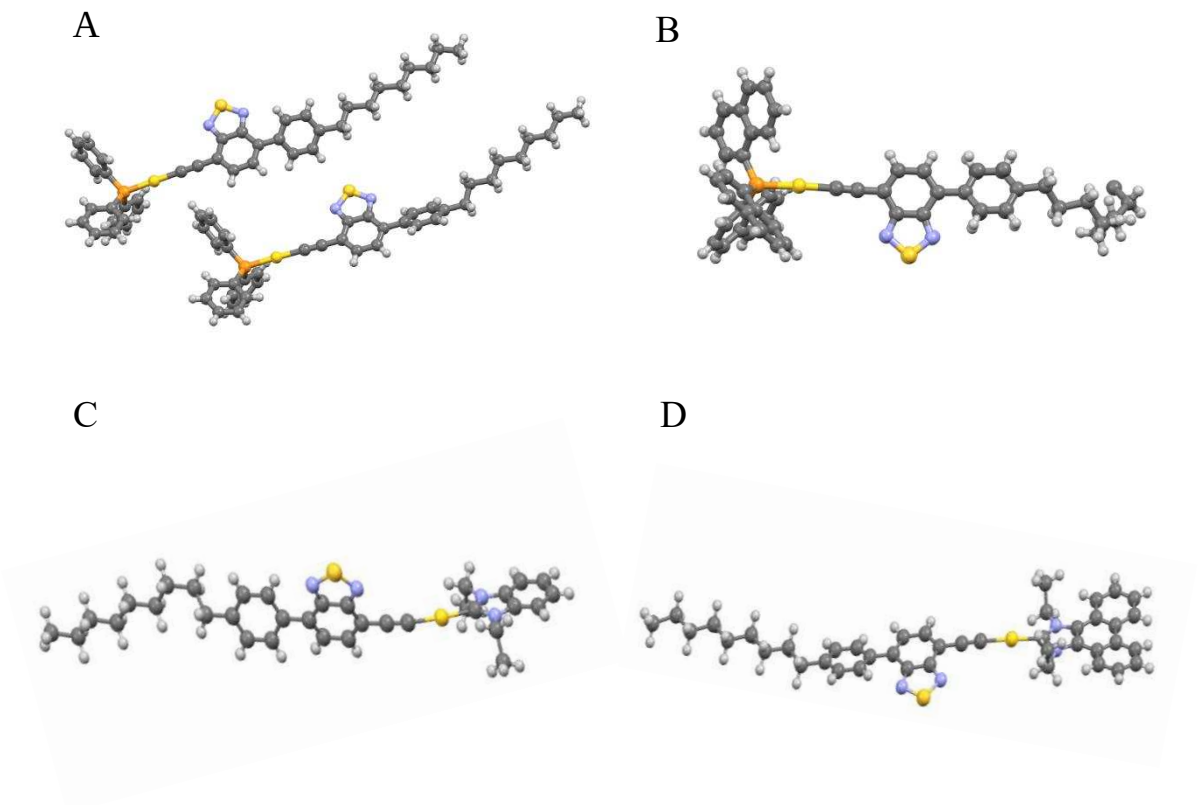


**Figure 5.3.** Representation of the X-ray crystal structures of **5.3** (A), **5.4** (B), **5.6** (C) and **5.7** (D).

The packing arrangement shows an alignment of the molecules due to the presence of an aliphatic chain in the case of complex **5.3**. In the case of **5.4**, the aliphatic chain is twisted at the end and the molecules are aligned due to the π-π stacking of the naphthyl rings (Figure 5.4). The difference in the resulting packing may be due to the steric hindrance of the phosphane in **5.4** that precludes a linear arrangement of the molecules. No aurophilic contacts are observed in the packing with Au···Au distances of 9.819 Å and 13.704 Å for **5.3** and **5.4** respectively.

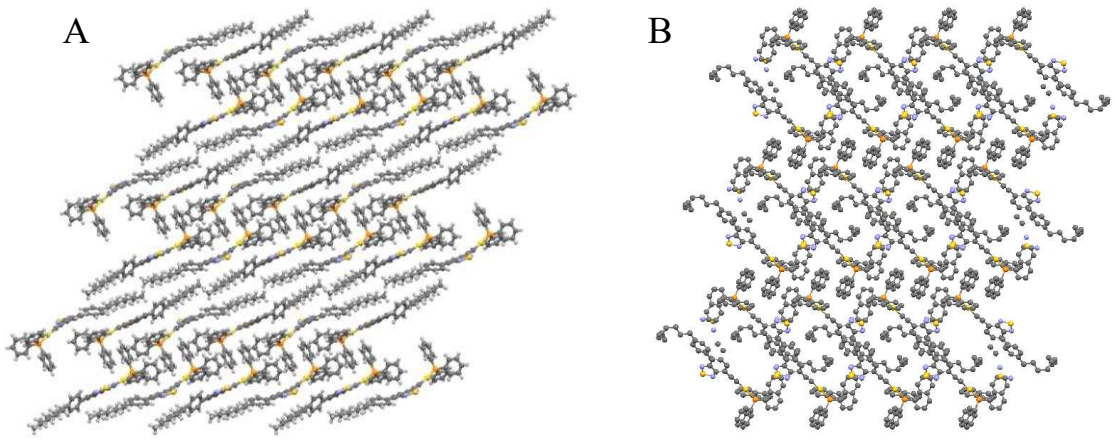


**Figure 5.4.** Representation of the 3D packing of **5.3** (A) and **5.4** (B).

The packing of compounds **5.6** and **5.7** shows an alignment of the molecules that forms dimeric species where the aliphatic chain is pointed in an antiparallel manner (Figure 5.5). In the case of compound **5.6**, this dimer is hold by non-covalent interactions such as N-H···$C_{sp}$, C-H···π. In the case of compound **5.7**, the dimer is hold by π-π-stacking and aurophilic interactions (Au···Au of 3.36 Å). The π-extended system of compound **5.7**, let the molecule stays in a planar mode and makes possible the establishment of aurophilic contacts due to the substitution of a phosphane for a planar imidazole that allows the approximation of the gold(I) atoms.

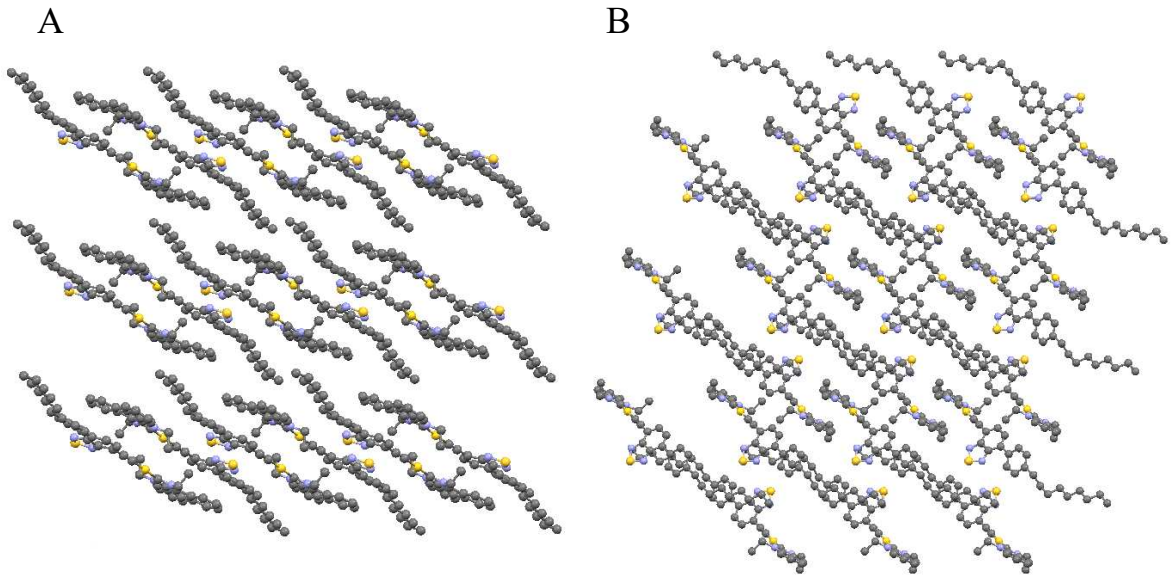


**Figure 5.5.** Representation of the 3D packing of **5.6** (A) and **5.7** (B).

### 5.2.3. Photophysical characterization

The absorption and emission spectra of all complexes **5.2-7** and **5.L** were recorded in $10^{-5}$ M dichloromethane solutions and solid state at room temperature and the obtained data is summarized in Table 5.2.

**Table 5.2.** Electronic absorption and emission data, quantum yields ($\Phi_{fl}$), lifetime ($\tau_{fl}$), $k_r$ and $k_{nr}$ of **5.L** and complexes **5.2-7**. Emission data, quantum yields, lifetimes, $k_r$ and $k_{nr}$ in solid state are in bold.

| **Compound** | Absorption $\lambda_{max}$ ($\varepsilon$ $cm^{-1}$ $M^{-1}$) | Emission | $\Phi_{fl}$ | $\tau_{fl}$ (ns) | $k_r$ ($ns^{-1}$) | $k_{nr}$ ($ns^{-1}$) |
|---|---|---|---|---|---|---|
| **5.L** | 270 (15454) 384 (8007) | 492/**485** | 0.83/**0.36** | 9.40/**5.8** | 0.088/**0.062** | 0.018/**0.11** |
| **5.2** | 287 (10454) 409 (7953) | 519/**517** | 0.86/**0.056** | 9.87/**3.92** | 0.087/**0.014** | 0.014/**0.24** |
| **5.3** | 293 (22355) 410 (12670) | 509/**514** | 0.87/**0.24** | 9.19/**2.01** | 0.094/**0.12** | 0.014/**0.37** |
| **5.4** | 300 (42905) 409 (11750) | 519/**517** | 0.62/**0.18** | 6.45/**3.78** | 0.096/**0.05** | 0.059/**0.22** |
| **5.5** | 298 (13000) 436 (5000) | 531/**523** | 0.88/**0.01** | 10.2/**4.08** | 0.086/**0.0024** | 0.012/**0.24** |
| **5.6** | 243 (22898) 297 (24455) 412 (8232) | 528/**528** | 0.93/**0.026** | 9.62/**3.59** | 0.097/**0.0072** | 0.0073/**0.27** |
| **5.7** | 257 (24271) 298 (15012) 419 (5265) | 525/**550** | 0.46/**0.03** | 9.15/**4.18** | 0.05/**0.0071** | 0.06/**0.23** |

The absorption spectra of compounds **5.2-4** display two bands: one at high energies related to the $\pi \rightarrow \pi^*$ transition of the molecule and another at lower energies assigned to a charge transfer (CT) transition.[28] The absorption spectra of compounds **5-7** display three absorption bands: the two highest energy bands are related to $\pi$-$\pi^*$ intraligand transition of the imidazol[29] and the benzothiadiazole and the lowest energy band is related to charge transfer (CT) transition. The charge transfer transition is ca. 40 nm red shifted in gold(I) complexes **5.2-7** with respect to **5.L**. This behavior is probably due to an increase in the conjugation through mixing of the metal d-orbital with the $\pi$-system of the ligand.[30]

Emission spectra were recorded in solution and in the solid state upon excitation of the samples at the lowest energy absorption band (ca. 410 nm) and it is observed that the emission of the complexes is ca. 30 nm red shifted upon coordination to **5.L** (Figures 5.6 and 5.7). The observed large Stokes' shifts (around 100 nm) are a consequence of the efficient intramolecular charge transfer (ICT).[31] There is no significant change in the emission in solution and in solid state for compounds **5.2-6**. In the case of compound **5.7**, a red shift in the emission in solid state is observed probably due to the presence of aurophilic interactions in the solid state.

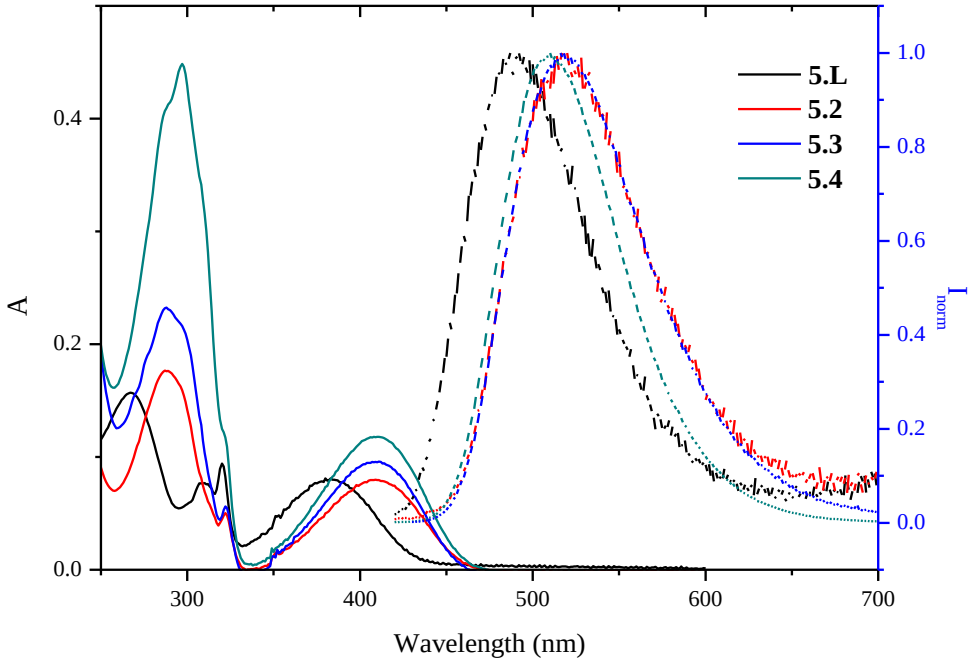


**Figure 5.6**. Absorption (solid lines) and emission (dash lines) spectra of **5.L** and gold(I) complexes **5.2-4** in dichloromethane.

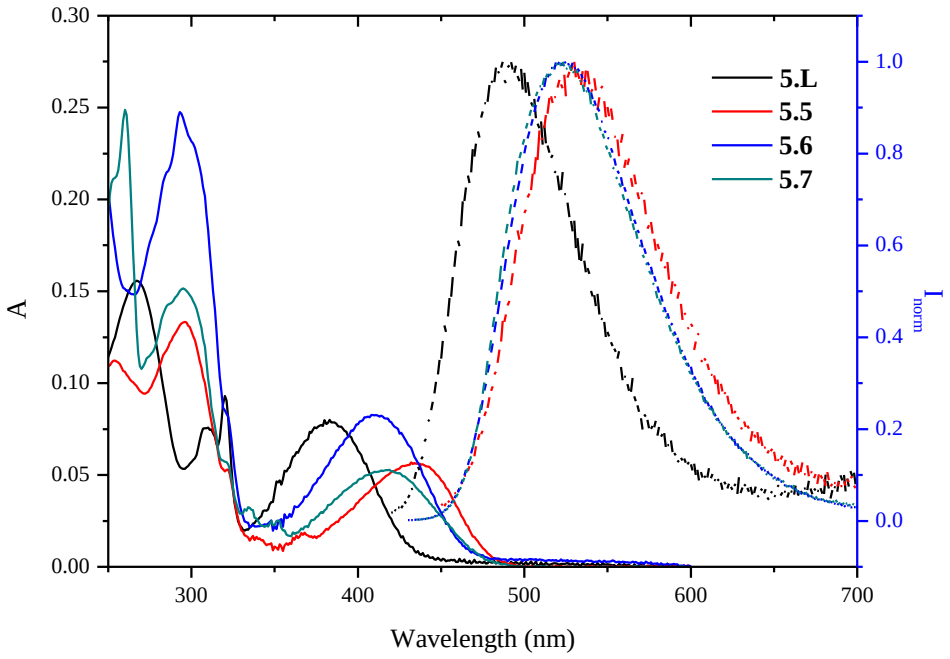


**Figure 5.7**. Absorption (solid lines) and emission (dash lines) spectra of **5.L** and gold(I) complexes **5.5-7** in dichloromethane.

Fluorescence quantum yields ($\Phi_{fl}$) and lifetimes ($\tau_{fl}$) are measured for all compounds in dichloromethane and in solid state (Table 5.2). In general, $\Phi_{fl}$ and $\tau_{fl}$ in solution are in the high-range order than other BTD derivatives.[13,32,33] There is no significant change in these values when the gold is coordinated to the BTD structure, except in the case of **5.4**, with the bulkiest phosphane and **5.7**, with the imidazole with the largest π-system, which display lower values in solution (Table 2). There is a decrease in the quantum yields in solid state as previously observed in some BTD derivatives previously reported in the literature, being more significant in the carbine derivatives **5.5-7**[34,35] that may perform more efficient intermolecular packing. In all cases, the fluorescence lifetime profile shows a single-exponential decay, giving the $\tau_{fl}$ values in the nanoseconds order, which are in agreement with the assignment of a transition between two singlet states (Figure 5.8).

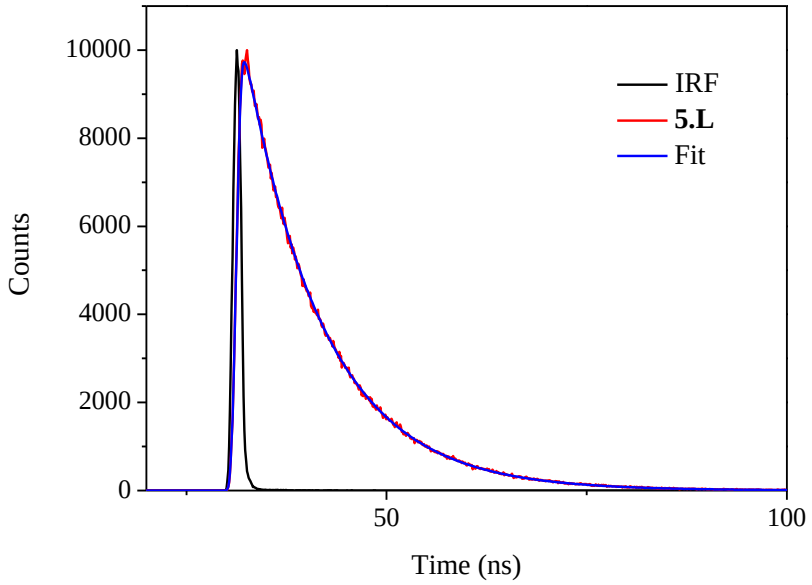


**Figure 5.8.** Fluorescent lifetime of **5.L** in dichloromethane solution

The fluorescence lifetimes are about 9 ns in the case of **5.L**, **5.2**, **5.3, 5.5-7** and 6 ns in the case of **5.4** and are in the order of expected for BTD derivatives, in the range of 2-10 ns.[35] The radiative ($k_F$) and non-radiative ($k_{nr}$) decay rate constants were calculated from the fluorescence quantum yields and lifetimes. In general, $k_r$ and $k_{nr}$ remain similar. There is a deviation of the tendency just in two cases: compound **5.4**, which presents the less electron-donating phosphane, a decrease of the fluorescence quantum yield and an increment of the non-radiative decay rate is observed. This behavior suggests a strong donor-acceptor interaction, leading to quenching in fluorescence.[36] A decrease of fluorescence quantum yield and a decrease of the radiative decay rate and an increase of the non-radiative decay rate is observed for compound **5.7**, with the imidazole with the largest π-system.

### 5.2.4. Solvent effect

BTD derivatives show commonly an emission dependence on the solvent polarity, as usually present chromophores with a charge transfer transition. For this reason, absorption and emission spectra of compounds **5.L** and **5.2-4** have been recorded in seven different solvents with a wide range of polarities (Figure 5.9). The solvents used in this work together with their respective parameters (α, β, $\pi^*$, n) employed in the correlations are presented in Table 5.3. Due to the lack of solubility of compounds **5.5-7** in a wide range of solvents, solvent effect has not been tested for them.

**Table 5.3.** α, β, $\pi^*$, n Parameters for the solvents used.[37]

| Solvent | α | β | $\pi^*$ | μ | $\varepsilon_r$ | n |
|---|---|---|---|---|---|---|
| Acetonitrile | 0.19 | 0.40 | 0.66 | 13.0 | 35.94 | 1.3442 |
| Ethyl acetate | 0 | 0.45 | 0.55 | 5.9 | 6.02 | 1,3722 |
| Dichloromethane | 0.3 | 0 | 0.82 | 3.8 | 8.93 | 1.4241 |
| Dimethylsulfoxide | 0 | 0.76 | 1 | 13.5 | 46.45 | 1.4793 |
| n-Hexane | 0 | 0 | -0.11 | 0 | 1.88 | 1.3749 |
| Methanol | 0.98 | 0.66 | 0.60 | 9.6 | 32.66 | 1.3288 |
| Tetrahydrofuran | 0 | 0.55 | 0.55 | 5.8 | 7.58 | 1.4072 |

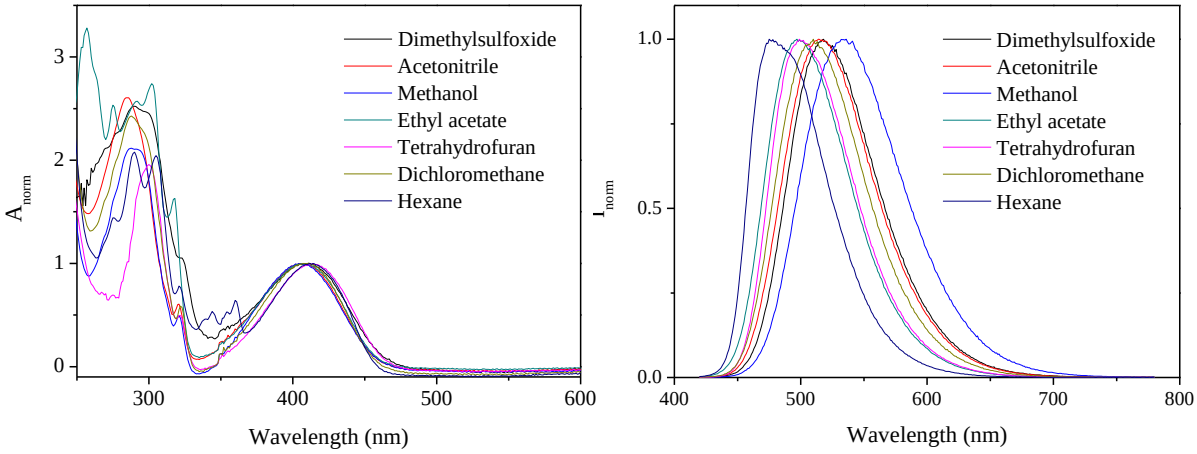


**Figure 5.9.** Normalized absorption (left) and emission (right) spectra of compound **5.3** recorded in solvents with different polarity.

The absorption spectra do not show a clear dependence on the solvent polarity. In contrast, the emission spectra of all compounds show a clear dependence on the solvent, presenting a large change in the emission maxima between hexane and methanol (around 60 nm). All complexes present a red shift of the emission and a decrease on the emission intensity when the solvent polarity increases. This behaviour is in agreement with the literature for BTD-containing donor-acceptor chromophores.[36]

Lippert-Mataga equation (1) was applied to estimate the excited state polarity from the recorded changes in the emission fluorescence with solvents of different polarizabilities. This equation expresses the magnitude of the Stokes' shift in terms of changes in the molecular dipole moment and the radius of the Onsager cavity.

$$\tilde{v}_a - \tilde{v}_f = \Delta f \frac{1}{4\pi\varepsilon_0} \frac{2(\mu_E - \mu_G)^2}{hca^3} + constant \quad (1)$$

where $\tilde{\upsilon}_a$ and $\tilde{\upsilon}_f$ are the respective absorption and emission energies in wavenumbers, $\varepsilon_0$ is the permittivity, $\mu_E$ and $\mu_G$ are, respectively, the magnitudes of excited and ground state dipole moments, h is the Planck's constant, c is the speed of the light and a is the Onsager cavity radius (calculated from the van der Waals volume[38]). The orientational polarizability Δf is defined as

$$\Delta f = \left[\frac{\varepsilon - 1}{2\varepsilon + 1} - \frac{n^2 - 1}{2n^2 + 1}\right] \quad (2)$$

where ε and n are solvent dielectric constant and refractive index respectively.

Plots of the Stokes' shift versus the orientational polarizability are represented in Figure 5.10 and the slopes, the variation of the dipolar moment in the ground and excited state, and the Onsager cavity radius are represented in Table 5.4.

**Table 5.4.** Lippert-Mataga slope, variation of the dipolar moment and Onsager cavity radius data of **5.L** and **5.2-4.**

| **Compound** | Slope ($cm^{-1}$) | a (Å) | $\mu_E$ - $\mu_G$ (D) |
|---|---|---|---|
| **5.L** | 6236 | 4.39 | 7.24 |
| **5.2** | 7298 | 4.89 | 9.20 |
| **5.3** | 7452 | 5.25 | 10.34 |
| **5.4** | 6757 | 5.58 | 10.79 |

A positive correlation between the Stokes' shift and the orientational polarizability factor implies an intramolecular charge transfer (ICT) mechanism in the excited state. A larger change in the dipole moment has been observed for gold(I) complexes **5.2-4**, indicating that these compounds are significantly more polar in the excited state than in the ground state. Hence, the interaction between the compound and the solvent becomes stronger in the excited state with increasing polarity of the solvent and lead to a quenching of the resulting luminescence.[39,40]

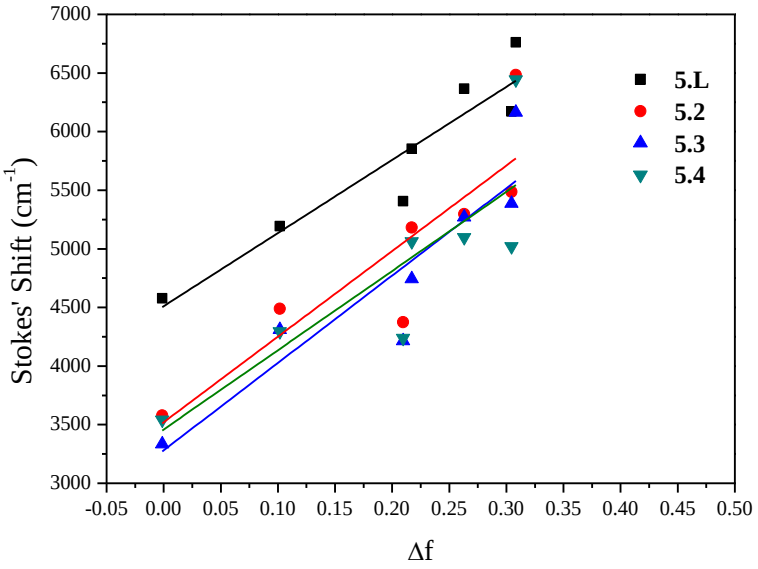


**Figure 5.10.** Lippert-Mataga plots determined for **5.L** and gold(I) complexes **5.2-4**.

The multiparametric Kamlet-Taft method was then applied in order to analyse in more detail the interaction between the compounds and the solvent. With this analysis, absorption and emission energies are correlated with different solvent properties according to equation 3.

$$\bar{\nu} = \bar{\nu_0} + a\alpha + b\beta + p(\pi^* + d\delta) \quad (3)$$

Where $\upsilon_0$ corresponds to the value of the absorption or the emission energies for a reference solvent; α is the index related to the solvent ability to act as a hydrogen-bond donor (or electron pair acceptor) toward a solute; β corresponds to the ability of bulk sovents to behave as a hydrogen-bond acceptors (or electron-pair donors); π* is the index of the solvent polarity/polarizability which indicates the solvent ability to stabilize a neighboring charge or dipole through non-specific dielectric interactions and finally, δ is the polarizavility correction factor for different solvents. Considering that often the contribution of δ is negligible equation 3 can be simplified as

$$\bar{\nu} = \bar{\nu_0} + a\alpha + b\beta + p\pi^* \quad (4)$$

Linear plots of $\bar{\upsilon}_{exp}$ versus $\bar{\upsilon}_{calc}$, like the exemplified for compound **5.4** (Figure 5.11), have been obtained for all compounds and the fitted parameters ($\bar{\upsilon}_0$, a, b and p), as well as slope and correlation coefficient are presented in Table 5.5.

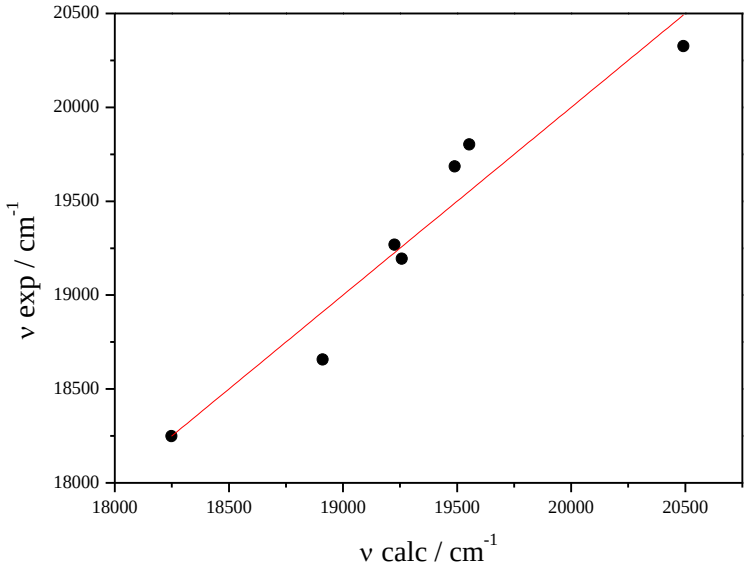


**Figure 5.11.** Plot of $\bar{\upsilon}_{exp}$ vs. $\bar{\upsilon}_{calc}$ for emission data of compound **5.4**.

Plots of $\bar{\upsilon}_{exp}$ versus $\bar{\upsilon}_{calc}$ yield slopes that are close to 1 and good correlation coefficients are obtained in all cases.

Inspection of Table 5.5 let us point out that the observed solvatochromism in the emission of compounds **5.L** and **5.2-4** is essentially reflected in a and p solute parameters, that means a higher sensitivity to the polarity/polarizability of solvent and to H-bond donor (or electron pair acceptor) of the solvent towards a solute.[41]

**Table 5.5.** $\bar{\upsilon}_0$, a, b and p values, in $cm^{-1}$, as well as slope and correlation coefficients obtained from Kamlet-Taft multiparametric of the emission data of **5.L** and **5.2-4.**

| **Compound** | $\bar{\upsilon}_0$ | a | b | p | Slope | $r^2$ |
|---|---|---|---|---|---|---|
| **5.L** | 21754 | -1083 | -684 | -1382 | 1.0 | 0.94 |
| **5.2** | 20471 | -1351 | -605 | -1038 | 1.0 | 0.98 |
| **5.3** | 20676 | -1121 | -690 | -937 | 1.0 | 0.95 |
| **5.4** | 20383 | -1145 | -631 | -992 | 1.0 | 0.93 |

### 5.2.5. Water/acetonitrile mixtures

The twisted conformation between the two aromatic rings of the BTD found in the crystal structures together with previous examples of BTD derivatives found in the literature[42] suggest the possibility of having aggregation induced emission (AIE) for the compounds under study.

Emission spectra, quantum yields, and lifetimes were measured in acetonitrile and in acetonitrile/water mixtures with an increasing water fraction in order to corroborate the AIE properties (Figure 5.12). The obtained data is summarized in Tables 5.6 and 5.7. These studies were not possible to be performed for compounds **5.4-7** due to the lack of solubility in the presence of small amounts of water.

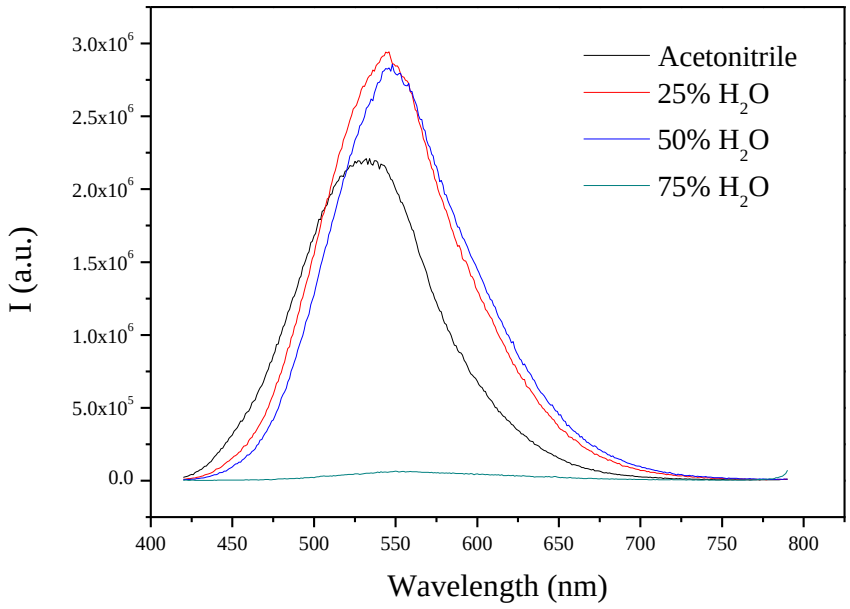


**Figure 5.12.** Emission spectra of **5.L** in acetonitrile and in acetonitrile/water mixtures with different water content.

**Table 5.6.** Quantum yields of **5.L**, **5.2** and **5.3** in acetonitrile and in acetonitrile/water mixtures with increasing water fractions.

| **Compound** | Acetonitrile | 25% $H_2O$ | 50% $H_2O$ | 75% $H_2O$ |
|---|---|---|---|---|
| **5.L** | 0.81 | 0.96 | 0.97 | 0.19 |
| **5.2** | 0.76 | 0.83 | 0.77 | 0.14 |
| **5.3** | 0.93 | 0.84 | 0.74 | 0.18 |

**Table 5.7.** Lifetimes (ns) of **5.L**, **5.2** and **5.3** in acetonitrile and in acetonitrile/water mixtures with increasing water fractions.

| **Compound** | Acetonitrile | 25% $H_2O$ | 50% $H_2O$ | 75% $H_2O$ |
|---|---|---|---|---|
| **5.L** | 9.8 | 13.7 | 14.1 | 13 |
| **5.2** | 10.8 | 11.4 | 12.6 | 12.6 |
| **5.3** | 11.1 | 11.1 | 11.6 | 12.1 |

A decrease in the absorption bands is observed for all compounds when the water contents increases, meaning that aggregation is taking place. A red shift is observed in the emission spectra for **5.L** (25 nm) and **5.2** (8 nm) upon increasing the water fraction up to 75% and up to 50% in the case of **5.3** (22 nm). Additionally, an increase of the quantum yield is observed when the water fraction reached 50% for **5.L** and 25% for gold(I) complex **5.2**. In the case of gold(I) complex **5.3**, a decrease of the quantum yield is observed at higher water fraction contents. A significant decrease of the quantum yield is observed for all compounds in the presence of large amount of water (beyond 50%) and in the case of **5.3** also a blue shift is recorded, suggesting a change on the aggregates' type under these conditions.

The increase of the quantum yield is attributed to the AIE mechanism that is dominating the effect of the solvent polarity.[43] The AIE phenomenon is more noticeable for **5.L** due to the presence of the lowest variation of the dipolar moment. Therefore, the effect of the solvent polarity is smaller. The aggregation process is dominating, in the case of **5.3**, only when the water fraction reached 75% and there is a blue shift in the emission and the emission intensity decrease is probably due to an aggregation induced quenching (ACQ) effect.

The radiative and non-radiative constants have been calculated and are summarized in Table 5.8. A significant decrease of the non-radiative constants has been observed when the water contents is above 50% for **5.L** and above 25% for **5.2** maybe due to the lack of mobility when the aggregates are formed that deactivates the non-radiative pathways.

**Table 5.8.** Radiative and non-radiative constants ($ns^{-1}$) of **5.L**, **5.2** and **5.3** in acetonitrile and in acetonitrile/water mixtures with increasing water fractions.

| **Compound** | Acetonitrile | | 25% $H_2O$ | | 50% $H_2O$ | | 75% $H_2O$ | |
|---|---|---|---|---|---|---|---|---|
| | $k_r$ | $k_{nr}$ | $k_r$ | $k_{nr}$ | $k_r$ | $k_{nr}$ | $k_r$ | $k_{nr}$ |
| **5.L** | 0.083 | 0.019 | 0.070 | 0.003 | 0.068 | 0.002 | 0.015 | 0.062 |
| **5.2** | 0.070 | 0.022 | 0.073 | 0.015 | 0.061 | 0.018 | 0.043 | 0.036 |
| **5.3** | 0.084 | 0.006 | 0.076 | 0.014 | 0.064 | 0.022 | 0.015 | 0.068 |

### 5.2.6. Mechanochromic properties.

The mechanochromic properties of **5.L** and gold(I) complexes **5.2-7** were also investigated. As a first screening step, the photoluminescence of the powder samples of the compounds under study were observed before and after mechanical stimuli. Only the gold(I) compounds that contain a carbene group as a second coordination position present some changes in the photoluminescence properties after the application of a mechanical stimuli. Interestingly, a correlation between the π-extended system character of the carbene and the mechanochromic properties was observed. Only small changes in the emission upon the application of pressure have been observed in the case of the gold(I) complex **5.5**, without a change in the crystalline phase. Different emission profiles were observed for complexes **5.6** and **5.7** when the solid is in powder or in crystal (Figure 5.12). The PXRD of complex **5.6** shows that the changes observed in the emission are due to a change on the orientation of the molecules. The single crystal is characterized by three explicit diffractions derived from the (001), (002) and (003) planes (Figure 5.13). Instead, different planes have been observed in the powder. A red shift of the emission of the gold(I) complex **5.7** is observed when the compound changes from the crystal to the powder form probably due to the presence of stronger aurophilic interactions in the powder. Generally speaking, the emission band is red shifted when aurophilic interactions are stronger due to larger destabilization of the HOMO energy level of the gold complexes. Some crystallinity seems to be observed when the solid are in contact with solvent vapors but without recovering completely the emission observed in the single crystal.

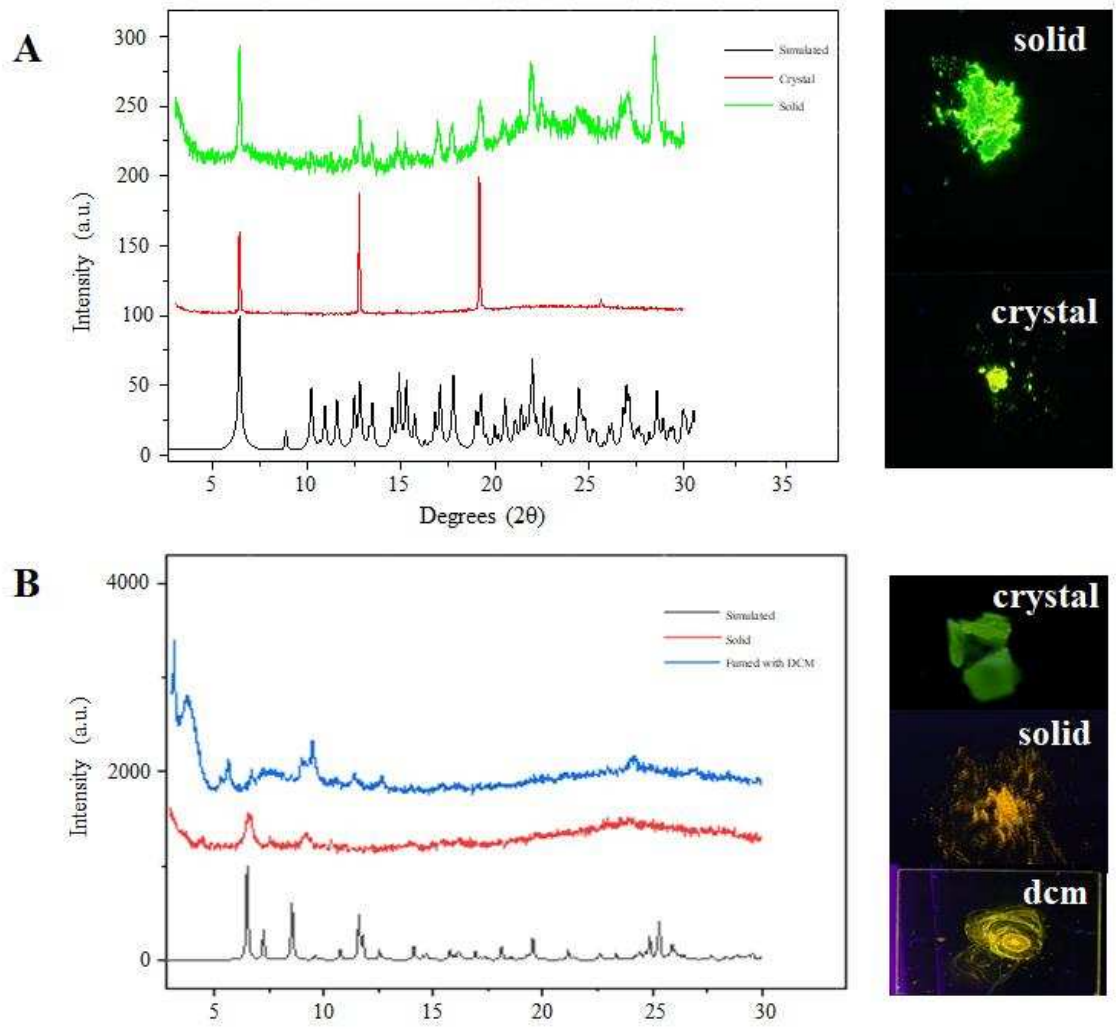


**Figure 5.13.** PXRD and photographs under UV light of **5.6** (A) and **5.7** (B).

### 5.2.7. Hybrid materials

The compounds were dispersed in solid matrixes of cellulose, polymethylmethacrylate (PMMA), polystyrene (PS) and a cyclic olefin copolymer, Zeonex in order to increase the quantum yield in solid state and block the non-radiative pathways for the decay of the singlet excited state, and to obtain gold(I) highly luminescent materials. The corresponding emission spectra were recorded and a blue shift of the emission maxima (around 10 nm) is observed in all cases when the compound is introduced in the matrixes. There is not a significant shift in the emission maxima between the different matrixes, being indicative that the polarity of the matrix is not affecting the resulting emission of those solvatochromic compounds.

The quantum yields and lifetimes were measured and are summarized in Tables 5.9 and 5.10. In general trends, there is an increase of the quantum yields and the lifetimes when

the compounds are introduced in the thin films. It must be highlighted that the quantum yields reached almost 1 in PMMA, PS and Zeonex matrixes for **5.L**, **5.2**, **5.3** and **5.6** and for the best of our knowledge, there are no precedents in the literature of BTD derivatives in polymer matrixes that presents such near unity quantum yields.

**Table 5.9.** Quantum yields of **5.L** and **5.2-4** in solid state and in cellulose, polymethylmethacrylate (PMMA), polystyrene (PS) and Zeonex matrixes.

| **Compound** | $\Phi_{fl}$ (solid) | $\Phi_{fl}$ (Celulose) | $\Phi_{fl}$ (PMMA) | $\Phi_{fl}$ (PS) | $\Phi_{fl}$ (Zeonex) |
|---|---|---|---|---|---|
| **5.L** | 0.36 | 0.91 | 0.96 | 0.95 | 0.93 |
| **5.2** | 0.056 | 0.91 | 0.95 | 0.94 | 0.92 |
| **5.3** | 0.24 | 0.89 | 0.94 | 0.97 | 0.96 |
| **5.4** | 0.18 | 0.31 | 0.41 | 0.41 | 0.45 |
| **5.5** | 0.01 | 0.12 | 0.13 | 0.13 | 0.31 |
| **5.6** | 0.026 | 0.87 | 0.9 | 0.93 | 0.83 |
| **5.7** | 0.03 | 0.56 | 0.57 | 0.58 | 0.53 |

**Table 5.10.** Lifetimes (ns) of **5.L** and **5.2-4** in solid state and in cellulose, polymethylmethacrylate (PMMA), polystyrene (PS) and Zeonex matrixes.

| **Compound** | $\tau_{fl}$ (solid) | $\tau_{fl}$ (Celulose) | $\tau_{fl}$ (PMMA) | $\tau_{fl}$ (PS) | $\tau_{fl}$ (Zeonex) |
|---|---|---|---|---|---|
| **5.L** | 5.80 | 9.69 | 9.07 | 8.01 | 8.4 |
| **5.2** | 3.92 | 8.32 | 8.54 | 7.75 | 8.51 |
| **5.3** | 2.01 | 7.82 | 8.83 | 7.09 | 7.69 |
| **5.4** | 3.78 | 6.79 | 3.89 | 3.62 | 4.32 |
| **5.5** | 4.08 | 6.93 | 7.02 | 6.49 | 7.43 |
| **5.6** | 3.59 | 8.02 | 8.22 | 6.93 | 6.74 |
| **5.7** | 4.18 | 6.93 | 5.62 | 5.31 | 5.59 |

Radiative and non-radiative constants have been calculated in order to rationalize the excellent recorded quantum yields (Table 5.11). In general, the introduction of the compounds in thin films decrease the non-radiative constants. In comparison with the luminescent properties in solid state, the introduction of the compounds in matrixes enhances the luminescent properties and allows the dispersion of the molecules avoiding aggregation processes that quench the resulting emission.

**Table 5.11.** Radiative and non-radiative constants ($ns^{-1}$) of **5.L** and **5.2-4** in solid state and in matrixes of cellulose, poly methyl methacrylate (PMMA), polystyrene (PS) and Zeonex.

| Compound | Solid | | Celulose | | PMMA | | PS | | Zeonex | |
|---|---|---|---|---|---|---|---|---|---|---|
| | $k_r$ | $k_{nr}$ | $k_r$ | $k_{nr}$ | $k_r$ | $k_{nr}$ | $k_r$ | $k_{nr}$ | $k_r$ | $k_{nr}$ |
| **5.L** | 0.062 | 0.11 | 0.094 | 0.009 | 0.11 | 0.004 | 0.12 | 0.006 | 0.11 | 0.008 |
| **5.2** | 0.014 | 0.24 | 0.25 | 0.025 | 0.11 | 0.006 | 0.12 | 0.008 | 0.11 | 0.009 |
| **5.3** | 0.12 | 0.37 | 0.11 | 0.014 | 0.11 | 0.007 | 0.14 | 0.004 | 0.12 | 0.005 |
| **5.4** | 0.05 | 0.22 | 0.046 | 0.10 | 0.11 | 0.15 | 0.11 | 0.16 | 0.10 | 0.13 |
| **5.5** | 0.0024 | 0.24 | 0.017 | 0.13 | 0.018 | 0.012 | 0.02 | 0.13 | 0.042 | 0.093 |
| **5.6** | 0.0072 | 0.27 | 0.10 | 0.016 | 0.11 | 0.012 | 0.13 | 0.010 | 0.12 | 0.025 |
| **5.7** | 0.007 | 0.23 | 0.08 | 0.063 | 0.10 | 0.076 | 0.11 | 0.079 | 0.09 | 0.084 |

## 5.3. Conclusions

The presence of phosphanes vs. carbenes at the second coordination position of the gold(I) at in two series of gold(I) complexes containing the same chromophoric unit (4-ethynyl-7-(4-nonylphenyl)benzo[c][1,2,5]thiadiazole) has a direct effect on their resulting solubities, solvatochromic and mechanochromic properties.

The incorporation of a carbene with an extended π-system allowed the possibility of having Au(I)···Au(I) contacts as shown in the crystal structure of some of the compounds. This fact affects the resulting mechanochromic properties displayed by compound **5.7**, having a red shift in the emission when a mechanic stimulus is present.

The incorporation of the compounds in polymer matrixes enhanced the emissive properties of the compounds allowing the possibility of the incorporation of these compounds in devices to produce highly luminescent materials.

## 5.4. Experimental Section

### 5.4.1. General procedures

All manipulations have been performed under prepurified $N_2$ using standard Schlenk techniques. All solvents have been distilled from appropriated drying agents. Commercial reagents triehylphosphane ($PEt_3$, Aldrich 99%), triphenylphosphane ($PPh_3$, Aldrich 99%), tri-1-naphthylphosphane ($PNaph_3$ Aldrich, 97%), imidazole (Aldrich >99.5%), iodoethane (Aldrich, 99%), 1H-Benzo[d]imidazole (Fluorochem), 9,10-phenanthrenequinone (Fluorochem), silver(I) oxide (Alfa Aesar, 99%) were used as received. The synthesis and characterization of 4-ethynyl-7-(4-nonylphenyl)benzo[c][1,2,5]thiadiazole (**5.L**) was carried out by Sr. Marcelo Echeverri from Instituto de Ciencia de Materiales de Madrid.

### 5.4.2. Physical measurements

Infrared spectra have been recorded on a FT-IR 520 Nicolet Spectrophotometer. $^1$H-NMR ($\delta$(TMS) = 0.0 ppm), $^{31}P\{^1H\}$-NMR ($\delta$(85% $H_3PO_4$) = 0.0 ppm) spectra have been obtained on a Varian Mercury 400 and Bruker 400 (Universitat de Barcelona). ElectroSpray-Mass spectra (+) has been recorded on a Fisons VG Quatro spectrometer (Universitat de Barcelona). Absorption spectra have been recorded on a Varian Cary 100 Bio UV- spectrophotometer and emission spectra on a Horiba-Jobin-Yvon SPEX Nanolog spectrofluorimeter (Universitat de Barcelona). Luminescent quantum yields were recorded using an Absolute PL quantum yield spectrometer from Hamamatsu Photonics upon excitation the samples at 400 nm. Fluorescence lifetimes were measured via the time-correlated single-photon counting technique (TCSPC) using DeltaPro fluorescence lifetime System from Horiba upon excitation of the sample with a 390nm nanoLED. X-ray structure determination were mounted on a Bruker four circle kappa-diffractometer equippedwith a Cu INCOATED microsource, operated at 30 W power (45kV, 0.60 mA) to generate Cu K$\alpha$ radiation ($\lambda$ = 1.54178 Å) and a Bruker VANTEC 500 area detector (microgap technology) (Instituto de Ciencias de Materiales de Madrid). Dynamic Light Scattering (DLS) measurements were carried out in a Zetasizer NanoS Spectrometer (Universitat de Barcelona). The samples were measured in quartz cuvettes.

### 5.4.3. Synthesis and Characterization

**Synthesis of [Au(4-ethynyl-7-(4-nonylphenyl)benzo[c][1,2,5]thiadiazole)]$_n$ (5.1)**

Sodium acetate (0.0102 g, 0.12 mmol) and [AuCl(tht)] (0.0191 g, 0.06 mmol) were added to a stirring solution of **5.L** (0.0212 g, 0.06 mmol) in $CH_2Cl_2$/MeOH (1:1) (10 mL) under $N_2$ atmosphere at room temperature. After stirring for 30 min the resulting orange suspension was filtered, washed with $CH_2Cl_2$/MeOH (1:1) (3 x 5 mL), and dried under vacuum. Yield 63% (20 mg). IR (KBr, $cm^{-1}$): ν(C≡C): 1970.

**Synthesis of [Au(4-ethynyl-7-(4-nonylphenyl)benzo[c][1,2,5]thiadiazole)($PEt_3$)] (5.2)**

31 μL of a solution 1.0 M of $PEt_3$ in THF was added to a stirring suspension of **5.1** (0.017 g, 0.030 mmol) in dichloromethane (10 mL) under $N_2$ atmosphere at room temperature. After stirring 1h the resulting yellow solution was concentrated to half volume and hexane (10 mL) was then added in order to favour precipitation. The resulting yellow solid was filtered and dried under vacuum. Yield 75% (15 mg).

$^{31}P\{^1H\}$ NMR ($CDCl_3$, ppm): 37.6. $^1H$ NMR ($CDCl_3$, ppm): 0.88 (t, J = 6.8 Hz, 3H), 1.15-1.4 (m, 21H), 1.66 (m, 2H), 1.83 (m, 6H), 2.67 (t, J = 7.7 Hz, 2H), 7.32 (d, J = 8Hz, 2H), 7.60 (d, J = 7.4 Hz, 1H), 7.78 (d, J = 7.3 Hz, 1H), 7.84 (d, J = 8Hz, 2H). IR (KBr, $cm^{-1}$): ν(C≡C): 2108. ESI-MS (+) m/z: 677.2391 ($[M + H]^+$, calc: 677.2315).

**Synthesis of [Au(4-ethynyl-7-(4-nonylphenyl)benzo[c][1,2,5]thiadiazole)($PPh_3$)] (5.3)**

Solid $PPh_3$ (0.0086, 0.033 mmol) was added to a stirring suspension of **5.1** (0.0185 g, 0.033 mmol) in dichloromethane (10 mL) under $N_2$ atmosphere at room temperature. After stirring 1h the resulting yellow solution was concentrated to half volume and hexane (10 mL) was then added in order to favour precipitation. The resulting yellow solid was filtered and dried under vacuum. Yield 74% (20 mg).

$^{31}P\{^1H\}$ NMR ($CDCl_3$, ppm): 42.1. $^1H$ NMR ($CDCl_3$, ppm): 0.88 (t, J = 6.8 Hz, 3H), 1.15-1.4 (m, 12H), 1.66 (m, 2H), 2.67 (t, J = 7.7 Hz, 2H), 7.33 (d, J = 8Hz, 2H), 7.43-7.63 (m, 16H), 7.81 (d, J = 7.4 Hz, 1H), 7.85 (d, J = 8Hz, 2H). IR (KBr, $cm^{-1}$): ν(C≡C): 2110. ESI-MS (+) m/z: 821.2392 ($[M + H]^+$, calc: 821.2315).

**Synthesis of [Au(4-ethynyl-7-(4-nonylphenyl)benzo[c][1,2,5]thiadiazole)(Tri-1-naphthylphosphane)] (5.4)**

Solid tris-1-naphthylphosphane (0.023, 0.056 mmol) was added to a stirring suspension of **5.1** (0.0303 g, 0.054 mmol) in dichloromethane (10 mL) under $N_2$ atmosphere at room temperature. After stirring 1h the resulting yellow solution was concentrated to half volume and hexane (10 mL) was then added in order to favour precipitation. The resulting yellow solid was filtered and dried under vacuum. Yield 76% (40 mg).

$^{31}P\{^1H\}$ NMR ($CDCl_3$, ppm): 21.8. $^1H$ NMR ($CDCl_3$, ppm): 0.87 (t, J = 6.8 Hz, 3H), 1.15-1.4 (m, 12H), 1.66 (m, 2H), 2.67 (t, J = 7.7 Hz, 2H), 7.28-7.37 (m, 8H), 7.50-7.62 (m, 4H), 7.71 (d, J = 7.4 Hz, 1H), 7.82 (d, J = 8 Hz, 2H), 7.97 (d, J = 7.9 Hz, 3H), 8.05 (d, J = 7.6 Hz, 3H), 8.83 (d, J = 8.3 Hz, 3H). IR (KBr, $cm^{-1}$): ν(C≡C): 2108. MALDI-TOF (+) m/z: 1021.2 ($[M + H + CH_3OH + H_2O]^+$, calc: 1021.3).

**Synthesis of N-ethyl.N'-ethylimidazolium iodide (Im1)**

Three steps are necessary for the synthesis of N-ethyl-N'-ethylimidazolium iodide. The first one is the deprotonation of the imidazole ring with a solution of sodium methoxide. Imidazole (0.29 g, 4.26 mmol) and small amount of acetonitrile (10 mL) were introduced into a solution of sodium methoxide (0.23 g, 4.25 mmol) in dry freshly distilled methanol at room temperature. After 15 min, the white suspension was formed and concentrated under reduced pressure. The dried white powder was dissolved in acetonitrile and iodoethane (2.03 g, 13.01 mmol) was added under nitrogen atmosphere. The mixture was heated at 85ºC for 24 h. After the first alkylation, the same procedure was used for the second alkylation. After cooling to room temperature, the solvent was removed by evaporation under vacuum, and the brown solid obtained was exhaustively washed with pentane and dried. Yield: 70% (373 mg)

$^1H$ NMR ($CD_3OD$, ppm): 1.55 (t, J = 4 Hz, 6H, N-$CH_2$-**$CH_3$** (ethyl)), 4.36 (q, J = 8 Hz, 4H, N-**$CH_2$**-$CH_3$ (ethyl)), 7.80 (s, 2H, CH-**CH**-N (imidazole)), 9.27 (s, 1H, N-**CH**-N (imidazole)). IR (KBr, $cm^{-1}$): ν(=CH-): 3075, ν(N=C): 1560. MALDI-TOF (+) m/z: 125.1 ($M^+$, calc: 125.1).

**Synthesis of 1,3-diethyl-1H-benzo[d]imidazol-3-ium iodide (Im2)**

Three steps are necessary for the synthesis of 1,3-diethyl-1H-benzo[d]imidazol-3-ium iodide. The first one is the deprotonation of the imidazole ring with a solution of sodium methoxide. 1H-Benzo[d]imidazole (0.3 g, 2.54 mmol) and small amount of acetonitrile (10 mL) were introduced into a solution of sodium methoxide (0.139 g, 2.57 mmol) in dry freshly distilled methanol at room temperature. After 15 min of stirring the white suspension was formed and concentrated under reduced pressure. The dried white powder was dissolved in acetonitrile and iodoethane (613 μL, 7.62 mmol) was added under nitrogen atmosphere. The mixture was heated at 85ºC for 24 h. After the first alkylation, the same procedure was used for the second alkylation. After cooling to room temperature, the solvent was removed by evaporation under vacuum, and the brown solid obtained was wash repeatedly with pentane and dried. Yield: 80% (356 mg).

$^1$H NMR (DMSO-$d_6$, ppm): 1.54 (t, J = 7.2 Hz, 6H, N-$CH_2$-**$CH_3$** (ethyl)), 4.51 (q, J = 7.2 Hz, 4H, N-**$CH_2$**-$CH_3$ (ethyl)), 7.69 (dd, J = 9.6 Hz, J = 3.2 Hz, 2H, C-CH-CH (benzo[d]imidazole)), 8.07 (dd, J = 9.6 Hz, J = 3.2 Hz, 2H, C-CH-CH (benzo[d]imidazole)), 9.74 (s, 1H, N-**CH**-N (benzo[d]imidazole)) IR (KBr, $cm^{-1}$): ν(=CH-): 3080, ν(N=C): 1555. ESI (+) m/z: 175.1217 ($M^+$, calc:175.1230)

**Synthesis of 1H-phenanthro[9,10-d]imidazole**

A mixture of 9,10-phenanthrenequinone (0.2 g, 0,96 mmol), formaldehyde (0.214 mL, 2.88 mmol), glacial acetic acid (5 mL) and ammonium acetate (1.55 g, 20.16 mmol) was refluxed for 4 h. After cooling at room temperature, the reaction mixture was diluted with water and neutralized with concentrated aqueous ammonia until pH 7. A light cream precipitate was formed. It was filtered, washed with water, acetone, dichloromethane, and ethyl ether and then dried. Yield: 98% (206 mg).

$^1$H NMR (DMSO-$d_6$, ppm): 7.48 (t, J = 7.2 Hz, 2H, $H_{phen}$), 7.59 (t, J = 7.2 Hz, 2H, $H_{phen}$), 8.01 (s, 1H, N-CH-NH), 8.42 (d, J = 8 Hz, 2H, $H_{phen}$), 8.75 (d, J = 8 Hz, 2H, $H_{phen}$), 13.38 (br. s, 1H, N-H). )) IR (KBr, $cm^{-1}$): ν(=CH-): 3070, ν(N=C): 1565. ESI (+) m/z: 219.09 ($[M+H]^+$, calc: 219.08).

**Synthesis of 1,3-diethyl-1H-phenanthro[9,10-d]imidazol-3-ium iodide (Im3)**

Three steps are necessary for the synthesis of 1,3-diethyl-1H-phenanthro[9,10-d]imidazol-3-ium iodide. The first one is the deprotonation of the imidazole ring. To a solution of 1H-phenanthro[9,10-d]imidazole (0.3 g, 1.37 mmol) in acetonitrile (5 mL) and DMSO (2 mL) was added sodium hydroxide (0.055 g, 1.38 mmol). The reaction mixture was stirred at room temperature for 2.5 h. The temperature was increased to 37ºC, and the reaction mixture was stirred at this temperature overnight. The solvent was removed until an oil was formed and make precipitate with diethyl ether. The dried solid was dissolved in DMF (5 mL) and iodoethane (332 μL, 4.11 mmol) was added. The mixture was heated at 130ºC during 24 h. After the first alkylation, the same procedure was used for the second alkylation. After cooling up to room temperature, water was added, and a red precipitate was formed. It was filtered, washed with water and ethyl ether and then dried. Yield: 50% (188 mg).

$^1$H NMR (DMSO-$d_6$, ppm): 1.68 (t, J = 7.2 Hz, 6H, N-$CH_2$-**$CH_3$** (ethyl)), 4.98 (q, J = 7.2 Hz, 4H, N-**$CH_2$**-$CH_3$ (ethyl)), 7.92 (m, 4H, $H_{phen}$), 8.61 (d, J = 8.4 Hz, 2H, $H_{phen}$), 9.12 (d, J = 8.4 Hz, 2H, $H_{phen}$), 9.74 (s, 1H, N-CH-N). IR (KBr, $cm^{-1}$): ν(=CH-): 3070, ν(N=C): 1565. ESI (+) m/z: 275.1563 ($M^+$, calc: 275.1543).

**Synthesis of (N-ethyl.N'-ethylimidazolium)gold(I) chloride**

Silver(I) oxide (0.0459 g, 0.19 mmol) was added to a solution of N-ethyl-N'-ethylimidazolium iodide (0.1 g, 0.33 mmol) in degassed dichloromethane (20 mL). The mixture was stirred under nitrogen for 6 h at 40ºC. [AuCl(tht)] (0.13 g, 0.33 mmol) was added after the mixture was cooled to room temperature and the mixture was stirred overnight. The solution was filtered through Celite and concentrated in vacuum to half volume and hexane (10 mL) was then added in order to favour precipitation. The resulting orange solid was filtered and dried under vacuum. Yield: 70% (47 mg).

$^1$H NMR ($CD_3OD$, ppm): 1.46 (t, J = 7.2 Hz, 6H, N-$CH_2$-**$CH_3$** (ethyl)), 4.21 (q, J = 7.6 Hz, 4H, N-**$CH_2$**-$CH_3$ (ethyl)), 7.29 (s, 2H, CH-**CH**-N (imidazole)). IR (KBr, $cm^{-1}$): ν(=CH-): 3090, ν(N=C): 1565. ESI (+) m/z: 348.077 ( $[M-Cl+CN+H]^+$, calc: 348.069).

**Synthesis of (1,3-diethyl-1H-benzo[d]imidazol-3-ium)gold(I) chloride**

Silver(I) oxide (0.038 g, 0.16 mmol) was added to a solution of 1,3-diethyl-1H-benzo[d]imidazol-3-ium iodide (0.1 g, 0.33 mmol) in degassed dichloromethane (20 mL). The mixture was stirred under nitrogen for 6 h at 40ºC. After the mixture was cooled to room temperature, [AuCl(tht)] (0.106 g, 0.33 mmol) was added and the mixture was stirred overnight at room temperature. The solution was filtered through Celite and concentrated in vacuum to half volume and hexane (10 mL) was added in order to favour precipitation. The resulting orange solid was filtered and dried under vacuum. Yield: 75% (49 mg)

$^1$H NMR ($CDCl_3$, ppm): 1.54 (t, J = 7.6 Hz, 6H, N-$CH_2$-**$CH_3$** (ethyl)), 4.54 (q, J = 7.2 Hz, 4H, N-**$CH_2$**-$CH_3$ (ethyl)), 7.43 (dd, J = 9.2 Hz, J = 3.2 Hz, 2H, C-CH-CH (benzo[d]imidazole)), 7.49 (dd, J = 9.2 Hz, J = 3.2 Hz, 2H, C-CH-CH (benzo[d]imidazole)). IR (KBr, $cm^{-1}$): ν(=CH-):3080, ν(N=C): 1555. ESI (+) m/z: 398.093 ($[M-Cl+CN+H]^+$, calc: 398.085).

**Synthesis of (1,3-diethyl-1H-phenanthro[9,10-d]imidazol-3-ium)gold(I) chloride**

1,3-diethyl-1H-phenanthro[9,10-d]imidazol-3-ium iodide (75 mg, 0.19 mmol) was mixed with $Ag_2O$ (43 mg, 0.18 mmol), 3 Å molecular sieves (0.1 g) and dry $CH_2Cl_2$ (5 mL) and stirred at 40 ºC for 72 h. Then, [AuCl(tht)] (59 mg, 0.19 mmol) was added and the mixture was stirred overnight at room temperature. The solution was filtered through Celite and concentrated in vacuum to half volume and hexane (5 mL) was added in order to favor precipitation. The resulting red solid was filtered and dried under vacuum. Yield: 45% (50 mg).

$^1$H NMR (DMSO-$d_6$, ppm): 1.38 (t, J = 7.08 Hz, 6H, N-$CH_2$-**$CH_3$** (ethyl)), 4.46 (q, J = 7.12 Hz, 4H, N-**$CH_2$**-$CH_3$ (ethyl)), 7.64 (t, J = 7.8 Hz, 2H, $H_{phen}$), 7.75 (t, J = 7.32, 2H, $H_{phen}$), 8.37 (d, J = 8.4 Hz, 2H, $H_{phen}$), 8.97 (d, J = 8.4 Hz, 2H, $H_{phen}$). IR (KBr, $cm^{-1}$): ν(=CH-): 3070, ν(N=C): 1565. ESI (+) m/z: 498.124 ( $[M-Cl+CN+H]^+$, calc: 498.117).

**Synthesis of [Au(4-ethynyl-7-(4-nonylphenyl)benzo[c][1,2,5]thiadiazole) (N-ethyl.N'-ethylimidazolium)] (5.5)**

To a stirred solution of 4-ethynyl-7-(4-nonylphenyl)benzo[c][1,2,5]thiadiazole (0.051 g, 0.14 mmol) in THF-MeOH (2:1 v/v, 25 mL) was added KOH (0.0193 g, 0.34 mmol). The reaction was stirred under nitrogen for 15 min. To stirred yellow solution was added (N-ethyl.N'-ethylimidazolium)gold(I) chloride (0.05 g, 0.14 mmol). The solution was stirred overnight under nitrogen. The mixture was concentrated in vacuum to half volume and hexane (10 mL) was added in order to favour precipitation. The resulting yellow solid was filtered and dried under vacuum. Yield: 60% (57 mg)

$^1$H NMR ($CD_3OD$, ppm): 0.90 (t, J = 7.2 Hz, 3H), 1.30-1.37 (m, 21H), 1.50 (t, J = 7.2 Hz, 6H, N-$CH_2$-**$CH_3$** (ethyl)), 1.68 (m, 2H), 2.70 (t, J = 7.6 Hz, 2H), 4.28 (q, J = 7.2 Hz, 4H, N-**$CH_2$**-$CH_3$ (ethyl)), 7.29 (s, 2H, CH-**CH**-N (imidazole)), 7.32 (d, J = 8 Hz, 2H), 7.72 (d, J = 5.6 Hz, 2H), 7.90 (d, J = 8 Hz, 2H). IR (KBr, $cm^{-1}$): ν(=CH-): 3090, ν(C≡C): 2108, ν(N=C): 1565. ESI (+) m/z: 683.248 ( $[M+H]^+$, calc: 683.240).

**Synthesis of [Au(4-ethynyl-7-(4-nonylphenyl)benzo[c][1,2,5]thiadiazole) (1,3-diethyl-1H-benzo[d]imidazol-3-ium)] (5.6)**

To a stirred solution of of 4-ethynyl-7-(4-nonylphenyl)benzo[c][1,2,5]thiadiazole (0.0445g, 0.12 mmol) in THF-MeOH (2:1 v/v, 25 mL) was KOH (0.0174 g, 0.31 mmol). The reaction was stirred under nitrogen for 15 min. To stirred yellow solution was added (1,3-diethyl-1H-benzo[d]imidazol-3-ium iodide)gold(I) chloride (0.05 g, 0.12 mmol). The solution was stirred overnight under nitrogen. The mixture was concentrated in vacuum to half volume and hexane (10 mL) was added in order to favour precipitation. The resulting yellow solid was filtered and dried under vacuum. Yield: 70% (61 mg).

$^1$H NMR ($CDCl_3$, ppm): 0.88 (t, J = 6.8 Hz, 3H), 1.27-1.35 (m, 21H), 1.66 (m, 2H), 2.68 (t, J = 8 Hz, 2H), 4.61 (q, J = 7.6 Hz, 4H, N-**$CH_2$**-$CH_3$ (ethyl)), 7.33 (d, J = 8.4 Hz, 2H), 7.42 (dd, J = 9.2 Hz, J = 2.8 Hz, 2H, C-CH-CH (benzo[d]imidazole)), 7.49 (dd, J = 9.2 Hz, J = 2.8 Hz, 2H, C-CH-CH (benzo[d]imidazole)), 7.62 (d, J = 7.6 Hz, 1H), 7.82 (d, J = 7.2 Hz, 1H), 7.86 (d, J = 8 Hz, 2H). IR (KBr, $cm^{-1}$): ν(=CH-):3080, ν(C≡C): 2110 ν(N=C): 1555. ESI (+) m/z: 733.262 ( $[M+H]^+$, calc: 733.256).

**Synthesis of [Au(4-ethynyl-7-(4-nonylphenyl)benzo[c][1,2,5]thiadiazole) (1,3-diethyl-1H-phenanthro[9,10-d]imidazol-3-ium)] (5.7)**

To a stirred solution of of 4-ethynyl-7-(4-nonylphenyl)benzo[c][1,2,5]thiadiazole (0.014g, 0.039 mmol) in THF-MeOH (2:1 v/v, 25 mL) was KOH (0.0054 g, 0.096 mmol). The reaction was stirred under nitrogen for 15 min. To stirred yellow solution was added (1,3-diethyl-1H-phenanthro[9,10-d]imidazol-3-ium)gold(I) chloride (0.02 g, 0.039 mmol). The solution was stirred overnight under nitrogen. The mixture was concentrated in vacuum to half volume and hexane (10 mL) was added in order to favour precipitation. The resulting yellow solid was filtered and dried under vacuum. Yield: 50% (6 mg).

$^1$H NMR ($CDCl_3$, ppm):0.88 (t, J = 6.2 Hz, 3H), 1.26-1.40 (m, 21H), 1.68 (t, J = 8.3 Hz, 2H), 1.74 (t, J = 7.2 Hz, 6H, N-$CH_2$-**$CH_3$** (ethyl)), 2.68 (t, J = 7.7 Hz, 2H), 5.22 (q, J = 7.2 Hz, 4H, N-**$CH_2$**-$CH_3$ (ethyl)), 7.34 (d, J = 8.1 Hz, 2H), 7.63 (d, J = 7.3 Hz, 1H), 7.76 (t, J = 8.3 Hz, 4H, $H_{phen}$), 7.84 (d, J = 7.4 Hz, 1H), 7.88 (d, J = 8.1 Hz, 2H), 8.41 (d, J = 8.2 Hz, 2H, $H_{phen}$), 8.86 (d, J = 8.2 Hz, 2H, $H_{phen}$). IR (KBr, $cm^{-1}$): ν(=CH-): 3070, ν(C≡C): 2110, ν(N=C): 1565. ESI (+) m/z: 833.327 ( $[M+H]^+$, calc: 833.287).

### 5.4.4. Preparation of matrixes doped with L and 2-7 complexes

Cellulose, PMMA, PS and Zeonex (Zeon Corporation, Japan) were used as matrix polymers. The films were prepared via drop-casting, using a mixture of dopant and host (Cellulose, PMMA, PS or Zeonex). Polymer solutions were prepared as follows: PMMA (MW 120000, 30% solution in dichloromethane), PS (MW 45000, 35% solution in dichloromethane). Cellulose (MW 30000, 20% in acetone), Zeonex (20% in chloroform). The same volume of a solution of the sample was added to a polymer solution at a concentration of 20 μg/mL. The films were drop-cast onto a quartz substrate at room temperature to avoid any thermal annealing.

## 5.5. References


1. Thomas, K. R. J., Lin, J. T., Velusamy, M., Tao, Y. T. and Chuen, C. H. Adv. Funct. Mater. **2004**, 14, 83–90.

2. Kono, T., Kumaki, D., Nishida, J., Sakanoune, T., Kakita, M., Tada, H., Tokito, S. and Yamashita, Y. Chem. Mater. **2007**, 19, 1218–1220.

3. Geng, Y., Pfattner, R., Campos, A., Hauser, J., Laukhin, V., Puigdollers, J., Veciana, J., Mas-Torrent, M., Rovira, C., Decurtins, S., and Liu, S. X. Chem. - A Eur. J. **2014**, 20, 7136–7143.

4. Neto, B. A. D., Lapis, A. A. M., Da Silva Júnior, E. N. and Dupont, J. Eur. J. Org. Chem. **2013**, 228–255.

5. Geng, Y., Pop, F., Yi, C., Avarvari, N., Grätzel, M., Decurtins, S. and Liu, S. X. New J. Chem. **2014**, 38, 3269–3274.

6. Pop, F., Seifert, S., Hankache, J., Ding, J., Hauser, A. and Avarvari, N. Org. Biomol. Chem. **2015**, 13, 1040–1047.

7. Neto, B. A. D., Carvalho, P. H. P. R. and Correa, J. R.. Acc. Chem. Res. **2015**, 48, 1560–1569.

8. Cozzolino, A. F., Vargas-Baca, I., Mansour, S. and Mahmoudkhani, A. H. J. Am. Chem. Soc. **2005**, 127, 3184–3190.

9. Ams, M. R., Trapp, N., Schwab, A., Milić, J. V. and Diederich, F. Chem. - A Eur. J. **2019**, 25, 323–333.

10. Yamashita, Y., Suzuki, K. and Tomura, M. Synth. Met. **2003**, 133–134, 341–343.

11. Bashirov, D. A., Sukhikh, T. S., Kuratieva, N. V., Naumov, D. Y., Konchenko, S. N., Semenov, N. A. and Zibarev, A. V. Polyhedron **2012**, 42, 168–174.

12. Goswami, S., Winkel, R. W. and Schanze, K. S. Inorg. Chem. **2015**, 54, 10007–10014.

13. Möller, A., Bleckenwegner, P., Monkowius, U. and Mohr, F. J. Organomet. Chem. **2016**, 813, 1–6.

14. Zhang, X., Zhang, X., Yang, B., Wang, S., Liu, M., Zhang, Y., Tao, L. and Wei, Y. RSC Adv. **2013**, 3, 9633–9636.

15. de Aquino, A., Caparrós, F. J., Truong, K. N., Rissanen, K., Ferrer, M., Jung, Y., Choi, H., Lima, J. C. and Rodríguez, L. Dalton Trans. **2021**, 50, 3806–3815.

16. de Aquino, A., Caparrós, F. J., Aullón, G., Ward, J. S., Rissanen, K., Jung, Y., Choi, H., Lima, J. C. and Rodríguez, L. Chem. - A Eur. J. **2021**, 27, 1810–1820.

17. Arcau, J., Andermark, V., Rodrigues, M., Giannicchi, I., Pérez-Garcia, L., Ott, I. and Rodríguez, L. Eur. J. Inorg. Chem. **2014**, 2014, 6117–6125.

18. Livi, S., Gérard, J. F. and Duchet-Rumeau, J. Chem. Commun. **2011**, 47, 3589–3591.

19. Tapu, D., Owens, C., Vanderveer, D. and Gwaltney, K.. **2009**, 270–276.

20. Caparrós, F. J., Outis, M., Jung, Y., Choi, H., Lima, J. C. and Rodríguez, L. Molecules 2020, **25**, 949–960.

21. Svahn, N., Moro, A. J., Roma-Rodrigues, C., Puttreddy, R., Rissanen, K., Baptista, P. V., Fernandes, A. R., Lima, J. C. and Rodríguez, L. Chem. - A Eur. J. **2018**, 24, 14654–14667.

22. Rubbiani, R., Kitanovic, I., Alborzinia, H., Can, S., Kitanovic, A., Onambele, L. A., Stefanopoulou, M., Geldmacher, Y., Sheldrick, W. S., Wolber, G., Prokop, A., Wölf, S. and Ott, I. J. Med. Chem. **2010**, 53, 8608–8618.

23. Lima, J. C. and Rodríguez, L. Chem. Soc. Rev. **2011**, 40, 5442–5456.

24. Hashmi, A. S. K. Acc. Chem. Res. **2014**, 47, 864–876.

25. Schmidbaur, H. and Schier, A. Chem. Soc. Rev. **2012**, 41, 370–412.

26. Meier-Menches, S. M., Aikman, B., Döllerer, D., Klooster, W. T., Coles, S. J., Santi, N., Luk, L., Casini, A. and Bonsignore, R. J. Inorg. Biochem. **2020**, 202, 110844.

27. Ibáñez, S., Poyatos, M. and Peris, E. J. Organomet. Chem. **2020**, 917, 121284.

28. Echeverri, M., Martin, I., Concellón, A., Ruiz, C., San Anselmo, M., Gutiérrez-Puebla, E., Serrano, J. L. and Gómez-Lor, B. ACS Omega **2018**, 3, 11857–11864.

29. Tanabe, I., Kurawaki, Y., Morisawa, Y. and Ozaki, Y. Phys. Chem. Chem. Phys. **2016**, 18, 22526–22530.

30. Goswami, S., Wicks, G., Rebane, A. and Schanze, K. S. Dalton Trans. **2014**, 43, 17721–17728.

31. Abeywickrama, C. S., Wiesinghe, K. J., Stahelin, R. V. and Pang, Y. Sensors Actuators, B Chem. **2019**, 285, 76–83.

32. Zhang, J., Konsmo, A., Sandberg, A., Wu, X., Nyström, S., Obermüller, U., Wegenast-Braun, B. M. Konradsson, P., Lindgren, M. and Hammarström, P. J. Med. Chem. **2019**, 62, 2038–2048.

33. Pina, J., De Melo, J. S., Breusov, D. and Scherf, U. Phys. Chem. Chem. Phys. **2013**, 15, 15204–15213.

34. Rietsch, P., Sobottka, s., Hoffmann, K., Hildebrandt, P., Sarkar, B., Resch-Genger, U. and Eigler, S. ChemPhotoChem **2020**, 4, 668–673.

35. Rietsch, P., Sobottka, S., Hoffmann, K., Popov. A. A., Hildebrandt, P., Sarkar, B., Resch-Genger, U. and Eigler, S. Chem. - A Eur. J. **2020**, 26, 17361–17365.

36. Misra, R., Gautam, P., Jadhav, T. and Mobin, S. M. J. Org. Chem. **2013**, 78, 4940–4948.

37. Reichardt, C. Solvents and solvents effects in organic chemistry. Wiley-VCH, **2003**.

38. Mukhopadhyay, A., Maka, V. K. and Moorthy, J. N. Phys. Chem. Chem. Phys. **2017**, 19, 4758–4767.

39. Gülseven Sidir, Y. and Sidir, I. Spectrochim. Acta - Part A Mol. Biomol. Spectrosc. **2013**, 102, 286–296.

40. Manning, S. J., Bogen, W. and Kelly, L. A. J. Org. Chem. **2011**, 76, 6007–6013.

41. Aliaga-Alcalde, N. and Rodríguez, L. Inorg. Chim. Acta **2012**, 380, 187–193.

42. Pazini, A., Maqueira, L., da Silveira Santos, F., Rodrigues Jardim Barreto, A., dos Santos Carvalho, R., Miranda Valente, F., Back, D., Queiroz Aucélio, R., Cremona, M., Rodembusch, F. S., and Limberger. Dyes. Pigment. **2020**, 178, 108377.

43. Jadhav, T., Dhokale, B. and Misra, R. J. Mater. Chem. C **2015**, 3, 9063–9068.

# CHAPTER 6

## Aggregation studies and biological activity of hybrid gold(I)/gold(0) systems

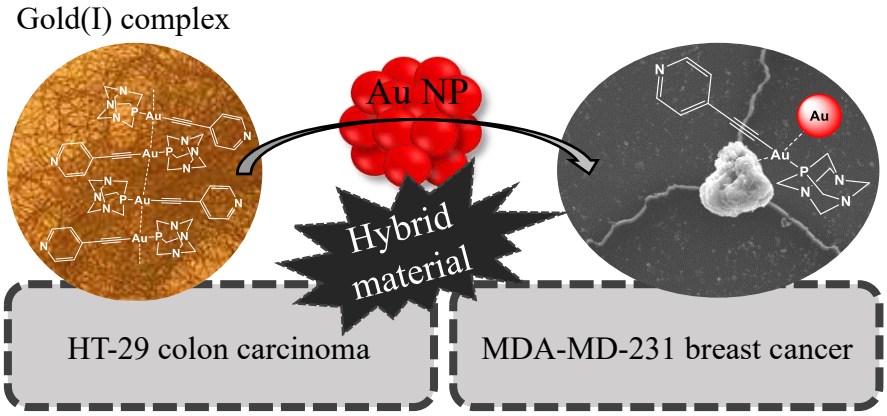


Part of this Chapter has been published in M. Dalmases, A. Pinto, P. Lippmann, I. Ott, L. Rodríguez, and A. Figuerola. Front. Chem. **2019**, 7, 60.

# 6. AGGREGATION STUDIES AND BIOLOGICAL ACTIVITY OF HYBRID GOLD(I)/GOLD(0) SYSTEMS

## 6.1. Introduction

The ability of small molecules to self-assemble by non-covalent interactions lead to the possibility of building supramolecular structures with a large number of specific functions, properties and morphologies.[1–3] In order to control the self-assembly, it is necessary a careful molecular design of the building blocks, where specific functional groups must be introduced for the construction of the resulting expected supramolecular structures. With this in mind, organometallic complexes present a rich chemistry due to the possibility of introducing weak non-covalent intra- or intermolecular bonds of different nature that are not common in pure organic compounds.[4] Among them, as it is previously said, metallophilic interactions may play an important role in the resulting supramolecular morphologies. In particular, gold(I) organometallic complexes have found to be excellent building blocks for the construction of plenty of different supramolecular assemblies with different shapes depending on the chemical structure and on the reaction conditions.[5] In these cases, aurophilic contacts, not only contribute in the stability of the assembly, but also in the resulting luminescent properties.[6,7]

Taking advantage of these aurophilic aggregation, it is also possible to construct gold(0) structures using a supramolecular system as a template. Thus, the application of an external stimuli such as heat or electron beam as a reducing agent, or directly catalytic amounts of a reductant can form plasmonic architectures in which the morphology of the previous supramolecular assembly has been maintained starting from Au(I) assemblies and finishing with Au(0) materials, at the nano- or micro- level, with the similar shape.[8–12] This methodology allows an easy control in the size and shape of the metal nanostructures. These two parameters, size and shape, strongly affect the optical properties of the gold nanostructures, that present an intense absorption band in the visible or near infrared region (NIR), known as the Localized Surface Plasmon Resonance (LSPR) (Figure 6.1).[13] The interaction of light with the metal surface results in a coupling of the free electrons of the metal and the light giving a coherent surface-confined oscillation with a resonant frequency that strongly depends on the material itself.

Therefore, the ability of selectively tune the LSPR features that result from these materials becomes increasingly important.

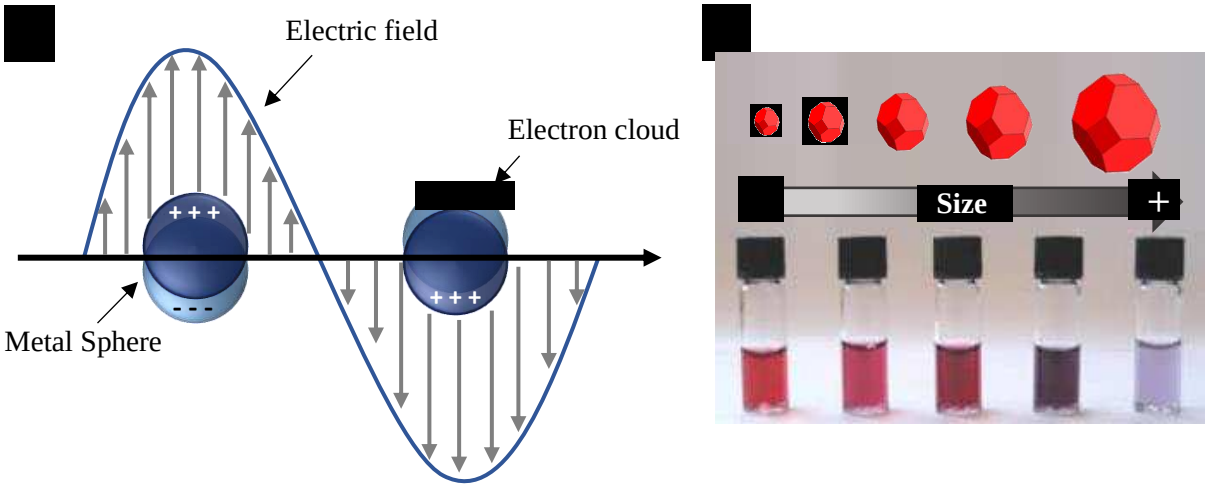


**Figure 6.1.** Schematic illustration of LSPR phenomenon (A) and figure that illustrates the relationship between the size and the optical properties (B).

It is known that supramolecular organogels consisting of multiple entangled fibrillary networks can be used to influence the shape and nanostructure of the inorganic material.[14] This synergy of the supramolecular chemistry and nanostructured materials have been widely used in the construction of hybrid materials, which can improve the individual properties and may be useful in the promising field of supramolecular devices.[15–18] Among all the possibilities, a good approach can be the incorporation of gold nanoparticles into a gold(I) supramolecular structure taking advantage of the metallophilic interactions that may happen also between an organometallic complex and the surface of the gold nanoparticles. In this way, the incorporation of gold nanoparticles in a supramolecular assembly of a low molecular weight gold(I) metallogelator was reported in the group a few years ago. This unconventional mixture allowed the complete solubilization of hydrophobic colloids in water due to the establishment of metallophilic interactions as well as being a way to tune the LSPR band.[19]

Based on this, the preparation of hybrid materials based on a combination of a gold(I) metallogelator and gold nanoparticles is presented in this chapter with the aim of studying the possible influence of the addition of the solubility of gold nanoparticles on aqueous or organic solvents on the resulting supramolecular structure and properties. Additionally, since the antitumoral properties against cancer cells are well known for both gold nanoparticles[20,21] and gold(I) compounds,[22,23] the biological activity of the resulting

hybrid systems (nanocomposites) has been studied and compared with the isolated gold(I) and gold(0) precursors.

## 6.2. Results and Discussion

### 6.2.1. Synthesis and Characterization

The synthesis of the nanocomposites consists of the mixture of an organometallic gold(I) compound and different amounts of a solution of dispersed gold nanoparticles. In this way, we used three different concentrations of nanoparticles, being called xxx_1 for the sample that contains the highest concentration of nanoparticles and xxx_3 for the lowest concentration one. The reaction was done in two different solvents in order to test if there are differences in the resulting aggregates. So, a hydrophobic solvent such as chloroform and a hydrophilic solvent such as water were chosen in these reactions. The nomenclature used for each of the nanocomposites is displayed in Scheme 6.1.

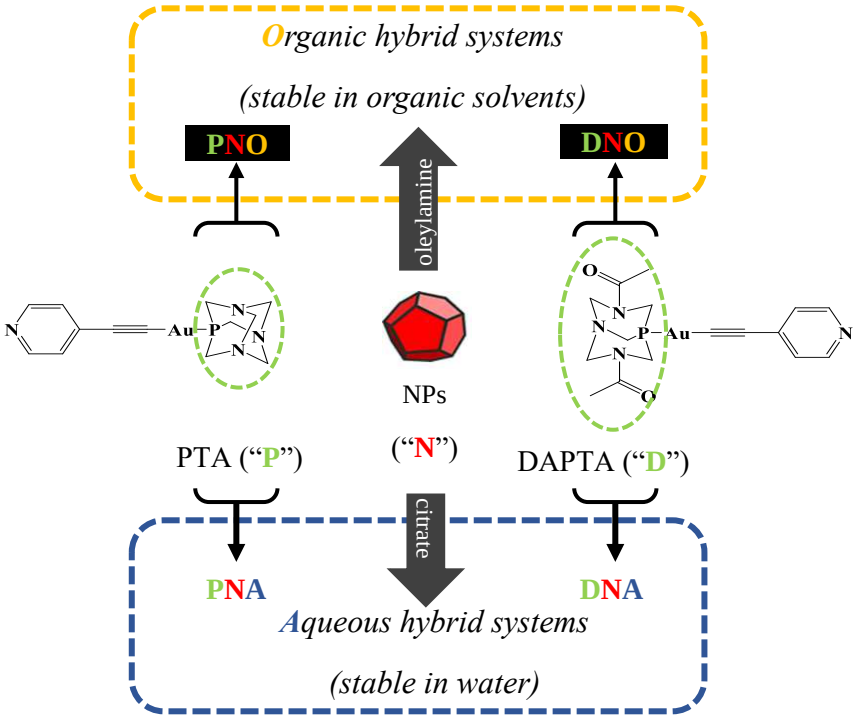


**Scheme 6.1.** Types of nanocomposites prepared, and description of the nomenclature used for each them. "N" indicates nanoparticles; "P", PTA phosphane; "D", DAPTA phosphane; "O", organic medium and "A", aqueous medium.

The characterization of the nanocomposites has been done with different techniques. The infrared spectra display the bands from the organometallic complex and from the stabilizing ligands of the nanoparticles, being an indicative of the presence of the both parts. Additionally, the alkynyl vibration band at 2100 $cm^{-1}$ is broadened with respect to the organometallic hydrogelator, being indicative of possible Au···π interaction between the nanoparticle surface and the pyridylethynyl group of the complex, in agreement with our previous reported data.[19] The UV-vis absorption spectra of the hybrid material systems present two different bands (Figure 6.2). On one hand, the band around 260 nm is attributed to the chromophoric unit of the gold(I) complex (4-ethynylpyridine).[24] On the other hand, the band at 500-600 nm is assigned to the surface plasmon resonance of the gold nanoparticles. Moreover, we observed that the amount of gold nanoparticles present in the nanocomposites has a direct effect in the recorded spectra. An increase of the intensity of the higher energy band is observed when larger amount of nanoparticles is used. A loss of the vibrational shape in the band is also observed as an evidence of the interaction between nanoparticles and the corresponding organometallic complex. Also, there is a slight red shift of 2 nm of the plasmonic band of gold nanoparticles with increasing interactions with the nanocomposite.

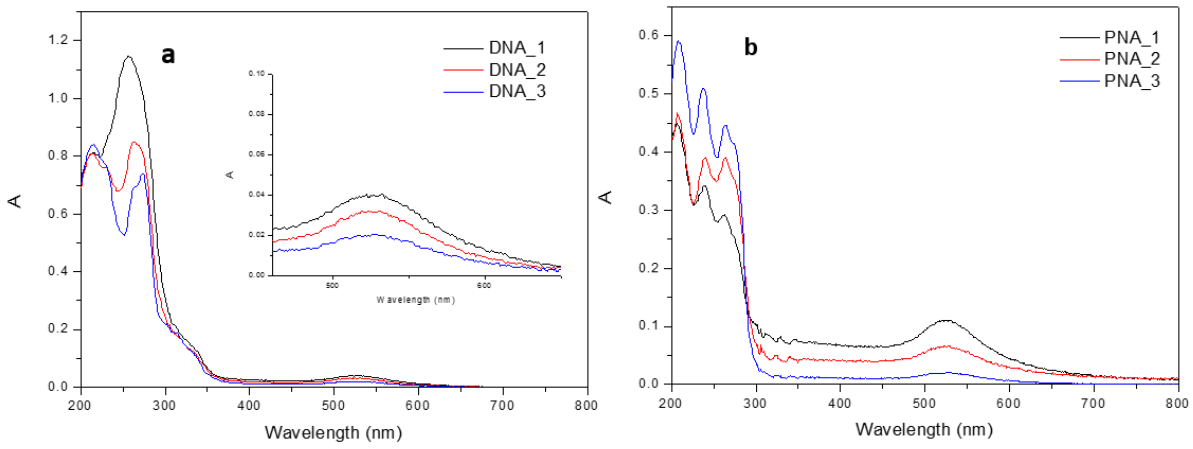


**Figure 6.2.** UV-Visible absorption spectra of (a) DNA_1-3 and (b) PNA_1-3 samples.

### 6.2.2. Aggregation studies

Aggregation studies in solid and in solution have been performed in order to better understand the interaction between the gold(I) complexes and the gold nanoparticles and how the amount of nanoparticles added affects the resulting assemblies. Scanning Electron Microscope (SEM) shows the size and the shapes of the aggregates in the solid state. Two kind of aggregates have been observed in the recorded micrographs: gold

agglomerates and long fibers. The first ones present sizes ranging between 100 and 300 nm approximately and are surrounded by a shell of the long fibers of the organometallic complex. In fact, a shrinkage of the aggregates was observed when the image is recorded with backscattered electrons, where only the elements that have a high atomic number have a bright contrast. Therefore, the significant reduction in the volume of the cluster is indicative of the presence of an organic shell around the metallic nanoparticles. The long fibers are in the microscale range and correspond to the aggregates formed through supramolecular interactions between the molecules of organometallic gold(I) complex, as previously identified.[10] The vanishing of these fibers when it is used the backscattering electrons mode confirms their organic origin.

A trend can be observed when we compare the micrographs of the nanocomposites formed at three different amounts of nanoparticles used. Generally speaking, higher amount of the aggregated nanocomposites is observed when the quantity of the nanoparticles used in the synthesis is larger, while few or none nanocomposite were found in samples that contain the less amount of gold nanoparticles. However, the trend of the fibers is the opposite, long fibers were only observed when the quantity of nanoparticles is low (Figure 6.3). In this way, the scarcity of gold nanoparticles allows the organometallic gold(I) complex to aggregate itself through supramolecular interactions. The trend is conserved independently of the solvent used; in water, the supramolecular structures of the organometallic part can be found even with the highest amount of gold nanoparticles. This can be attributed to the better capacity of this complex to aggregate in water in comparison with chloroform.

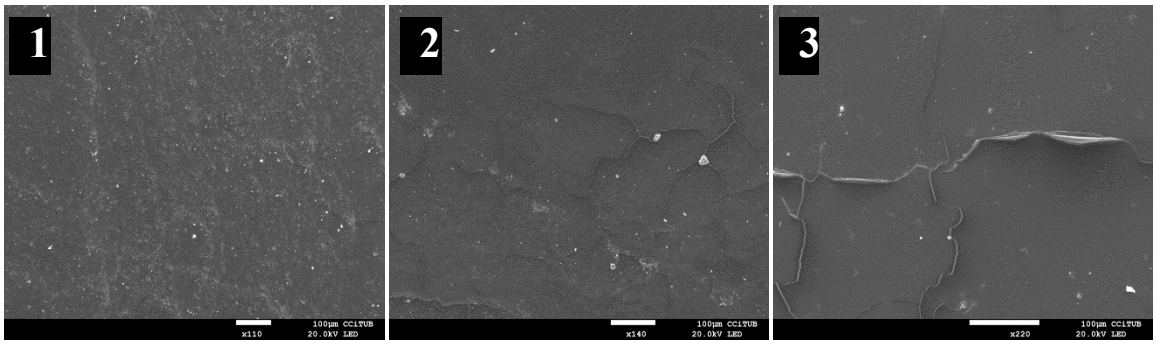


**Figure 6.3.** SEM micrographs of DNO_1 (1), DNO_2 (2) and DNO_3 (3) showing the topographical micrographs recorded with secondary electrons.

Aggregation studies in solution were performed in order to know if these aggregates also exist in solution or are only formed when the sample is dried. The presence and size of

the aggregates was firstly analysed by Dynamic Light Scattering (DLS) for those samples prepared with the highest (xxx_1) and medium (xxx_2) amount of gold nanoparticles at room temperature. Samples with less amount of nanoparticles (xxx_3) were not measured since very few aggregates of the nanocomposite were observed by SEM. Two additional diluted concentrations (i.e. with DNO_1_1 being the as-prepared sample, and DNO_1_2 and DNO_1_3 the samples derived from 1/500 and 1/1000 dilution). Diluted samples (xxx_x_3) do not present any evidence of aggregates in solution. DLS measurements of the other samples (xxx_x_1 and xxx_x_2) confirms the sizes observed by SEM, being of hundreds of nanometres as well as a population of some microscale aggregates. DLS data shows aggregates in the range of 20-60 nm in some samples, that were not observed in SEM micrographs. This kind of aggregates may be found at the initial state of the aggregates formation and then, when the sample is dried, they tend to agglomerate. In general trend, the samples (xxx_x_2) contain two populations of aggregates whereas more concentrated samples (xxx_x_1) are more homogeneous (Figure 6.4). Thus, it seems that lower concentrations favours the large aggregation of the organometallic compound instead of forming only aggregates of nanocomposite.

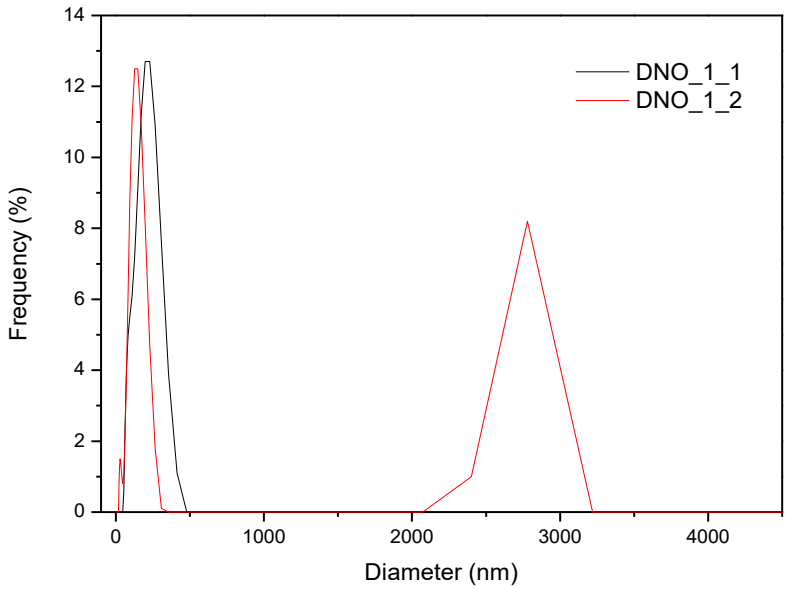


**Figure 6.4.** Size distribution obtained by Dynamic Light Scattering (DLS) for DNO_1_1 and DNO_1_2 samples in chloroform.

Small Angle X-ray Scattering (SAXS) studies were performed in order to know the size and the shape of the aggregates in the early stage. The measurements were performed with the same set of samples as in DLS and at different temperatures (from 20 to 40ºC in

a 5ºC gradient, for better analysis of the aggregates' formation). The low-resolution structures were reconstructed ab initio from the scattering patterns using the DAMMIN program (Figure 6.5).[25]

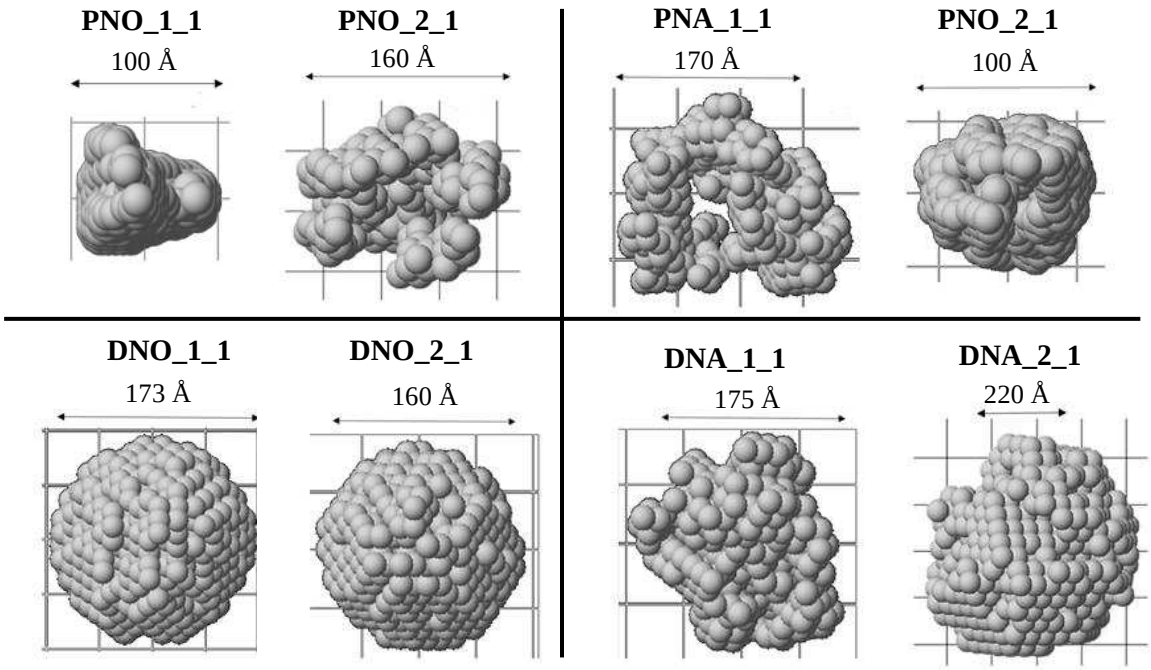


**Figure 6.5.** DAMMIN low resolution structures reconstructed from SAXS patterns for PNX_x_x and DNX_x_x at 20ºC. Grid: 50 Å.

The samples with the lowest amount of nanoparticles (xxx_3) were not measured due to the lack of aggregation detected in DLS studies. No aggregation was observed for more diluted samples (xxx_x_3), as in DLS measurements, while appreciable degrees of aggregation were measured for the other more concentrated two solutions. These data seem to point out the existence of a critical concentration of aggregates below which they lose their stability. In general, the size of the aggregates is between 10 and 30 nm which in general agrees with the small aggregates observed in DLS measurements for some samples. The values obtained by DLS and SAXS highlight the possibility that the large aggregates (100 - 300 nm) observed in SEM can be formed by smaller subunits (10 - 60 nm) that are merged together with time and upon drying the solutions. Therefore, gold nanoparticles are mainly wrapped within a network of organometallic complex forming small agglomerates and then, they tend to aggregate through non-covalent interactions to

form larger structures. No clear trend was observed with the variation of the temperature, only in the case of DNO_2, that a significant increase on the size was detected. This can be due to the higher solubility in water of the DAPTA phosphane and the increase of temperature favors the intermolecular hydrophobic interactions. So, the size of the aggregates increases due to the capacity of the DAPTA moiety to avoid the contact with the organic solvent. Some trend can be observed regarding the amount of nanoparticles added. In organic media, PNO nanocomposites increase the size when the number of nanoparticles decreases. On the contrary, DNO nanocomposites follow the opposite trend, their size decrease together with the amount of nanoparticles. This could be rationalized in terms of solubility: the presence of more nanoparticles leads to the formation of more quantity of nanocomposites, so DAPTA (in DNO) presents lower solubility than PTA (in PNO) in organic media and in this way, they tend to present larger aggregates when the concentration of nanoparticles increases. It is not surprising that in aqueous media we observe the inverse trend: PNA nanocomposites are smaller when the nanoparticles added decrease while DNA nanocomposites, on the contrary increase.

### 6.2.3. Biological assays.

Previous experiments demonstrate the biological activity of [Au(C≡Cpy)($PR_3$)] ($PR_3$ = PTA and DAPTA) complexes and showed the preference for the PTA over the DAPTA phosphane ligand as metallodrugs. The effects against the tumour cells are clearly related to the presence of gold atoms in the complexes. Hence, as it is also well-known the potential antitumoral activity of gold nanoparticles, we envisaged that the biological activity of the synthesized nanocomposites deserved their investigation, in order to compare if the resulting activity improves the corresponding to their individual counterparts (organometallic hydrogelators and nanoparticles separately). In this way, the nanocomposites synthesized have been tested in two different tumour cells: HT-29 colon carcinoma and MDAMB-231 breast cancer (Table 6.2). It can be directly observed in Table 6.2 that the hybrid systems present higher cytotoxicity than their respective counterparts. This may be a nice cooperative effect of both parts, the organometallic and the nanoparticles. Considering the effect of the solvent, the nanocomposites synthesized in the organic media present higher cytotoxicity than those synthesized in aqueous media. The DAPTA nanocomposites show higher cytotoxicity with respect to the PTA nanocomposites in aqueous media. This may be due to the highest solubility of the

DAPTA phosphane in that solvent. On the other hand, the nanocomposites soluble in organic media present the highest cytotoxicity and those with better activity are those with smaller aggregates size (PNO_1 and DNO_2). This may be ascribed to the better capacity of entering the cells. No significant preference of the nanocomposites has been observed for one specific tumour cell although, in general, better activity can be observed against MDA-MB-231 cell line.

**Table 6.2.** $IC_{50}$ values of the different hybrid systems and corresponding counterparts.

| Compound | HT-29 (mM) | MDA-MB-231 (mM) |
|---|---|---|
| **DNA_1** | 6.14 ± 0.29 | > 10 |
| **DNA_2** | > 6.40 | > 7.7 |
| **PNA_1** | > 10 | > 10 |
| **PNA_2** | > 10 | > 10 |
| **DNO_1** | 3.41 ± 0.29 | 1.73 ± 0.44 |
| **DNO_2** | 2.76 ± 0.23 | > 1.4 |
| **PNO_1** | 1.82 ± 0.32 | 1.00 ± 0.17 |
| **PNO_2** | 4.16 ± 0.38 | 2.02 ± 0.40 |
| **Org NPs** | 5.39 ±0.89 | 6.01 ± 0.85 |
| **Aqueous NPs** | > 10 | > 10 |
| **AupyPTA**[a] | 56.09 ± 3.05 | 52.32 ± 4.76 |
| **AypyDAPTA**[a] | 74.78 ± 9.34 | 34.07 ± 3.51 |

[a] From ref;[26] results of independent repeated experiments are presented

## 6.3. Conclusions

The reaction of gold(I) complexes with gold nanoparticles gives rise to the correct formation of hybrid materials (nanocomposites) both in water and in organic (chloroform) media. SEM, DLS and SAXS reveal the influence of the amount of nanoparticles added in the reaction on the resulting aggregates' size and shape of the resulting nanocomposites. The lower $IC_{50}$ values obtained for the hybrid material compared with the individual counterparts suggest the existence of a synergetic effect. These results represent the beginning for the exploitation of these novel nanocomposites in the biomedical field.

## 6.5. Experimental Section

### 6.5.1. General procedures

Commercial reagents 1,3,5-triaza-7-phosphatricyclo[3.3.1.13.7]decane (PTA; 97%, Aldrich), 3,7-diacetyl-1,3,7-triaza-5-phosphabicyclo[3.3.1]nonane (DAPTA; 97%, Aldrich), Gold(III) chloride trihydrate ($HAuCl_4 \cdot 3H_2O$, ≥99.9, Aldrich), trisodium citrate dihydrate ($HOC(COONa)(CH_2COONa)_2 \cdot 2H_2O$, Aldrich), oleylamine (OLAm, 70%, Aldrich), oleic acid (OLAc, ≥99%, Aldrich), 1-octadecene (ODE, 90%, Aldrich), 2-Propanol (iPrOH, for HPLC, VWR Chemicals), and chloroform (CHCl3, 99.2%, VWR Chemicals) have been used as received. The synthesis and characterization of gold(I) complexes was carried out by Dr. Elisabet Aguiló from *Departament d'Inorgànica i* Orgànica, Universitat de Barcelona. Literature methods were used to prepare [Au(C≡C-$C_5H_4N$)(PTA)][24] and [Au(C≡C-$C_5H_4N$)(DAPTA)][10] compounds. The correct formation of the compounds was checked by $^1H$ NMR where the same pattern as the reported was obtained. Synthesis and characterization of gold nanoparticles was carried out by Dr. Mariona Dalmases from *Departament d'Inorgància i Orgànica*, Universitat de Barcelona. The synthesis of hydrophilic gold NPs was based on that reported by Turkevish and co-workers[27] and the synthesis of the hydrophobic gold NPs was adapted from that described by Yu and co-workers.[28] Transmission Electron Microscope (TEM) micrograph was used to evaluate the morphological and size distribution of the nanoparticles. The hydrophilic nanoparticles comprise a significant distribution of shapes: spherical, triangular and elongated whereas, the hydrophobic nanoparticles shown only spherical faceted nanoparticles. Both shown an average diameter of ca. 14 nm.

### 6.5.2. Physical measurements

A JEOL 2000 FX II conventional TEM operating at an accelerating voltage of 80 kV was used. Scanning electron microscopy (SEM) was carried out at 20 kV using J-7100F (Jeol) equipped with a thermal field electron source. Dynamic Light Scattering (DLS) measurements were carried out in a Zetasizer NanoS Spectrometer. The samples were measured in quartz cuvettes. IR spectra were recorded with a FTIR 520 Nicolet Spectrophotometer. For the measurements, a pellet of a mixture of the sample and KBr was used. A Cary 100 Scan 388 Varian UV/Vis spectrophotometer was used quartz cuvettes for optical characterization. SAXS was performed on the NCD-SWEET

beamline at the ALBA Synchrotron at 12.4 keV, and the distance sample/detector was 6.2 m to cover the range of momentum transfer of $0.028 < q < 2.56$ nm−1. The data were collected on a Pilatus3S 1M detector with a pixel size of 172.0 × 172.0 μm2. The exposure time was 30 s.

### 6.5.3. Synthesis of hybrid organometallic supported NPs

**Au-DAPTA nanocomposites in organic media (DNO systems)**

[Au(C≡C-$C_5H_4N$)(DAPTA) (0.0042 g, 0.0073 mmol) were dissolved in 8 mL of chloroform and mixed with a solution of hydrophobic Au nanoparticles dispersed in chloroform at room temperature. The solution was shaken for 24 h. After this time, the solution was centrifuged and the resultant precipitated was redispersed in chloroform.

**Au-PTA nanocomposites in organic media (PNO systems)**

The functionalization of hydrophobic Au nanoparticles with [Au(C≡C-$C_5H_4N$)(PTA)] was adapted from the protocol described above but using 0.0013 g (0.0085 mmol) of [Au(C≡C-$C_5H_4N$)(PTA)] instead of [Au(C≡C-$C_5H_4N$)(DAPTA)].

**Au-DAPTA and Au-PTA nanocomposites in aqueous media (DNA and PNA systems, respectively)**

The synthesis of Au-DAPTA (or -PTA) nanocomposites was carried out following the same procedure described for the nanocomposites in organic media but substituting the chloroform for deionized water.

Three different samples of each nanocomposite were synthesised using different amounts of Au NPs. The volumes of Au NPs solution in each case are compiled in Table 6.3.

**Table 6.3.** Volumes of Au NP solution used in each synthesis. The concentration of Au NPs in aqueous solution was 0.015 μM and in organic solution 2.33 μM

| SAMPLE | Volume of Au NP solution |
|---|---|
| DNO_1 | 540 μL hydrophobic Au NPs |
| DNO_2 | 270 μL hydrophobic Au NPs |
| DNO_3 | 54 μL hydrophobic Au NPs |
| DNA_1 | 1600 μL hydrophilic Au NPs |
| DNA_2 | 800 μL hydrophilic Au NPs |
| DNA_3 | 160 μL hydrophilic Au NPs |
| PNO_1 | 540 μL hydrophobic Au NPs |
| PNO_2 | 270 μL hydrophobic Au NPs |
| PNO_3 | 54 μL hydrophobic Au NPs |
| PNA_1 | 1600 μL hydrophilic Au NPs |
| PNA_2 | 800 μL hydrophilic Au NPs |
| PNA_3 | 160 μL hydrophilic Au NPs |

## 6.6. References


1. Mayoral Muñoz, M. J. and Fernández, G. Chem. Sci. **2012**, 3, 1395–1398.
2. Sevim, S., Sorrenti, A., Franco, C., Furukuma, S., Pané, S., deMello, A. J. and Puigmartí-Luis, J. Chem. Soc. Rev. **2018**, 47, 3788–3803.
3. Sun, Q. F., Iwasa, J., Ogawa, D., Ishido, Y., Sato, S., Ozeki, T., Sei, Y., Yamaguchi, K. and Fujita, M. Science **2010**, 328, 1144–1147.
4. Zhang, J. and Su, C. Y. Coord. Chem. Rev. **2013**, 257, 1373–1408.
5. Lima, J. C. and Rodríguez, L. Inorganics **2015**, 3, 1–18.
6. Rodríguez, L., Ferrer, M., Crehuet, R., Anglada, J. and Lima, J. C. Inorg. Chem. **2012**, 51, 7636–7641.
7. Schmidbaur, H. and Schier, A. Chem. Soc. Rev. **2012**, 41, 370–412.
8. Aguiló, E., Dalmases, M., Lin, M., Lima, J. C., Gavara, R., Figuerola, A., Llorca, J. and Rodríguez, L. Dalton Trans. **2020**, 49, 4200–4205.
9. Ezquerra, R., Eaves, S. G., Bock, S., Skelton, B. W., Pérez-Murano, F., Cea, P., Martín, S. and Low, P. J. J. Mater. Chem. C **2019**, 7, 6630–6640.
10. Aguiló, E., Gavara, R., Lima, J. C., Llorca, J. and Rodríguez, L. J. Mater. Chem. C **2013**, 1, 5538–5547.
11. Ballesteros, L. M., Martín, S., Cortés, J., Marqués-González, S., Pérez-Murano, F., Nichols, R. J., Low, P. J. and Cea, P. Adv. Mater. Interfaces **2014**, 1, 1–6.
12. Muhich, C. L., Qiu, J., Holder, A. M., Wu, Y. C., Weimer, A. W., Wei, W. D., McElwee-White, L. and Musgrave, C. B. ACS Appl. Mater. Interfaces **2015**, 7, 13384–13394.
13. Motl, N. E., Smith, A. F., Desantis, C. J. and Skrabalak, S. E. Chem. Soc. Rev. **2014**, 43, 3823–3834.
14. Van Bommel, K. J. C., Friggeri, A. and Shinkai, S. Angew. Chemie - Int. Ed. **2003**, 42, 980–999.
15. Vemula, P. K. and John, G. Chem. Commun. **2006**, 2218–2220.
16. Ray, S., Das, A. K. and Banerjee, A. Chem. Commun. **2006**, 2816–2818.

17. Vemula, P. K., Aslam, U., Mallia, V. A. and John, G. Chem. Mater. **2007**, 19, 138–140.

18. Bardelang, D., Zaman, M. B., Moudrakovski, L., Pawsey, S., Mageson, J. C., Wang, D., Wu, X., Ripmeester, J. A., Ratcliffe, C. I. and Yu, K. Adv. Mater. **2008**, 20, 4517–4520.

19. Dalmases, M., Aguiló, E., Llorca, J., Rodríguez, L. and Figuerola, A. ChemPhysChem **2016**, 2190–2196.

20. Boisselier, E. and Astruc, D. Chem. Soc. Rev. **2009**, 38, 1759–1782.

21. Bromma, K. and Chithrani, D. B. Nanomaterials **2020**, 10, 1–25.

22. Lima, J. C. and Rodriguez, L. Anticancer. Agents Med. Chem. **2011**, 11, 921–928.

23. Yue, S., Luo, M., Liu, H. and Wei, S. Front. Chem. **2020**, 8.

24. Gavara, R., Llorca, J., Lima, J. C. and Rodríguez, L. Chem. Commun. **2013**, 49, 72–74.

25. Svergun, D. I. Biophys. J. **1999**, 76, 2879–2886.

26. Arcau, J., Andermark, V., Aguiló, E., Gandioso, A., Moro, A., Cetina, M., Lima, J. C., Rissanen, K., Ott, I and Rodríguez, L. Dalton Trans. **2014**, 43, 4426–4436.

27. Turkevich, J., Stevenson, P. C., Turkevich, B. J. and Stevenson, P. C. J. Phys. Chem. **1953**, 57, 670–673.

28. Perez, G., Araujo, J., Romero, P. and Solorzano, G. Microsc. Microanal. **2020**, 26, 2818–2819.

# CHAPTER 7

## Effect of the aggregation on the biological activity of gold(I) complexes

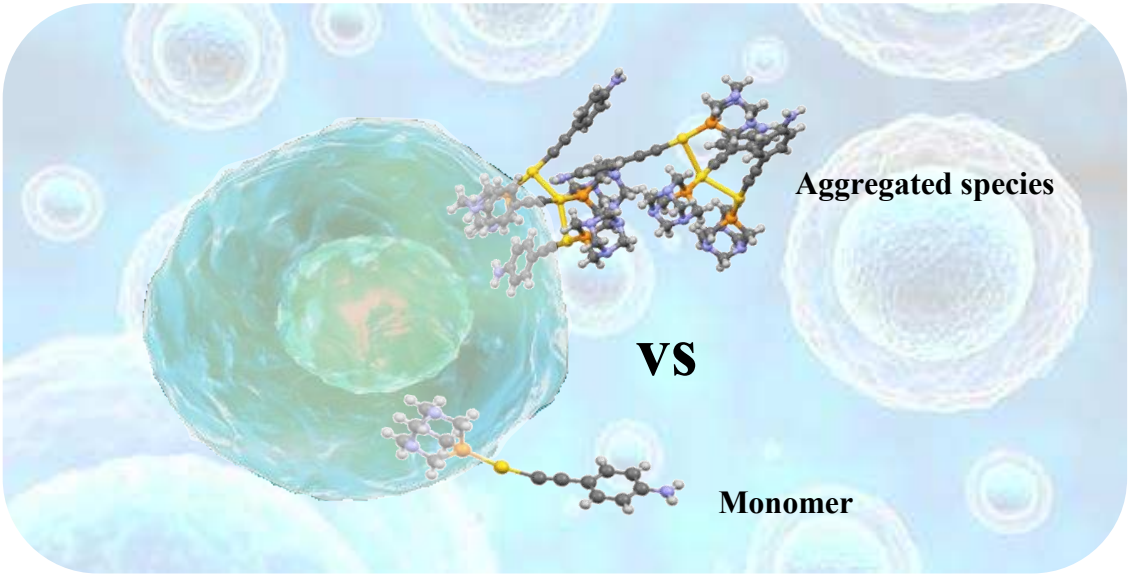


Part of this Chapter has been submitted A. Pinto, C. Roma-Rodrigues, J. Ward, R. Puttreddy, K. Rissanen, P. Baptista, A. Fernandes, J.C. Lima, L. Rodríguez Inorg. Chem. ic-2021-02359y.R1.

# 7. EFFECT OF THE AGGREGATION ON THE BIOLOGICAL ACTIVITY OF GOLD(I) COMPLEXES

## 7.1. Introduction

The use of gold compounds in medicine began with the discovery of the bacteriostatic behaviour of gold cyanide $K[Au(CN)_2]$ towards the mycobacteria and it was subsequently introduced as a therapy for the tuberculosis treatment. Its toxicity made evolve gold drugs to other gold species such as gold(I) thiolate complexes.[1] Later, the suggestion that the mycobacteria could be an agent that can cause rheumatoid arthritis, allows to confirm the effectiveness of gold compounds for this treatment. Since then, gold drugs have been used to treat a variety of other rheumatic diseases including psoriatic arthritis, juvenile arthritis, or palindromic rheumatism.[2] The study of the mechanism of action together with the discovery of metal compounds such as cisplatin for chemotherapy allows the most interesting advances in the pharmacology of gold drugs, expanding the use of gold compounds not only in the treatment of rheumatoid arthritis but also in other fields such as anticancer medicine or antimicrobial medicine. Nowadays, gold complexes have exhibited excellent antiproliferative activity in several tumour cell lines[3–8] and, in particular, Auranofin is on clinical trials for the treatment of leukaemia cancer.[9]

Platinum-based drugs present side effects and some cancer cell lines develop resistance for this kind of drugs. For this reason, non-platinum drugs have gained more attention, especially gold(I) complexes, bearing a softer metal centre. They show lower interaction with DNA than platinum drugs due to a tight interaction with the nitrogen donor atoms of the nucleobases. This fact suggests that gold(I) compounds use different mechanisms of action for their antiproliferative activity. The cytotoxic effects of gold(I) compounds may come from the interaction between the residues of the proteins of specific enzymes inducing a suppression of their activity. Gold has a tendency to bind sulfur and selenium donor ligands and, consequently, most of the enzymes containing these residues could be potential targets.

Thioredoxin reductase (TrxR) is a homodimeric protein that belongs to the family of glutathione reductase acting as enzymes. It catalyses the NADPH-dependent reduction of

thioredoxin (Trx) disulfide and many other oxidized cell constituents. This enzyme is involved in numerous metabolic pathways and pathophysiological conditions (tumours, infectious diseases, rheumatoid arthritis, etc).[10] Due to its antioxidant properties, the thioredoxin system is regarded as preventing cells from oxidative stress, which is a key factor for DNA damage. Over expression of TrxR has been observed in numerous tumour cell lines and high levels of this substrate have been associated with the resistance to the cisplatin.[11] The active site of TrxR contains a selenocysteine motif involved in the catalytic mode of action of the enzyme. Based on the affinity of gold(I) centre, a preferred binding with this residue is suggested and can act as an inhibitor agent. Although TrxR enzyme appears as the main target of gold(I) drugs and their mechanism is not completely understood yet, other targets such as aquaporin-3,[12] zinc finger proteins such as poly(adenosnediphosphate riose)polymerase-1 (PARP-1),[13] quadruplex DNA[14,15] and other thiolate dependent enzymes, such as human glutathione reductase (hGR), glutathione peroxidase (GpX), glutathione-S-transferases (GSTs) and cysteine protease[16] may not be discarded.

Some parameters must be considered in order to design a gold(I) metallodrug. The stability of the complex in the biological media is an important feature and, for this reason, strong ligand-metal bonds have been mainly chosen. The more frequent ligands used to build biologically active gold complexes are thiolates,[17] dithiocarbamates,[18] phosphanes,[19] N-heterocyclic,[20] thiourea,[21] or alkynyl.[22] Another important parameter is the drug distribution and the uptake of the agents into the cells. In this way, a balance between hydrophilicity and lipophilicity is required for the drug to be water soluble (i.e., soluble in the biological medium) and at the same time be able to pass through the phospholipid cellular membrane.[23–25] The lipophilicity of compounds is a very important parameter in optimizing the biodistribution and the biological activity. Some physicochemical studies on $[Au(dppe)_2]^+$ and some analogues revealed a correlation between drug lipophilicity, cellular uptake and biological activity.[26]

On other hand, it is well known that gold(I) complexes tend to aggregate yielding supramolecular structures via non-covalent interactions such as hydrogen bonding, π-π stacking and in particular by the establishment of Au···Au interactions.[27,28] These supramolecular architectures can be favoured in aqueous media even at diluted conditions.[29–34] Since biological assays are in aqueous media, the aggregation process

cannot be discarded. Although some studies regarding this field have been found in the literature related to anticancer drugs based on pure organic structures and with nanoparticles,[35,36] to the best of our knowledge, the consideration of the aggregation parameter has not precedent in the literature with metallodrugs and is also of great relevance for further drug design.

In this context, we previously designed and synthesized in our group a series of mono- and dinuclear gold(I) complexes containing the same chromophoric unit, 4-ethynylaniline, and a different phosphane located at the second position varying their aromaticity and the rigidity (Figure 7.1).[37] This family of compounds was tested against two different cancer cell lines (human colorectal, HCT116 and ovarian carcinoma, A2780) and we could draw some important conclusions: 1) mononuclear complexes present higher cytotoxicity and better selectivity for A2780 ovarian cells than dinuclear complexes; 2) the complex that contains tri(1-naphthyl)phosphane shows a great selectivity for A2780 ovarian cells with no cytotoxic effect on normal fibroblast, making it a very interesting candidate for this treatment; 3) the flexibility of the dinuclear complexes has a direct positive influence on the resulting biological activity.

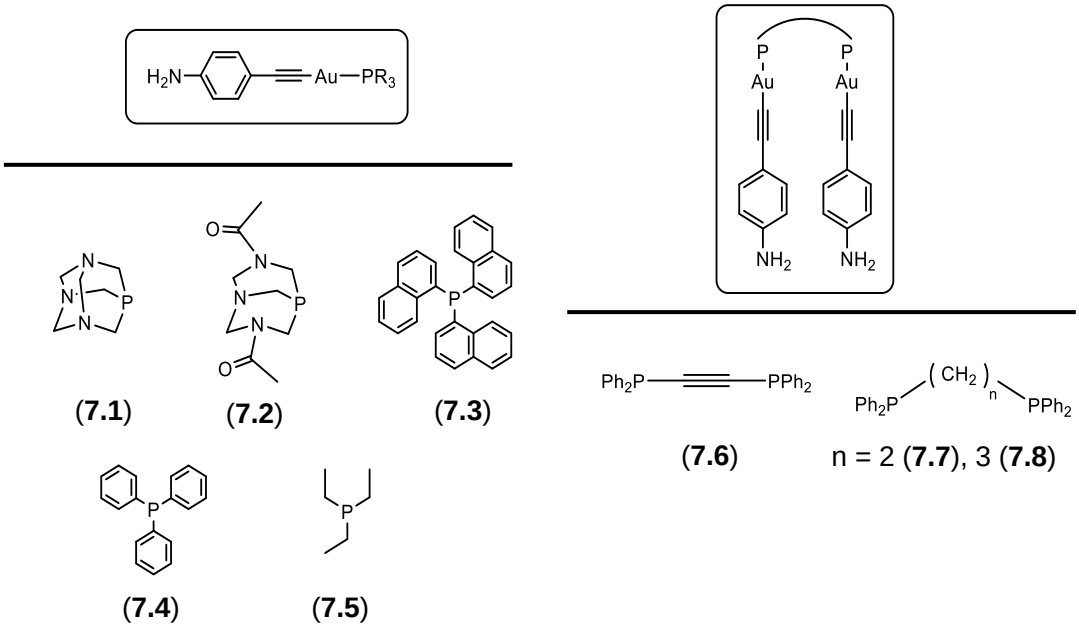


**Figure 7.1.** Chemical structure of the gold(I) complexes with biological activity studied in this work.

Taking into consideration the important results previously obtained in the group, in this work, we have been focused on a careful analysis of the behaviour of the metallodrugs

before entering the cells. That is, how the molecules enter the cells and a detailed and complete analysis of their aggregation in order to retrieve some denoted information of great relevance for future gold(I) metallodrugs development and understanding. Additionally, since the gold(I) complex containing tri(1-naphthyl)phosphane shows a great selectivity towards A2780 ovarian cells, we have designed a new family of compounds having a phosphane with a substituted naphthyl group (Figure 7.2) in order to see the effect on the biological activity of the substituents in this moiety and to analyse if naphthyl units have positive effect on the biological activity of gold(I) metallodrugs.

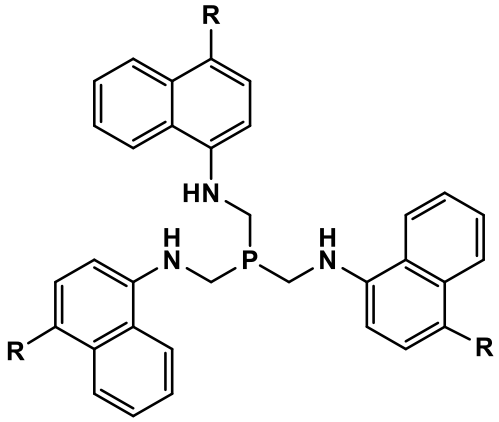


**R = H (P1), Cl (P2), Br (P3)**

**Figure 7.2.** P{$CH_2$-1-N(H)naphthyl}$_3$ phosphane used for the synthesis of the new family of gold(I) complexes.

## 7.2. Results and discussion

### 7.2.1. Synthesis and characterization

The complexes **7.1-8** have been prepared following the method previously reported by us.[37] The recorded spectroscopic data indicates their correct formation in pure form.

The complexes **7.9-11** were synthesized by the reaction of the previously synthesized polymer [Au(4-ethynylaniline)]$_n$ and the corresponding P{$CH_2$-1-N(H)naphthyl}$_3$ phosphane[38] (Scheme 7.1) following the established method previously reported by us with slight modifications.[37] Several recrystallizations were necessary in order to obtain the compounds in pure form and to remove the traces of the [$(PR_3)_2$Au]Cl subproduct that remains in solution.

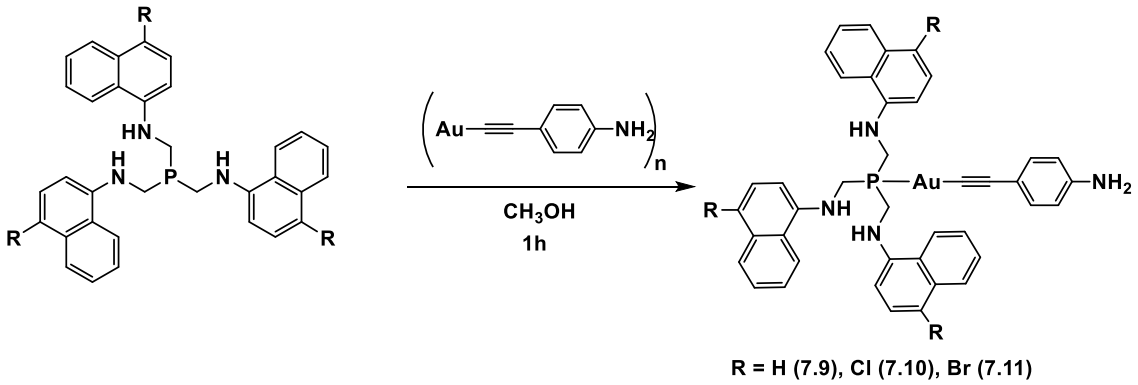


**Scheme 7.1.** Synthesis of the gold(I) complexes **7.9-11**.

Complexes **7.12-14** were synthesized by the addition in two different steps of one equivalent of the phosphane to an initial solution of [AuCl(tht)] (Scheme 7.2).[39,40]

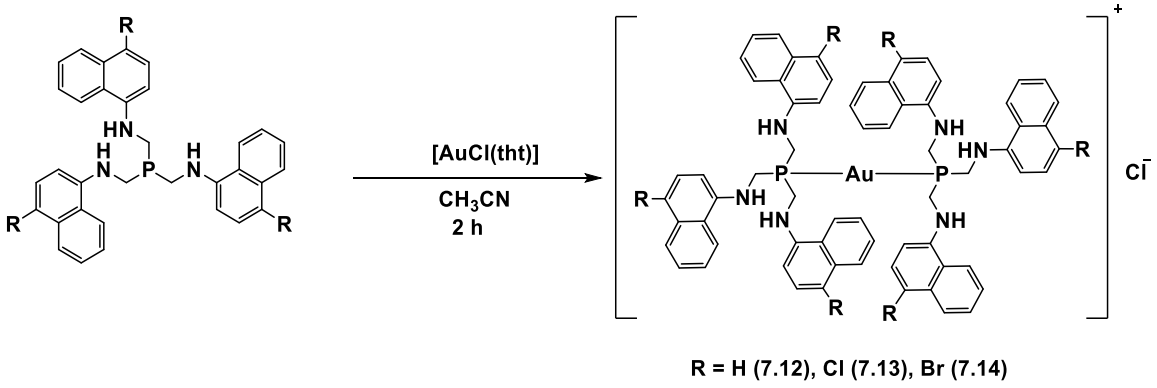


**Scheme 7.2.** Synthesis of the gold(I) complexes **7.12-14**.

The characterization of the complexes by $^{1}H$ and $^{31}P\{^{1}H\}$ NMR and IR spectroscopy, ESI-MS(+) spectrometry evidences the correct formation of the desired products and their purity. $^{1}H$ NMR spectra display the pattern of the phosphane and the aniline in the case of complexes **7.9-11**. $^{31}P\{^{1}H\}$ NMR spectra display a single resonance in all cases, which is 60 ppm downfield shifted with respect to the free phosphane. IR spectra display the υ(C≡C) vibration at ca. 2100 $cm^{-1}$ in the case of complexes **7.9-11** and υ(N–H) vibration in all complexes. Mass spectra show a final evidence of the correct formation of the desired products by the identification of the monoprotonated species $[M+H]^+$ and $[M+Na]^+$ or $[M+K]^+$ species in the case of complexes **7.9-11** and the molecular peak $[M]^+$ in the case of **7.12-14**.

### 7.2.2. Photophysical characterization

The absorption and emission spectra of the uncoordinated phosphanes **P1-3** and gold complexes **7.9-14** were recorded in $10^{-5}$ M dimethyl sulfoxide solutions at room temperature and the obtained data are summarized in Table 7.1.

**Table 7.1.** Electronic absorption and emission data, quantum yield of complexes **7.9-14** and uncoordinated phosphanes in dimethyl sulfoxide.

| Compound | Absorption $\lambda_{max}$ ($10^3$ ε $cm^{-1}$ $M^{-1}$) | Emission | $\Phi_{fl}$ | $\tau_F$ (ns) | $k_F$ ($ns^{-1}$) | $k_{nr}$ ($ns^{-1}$) |
|---|---|---|---|---|---|---|
| **P1** | 344 (23.5) | 430 | 0.32 | 3.97 | 0.08 | 0.171 |
| **P2** | 360 (24.2) | 446 | 0.26 | 2.82 | 0.092 | 0.262 |
| **P3** | 360 (21.6) | 446 | 0.13 | 1.47 | 0.088 | 0.591 |
| **7.9** | 324 (34.4) | 420 | 0.026 | 0.215 | 0.120 | 4.530 |
| **7.10** | 342 (27.3) | 431 | 0.019 | 0.188 | 0.101 | 5.218 |
| **7.11** | 342 (28.3) | 428 | 0.015 | 0.180 | 0.083 | 5.472 |
| **7.12** | 339 (25.9) | 426 | 0.027 | 0.392 | 0.068 | 2.482 |
| **7.13** | 354 (26.5) | 439 | 0.021 | 0.882 | 0.023 | 1.109 |
| **7.14** | 354 (41.2) | 437 | 0.01 | 1.01 | 0.01 | 0.980 |

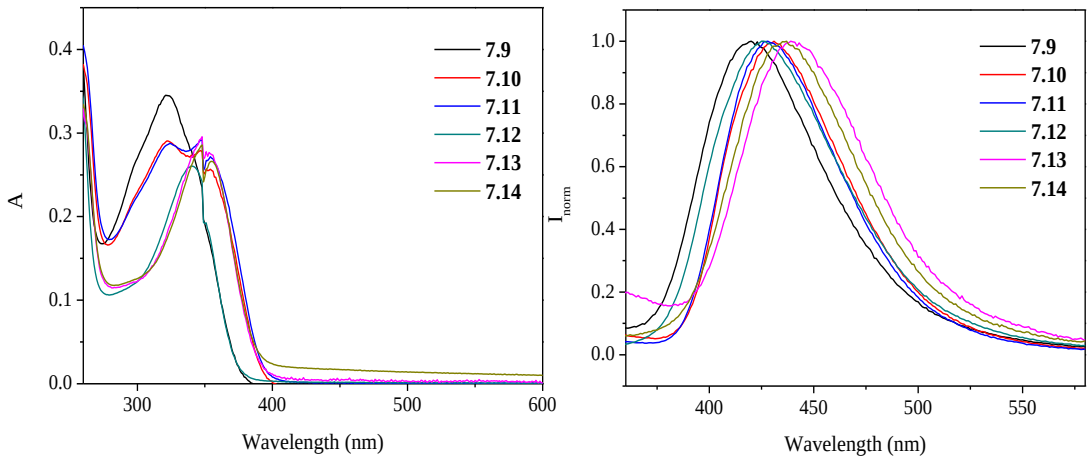


**Figure 7.3.** Absorption (left) and normalized emission (right) spectra of complexes **7.9-14** in dimethyl sulfoxide.

The absorption spectra of all the compounds in dimethyl sulfoxide displays one absorption band at 320-350 nm. The absorption spectra of the gold(I) complexes display the same profile as the corresponding spectra of the uncoordinated phosphanes P{$CH_2$-1-$NHC_{10}H_6$(4-R)}$_3$, but ca. 20 nm blue-shifted (Table 7.1) and it is thus assigned to the π-π* transition of the naphthyl moiety of the phosphane. The same trend is observed in the emission spectra. The recorded blue shift (Figure 7.3) may be ascribed to the change on the closed conformation of the free phosphane (due to intramolecular N-H···N interactions)[38] upon coordination to the metal atom.

A red shift is observed in all cases when a halogen atom is incorporated into the chemical structure due to an electronegativity effect. Such electronegativity effect occurs if either the HOMO or the LUMO is particularly stabilized, and it is especially pronounced in molecules with disjoint orbital structures, where HOMO and LUMO are localized on different parts of the molecule.[41] Moreover, the effect of chlorine and bromine substituents on the resulting emission is almost identical. This is however consistent with the similar inductive and mesomeric properties of these two halogens (Br: F = + 0.45, R = - 0.22, Cl: F = + 0.42, R = - 0.19, F = field effect parameter, R = resonance parameter). That is, both substituents function as moderately inductive (σ) electron withdrawing group and as weak π-donor, as indicated by the Swain-Lupton parameters quantifying these two effects.[41,42]

Emission spectra recorded at 77 K in dimethyl sulfoxide (Figure 7.4) show that only gold(I) complexes present a phosphorescence band at ca. 575 nm in agreement with the effect of the heavy atom in the possible intersystem crossing and population of the triplet state. Gold(I) compounds that contain the P{$CH_2$-1-$NHC_{10}H_6$(4-**Br**)}$_3$ phosphane, present the lowest phosphorescence emission.

The fluorescence quantum yields in dimethyl sulfoxide are between 1 and 3% and follow the trend R = H > Cl > Br. The lowest fluorescence quantum yields observed for gold(I) compounds also confirms that gold(I) is populating the triplet state, which is much more favoured when a second heavy atom is included in the chemical structure of the molecule (Cl, Br). The radiative and non-radiative rate constants were calculated from the fluorescence quantum yields and lifetimes. In general, the radiative constant remain similar, while it is in the non-radiative where the addition of gold(I) atom promotes these deactivation pathways, also in agreement with the observed phosphorescence emission.

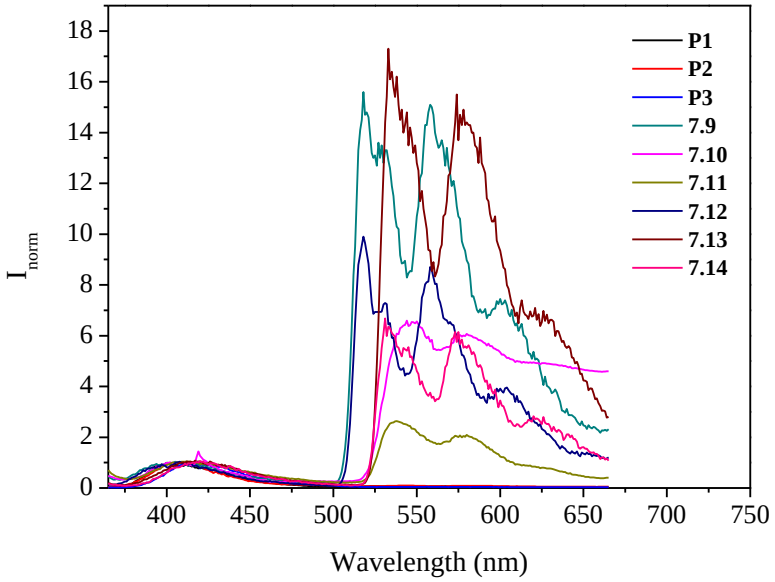


**Figure 7.4.** Emission spectra of phosphanes **P1-3** and gold(I) complexes **7.9-14** at 77 K (fluorescence band is normalized).

### 7.2.3. X-ray crystal ctructure determination

Slow evaporation of dichloromethane/hexane solutions provided single crystals suitable for X-ray diffraction resolution of the structures of **7.1**, **7.4**, **7.5** and **7.13**.

Complexes **7.1**, **7.4** and **7.5** present a linear coordination at the Au(I) center, with the P-Au-C angles ranging between 173-177º. The P-Au and Au-C bond parameters are in good agreement with those of previously reported for compounds that contain 4-ethynylaniline as a ligand.[37] The three complexes display N−H···$C_{sp}$ and C−H···π interactions in the 3D crystal packing, similar to the previous complexes reported by us.[37]

The complex **7.1** crystalizes in two different modes; as two trimers with molecules twisted in antiparallel form and connected through aurophilic interactions (**7.1a**) and as a discrete molecule (**7.1b**), as shown in Figure 7.5. The main difference between the two modes is the presence of a solvent molecule in the crystal that leads to the formation of trimers. Even though compound **7.1** also crystallizes in a discrete structure (**7.1b**) where aurophilic interactions can be observed in the 3D packing. The conformation found for **7.1a** is observed in previous complexes reported that contains 1,3,5-triaza-7-phosphaadamantane as a phosphane.[33]

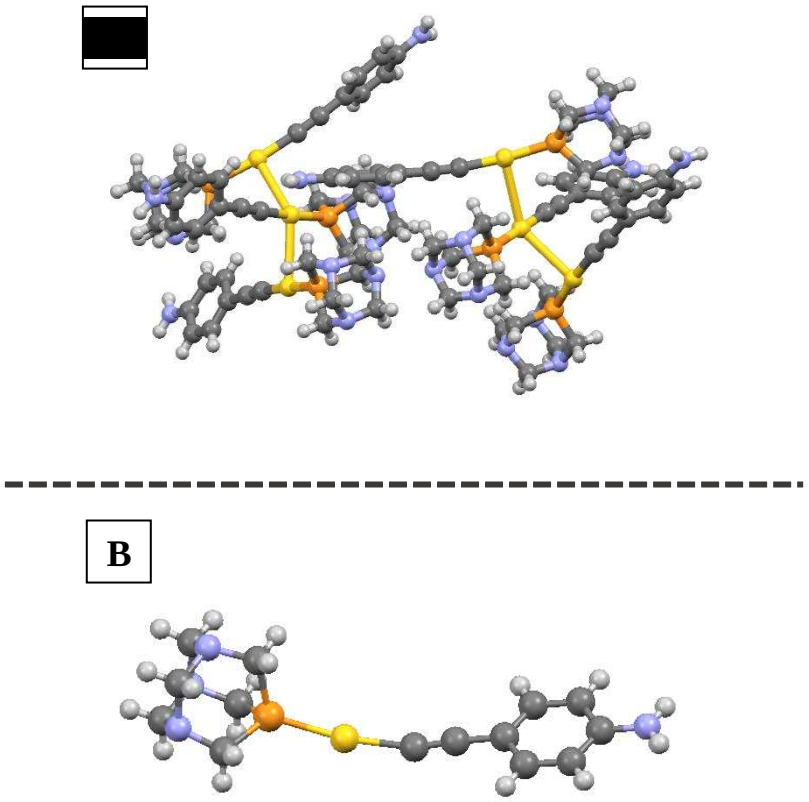


**Figure 7.5**. X-ray crystal structures of **7.1a** (A), **7.1b** (B). Yellow: gold; orange: phosphorus; black: carbon; light blue: nitrogen; pale grey: hydrogen. Solvents have been omitted for clarity.

Complex **7.4** crystalizes as a dimer in antiparallel mode and complex **7.5** as a discrete structure . (Figure 7.6). In the 3D packing of both complexes, the molecules are oriented by the interactions between $NH_2$ and C≡C groups. This kind of interactions play a significance role in the stabilization of the arrangement also in other complexes found in the literature that contains an ethynylaniline in the chemical structure.[37]

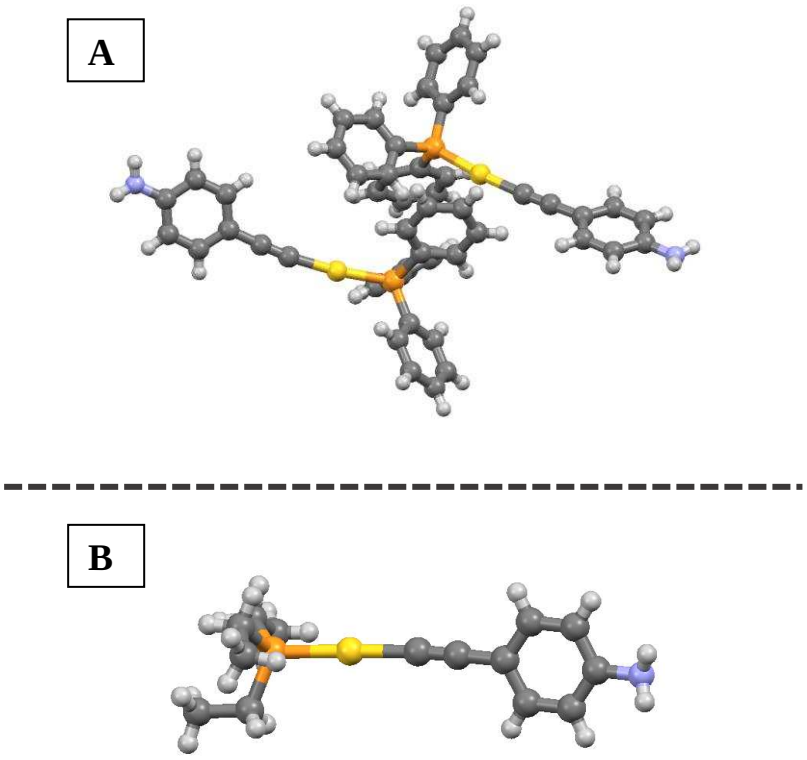


**Figure 7.6**. X-ray crystal structures of **7.4** (A), **7.5** (B). Yellow: gold; orange: phosphorus; black: carbon; light blue: nitrogen; pale grey: hydrogen. Solvents have been omitted for clarity.

Complex **7.13** crystallizes as a single molecule with two molecules of methanol (Figure 7.7). A linear geometry is observed around the metal atom with a P-Au-P angle of 180º similar to other $[(PR_3)_2Au]Cl$ complexes.[43] The P-Au bond distance is in a good agreement with those found in other gold-phosphane complexes.[39,40] The angle of P-$CH_2$-N is around 111º which is similar to other gold(I) complexes with similar phosphanes[38] and is smaller with respect to the uncoordinated phosphane due to a higher steric hindrance when the gold(I) is coordinated and the phosphanes become closer. The complex displays intramolecular short N-H···Cl, Cl··$\pi$, Cl···Cl[44] contacts in the 3D crystal packing. The packing arrangement shows that the molecules form a chain due to the presence of hydrogen bonding of the N-H of the molecule, the chlorine that acts as a counterion and the methanol molecules present in the crystal structure.

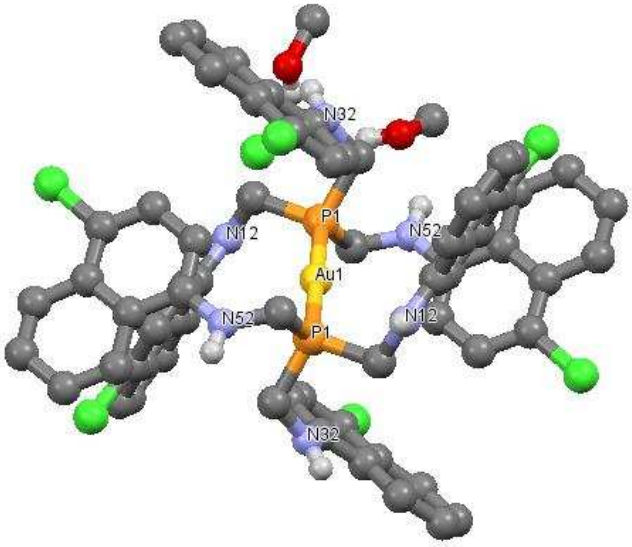


**Figure 7.7.** X-Ray crystal structure of **7.13**. Yellow: gold; orange: phosphorous; black: carbon; light blue: nitrogen; green: chlorine; red: oxygen (All hydrogen atoms except on N have been removed for clarity).

### 7.2.4. Biological assays

The cytotoxicity of the new gold(I) complexes **7.9-14** was analyzed in order to compare the results with the previously studied gold(I) complex containing trinaphthylphosphane (**7.3**) that was the best one regarding both cytotoxicity and selectivity. MTS assays were performed on the representative human cancer cell lines: ovarian cisplatin sensitive, A2780, and colorectal carcinoma, HCT116. The cell viability was observed to be dependent on the concentration for compounds **7.9** and **7.12** that do not contain a halogen atom in the naphthalene moiety (see Figures 7.8 and 7.9).

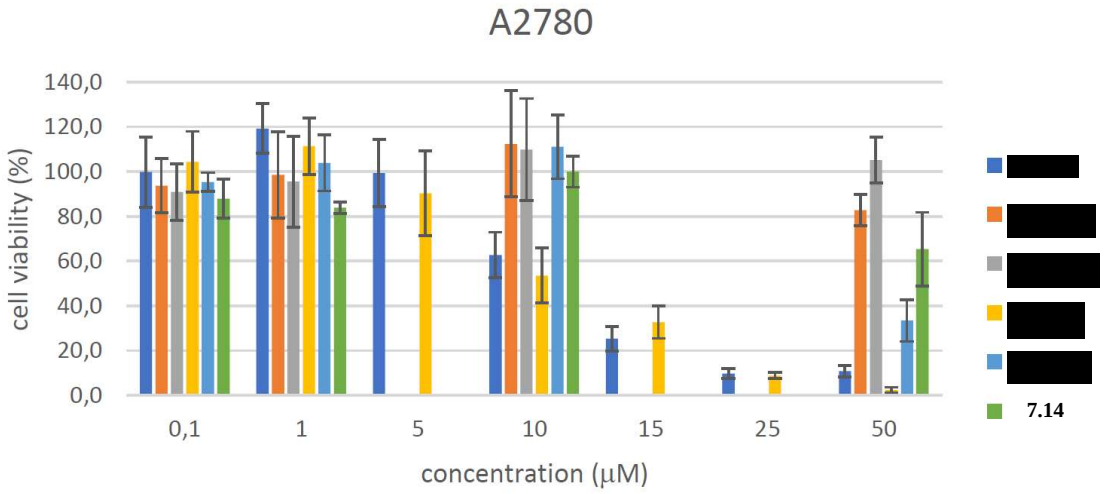


**Figure 7.8**. Cytotoxicity of complexes **7.9–14** in the A2780 cell lines after incubation for 48 h with increasing concentration of the complex. Cell viability was determined by means of the MTS assay. Data normalized against the control (0.1 %(v/v) DMSO).

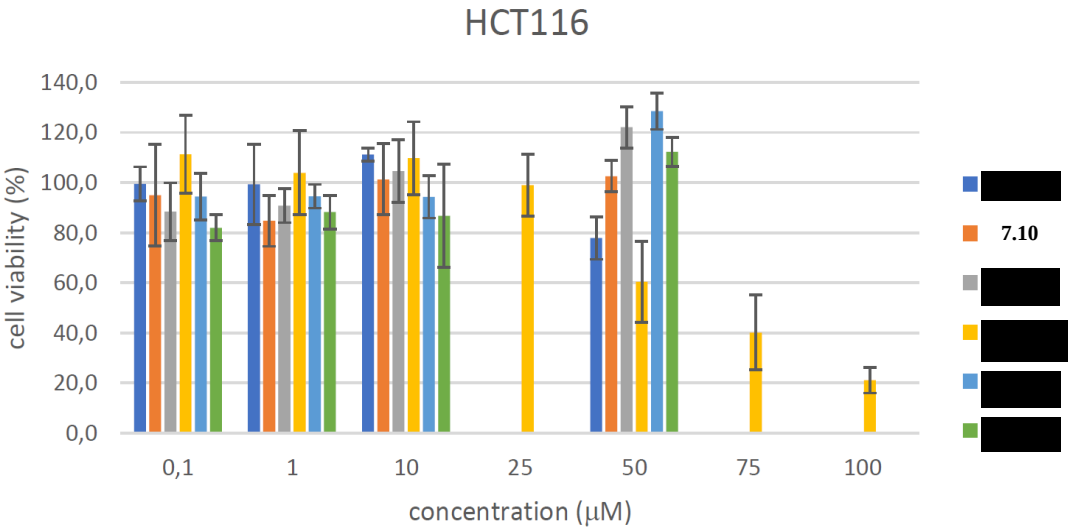


**Figure 7.9.** Cytotoxicity of complexes **7.9–14** in the HCT116 cell lines after incubation for 48 h with increasing concentration of the complex. Cell viability was determined by means of the MTS assay. Data normalized against the control (0.1 %(v/v) DMSO).

$IC_{50}$ values are higher for the complexes **7.9-14** with respect to the complex **7.3** containing the trisnaphthylphosphane ($PNaph_3$) and thus, the compounds are less active (Table 7.2). The introduction of the -$CH_2$-NH- moiety between the phosphorous and the naphthalene seems to affect negatively the cytotoxicity of these compounds. On the other hand, the introduction of a halogen in the chemical structure of the naphthalene decreases the cytotoxicity of the complexes.

**Table 7.2.** $IC_{50}$ values of complexes **7.1-14**.

| Compound | A2780 | HCT116 | Fibroblast |
|---|---|---|---|
| **7.1**[a] | 1.7 ± 0.4 | 18.2 ± 8.1 | 19.0 ±7.3 |
| **7.2**[a] | 17.4 ± 1.0 | 77.5 ±0.1 | 70.4 ± 3.5 |
| **7.3**[a] | 2.3 ± 0.1 | >100 | >100 |
| **7.4**[a] | 0.1 ± 0.0 | 8.7 ± 1.8 | 5.3 ± 0.7 |
| **7.5**[a] | 0.3 ± 0.1 | 6.5 ± 0.1 | 1.0 ± 0.4 |
| **7.6**[a] | 10.9 ± 3.7 | 59.5 ± 17.5 | 96.3 ± 4.5 |
| **7.7**[a] | 0.3 ± 0.0 | 1.9 ± 0.3 | 15.2 ± 1.8 |
| **7.8**[a] | 0.3 ± 0.1 | 1.3 ± 0.0 | 36.4 ± 0.0 |
| **7.9** | 10.24 ± 1.02 | >50 | >50 |
| **7.10** | >50 | >50 | >50 |
| **7.11** | >50 | >50 | >50 |
| **7.12** | 10.12 ± 0.46 | 52.3 ± 1.3 | >50 |
| **7.13** | >50 | >50 | >50 |
| **7.14** | >50 | >50 | >50 |

[a] From ref.[37]

### 7.2.5. Correlation between aggregation and the mechanism to enter the cells

7.2.5.1. Aggregations studies

Gold(I) complexes, with similar chemical structure to the compounds under study in this work, have been found to aggregate in solution.[31,45] Hence, aggregation studies have been performed with the current complexes in order to try to retrieve some correlation between the biological activity and the aggregation behavior. Since complexes **7.9-14** do not present relevant cytotoxicity towards ovarian cisplatin-sensitive (A2780) and colorectal carcinoma (HCT116), the studies correlating the aggregation vs biological properties have not been performed.

The critical concentration aggregation (CAC) is defined as the concentration where the aggregates start to be formed. This concentration depends on the interaction between the complex and the solvent. In this way, the absorption and emission spectra at different concentrations were recorded in water-dimethyl sulfoxide mixtures. The representation of the concentration vs the absorption or emission maxima gives a plateau (Figure 7.10),

which is the point where the molecules start to aggregate. It is thus ascribed as the critical concentration aggregation (CAC). The obtained values are summarized in the Table 7.3.

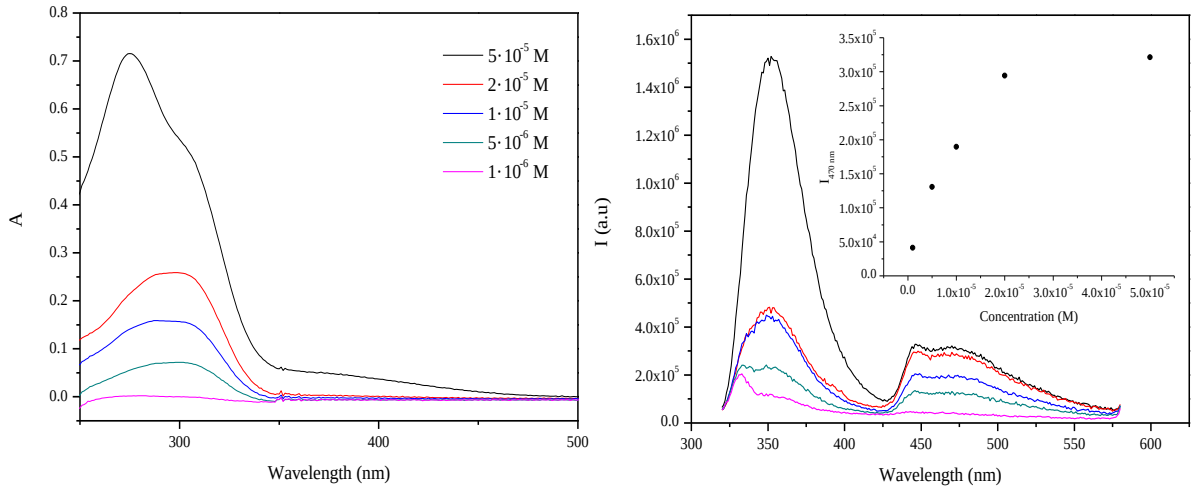


**Figure 7.10.** Absorption (left) and emission (right) spectra of compound **7.1** at different concentrations (inset: plot intensity vs the concentration at the 470 nm maxima).

All complexes tend to aggregate between $5\cdot10^{-6}$ - $1\cdot10^{-5}$ M where a new absorption band around 400 nm appears together with an increase on the baseline due to the dispersion effect of the aggregates. A second emission band also appears at longer wavelengths, around 470 nm, due to the aggregates. The complexes **7.1** and **7.2** that contain the more water soluble phosphane (PTA and DAPTA respectively) present the largest CAC. This is due to the highest solubility of these phosphanes in water and thus the aggregates start to form at higher concentrations. The other complexes present similar CAC except complex **7.8** that shows the lowest CAC due to solubility issues.

**Table 7.3.** Values of the critical aggregation concentration of complexes **7.1-8**.

| Compound | CAC |
|---|---|
| **7.1** | $1.75 \cdot 10^{-5}$ M |
| **7.2** | $2 \cdot 10^{-5}$ M |
| **7.3** | $10^{-5}$ M |
| **7.4** | $10^{-5}$ M |
| **7.5** | $10^{-5}$ M |
| **7.6** | $10^{-5}$ M |
| **7.7** | $10^{-5}$ M |
| **7.8** | $5 \cdot 10^{-6}$ M |

NMR studies have been performed at different concentrations in water-dimethyl sulfoxide mixtures in order to analyze in more detail which part of the molecule is more affected in the aggregation process. In the case of the more water soluble phosphanes PTA and DAPTA (compounds **7.1** and **7.2** respectively) a shift in the protons on the phosphane and also in the phosphorous signal can be detected together with the presence of secondary signals in the pyridine group that indicates the presence of new aggregated structures. A downfield shift in the $^{31}$P NMR was also observed. This behavior is in agreement with the presence of aggregated assemblies at higher concentrations where both parts of the molecule (phosphane an aniline group) are affected. This may be correlated with what was previously displayed in the X-ray crystal structures due to the aurophilic contacts (in the nearby of the phosphorous atom) and N-H$\cdots\pi$ interactions are involved in the intermolecular contacts (affecting the NMR chemical shift). In the case of compound **7.5**, that contains a triethylphosphane, only the aniline protons are affected with no effect neither in the protons of the phosphane nor in the $^{31}$P NMR. However, both the aniline and the phosphane groups are affected in compound **7.4**, that contains a triphenylphosphane (Figure 7.11). Although these two compounds present the same kind of intermolecular interactions in the crystal structure, the solubilization of compound **7.4** in a water-dimethyl sulfoxide mixture promotes the presence of intermolecular contacts between the phenyl groups (C-H$\cdots\pi$) observed in the X-ray structure. These interactions may be maintained in solution (aggregated form) and may explain the involvement of the phosphane in this process (a part from the N-H$\cdots\pi$ interaction involving the aniline).

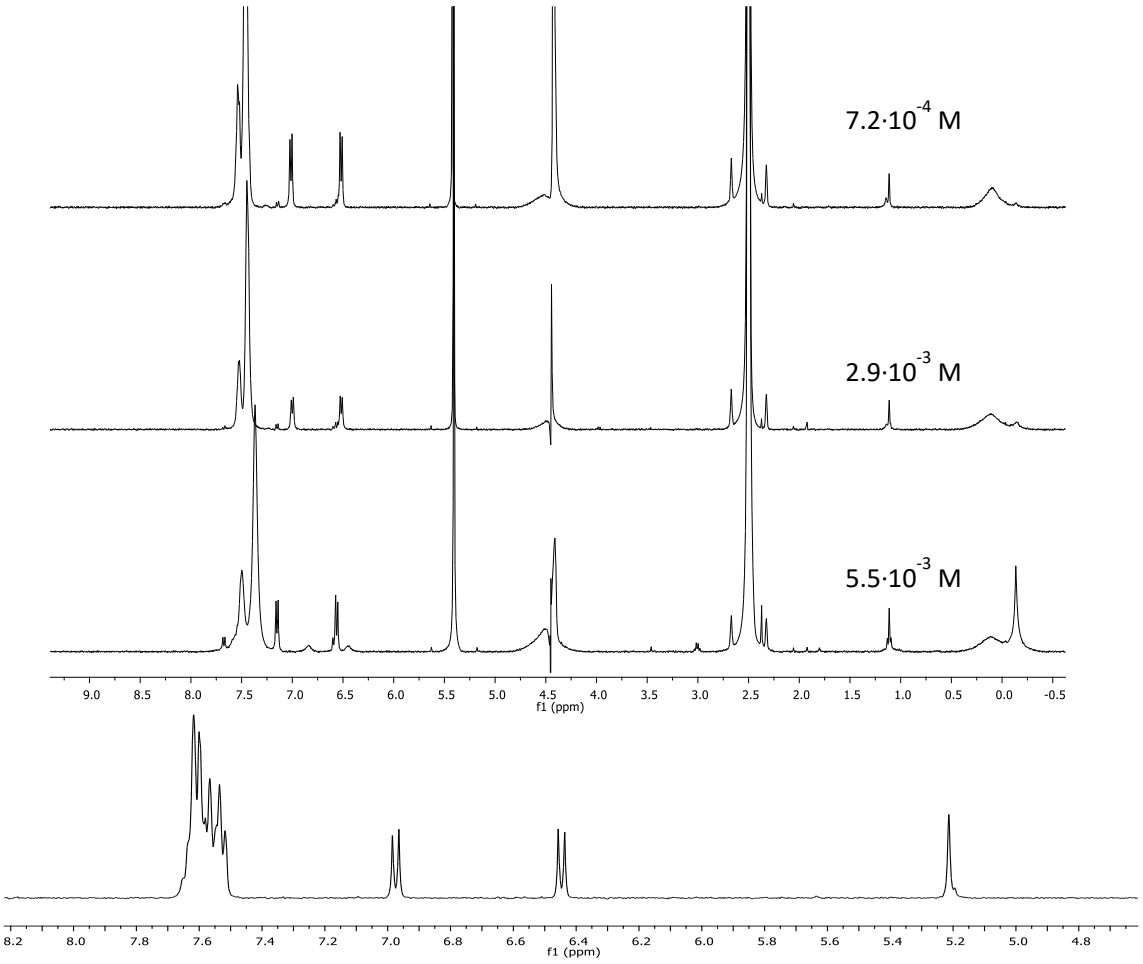


**Figure 7.11.** $^{1}$H-NMR spectra of **7.4** at different concentrations in a mixture of $D_2O$:DMSO-$d_6$ (above). $^{1}$H NMR spectra of **7.4** in DMSO-$d_6$ (below).

Only the protons of the aniline are affected by the concentration in the NMR of the compounds that are less soluble in the mixture of solvents used (**7.3**, **7.6**, **7.7** and **7.8**) due to a conformation where this group is involved in the aggregation process and somehow the aniline can be blocked through π-π stacking (found in the crystal structure previously reported by us).[37]

7.2.5.2. Aggregation vs biological properties

We have observed that gold(I) complexes **7.1-8** aggregate in dimethyl sulfoxide:water mixtures and we could get some information regarding the parts of the molecule that are involved. Aiming at correlating the aggregation of these compounds with the biological properties, it is firstly necessary to determine which species are being uptaken in the cells, the monomers or the aggregates. To elucidate this question, absorption spectra and

dynamic light scattering (DLS) experiments have been recorded at different times (crucial points for the biological assays) and at the same conditions used for the biological experiments (aqueous solutions with 0.1% of DMSO at 37 ºC). Times 0h, 1h, 3h and 6h have been chosen since they are relevant in the biological culture. A decrease in the absorption band and an increase of the baseline was observed at longer times due to an increase of the formation of the aggregates (Figure 7.12).

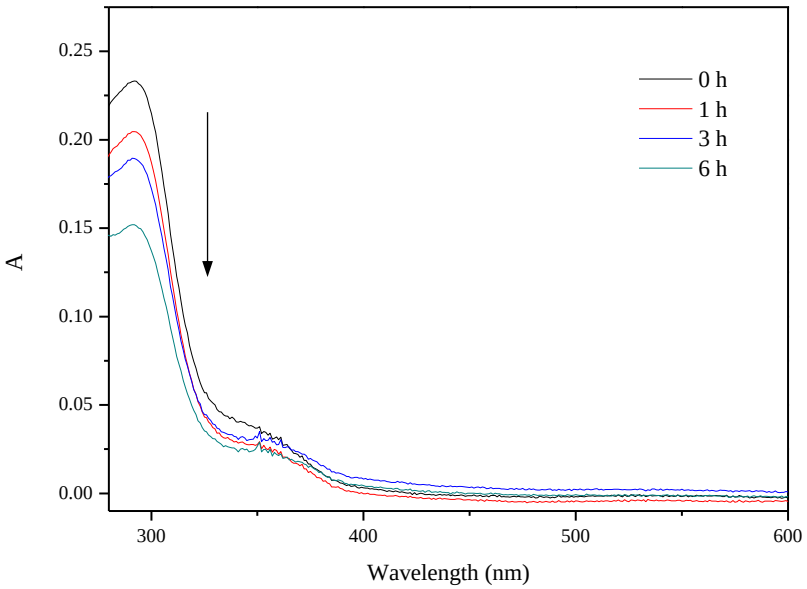


**Figure 7.12.** Absorption spectra of a $10^{-5}$M aqueous solution (containing 0.1% DMSO) of **7.5** at different times.

Additionally, dynamic light scattering (DLS) studies reveal that at this starting point the aggregated form is the species present in the solution. Initially, compounds **7.1**, **7.2**, **7.5**, **7.7** and **7.8** present aggregates around 200 nm and **7.3**, **7.4** and **7.6** display larger aggregates due to a lower solubility in the medium. Different trends can be observed at the different times where the measurements were recorded: the more soluble compounds show an increase of the size at longer times, as expected for aggregation processes, which are usually more favored with time. On the other hand, the size of the aggregates decreases with time in the case of the less soluble compounds. This may be ascribed to an increase of the aggregates or the appearance of precipitates with time being those maintained in the suspensions smaller or more homogeneous (sharper signals) (Figure 7.13 left). Similar experiments carried out in biological media (in PBS) show that in this medium aggregation is still present although smaller sizes can be detected in all cases.

The aggregates are also maintained in the presence of a biological relevant protein, bovine serum albumin (BSA), but becoming smaller (Figure 7.13 right).

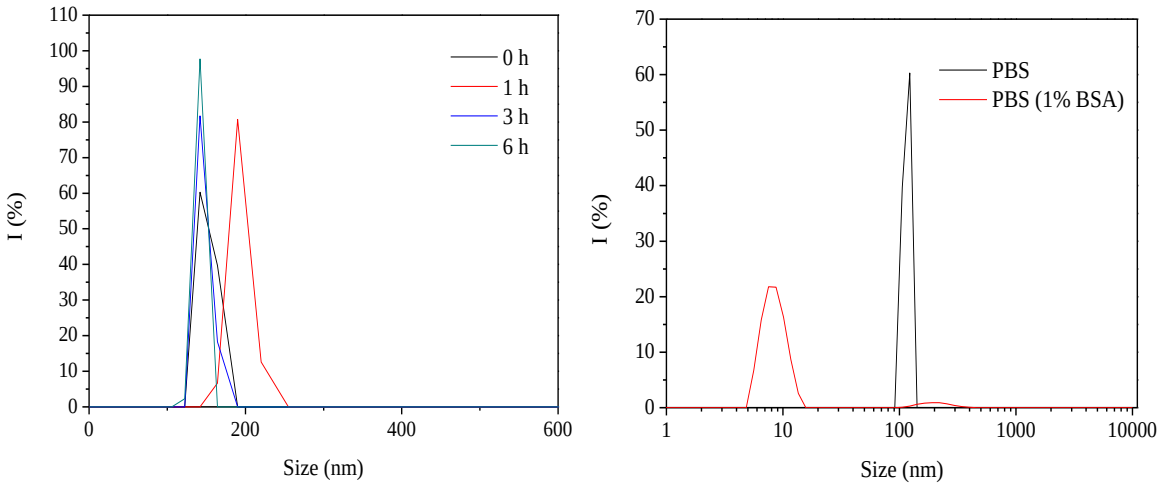


**Figure 7.13.** Dynamic light scattering (DLS) spectra of **7.5** of a $10^{-5}$M aqueous solution (containing 0.1% DMSO) at different times (left) and of a $10^{-5}$M PBS solution (black line) and in presence of 1% BSA protein (red line).

Small Angle X-ray Scattering (SAXS) experiments were also performed in order to verify if smaller aggregates might be present in the solutions at the biological temperature conditions. The low-resolution structures were reconstructed ab initio from the scattering patterns using the DAMMIN program. As it can be observed in Table 7.4, small aggregates exist in all cases with a size around 200 - 400 Å, being a final evidence of the presence of even smaller aggregates in the solutions of the studied metallodrugs.

**Table 7.4.** Size of the small aggregates of the complexes retrieved through SAXS experiments under analogous conditions than those used for the biological assays.

| **Compound** | **7.1** | **7.2** | **7.3** | **7.4** | **7.5** | **7.6** | **7.7** | **7.8** |
|---|---|---|---|---|---|---|---|---|
| **Size** (Å) | 269 | 263 | 284 | 189 | 254 | 275 | 389 | 225 |

Thus, the first hypothesis is that the samples are introduced in the cells already as aggregates whose size decreases in the presence of biological proteins. But how is the mechanism to enter the cells? The cell membrane is a semipermeable barrier and it only allows the transport of compounds with small molecular size, which can be transported using channels and specific carriers.[46] But not only the size is important, also the hydrophobic character of the complex is crucial to know how easily it crosses the cell

membrane. The hydrophobic character of a derivative can be measured experimentally by testing the relative distribution in an n-octanol/water mixture. Hydrophobic molecules will prefer to dissolve in the n-octanol layer of this two-phase system, whereas hydrophilic molecules prefer the aqueous layer. The relative distribution is known as the partition coefficient (P) and is obtained from the following equation:

$$P = \frac{Concentraton\ of\ the\ derivative\ in\ octanol}{Cocentration\ of\ the\ derivative\ in\ aqueous\ solution}$$

In general, hydrophobic compounds present higher P values, whereas lower P values are obtained for hydrophilic compounds. In this way, the partition coefficients of the compounds were retrieved through absorption spectra in water/octanol mixtures and we were only able to determine this parameter for those complexes that present some solubility in octanol (compounds **7.3-5** and **7.8**) (Table 7.5). The observed trend is **7.8** > **7.4** > **7.3** > **7.5**. Thus, the $logK_{ow}$ values seem to be related with the corresponding hydrophobicity of the complexes and we can suggest that the compounds that present a more aromatic or more rigid phosphane (less soluble in water) might cross the membranes more easily.

**Table 7.5.** Partition coefficient for compounds **7.3**, **7.4**, **7.5** and **7.8**.

| **Compound** | Partition coefficient | $logK_{ow}$ |
|---|---|---|
| **7.3** | 2.1 | 0.3 |
| **7.4** | 4.5 | 0.7 |
| **7.5** | 1.2 | 0.1 |
| **7.8** | 6.9 | 0.8 |

In terms of size, it is expected that the monomers may enter the cell via passive or an active pathway, while aggregates with more than 200 nm might require energy-dependent pathways, such as endocytosis for internalization.[36,47] The activity of cellular transporters are temperature dependent, while the energy-dependent mechanisms will be mostly inhibited at lower temperature.[48,49] The percentage of intracellular gold was evaluated in A2780 cells incubated with complexes for 3 h at 4ºC. These experiments were performed in colaboration with the group of Dr. Alexandra Fernandes and Dr. Pedro V. Baptista at the UCIBIO-REQUIMTE (Universidade NOVA de Lisboa). We considered for these

analyses those complexes that present gold internalization levels higher than 4% (complex **7.4**, **7.5**, **7.7** and **7.8**) which is the sensitivity of the inductively coupled plasma atomic emission spectrometry (ICP-AES) technique. A slight deacrease on the internalized gold was observed when cells were incubated at 4ºC relative to incubation at 37ºC (Figure 7.14). Only in the case of **7.5**, a decrease on the interanalized gold (from 3.9% at 37ºC to 0.38% at 4ºC) was observed. In general, these results suggest that gold(I) complexes might enter the A2780 cells via a passive mechanism. In the case of compound **7.5**, although the decrease of internalization might induce to consider that the uptaking of this compound is via an active transport mechanism, it is important to note that passive difussion is also affected by lower temperature.

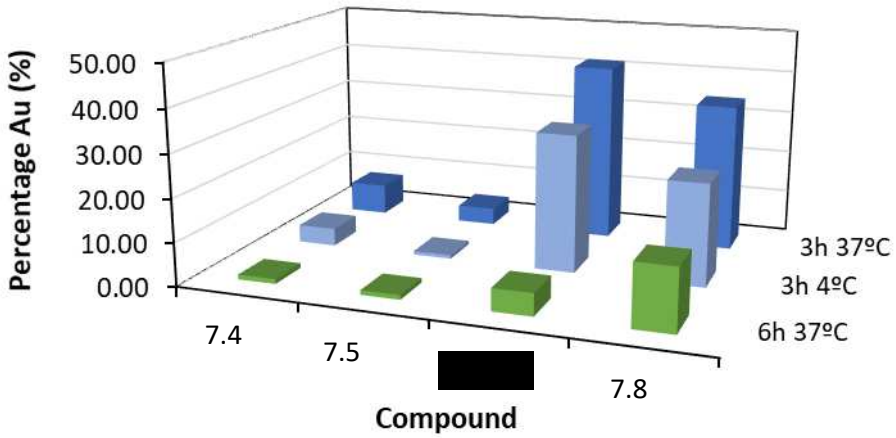


**Figure 7.14.** Internalization of complexes **7.4**, **7.5**, **7.7** and **7.8** in ovarian cancer cells A2780 after 3h at 37ºC (dark blue) and 4ºC (light blue) and after 6h at 37ºC (green). Bars represent the percentage of gold in cells relative to the total amount of gold found in the media and cells for each sample.

A decrease on the internalization is observed after 6h in all complexes. Complex **7.7** presents the highest alteration (from 41.7% after 3h to 5.2% internalized after 6h). This observed decrease can be ascribed to the increase of the size of aggregates with time in the case of compounds more soluble in water or the precipitation over time for compounds that are less water soluble, previously seen in the DLS experiments.

Dark field microscopy analysis was performed in order to know how the compounds are interacting with the cell membrane. Compounds with higher partition coefficient (**7.4** and **7.8**) were chosen. A2780 cells were exposed for 3h with gold(I) complexes or with 0.1%

(v/v) DMSO as control sample. Only cells incubated with complex **7.4** present bright spots in the cell membrane, consistent with denser material and hence to the presence of aggregates (Figure 7.15). These results suggest that, in the case of **7.4**, aggregates interact with the cell membrane and are then internalized in this form.

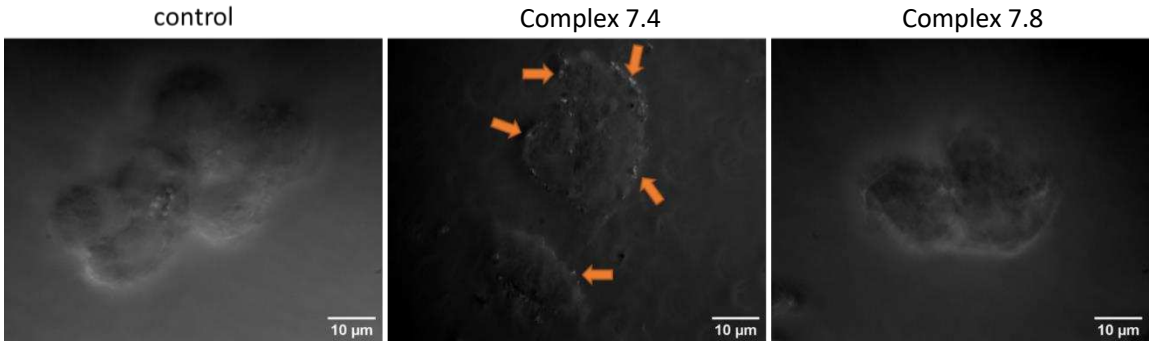


**Figure 7.15.** Analysis of complexes **7.4** and **7.8** internalization in the aggregated form. Ovarian cancer cell line A2780 was incubated for 3h with the $IC_{50}$ of each complex (0.1 µM for complex **7.4** and 0.3 µM for complex **7.8**) or 0.1 % (v/v) DMSO for control purposes, and then fixed with formaldehyde 4% (w/v). Images were acquired in a Ti-U Eclipse inverted microscope using a Dark field condenser. Orange arrows point to bright spots consistent with the presence of complex **7.4** aggregates.

Previous studies carried out for these compounds, suggested a correlation between complex internalization and its cytotoxicity. In general, gold(I) compounds that present higher internalization display also higher cytotoxicity (lower $IC_{50}$ values), as can be seen in Figure 7.16. However, dinuclear compounds with similar $IC_{50}$ values compared to mononuclear analogous complexes showed higher intracelular %Au. Interestingly, complexes **5**, **7** and **8** with lower aggregates' size (~ 200 nm) in DLS measurements present the same $IC_{50}$ in ovarian cancer cell.

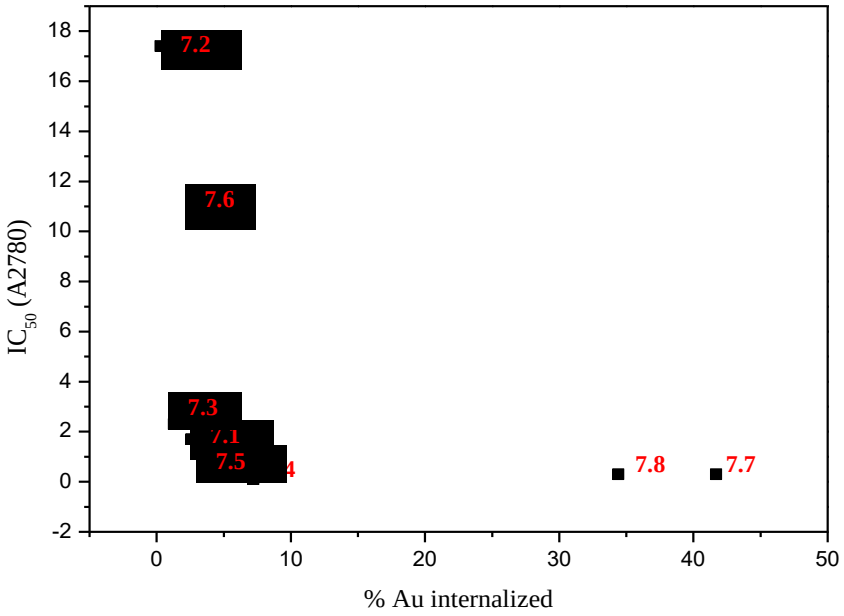


**Figure 7.16.** Plot of %Au internalized vs $IC_{50}$ values against A2780 cell line.

Altogether, the results suggest that although the internalization in the aggregated form cannot be excluded, the highest cytotoxicity of complex **7.4** might be correlated with its higher aggregate size and its hydrophobicity that can cross more easily the cell membrane via a passive transport.

Since different behavior has been observed for mononuclear and dinuclear compounds, the intracellular distribution within cellular organelles was assayed in order to elucidated the effect of gold(I) complexes on A2780 cells. Cellular fractionation using a detergent-based cell fractionation kit was used as a methodology to separate the cell contents into three fractions: cytosolic fraction, mitochondrial fraction (composed by membranes and organelles) and nuclear fraction (composed by the nuclei and cytoskeleton). The results obtained suggest that while mononuclear complexes are mainly found in the cytosolic fraction, the dinuclear complexes are mainly at the fractions composed by nuclei and cytoskeleton (Figure 7.17).

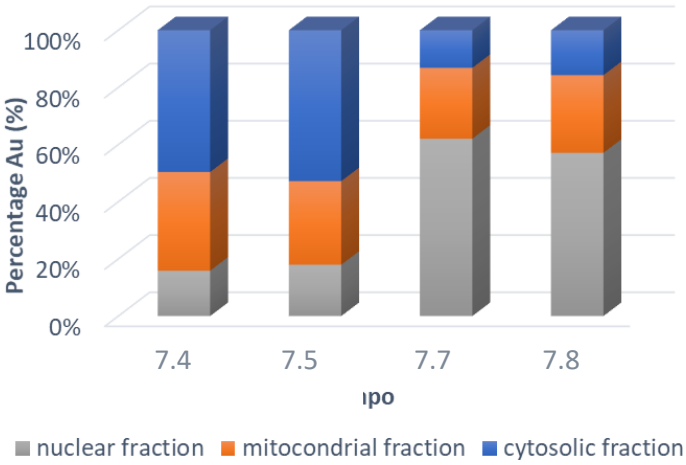


**Figure 7.17.** Distribution of complexes **7.4**, **7.5**, **7.7** and **7.8** in the ovarian carcinoma cell line A2780. Cells were exposed to 10x IC50 of each complex for 3h at 37ºC. Cells were then fractionated using Cell fractionation kit (Cell signaling technologies) into cytosolic fraction, mitochondrial fraction (composed by membrane and organelles) and nuclear fraction (composed by nucleus and cytoskeleton). The concentration of gold in each fraction was measured by ICP-AES and the represented percentage of gold in each bar is the gold in each fraction relative to the sum of gold in all fractions.

The different behavior observed between mononuclear and dinuclear compounds and their different cytotoxicity behavior suggest different targets. A proteomic analysis made by Modesti and coworkers[50] showed that gold compounds can interact with actin or actin related proteins in A2780 cells and they observed a decrease on the expression of two actin isoforms when cells were incubated with auranofin and Auoxo6. The modification or reorganization of these proteins of the cytoskeleton can cause the apoptosis of the cell.[51] In this way, the interaction of complexes **7.4** (mononuclear) and **7.8** (dinuclear) with actin was examined (Figure 7.18). The results show that both complexes present some interaction with actin, causing the formation of actin agglomeration. Major actin modifications was observed for complex **7.8**, being more significant after 3h of incubation, where the actin filament were more disorganized than cells incubated with DMSO (control) or with complex **7.4**. These results suggest that complex **7.8** destabilizes the action cytoskeleton of the cells in major degree probably due to a cooperative effect between the two gold(I) complexes.[52]

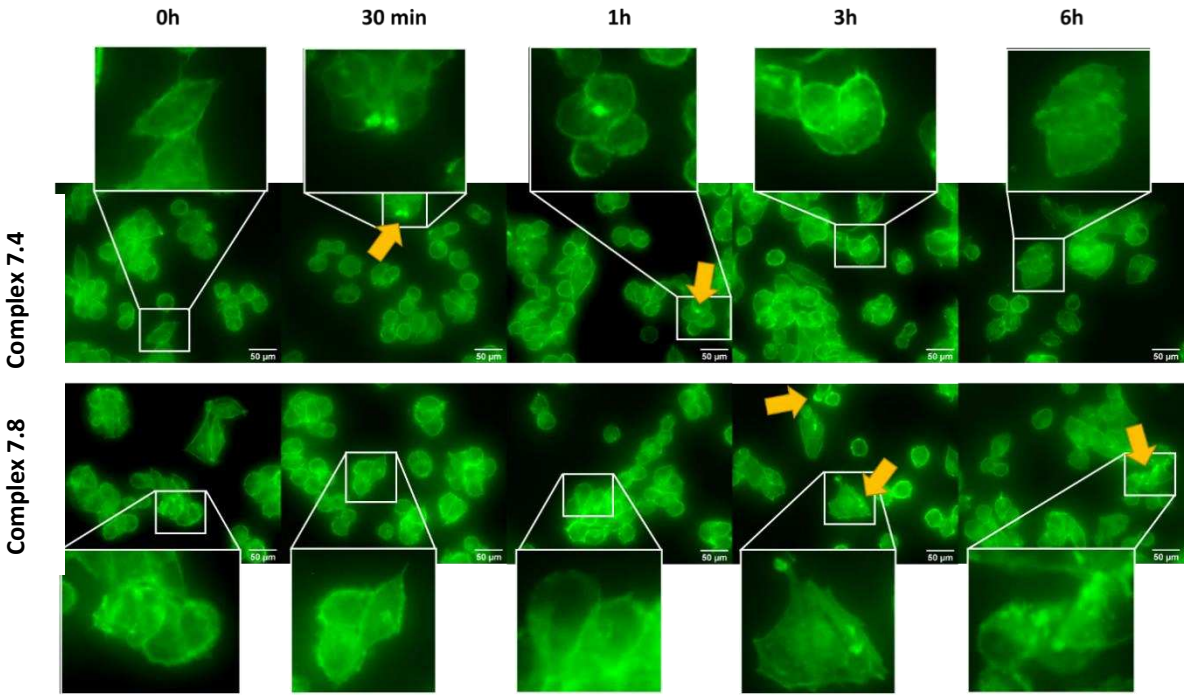


**Figure 7.18.** Interaction of complexes **7.4** and **7.8** with actin. Ovarian cancer cell line A2780 was incubated for 0h, 30 min, 1h, 3h and 6h with the $IC_{50}$ of each complex (0.1 μM for complex **7.4** and 0.3 μM for complex **7.8**) and then fixed with formaldehyde 4% (w/v). Cells were stained with AlexaFluor 488 phalloidin (Invitrogen) and images were acquired in a Ti-U Eclipse inverted microscope with green filter cube (excitation filter range 465-495 nm and emission filter range at 515-555 nm). Orange arrows point to actin agglomerations in cells.

Thus, aggregation seems to be involved in a possible passive mechanism to enter the cell but the final effect once the compounds are within the cell, is expected to be more affected by cooperative effect related to nuclearity of the metallodrug.

## 7.3. Conclusions

The use of complementary techniques revealed that aggregates are mantained in solution even at low concentrations. DLS experiments show that at the very beginning these aggregates already exist. The correlation between the biological activity previously studied and the aggregation studies let us to asume that aggregates are the species that cross the cellular membrane possibly through passive diffusion mechanim. Nevertheless, the biological activity and localization seems to be more related to the nuclearity of the complexes.

Taking into consideration the previous results, a series of neutral and cationic gold(I) compounds with a phosphane that contain a naphtyl moiety ($P\{CH_2\text{-}1\text{-}NHC_{10}H_6(4\text{-}R)\}_3$, R = H, Cl, Br) has been successfully synthesized and their biological activity studied. It has been observed that the introduction of an amine group between the naphthyl and the phosphorous decreases the resulting biological activity.

To the best of our knowledge, the correlation between the mechanism used for the metallodrug to enter the cells and the aggregation process has not precedent in the literature. This study can be of great relevance to better understand the activity of the gold(I) drugs and for further design of new active molecules.

## 7.4. Experimental Section

### 7.4.1. General procedures

All manipulations have been performed under prepurified $N_2$ using standard Schlenk techniques. All solvents have been distilled from appropriated drying agents. 4-ethynylamine (Aldrich, 97%) was used as received. Literature methods were used to prepare $[Au(C\equiv C\text{-}C_6H_4NH_2)]_n$,[37] and 4-ethynylaniline gold(I) complexes containing monophosphane (1,3,5-triaza-7-phosphaadamantane (PTA; **7.1**), 3,7-diacetyl-1,3,7-triaza-5-phosphabicyclo[3.3.1]nonane (DAPTA; **7.2**), and $PR_3$, with R=naphthyl (**7.3**), phenyl (**7.4**), and ethyl (**7.5**) and diphosphane (bis(diphenylphosphano)acetylene (dppa; **7.6**), 1,2-bis(diphenylphosphano)ethane (dppe; **7.7**), and 1,3-bis(diphenylphosphano)propane (dppp; **7.8**).[37] $P\{CH_2\text{-}1\text{-}NHC_{10}H_6(4\text{-}H)\}_3$ (**P1**), $P\{CH_2\text{-}1\text{-}NHC_{10}H_6(4\text{-}Cl)\}_3$ (**P2**) and $P\{CH_2\text{-}1\text{-}NHC_{10}H_6(4\text{-}Br)\}_3$ (**P3**) were provided by Prof. Martin B. Smith from Department of Chemistry, Loughborough University, Loughborough, UK.

### 7.4.2. Physical measurements

Infrared spectra have been recorded on a FT-IR 520 Nicolet Spectrophotometer. $^1H$ NMR ($\delta$(TMS) = 0.0 ppm), $^{31}P\{^1H\}$ NMR ($\delta$(85% $H_3PO_4$) = 0.0 ppm) spectra have been recorded on a Varian Mercury 400 and Bruker 400 (Universitat de Barcelona). ElectroSpray-Mass spectra (+) has been recorded on a Fisons VG Quatro spectrometer (Universitat de Barcelona). Absorption spectra have been recorded on a Varian Cary 100 Bio UV- spectrophotometer and emission spectra on a Horiba-Jobin-Yvon SPEX Nanolog spectrofluorimeter (Universitat de Barcelona). Luminescent quantum yields were recorded using an Absolute PL quantum yield spectrometer from Hamamatsu Photonics upon excitation the samples at 300 nm. Dynamic Light Scattering have been obtained on a Zetasizer Nano S of MALVERN (Parc Científic de Barcelona). The samples were measured in quartz cuvettes. SAXS was performed on the NCD-SWEET beamline at the ALBA Synchrotron at 12.4 keV, and the distance sample/detector was 6.2 m to cover the range of momentum transfer of $0.028 < q < 2.56$ $nm^{-1}$. The data were collected on a Pilatus3S 1M detector with a pixel size of 172.0 x 172.0 $\mu m^2$. The exposure time was 30 s. The q-axis calibration was obtained by measuring silver behenate.[53] The program pyFAI was used to integrate the 2D SAXS data into 1D data.[54] The data were

then subtracted by the background using PRIMUS software.[55] The maximum particle dimension Dmax and the pair distance Distribution P (r) were determined with GNOM.[56] The low resolution structure of aggregates was reconstructed ab initio from the initial portions of the scattering patterns using the program DAMM.[57] The crystal data and experimental details for the data collection of **7.1**, **7.4, 7.5** and **7.13** were made by Jas Ward in collaboration with the group of Prof. Kari Rissanen from University of Jyväskylä. The single crystal data for all compounds were collected using a Bruker-Nonius KappaCCD diffractometer with an APEX-II detector with graphite-monochromatized Mo-$K_\alpha$ ($\lambda$ = 0.71073 Å) radiation. CCDC-2070637 (**7.1a**), CCDC-2070638 (**7.1b**), CCDC-2070639 (**7.4**) and CCDC-2070640 (**7.5**) contain the supplementary crystallographic data for these structures. These data can be obtained free of charge from The Cambridge Crystallographic Data Centre via www.ccdc.cam.ac.uk/data_request/cif.

### 7.4.3. Synthesis and Characterization

**Synthesis of [Au(4-ethynylaniline)(P1)] (7.9)**

Solid **P1** (39 mg, 0.078 mmol) was added to a stirring suspension of $[Au(C{\equiv}C\text{-}C_6H_4NH_2)]_n$ (25 mg, 0.079 mmol) in methanol (10 mL) under $N_2$ atmosphere at room temperature. After 1h of stirring, the solution was concentrated to the half and diethyl ether was added in order to favour the precipitation. The resulting yellow solid was filtered and dried under vacuum. Yield 51% (32 mg).

$^{31}P\{^1H\}$ NMR (DMSO-$d_6$, 400 MHz): $\delta$ = 26.1 ppm; $^1H$ NMR (DMSO-$d_6$, 400 MHz): $\delta$ = 4.30 (d, J = 6.12 Hz, 6H, $CH_2$), 5.09 (s, 2H, $NH_2$), 6.35 (d, J= 8.64, 2H, $H_\alpha$), 6.62 (m, 3H, Naph), 6.77 (d, J= 8.56 Hz, 2H, $H_\beta$), 6.86 (d, J = 7.56 Hz, 3H, Naph), 7.15 (d, J = 8.08 Hz, 3H, Naph), 7.22 (t, J = 7.68 Hz, 3H, Naph), 7.45 (m, 3H, Naph), 7.78 (d, J = 7.2 Hz, 3H, Naph), 8.14 (d, J = 7 Hz, 3H, Naph); IR (FT): $\upsilon$ = 3451 (s), 3349 $cm^{-1}$ (s, N-H), 2101 (w, C≡C); ESI (+) m/z: 813.239 ($[M+H]^+$, calc: 812.234), 835.224 ($[M+Na]^+$, calc: 835.224), 851.201 ($[M+K]^+$, calc: 851.198).

**Synthesis of [Au(4-ethynylaniline)(P2)] (7.10)**

Complex **7.10** was synthesized following the same experimental procedure reported for **7.9** but by using **P2** instead of **P1**. A yellow solid was obtained in a yield of 60 % (43 mg).

$^{31}P\{^{1}H\}$ NMR (DMSO-$d_6$, 400 MHz): δ = 25.3 ppm; $^{1}H$ NMR (DMSO-$d_6$, 400 MHz): δ = 4.27 (d, J = 5.36 Hz, 6H, $CH_2$), 5.05 (s, 2H, $NH_2$), 6.32 (d, J = 8.2 Hz, 2H, $H_\alpha$), 6.72 (d, J = 8.2 Hz, 2H, $H_\beta$), 6.78 (d, J = 8.2 Hz, 3H, Naph), 7.28 (d, J = 8.3 Hz, 3H, Naph), 7.54 (t, J = 7.36 Hz, 3H, Naph), 7.61 (t, J = 8.12 Hz, 3H, Naph), 8.03 (d, J = 8.3 Hz, 3H, Naph), 8.20 (d, J = 8.3 Hz, 3H, Naph); IR (FT): υ = 3449 (s), 3353 $cm^{-1}$ (s, N-H), 2103 (w, C≡C); ESI (+) m/z: 915.122 ($[M+H]^+$, calc: 915.117), 937.107 ($[M+Na]^+$, calc: 937.107), 953.079 ($[M+K]^+$, calc: 953.081).

**Synthesis of [Au(4-ethynylaniline)(P3)] (7.11)**

Complex **7.11** was synthesized following the same experimental procedure reported for **7.9** but by using **P3** instead of **P1**. A purple solid was obtained in a yield of 59 % (41 mg).

$^{31}P\{^{1}H\}$ NMR (DMSO-$d_6$, 400 MHz): δ = 25.4 ppm; $^{1}H$ NMR (DMSO-$d_6$, 400 MHz): δ = 3.92 (d, J = 6.2 Hz, 6H, $CH_2$), 4.71 (s, 2H, $NH_2$), 5.97 (d, J = 8.4 Hz, 2H, $H_\alpha$), 6.39 (d, J = 8.3 Hz, 2H, $H_\beta$), 6.41 (d, J = 8.4 Hz, 3H, Naph), 7.11 (d, J = 8.3 Hz, 3H, Naph), 7.18 (t, J = 7 Hz, 3H, Naph), 7.26 (t, J = 8.3 Hz, 3H, Naph), 7.64 (d, J = 7.8 Hz, 3H, Naph), 7.83 (d, J = 8.6 Hz, 3H, Naph); IR (FT): ): υ = 3453 (s), 3348 $cm^{-1}$ (s, N-H), 2099 (w, C≡C) ; ESI (+) m/z: 1046.965 ($[M+H]^+$, calc: 1046.966), 1068.960 ($[M+Na]^+$, calc: 1068.956), 1084.942 ($[M+K]^+$, calc: 1084.930).

**Synthesis of $[Au(P1)_2]Cl$ (7.12)**

Complex **7.12** was prepared following the procedure previously reported in the literature[39] in a yield of 78 % (77 mg)

$^{31}P\{^{1}H\}$ NMR (DMSO-$d_6$, 400 MHz): δ = 15.9 ppm; $^{1}H$ NMR (DMSO-$d_6$, 400 MHz): δ = 3.79 (d, J = 5.7 Hz, 12H, $CH_2$), 6.70 (m, 12H, Naph), 7.07 (d, J = 8.2 Hz, 6H, Naph), 7.44 (m, 12H, Naph), 7.77 (d, J = 7.12 Hz, 6H, Naph), 8.13 (d, J = 7.76 Hz, 6H, Naph); IR (FT): υ = 3400 $cm^{-1}$ (s, N-H); ESI (+) m/z: 1195.401 ( $[M]^+$, calc: 1195.402).

**Synthesis of [Au(P2)$_2$]Cl (7.13)**

Complex **7.13** was synthesized following the same experimental procedure reported for **7.12** but using **P2** instead of **P1**. A solid was obtained in a yield of 64 % (72 mg).

$^{31}P\{^1H\}$ NMR (DMSO-$d_6$, 400 MHz): δ = 11.3 ppm; $^1H$ NMR (DMSO-$d_6$, 400 MHz): δ = 3.91 (d, J = 4 Hz, 12H, $CH_2$), 5.71 (d, J = 8.3 Hz, 6H, Naph), 6.34 (d, J = 7.7 Hz, 6H, Naph), 7.00 (m, 6H, Naph), 7.62 (m, 6H, Naph), 7.97 (d, J = 8.04 Hz, 6H, Naph), 8.25 (d, J = 8.4 Hz, 6H, Naph); IR (FT): υ = 3410 $cm^{-1}$ (s, N-H); ESI (+) m/z: 1399.162 ( $[M]^+$, calc: 1399.168).

**Synthesis of [Au(P3)$_2$]Cl (7.14)**

Complex **7.14** was synthesized following the same experimental procedure reported for **7.12** but using **P3** instead of **P1**. A solid was obtained in a yield of 75 % (101 mg).

$^{31}P\{^1H\}$ NMR (DMSO-$d_6$, 400 MHz): δ = 8.8 ppm; $^1H$ NMR (DMSO-$d_6$, 400 MHz): δ = 3.95 (d, J = 5.5 Hz, 12H, $CH_2$), 5.58 (d, J = 8.16 Hz, 6H, Naph), 6.36 (d, J = 8.12 Hz, 6H, Naph), 7.08 (m, 6H, Naph), 7.60 (m, 6H, Naph), 7.90 (d, J = 7.92 Hz, 6H, Naph), 8.25 (d, J = 8.3 Hz, 6H, Naph); IR (FT): υ = 3413 $cm^{-1}$ (s, N-H); ESI (+) m/z: 1662.857 ( $[M]^+$, calc: 1662.865).

### 7.4.4. Aggregation studies

Critical aggregation concentration was obtained by recording the absorption, excitation and emission spectra at different concentrations ($5\cdot10^{-5}$-$10^{-6}$ M) in a mixture of dimethyl sulfoxide and water (50:50 in the case of **7.1-5** and **7.8** or 60:40 in the case of **7.6** and **7.7**).

NMR studies at different concentrations ($5.5\cdot10^{-3}$-$2.4\cdot10^{-4}$) were carried out by dissolving the corresponding amount of the compound in a DMSO-$d_6$:$D_2O$ mixtures, (50:50 in the case of **7.1-5** and **7.8** or 60:40 in the case of **7.6** and **7.7**).

The samples for SAXS experiments were prepared one week before in order to favour the aggregation processes at different concentrations ($10^{-4}$-$5\cdot10^{-6}$ M) in water for **7.1** and **7.2** and in water and tetrahydrofuran mixtures (50:50) for **7.3-8**.

Time dependent studies of $10^{-5}$M water solutions containing 0.1% of dimethyl sulfoxide were followed by absorption and dynamic light scattering (DLS) at different times (0, 1, 3 and 6 hours) at 37ºC.

### 7.4.5. Partition coefficient

Partition coefficient was calculated following literature methods.[58] A known amount of the compound was dissolved in 1-octanol. Equal volumes of this solution and water was mixed and stirred for 24 h at room temperature. After 24 h, the solution was transferred into 60 mL of separating funnel and allowed to stand in order to separate the aqueous and organic layer. The organic layer was then analysed by UV-vis spectrophotometer.

### 7.4.6. Biological assays

Biological assays were made by Dr. Catarina Roma-Rodrigues in collaboration from the group of Dr. Alexandra R. Fernandes and Dr. Pedro V. Baptista from Universidade NOVA de Lisboa.

#### Cell culture and cell culture maintenance

Human ovarian carcinoma, A2780, purchased from ATCC (Manassas, VA, USA) were grown and maintained in RPMI 1640 medium (Gibco, ThermoFisher Scientific, Waltham, MA, USA) supplemented with 10% (v/v) fetal bovine serum (FBS, Gibco, ThermoFisher Scientific), 1% (v/v) non-essential aminoacids (MEM, Gibco, ThermoFisher Scientific) and a mixture of 100 U/mL Penicillin and 100 μg/mL Streptomycin (Gibco, ThermoFisher Scientific) at 37ºC, 5% (v/v) $CO_2$ in an humidified atmosphere.

#### Cellular uptake of complexes 5.4, 5.5, 5.7 and 5.8 by A2780 cells

To evaluate the internalization of the complexes, $2x10^6$ A2780 cells were seeded in a 25 $cm^2$ T-flask and let to adhere for 24h. Afterwards, the media was replaced by fresh media supplemented with 10 times the respective $IC_{50}$ of each complex and incubated for 3h at 37ºC and 4ºC or for 6h at 37ºC. The supernatant was transferred to a clean tube and cells were washed with phosphate buffer saline (PBS) that was added to the supernatant containing tube. Cells were then detached with Tryple express (TE, ThermoFisher Scientific) and pelleted with a 500 xg centrifugation for 5 min. The supernatant was

transferred to the supernatant containing tube and both cells and supernatant samples were incubated with aqua regia overnight. The amount of gold in each sample was quantified with ICP-AES. The percentage of intracellular gold was calculated by dividing the gold concentration in cells by the sum of gold concentrations in respective supernatant and cell pellet.

**Distribution of complexes 5.4, 5.5, 5.7 and 5.8 in cellular fractions**

A2780 cells were seeded in 25 $cm^2$ T-flasks in a density of $6x10^5$ cells/mL. After 24h, cells were exposed to fresh media supplemented with $IC_{50}$ of each complex and incubated for 3h at 37ºC, 5% (v/v) $CO_2$ in a humidified atmosphere. Afterwards, cells were collected with a cell scratcher in PBS, pelleted with a 500 xg centrifugation for 5 min and fractionated with Cell fractionation kit (Cell Signalling Technologies, Danvers, MA, USA) according to the manufacturer's instructions. With this protocol three fractions are obtained, the cytoplasmic fraction, the mitochondrial fraction, composed by membranes and organelles, and the nuclear fraction. After incubation of each obtained fraction with aqua regia, the amount of gold was quantified with ICP-AES. The percentage of gold in each fraction was calculated by dividing the gold concentration in the specific fraction with the sum of gold concentrations in respective cytoplasmic, mitochondrial, and nuclear fractions.

**Interaction of complexes 5.4 and 5.8 with actin**

A2780 cells were seeded in a 24-well plate in a cell density of 37500 cells/well. After 24h, the media was replaced by the $IC_{50}$ of complex **7.4** (0.1 μM), the $IC_{50}$ of complex **7.8** (0.3 μM) or 0.1 % (v/v) DMSO, the vehicle solvent of complexes. After 0h, 30 min, 1h, 3h or 6h incubation, cells were fixed with formaldehyde 4% (w/v) (Sigma Aldrich, Merck, Kenilworth, NJ, USA) for 15 min and washed three times with PBS. Cell membrane was then disrupted through a 5 min incubation with triton 0.1% (v/v) (Sigma Aldrich, Merck), washed three times with PBS and cells were incubated for 30 min with BSA 1% (w/v) (NZYtech, Lisbon, Portugal) and 20 min with AlexaFluor 488 phalloidin (Invitrogen, ThermoFisher Scientific) as previously described. After washing three times with PBS, cells were visualized with a Ti-U Eclipse inverted microscope with green filter cube (excitation filter range 465-495 nm and emission filter range at 515-555 nm) and images were acquired with respective microscope software. Three different images with

around 20 cells were acquired per sample with 40x objective or 5 different images with around 5 cells were acquired with 100x objective.

**Dark field analysis**

A2780 cells were seeded in a 24-well plate in a cell density of 37500 cells/well. After 24h, the media was replaced by the $IC_{50}$ of complex **7.4** (0.1 μM), the $IC_{50}$ of complex **7.8** (0.3 μM) or 0.1 % (v/v) DMSO, the vehicle solvent of complexes. After 3h incubation cells were fixed with formaldehyde 4% (w/v) (Sigma Aldrich, Merck) for 15 min and washed three times with PBS. Cells were visualized with a Ti-U Eclipse inverted microscope using a dark field condenser and 100x objective. Five different images with around 5 cells were acquired per sample.

## 7.5. References


1. Hanzlik, R. P. Annu. Rep. Med. Chem. **1973**, 8, 294–302.
2. Champion, G. D., Graham, G. G. and Ziegler, J. B. *Bailliere's Clinical* Rheumatology **1990**, 4, 491–534.
3. Ott, I. Coord. Chem. Rev. **2009**, 253, 1670–1681.
4. Brown, T. Harv. Bus. Rev. **2008**, 86, 84–92.
5. Che, C. M. and Sun, R. W. Y. Chem. Commun. **2011**, 47, 9554–9560.
6. Bertrand, B. and Casini, A. Dalton Trans. **2014**, 43, 4209–4219.
7. Zou, T., Lum, C. T., Lok, C. N., Zhang, J. J. and Che, C. M. Chem. Soc. Rev. **2015**, 44, 8786–8801.
8. Zhou, L., Liu, H., Liu, K. and Wei, S. Front. Pharmacol. **2021**, 12, 1–15.
9. https://clinicaltrials.gov/ct2/show/NCT01419691 (30/03/2021).
10. Becker, K., Gromer, S., Heiner Schirmer, R. and Müller, S. Eur. J. Biochem. **2000**, 267, 6118–6125.
11. Urig, S. and Becker, K. Semin. Cancer Biol. **2006**, 16, 452–465.
12. De Almeida, A., Mósca, A. F., Wragg, D., Wenzel, M., Kavanagh, P., Barone, G., Leoni, S., Soveral, G. and Casini, A. Chem. Commun. **2017**, 53, 3830–3833.
13. Jacques, A., Lebrun, C., Casini, A., Kieffer, I., Proux, O., Latour, J. M. and Sénèque, O. Inorg. Chem. **2015**, 54, 4104–4113.
14. Meier-Menches, S. M., Aikman, B., Dóllerer, D., Klooster, W. T., Coles, S. J., Santi, N., Luk, L., Casini, A. and Bonsignore, R. J. Inorg. Biochem. **2020**, 202, 110844.
15. Wragg, D., de Almeida, A., Bonsignore, R., Kühn F. E., Leoni, S. and Casini, A. Angew. Chem. Int. Ed. **2018**, 130, 14732–14736.
16. Silva, M. J. S. A., Gois, P. M. P. and Gasser, G. ChemBioChem **2021**, 22, 1740–1742.

17. Ott, I., Qian, X., Xu, Y., Vlecken, D. H. W., Marques, I. J., Kubutat, D., Will, J., Sheldrick, W. S., Jesse, P., Prokop, A. and Bagowski, C. P. J. Med. Chem. **2009**, 52, 763–770.

18. Ronconi, L., Giovagnini, L., Marzano, C., Bettìo, F., Graziani, R., Pilloni, G. and Fregona, D. Inorg. Chem. **2005**, 44, 1867–1881.

19. Urig, S., Fritz-Wolf, K., Réau, R., Herold-Mende, C., Tóth, K., Davioud-Charvet, E. and Becker, K. Angew. Chemie - Int. Ed. **2006**, 45, 1881–1886.

20. Baker, M. V., Barnard, P. J., Berners-Price, S. J. Brayshaw, S. K., Hicey, J. L., Skelton, B. W. and White, A. H. Dalton Trans. **2006**, 6, 3708–3715.

21. Yan, K., Lok, C. N., Bierla, K. and Che, C. M. Chem. Commun. **2010**, 46, 7691–7693.

22. Meyer, A., Bagowski, C. P., Kokoschka, M., Stefanopoulou, M., Alborzinia, H., Can, S., Vlecken, D. H., Sheldrick, W. S., Wölf, S. and Ott, I. Angew. Chem. Int. Ed. **2012**, 51, 8895–8899.

23. Humphreys, A. S., Filipovska, A., Berners-Price, S. J., Koutsantoni, A., Skelton, B. W. and White, A. H. Dalton Trans. **2007**, 43, 4943–4950.

24. Bergamini, P., Bertolasi, V., Marvelli, L, Canella, A., Gavioli, R., Mantovani, N., Mañas, S. and Romerosa, A. Inorg. Chem. **2007**, 46, 4267–4276.

25. Hajji, L., Saraiba-Bello, C., Romerosa, A., Segovia-Torrente, G., Serrano-Ruiz, M., Bergamini, P. and Canella, A. Inorg. Chem. **2011**,50, 873–882.

26. McKeage, M. J., Berners-Price, S. J., Galettis, P., Bowen, R. J., Brouwer, W., Ding, L., Zhuang, L. and Baguleu, B. Cancer Chemother. Pharmacol. **2000**, 46, 343–350.

27. Petrenko, A., Belyakov, S. and Arsenyan, P. Mendeleev Commun. **2020**, 30, 572–573.

28. Raubenheimer, H. G. and Schmidbaur, H. Organometallics **2012**, 31, 2507–2522.

29. Aguiló, E., Moro, A. J., Gavara, R., Alfonso, I., Pérez, Y., Zaccaria, F., Fonseca Guerra, C., Malfois, M., Baucells, C., Ferrer, M., Lima, J. C. and Rodríguez, L. Inorg. Chem. **2018**, 57, 1017–1028.

30. Gavara, R., Aguiló, E., Guerra, C. F., Rodríguez, L. and Lima, J. C. Inorg. Chem. **2015**, 54, 5195–5203.

31. Moro, A. J., Rome, B., Aguiló, E., Arcau, J., Puttreddy, R., Rissanen, K., Lima, J. C. and Rodríguez, L. Org. Biomol. Chem. **2015**, 13, 2026–2033.

32. Pinto, A., Svahn, N., Lima, J. C. and Rodríguez, L. Dalton Trans. **2017**, 46, 11125–11139.

33. Gavara, R., Pinto, A., Donamaría, R., Olmos, M. E., López de Luzuriaga, J . M. and Rodríguez, L. Inorg. Chem. **2017**, 56, 11946–11955.

34. Pinto, A., Hernández, G., Gavara, R., Aguiló, E., Moro, A. J., Aullón, G., Malfois, M., Lima, J. C. and Rodríguez, L. New J. Chem. **2019**, 43, 8279–8289.

35. Owen, S. C., Doak, A. K., Wassam, P., Shoichet, M. S. and Shoichet, B. K. ACS Chem. Biol. **2012**, 7, 1429–1435.

36. Prabha, S., Arya, G., Chandra, R., Ahmed, B. and Nimesh, S. Artif. Cells, Nanomedicine Biotechnol. **2016**, 44, 83–91.

37. Svahn, N., Moro, A. J., Roma-Rodrigues, C., Puttreddy, R., Rissanen, K., Baptista, P. V., Fernandes, A. R., Lima, J. C. and Rodríguez, L. Chem. - A Eur. J. **2018**, 24, 14654–14667.

38. Carpenter-Warren, C. L., Cunnington, M., Elsegood, M. R. J., Kenny, A., Hill, A. R., Miles, C. R. and Smith, M. B. Inorg. Chim. Acta **2017**, 462, 289–297.

39. Assefa, Z., Forward, J . M., Grant, T. A., Staples, R. J., Hanson, B. E., Mohamed, A. A. and Fackler, J. P. Inorg. Chim. Acta **2003**, 352, 31–45.

40. Svahn, N., Sanz, I., Rissanen, K. and Rodríguez, L. J. Organomet. Chem. **2019**, 897, 170–177.

41. Appleton, A. L., Brombosz, S. M., Barlow, S., Sears, J. S., Bredas, J. L., Marder, S. R. and Bunz, U. H F. Nat. Commun. **2010**, 1, 1–6.

42. Hansch, C., Leo, A. and Taft, R. W. A. Chem. Rev. **1991**, 91, 165–195.

43. Bowmaker, G. A., Brown, C. L., Hart, R. D., Healy, P. C., Rickard, C. E. F. and White, A. H. J. Chem. Soc. Dalton Trans. **1999**, 3, 881–889.

44. Bui, T. T. T., Dahaoui, S., Lecomte, C., Desiraju, G. R. and Espinosa, E. Angew. Chem. Int. Ed. **2009**, 121, 3896–3899.

45. Gavara, R., Llorca, J., Lima, J. C. and Rodrígez, L. Chem. Commun. **2013**, 49, 72–74.

46. Ruseska, I. and Zimmer, A. Beilstein J. Nanotechnol. **2020**, 11, 101–123.

47. Rejman, J., Oberle, V., Zuhorn, I. S. and Hoekstra, D. Biochem. J. **2004**, 377, 159–169.

48. dos Santos, T., Varela, J., Lynch, I., Salvati, A. and Dawson, K. A. PLoS One **6**, **2011**, 6, 1–10.

49. Chen, M. L., Yi, L., Jin, X., Xie, Q., Zhang, T., Zhou, X., Chang, H., Fu, Y. J., Zhu, J. D., Zhang, Q. Y. and Mi, M. T. J. Nutr. Biochem. **2013**, 24, 1823–1829.

50. Guidi, F., Landini, I., Puglia, M., Magherini, F., Gabbiani, C., Cinellu, M. A., Nobili, S., Fiaschi, T., Bini, L., Mini, E., Messori, L. and Modesti, A. Metallomics **2012**, 4, 307–314.

51. Suarez-Huerta, N., Mosselmans, R., Dumont, J. E. and Robaye, B. J. Cell. Physiol. **2000**,184, 239–245.

52. Liu, W. and Gust, R. Coord. Chem. Rev. **2016**, 329, 191–213.

53. Huang, T. C., Toraya, H., Blanton, T. N. and Wu, Y. J. Appl. Crystallogr. **1993**, 26, 180–184.

54. Kieffer, J. and Karkoulis, D. J. Phys. Conf. Ser. **2013**, 425, 1–5.

55. Konarev, P. V., Volkov, V. V., Sokolova, A. V., Koch, M. H. J. and Svergun, D. I. J. Appl. Crystallogr. **2003**, 36, 1277–1282.

56. Svergun, D. I. J. Appl. Crystallogr. **1992**, 25, 495–503.

57. Svergun, D. Biophys. J. **1999**, 76, 2879–2886.

58. Baluja, S., Kulshrestha, A. and Movalia, J. Rev. Colomb. Ciencias Químico-Farmacéuticas **2017**, 46, 342–356.

# CHAPTER 8

## Effect of the incorporation of an amphiphilic moiety on the resulting supramolecular assemblies

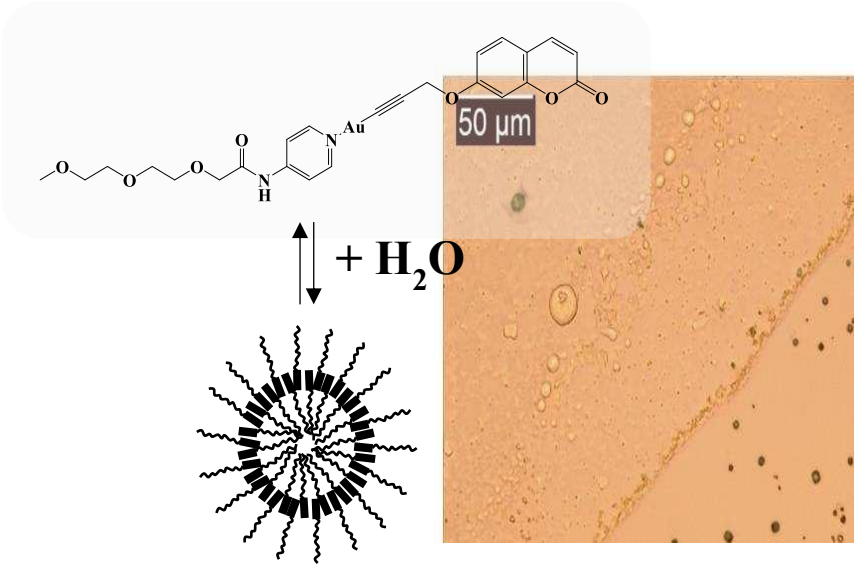


Unpublished work.

# 8. EFFECT OF THE INCORPORATION OF AN AMPHIPHILIC MOIETY ON THE RESULTING SUPRAMOLECULAR ASSEMBLIES

## 8.1. Introduction

The self-assembly of small molecules is a powerful bottom-up approach for the preparation of nanomaterials and has received great attention in the past decade.[1,2] Molecular self-assembly represents a very attractive way to create a large variety of supramolecular structures and offers different advantages thanks to its reversibility, which can confer the ability of changing different properties by an external stimulus. This technologically relevant science led many research groups to take advantage of non-covalent interactions in order to construct supramolecular structures with different morphologies and with specific functions.[3–6] In particular, controlling supramolecular interactions in water has become an attractive feature since the use of water as solvent provides promising benefits with respect to environmental impact and provides also a better understanding and control of the major processes in nature. One of the main challenges of supramolecular chemistry in aqueous media is the design of synthetic structures stable in this medium. Complex systems present usually several restrictions in terms of solubility, that governs the type of building blocks that can be obtained. Moreover, the competitive influence of water must be also considered due to the strong hydration of the individual molecules affecting the non-covalent processes.[7]

Several strategies can be followed in order to avoid these drawbacks. Among them, the use of amphiphilic systems, inspired from the intracellular components of the biological membranes, allows to control and create a wide variety of supramolecular structures.[8] The arrangement of the molecules that contain an amphiphilic group usually is driven by hydrophilic and hydrophobic interactions that allows constructing supramolecular structures due to repulsive interactions with the aqueous media. This strategy has been followed by different research groups. For example, Lee and co-workers studied the self-assembly of a laterally grafted bent-rod amphiphile in water or Aida and co-workers performed the self-assembly studies with an amphiphilic hexa-peribenzocoronene derivates.[9] In particular, and regarding our work, it is interesting to highlight how the self-

assembly of luminescent transition metal complexes, can be used as an effective strategy to modulate their photophysical properties, such as the emission wavelength, excited state lifetime or the photochemical stability.[10] Within this field, gold(I) complexes are exceptionally appealing due to the well-known weak Au(I)···Au(I) interactions, being some of the strongest metallophilic interactions which are comparable to hydrogen bonding,[11] and are directly involved on the resulting assemblies and properties.[12,13]

In this context, small molecules containing the gold(I) alkynyl unit are attractive building blocks for the construction of organometallic materials due to the preference of gold(I) for a linear coordination geometry and the π-unsaturated nature of the acetylide unit. The addition of a water-soluble phosphane as a secondary coordination position favours the solubility of gold(I) compounds in water. Additionally, as previously observed in our group, they govern the construction of supramolecular structures with different morphologies that are also strongly affected by the introduction of a charge in the chemical structure or on the chromophoric unit used (Figure 8.1).[14–16]

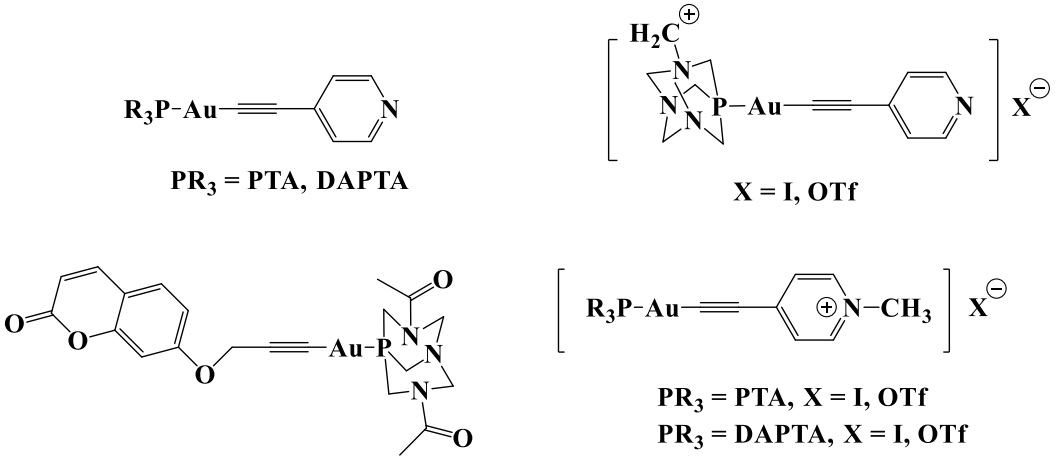


**Figure 8.1.** Molecular structures of gold(I) alkynyl complexes previously studied in the research group that give rise to supramolecular assemblies in water.

Another approach to ensure the solubility of the molecules in water is by attaching a polar group in the chemical structure of the molecule. Poly(ethylene glycol) (PEG) is an amphiphilic moiety with a hydrophilic character that can give a good aqueous solubility to metal complexes. Moreover, its amphiphilic character ensures the resulting supramolecular assemblies through strong non-covalent interactions. This ligand has been barely used in organometallic chemistry and the resulting complexes may be used for bioimaging purposes since the incorporation of a PEG moiety significantly improve the

solubility of the molecules in water.[1] Despite this, some applications are found as catalysts[17] or in controlling the self-assembling with the aim of changing the luminescent properties are also described.[18,19]

In this context, we have designed gold(I) complexes containing a pyridil type ligand with a PEG moiety incorporated in their chemical structure. Pyridyl type ligands are widely used in coordination chemistry due to their coordination ability properties. However, the number of gold(I) pyridine complexes is less and can be a hidden potential.[20–23] Also the incorporation of two different chromophores (previously used in this thesis) as the second coordination position was employed in order to introduce luminescent properties to these systems. Aggregation studies and potential applications derived from them have been also explored, since the pyridine ligand contains an amphiphilic group, which may induce this aggregations.

## 8.2. Results and Discussion

### 8.2.1. Synthesis and characterization

The synthetic route of the final gold(I) complexes involves various steps. Firstly, the synthesis of N-(4-pyridyl)2-[2-(2-methoxyethoxy)ethoxy] acetic acid amide (**8.1**) that was synthesized following the literature method summarized in Scheme 8.1.[18]

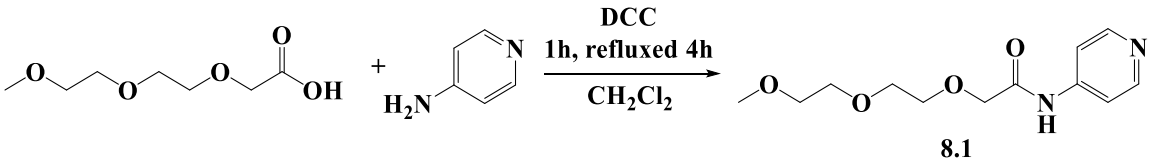


**Scheme 8.1.** Synthesis of N-(4-pyridyl)2-[2-(2-methoxyethoxy)ethoxy] acetic acid amide (**8.1**).

This reaction is a nucleophilic acyl substitution that affects a carboxylic acid and an amine. This process needs an auxiliary reagent, in this case N,N'-dicyclohexylcarbodiimide (DCC), otherwise an acid-base reaction between the acid and the amine would occur. The correct formation of **8.1** was checked by $^{1}$H NMR, IR and mass spectrometry. A downfield shift (0.2 ppm) of the aromatic protons and the presence of the proton of the amide at ca. 9 ppm was observed in the $^{1}$H NMR spectrum. ESI-

MS(+) shows a peak of the monoprotonated $[M+H]^+$ species as a final evidence of the correct formation of the product.

The introduction of gold(I) was carried out by the reaction of the alkynyl derivatives, 4-ethynylaniline (**8.L3**) or 7-propargylcoumarin (**8.L4**), with a common gold(I) precursor. This one consists of the reaction of **8.1** with [AuCl(tht)] in order to obtain the complex **8.2**. Its successful formation was proved by $^1$H NMR, where a variation in the chemical shift was observed in the aromatic region. Finally, alkynyl derivatives were deprotonated with a strong base and then complex **8.2** was added in order to form the desired products **8.3** and **8.4** (Scheme 8.2).

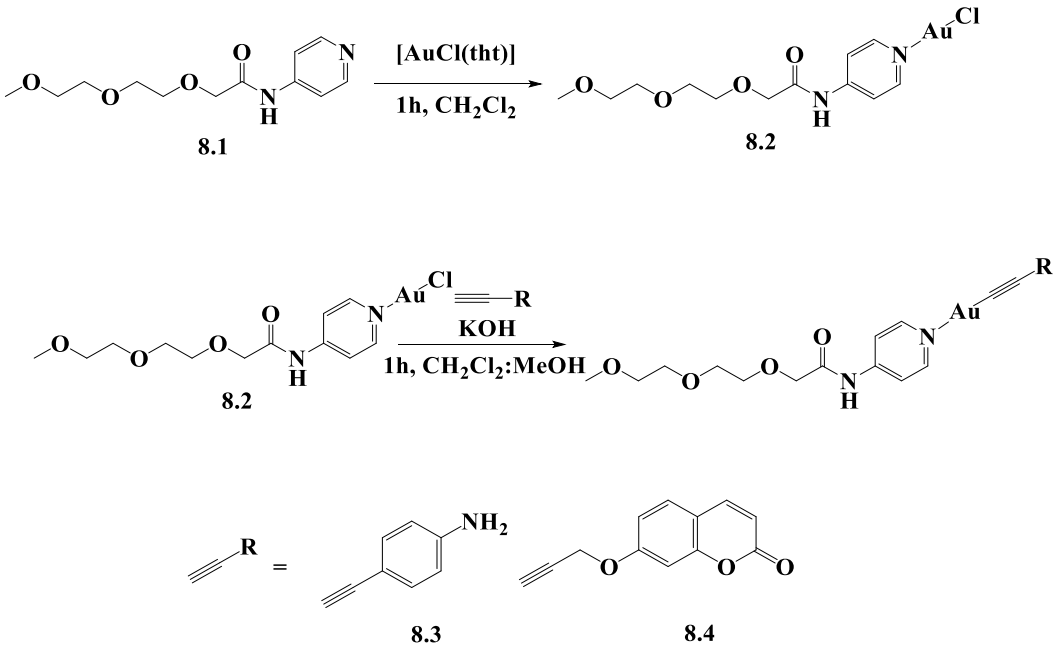


**Scheme 8.2.** Synthetic route followed for the synthesis of complexes **8.3** and complexes **8.4**.

$^1$H NMR spectra confirm the correct formation of the complexes due to the disappearance of the terminal alkynyl proton and a slight upfield shift (0.04 ppm) of the protons close to the gold(I) atom (Figure 8.2). It was also confirmed by ESI-MS(+) with the detection of the monoprotonated $[M+H]^+$ species in both cases.

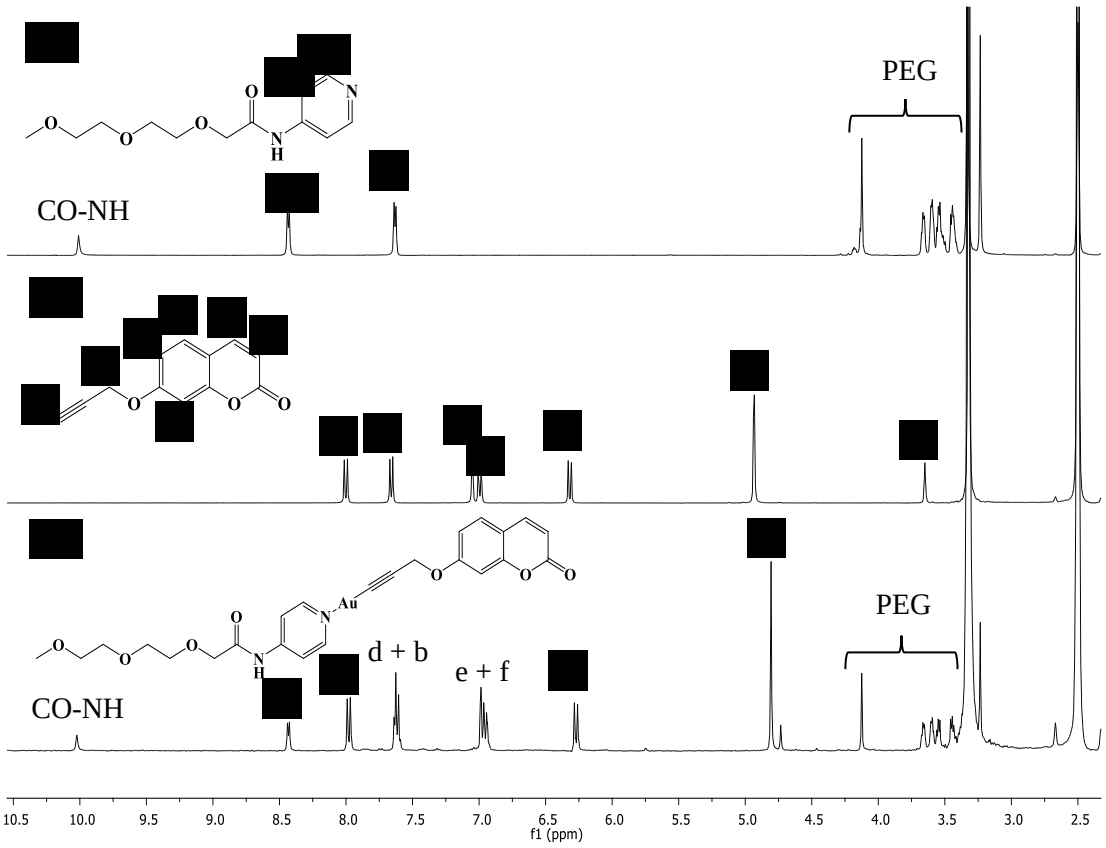


**Figure 8.2.** $^{1}$H NMR spectra of **8.1** (a), 7-propargylcoumarin (b) and **8.4** (c) in DMSO-$d_6$.

### 8.2.2. Photophysical characterization

The absorption and emission spectra of all complexes have been recorded in $10^{-5}$ M acetonitrile solutions at room temperature and the obtained data are summarized in Table 8.1.

**Table 8.1.** Electronic absorption and emission data, of **8.1**, **8.L3** and **8.L4** and complexes **8.3** and **8.4** in acetonitrile.

| Compound | Absorption, nm $\lambda_{max}$ ($10^3$ ε $cm^{-1}$ $M^{-1}$) | Emission (nm) |
|---|---|---|
| **8.1** | 240 (16.6) | - |
| **8.L3** | 273 (7.9) | 346 |
| **8.L4** | 316 (16.0) | 381 |
| **8.3** | 235 (11.1), 288 (19) | 348 |
| **8.4** | 237 (16.5), 322 (18.0) | 386 |

The absorption spectra of the gold(I) complexes **8.3** and **8.4** display two absorption bands: one at high energies (ca. 230 nm) related to the π-π* transition located in the pyridine ring and another at lower energies (ca. 300 nm) due to the π-π* of the alkynyl derivatives, 4-ethynylaniline (**8.L3**) or 7-propargylcoumarin (**8.L4**) (Figure 8.3). The band at lower energies in both gold(I) complexes is slightly red shifted when the gold(I) is coordinated to the chemical structure probably due to a participation of the d-orbital in the transition.[24]

Emission spectra were recorded in solution upon excitation of the samples at the lowest energy absorption band. The emission of the gold(I) complexes is observed to be ligand-centered fluorescence without a significant red shift in the emission maxima.

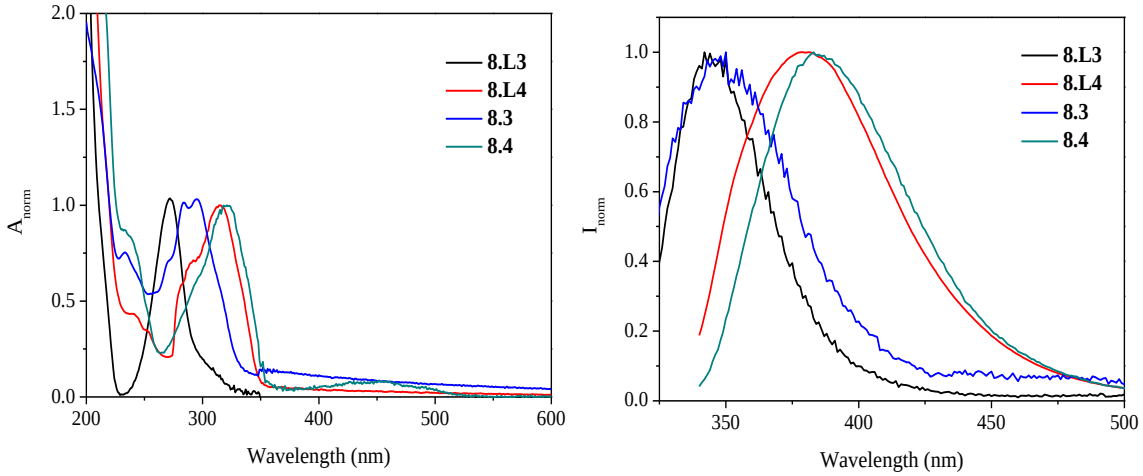


**Figure 8.3.** Absorption (left) and emission (right) spectra of **8.L3** and **8.L4** and gold(I) complexes **8.3** and **8.4** in acetonitrile.

### 8.2.3. Aggregation studies

The gold(I) complexes **8.3** and **8.4** contain a hydrophobic chromophore and a hydrophilic triethylene glycol pendant group, that are expected to induce aggregation in water. In addition, the presence of an amide group, capable of favouring the establishment of additional directional hydrogen bonds may play an important role in the resulting self-assembly process.

For this reason, absorption and emission spectra were recorded for **8.3** and **8.4** at different concentrations ($2.5 \cdot 10^{-6}$ M – $10^{-4}$ M). A linear trend is observed in the plot of the absorption and the emission vs the concentration (Figure 8.4). Therefore, aggregation is not expected to occur when the concentration increases.

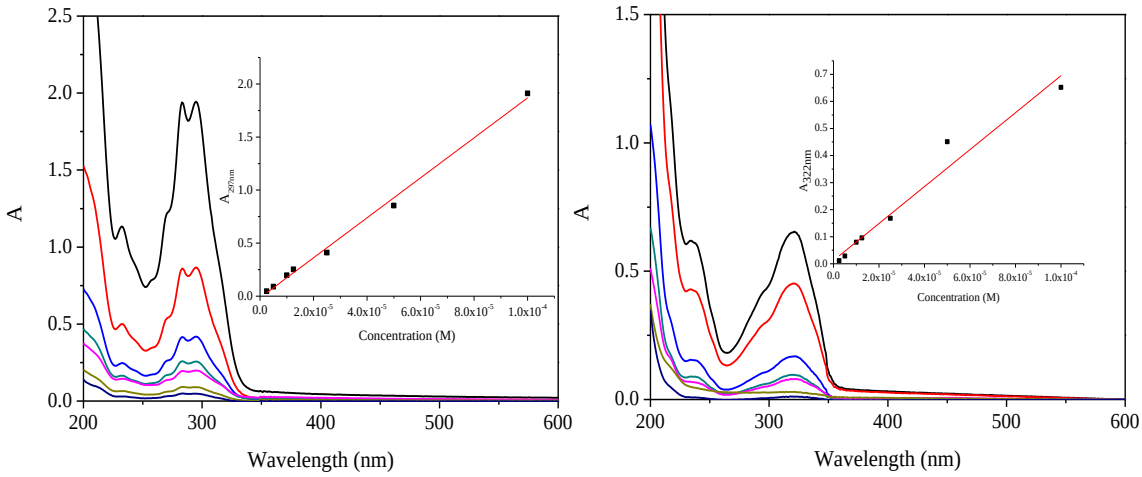


**Figure 8.4.** Absorption spectra of **8.3** (left) and **8.4** (right) at different concentrations (inset: plot c absorption maxima vs the concentration).

Studies of the luminescent properties in a solvent/non-solvent mixture have been performed in order to induce the aggregation of the gold(I) complexes. Water/acetonitrile mixtures (25% to 75%) were chosen since the complexes are well solubilized in acetonitrile and the introduction of water, which acts as the non-solvent, can induce their aggregation. Additionally, similar experiments were carried out with gold(I) complexes containing the PTA and DAPTA phosphanes and the same chromophoric unit used for **8.3** and **8.4** for comparison purposes (Figure 8.5).

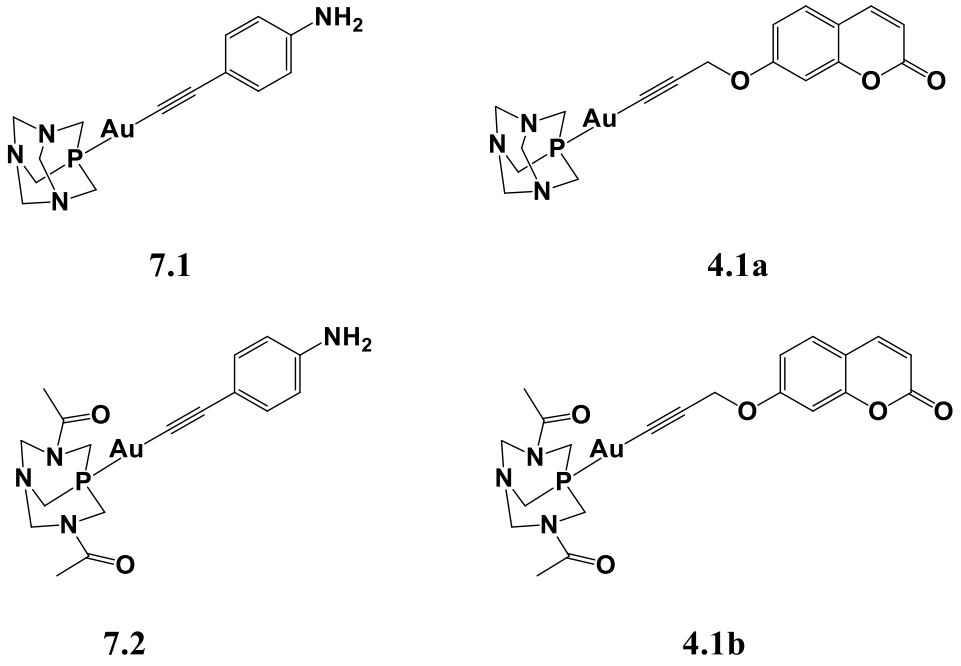


**Figure 8.5.** Gold(I) complexes used to compare the aggregation process with the gold(I) complexes synthesized in this chapter.

Absorption and emission spectra were recorded for **8.3**, **7.1-2**, **8.4** and **4.1a-b** at different water contents (25% to 75%). A blue shift (10 nm) is observed for those compounds that contain 4-ethynylaniline (**8.L3**) as a chromophore. In the case of **8.3** the absorption band is the same to the **8.L3** absorption when the water contents reaches 75%. This is probably due to a degradation of the compound and the more labile character of the pyridine group. No significant change in the absorption spectra was observed for those compounds containing 7-propargylcoumarin (**8.L4**) as a chromophore and PTA (**4.1a**) or DAPTA (**4.1b**) as a phosphane. On the other hand, the incorporation of a hydrophilic PEG moiety (**8.4**) induces a decrease of the absorption band together with an increase of the baseline in agreement with the aggregation process. In all cases, the intensity of the emission increases at higher water contents, due to an aggregation induced emission (AIE) process. The most interesting data were retrieved from the emission of the gold(I) complex **8.4**, since a new band appears at longer wavelength when the water contents increases (Figure 8.6). This band is attributed to the excimer of the coumarin unit, according to the literature.[25]

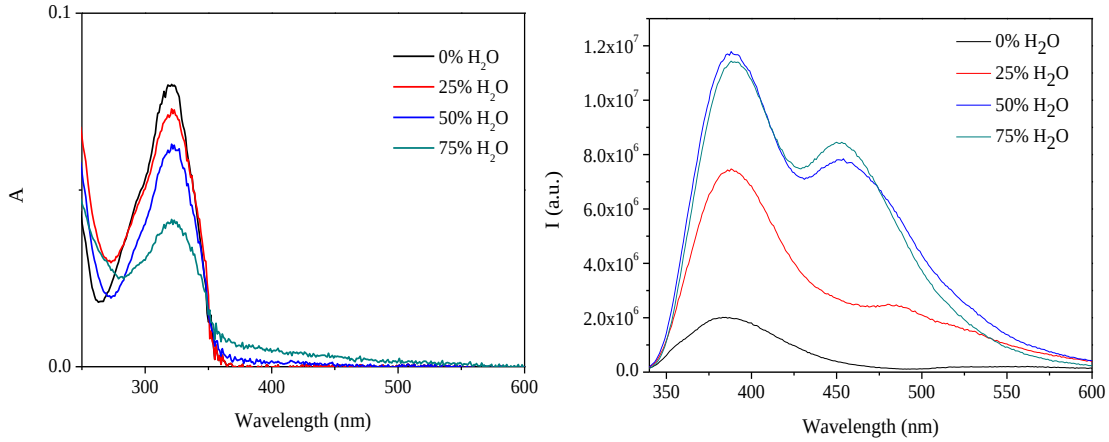


**Figure 8.6.** Absorption (left) and emission (right) spectra of **8.4** in acetonitrile/water mixtures.

Thus, the incorporation of the hydrophilic triethylene glycol pendant group as a second coordination position in the gold(I) complex that contains 7-propargylcoumarin (complex **8.4**) induces the formation of an excimer, meaning that the hydrophobic part of the molecules stays closer to each other in the resulting aggregates, as exemplified in Figure 8.7.

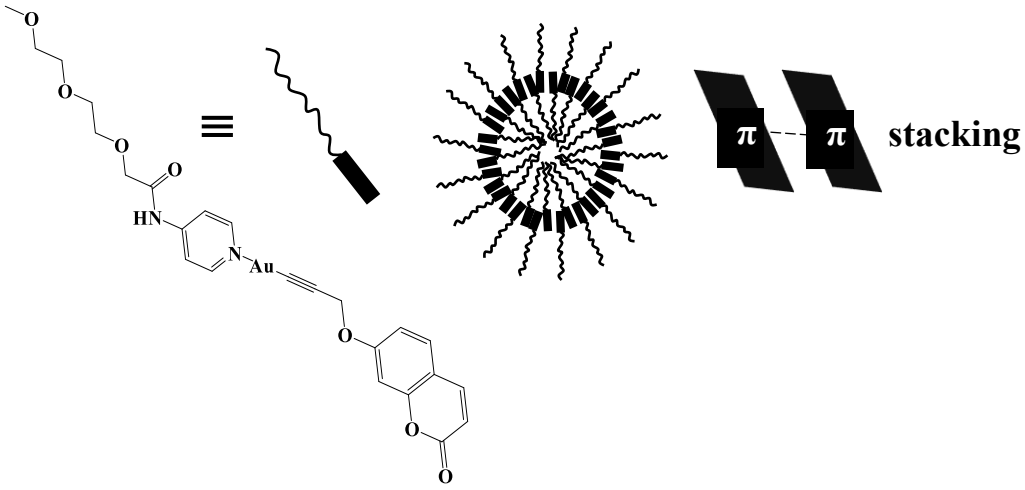


**Figure 8.7.** Illustration of the supramolecular self-assembly expected for complex **8.4**. Left, chemical formula and schematic representation of complex **8.4** and right, schematic illustration of the expected assembly.

### 8.2.4. Characterization of the aggregates

An in depth characterization of the resulting aggregates in solution and in solid state has been performed for the gold(I) complex **8.4**. Dynamic light scattering (DLS) measurements showed the formation of aggregates in pure acetonitrile with a relatively narrow distribution (220 nm). Thus, aggregation already exists in the absence of water, in a good solvent such as acetonitrile, as previously observed in other gold(I) complexes.[26] The addition of different amounts of water induces an increase of the size of the aggregates (ca. 400 nm) and a broadening of the size distribution (Figure 8.8). This data is in agreement with the results obtained from the absorption and emission spectra at different acetonitrile/water ratios and the appearance of aggregates where the chromophoric unit is directly involved.

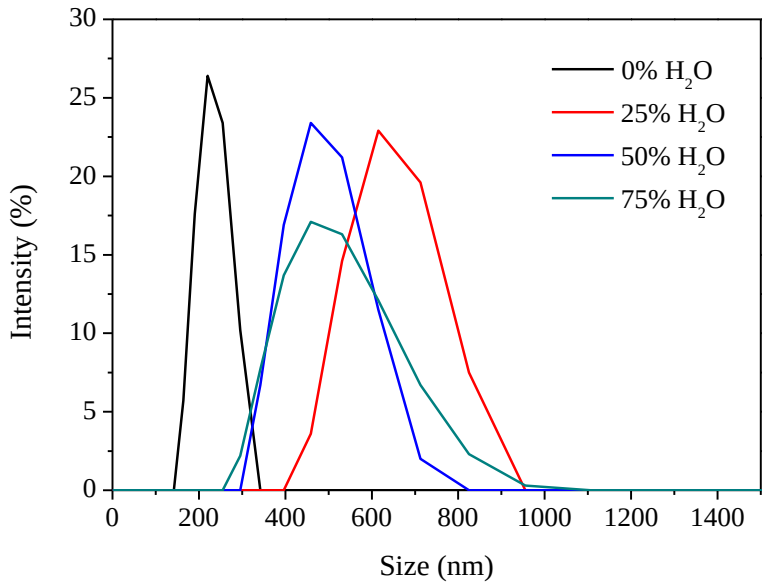


**Figure 8.8.** Size distribution obtained by Dynamic Light Scattering (DLS) for **8.4** at different water/acetonitrile ratios.

Small Angle X-ray Scattering (SAXS) studies were performed in order to analyze the size and the shape of the aggregates in an early stage. SAXS measurements have been performed in the NCD (Non Crystalline Diffraction) beamline at the Alba Synchrotron. The measurements were performed with $10^{-5}$ M solutions of the gold(I) complex **8.4** dissolved in acetonitrile/water mixtures. The low-resolution structures were reconstructed ab initio from the scattering patterns using the DAMMIN program (Figure 8.9).

One general tendency can be observed: the aggregates exist even in early stages and they have a larger size at higher water contents. These results are in agreement with the data obtained in the DLS experiments and confirm that the aggregation process is more favoured when increasing the water contents (non-solvent) in the solvent mixture.

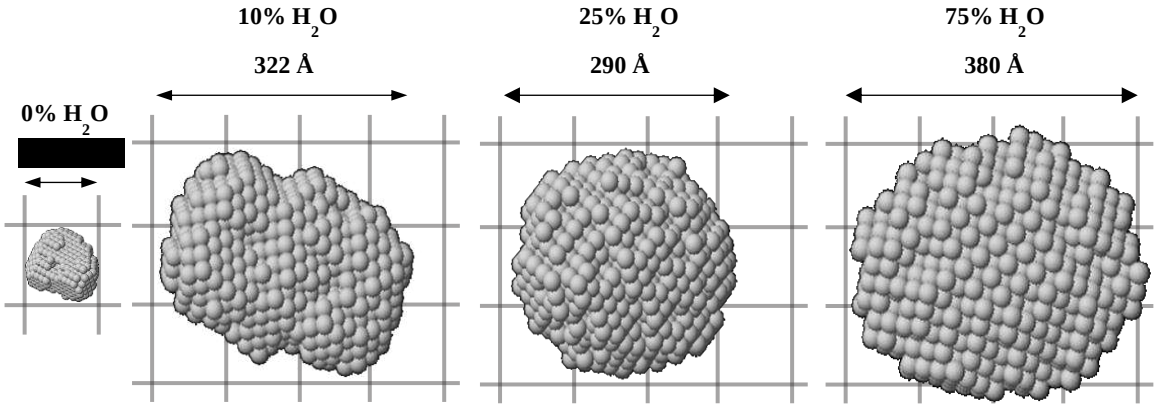


**Figure 8.9.** DAMMIN low resolution structures reconstructed from SAXS patterns for **8.4** at different water/acetonitrile ratios.

Optical microscopy has been used to determine the size and the shapes of the aggregates in dried samples after aggregation in solution. The samples were prepared by the deposition of solutions of gold(I) complex **8.4** with different acetonitrile/water mixtures onto a quartz substrate and let them dry. The aggregates can be detected by optical microscopy when the water contents reaches up to 50%, in agreement with more favoured aggregation. The optical microscopy images show the existence of micrometric dendritic structures and some spherical aggregates (Figure 8.10). It is expected that the more tangled supramolecular structure comes from the junction of the spherical aggregates as previously seen for gold(I) complexes.[27]

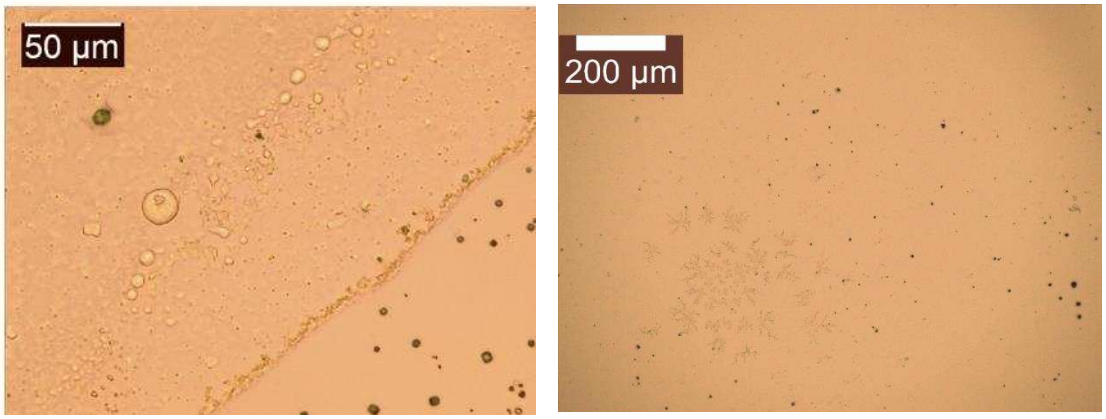


**Figure 8.10.** Optical microscopy image of dried solution of **8.4** in acetonitrile/water mixtures (25/75).

### 8.2.5. Molecular recognition of naphthalene derivatives

The emissive properties of the gold(I) complex **8.4** in acetonitrile/water mixtures together with the obtained micellar supramolecular assembly encouraged us to use this gold(I) complex as host for molecular recognition of hydrophobic species in water, such as naphthalene derivatives. With this goal in mind, three different naphthalene compounds (Figure 8.11), which differ in the substituents and the capability to perform different weak interactions with the host system, were chosen as guests. Absorption and emission titrations were performed in acetonitrile/water mixtures (25:75) and the changes on the spectroscopic properties were followed upon addition of different amounts of the corresponding guest.

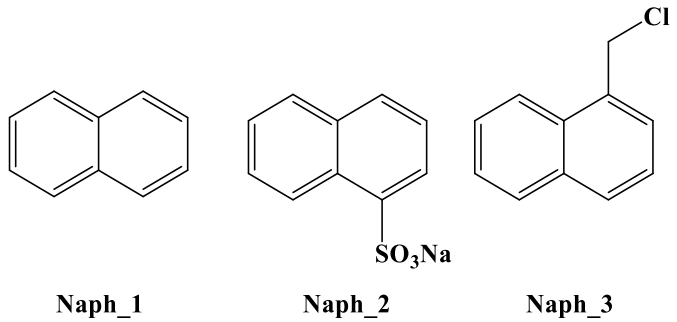


**Figure 8.11.** Naphthalene derivatives used as a guests.

No significant changes were recorded in the absorption spectra of the host, a part from the expected presence of increasing amounts of the guest molecules (Figure 8.12 left). Some changes were observed in the emission spectra. In general trends, the formation of 1:1 host:guest adducts can be expected for all the naphthalene derivatives as exemplified in figure 8.12 right for the **Naph_1** guest, although the small recorded changes in the emission spectra. Different behaviour has been observed depending on the guest. The emission intensity of both the monomer and the excimer decreases in the presence of the guest in the case of **Naph_1** and **Naph_2**. On the contrary, the excimer is more favoured when **Naph_3** is present in the solution. Considering the monomer/excimer ratio, an increase of the excimer has been observed for **Naph_1** and **Naph_3** (mainly **Naph_3**). In contrast, no significant changes have been observed for **Naph_2** (Figure 8.13). Altogether, some conclusions can be retrieved: 1) the substituents of the naphthalene guest molecule affect the resulting host-guest processes; 2) the incorporation of a negative charge in the naphthalene structure (**Naph_2**) does not affect the excimer band, and therefore, the aggregates' formation; 3) the incorporation of a chloride substituent, able to establish hydrogen bonds with the host, promotes the formation of the excimer formation and consequently, it has more affinity with the aggregated form of the host.

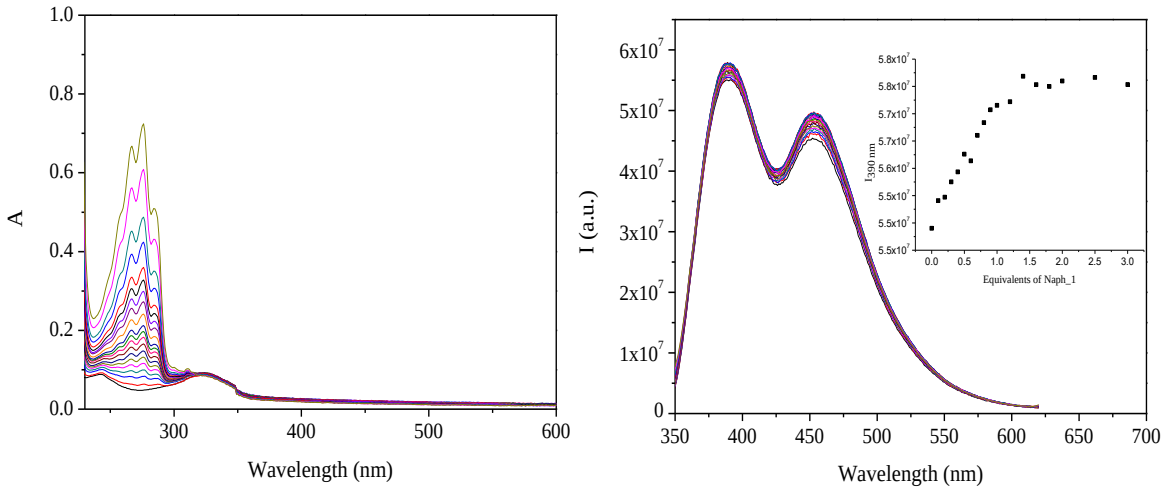


**Figure 8.12.** Absorption (left) and emission (right) spectra of **8.4** in the presence of different amounts of **Naph_1**. Inset: variations of the emission maxima at 390 nm against **Naph_1**.

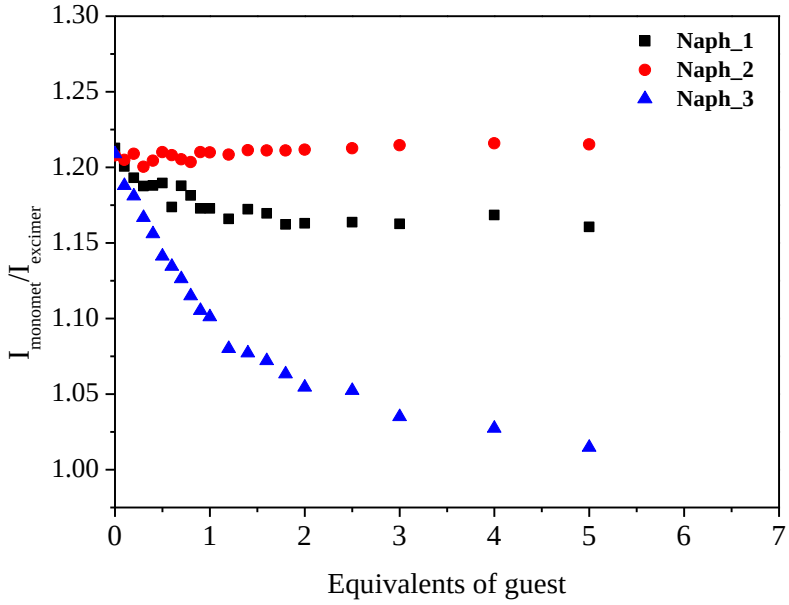


**Figure 8.13**. Plot representing the monomer/ excimer ratio variations vs number of equivalents of the guest added.

## 8.3. Conclusions

A series of gold(I) complexes containing N-(4-pyridyl)2-[2-(2-methoxyethoxy)ethoxy]acetic acid amide and two different chromophores located at the second coordination position have been successfully synthesized.

The incorporation of a hydrophilic triethylene glycol pendant group allows the formation of an excimer in the case of complex **8.4** in acetonitrile/water mixtures and the aggregates of this compound have been evidenced and characterized by DLS, SAXS and optical microscopy.

The micellar structure formed in acetonitrile/water mixtures (25/75) of complex **8.4** allows the possibility of using it as a host for the recognition of naphthalene derivatives. The substituent in the chemical structure of the naphthalene plays an important role, being the one that contains a chloride (**Naph_3**) the guest that interacts stronger with the excimer of the host probably due to the establishment of hydrogen bonds.

## 8.4. Experimental Section

### 8.4.1. General procedures

All manipulations have been performed under prepurified $N_2$ using standard Schlenk techniques. All solvents have been distilled from appropriated drying agents. Commercial reagents 4-aminopyridine (Aldrich, 98%), N,N'-dicyclohexylcarbodiimide (Aldrich, 99%), 2-[2-(2-methoxyethoxy)ethoxy]acetic acid (Aldrich), 4-ethynylaniline (Aldrich, 97%), propargyl bromide (Aldrich, 80wt. % toluene), 7-hydroxy-1-benzopyran-2-one (Aldrich) were used as received. Literature methods were used to prepare 7-(prop-2-in-1-yloxy)-1-benzopyran-2-one.[29]

### 8.4.2. Physical measurements

Infrared spectra have been recorded on a FT-IR 520 Nicolet Spectrophotometer. $^{1}$H-NMR (δ(TMS) = 0.0 ppm), $^{31}$P{$^{1}$H}-NMR (δ(85% $H_3PO_4$) = 0.0 ppm) spectra have been obtained on a Varian Mercury 400 and Bruker 400 (Universitat de Barcelona). ElectroSpray-Mass spectra (+) has been recorded on a Fisons VG Quatro spectrometer (Universitat de Barcelona). Absorption spectra have been recorded on a Varian Cary 100 Bio UV- spectrophotometer and emission spectra on a Horiba-Jobin-Yvon SPEX Nanolog spectrofluorimeter (Universitat de Barcelona). Dynamic Light Scattering (DLS) measurements were carried out in a Zetasizer NanoS Spectrometer (Universitat de Barcelona). The samples were measured in quartz cuvettes. SAXS experiments were performed on the NCD-SWEET beamline at the ALBA Synchrotron at 12.4 keV, and the distance sample/detector was 6.2 m to cover the range of momentum transfer of $0.028 < q < 2.56$ nm$^{-1}$. The data were collected on a Pilatus3S 1M detector with a pixel size of 172.0 x 172.0 μm$^2$. The exposure time was 30 s. The q-axis calibration was obtained by measuring silver behenate.[30] The program pyFAI was used to integrate the 2D SAXS data into 1D data.[31] The data were then subtracted by the background using PRIMUS software.[32] The maximum particle dimension Dmax and the pair distance Distribution P (r) were determined with GNOM.[33] The low resolution structure of aggregates was reconstructed ab initio from the initial portions of the scattering patterns using the program DAMM.[34] Optical microscopy images were acquired on a Leica ICC50 W microscope equipped with a Nikon DXM1200F digital camera.

### 8.4.3. Synthesis and Characterization

**Synthesis of N-(4-pyridyl)2-[2-(2-methoxyethoxy)ethoxy]acetic acid amide (pyPEG)**

According to the literature procedure,[18,19] 2-[2-(2-methoxyethoxy)ethoxy]acetic acid (5.724 g, 32.13 mmol) and 4-aminopyridine (2.005 g, 21.31 mmol) were dissolved in 100 mL of $CHCl_3$. Then N,N'-dicyclohexylcarbodiimide (DCC) (6.590 g, 31.94) was added in consecutive small aliquots. During the addition, a white precipitate was formed. The solution was stirred for one hour at room temperature and then refluxed for four hours. After cooling down to room temperature, the solution was filtered, and the filtrate concentrated under vacuum. The resulting crude yellow oil was purified by column chromatography on silica gel using AcOEt to AcOEt/MeOH 9:1, monitoring the process by TLC till obtaining the pure product, which was a pale-yellow oil. Yield: 16% (860 mg).

$^1$H NMR ($CDCl_3$, ppm): 3.37 (s, 3H, -$CH_3$), 3.58-3.78 (m, 8H, $CH_3$-O-$CH_2$-$CH_2$-O-$CH_2$-$CH_2$), 4.11 (s, 2H, CO-$CH_2$), 7.59 (d, J = 6.0 Hz, 2H, $N_{py}$-CH-CH), 8.51 (d, J = 6.0 Hz, 2H, $N_{py}$-CH), 8.99 (br. s, 1H, N-H). IR (KBr, $cm^{-1}$): ν(N-H): 3079, ν(C=O): 1703, ν(C=N): 1594. ESI-MS (+) m/z: 255.1647 ($[M + H]^+$, calc: 255.1339).

**Synthesis of [AuCl(pyPEG)] (8.2)**

[AuCl(tht)] (0.1999 g, 0.6228 mmol) was dissolved in $CH_2Cl_2$ (5 mL) in a purged Schlenk protected with aluminium foil. pyPEG (0.1558 g, 0.6131 mmol) was dissolved in $CH_2Cl_2$ (5 mL). The pyPEG solution was added dropwise to the [AuCl(tht)] solution under stirring, resulting in a white suspension. After 1 h of stirring, the reaction mixture was concentrated in vacuum to half volume and hexane (5 mL) was then added in order to favour precipitation. The resulting white solid was filtered and dried under vacuum. Yield: 69% (128 mg).

$^1$H NMR ($CDCl_3$, ppm): 3.38 (s, 3H, -$CH_3$), 3.60-3.78 (m, 8H, $CH_3$-O-$CH_2$-$CH_2$-O-$CH_2$-$CH_2$), 4.15 (s, 2H, CO-$CH_2$), 7.89 (d, J = 6.0 Hz, 2H, $N_{py}$-CH-CH), 8.40 (d, J = 6.0 Hz, 2H, $N_{py}$-CH), 9.53 (br. s, 1H, N-H). IR (KBr, $cm^{-1}$): ν(N-H): 3452, ν(C=O): 1714, ν(C=N): 1622.

**Synthesis of [Au(4-ethynylaniline)(pyPEG)] (8.3)**

4-ethynylaniline (0.0148 g, 0.1263 mmol) was reacted with KOH (0.0196 g, 0.3493 mmol) in MeOH (5 mL) under $N_2$ atmosphere. [AuCl(pyPEG)] (0.0596 g, 0.1225 mmol) was dissolved in $CH_2Cl_2$ (5 mL) and this solution was added dropwise to the previous one, leading to the formation of a reddish brown solid. After 1 h of stirring, the reaction mixture was concentrated under vacuum to half volume and hexane (5 mL) was then added in order to favour precipitation. The resulting reddish solid was filtered and dried under vacuum. Yield: 59% (41 mg).

$^1$H NMR (acn-$d_3$, ppm): 3.30 (s, 3H, -$CH_3$), 3.48-3.75 (m, 8H, $CH_3$-O-$CH_2$-$CH_2$-O-$CH_2$-$CH_2$), 4.05 (s, 2H, CO-$CH_2$), 4.07 (s, 2H, -$NH_2$), 6.49 (d, J = 8.2 Hz, 2H, $H_\alpha$), 7.00 (d, J = 8.2 Hz, 2H, $H_\beta$), 7.61 (d, J = 6.0 Hz, 2H, $N_{py}$-CH-CH), 8.45 (d, J = 6.0 Hz, 2H, $N_{py}$-CH), 9.03 (br. s, 1H, N-H). IR (KBr, cm$^{-1}$): ν(N-H): 3436, ν(C≡C): 1996, ν(C=O): 1715, ν(C=N): 1619. ESI-MS (+) m/z: 568.1496 ([M + H]$^+$, calc: 568.1505).

**Synthesis of [Au(7-propargylcoumarin)(pyPEG)] (8.4)**

7-propargylcoumarin (0.0184 g, 0.0919 mmol) was treated with KOH (0.0112 g, 0.1996 mmol) in MeOH (5 mL) under $N_2$ atmosphere. [AuCl(pyPEG)] (0.0447 g, 0.0918 mmol) was dissolved in $CH_2Cl_2$ (5 mL) and this solution was added dropwise to the previous, leading to the formation of an ochre solid. After 1 h of stirring, the reaction mixture was concentrated under vacuum to half volume and hexane (5 mL) was then added in order to favour precipitation. The resulting pale brown solid was filtered and dried under vacuum. Yield: 63% (31 mg).

$^1$H NMR (DMSO-$d_6$, ppm): 3.24 (s, 3H, -$CH_3$), 3.42-3.68 (m, 8H, $CH_3$-O-$CH_2$-$CH_2$-O-$CH_2$-$CH_2$), 4.13 (s, 2H, -$NH_2$), 4.81 (s, 2H, C≡C-$CH_2$), 6.29 (d, J = 9.5 Hz, 1H, O-CO-CH), 7.00-6.94 (m, 2H, $CH_2$-O-C-CH), 7.61 (d, J = 8.5 Hz, 1H, O-CO-CH-CH-C-CH), 7.64 (d, J = 6.0 Hz, 2H, $N_{py}$-CH-CH), 7.99 (d, J = 9.5 Hz, O-CO-CH-CH), 8.44 (d, J = 6.0 Hz, 2H, $N_{py}$-CH), 10.03 (br. s, 1H, N-H). IR (KBr, cm$^{-1}$): ν(N-H): 3436, ν(C≡C): 2135, ν(C=O): 1720, ν(C=N): 1612. ESI-MS (+) m/z: 651.1409 ([M + H]$^+$, calc: 651.1400).

## 8.5. References


1. De Loos, M., Feringa, B. L. and Van Esch, J. H. European J. Org. Chem. **2005**, 17, 3615–3631.

2. McCullagh, M., Prytkova, T., Tonzani, S., Winter, N. D. and Schatz, G. C. J. Phys. Chem. B **2008**, 112, 10388–10398.

3. Zhuang, X., Mai, Y., Wu, D., Zhang, F. and Feng, X. Adv. Mater. **2015**, 27, 403–427.

4. Lehn, J. M. Chem. Soc. Rev. **2007**, 36, 151–160.

5. Yan, X., Wang, F., Zheng, B. and Huang, F. Chem. Soc. Rev. **2012**, 41, 6042–6065.

6. Wang, J., Huang, Z., Ma, X. and Tian, H. Angew. Chem. Int. Ed. **2020**, 59, 9928–9933.

7. Oshovsky, G. V., Reinhoudt, D. N. and Verboom, W. Angew. Chem. Int. Ed. **2007**, 46, 2366–2393.

8. Levin, A., Hakala, T. A., Schnaider, L., Bernardes, G. J. L., Gazit, E. and Knowles, T. P. J. Nat. Rev. Chem. **2020**, 4, 615–634.

9. Mayoral Muñoz, M. J. and Fernández, G. Chem. Sci. **2012**, 3, 1395–1398.

10. Kemper, B., Hristova, Y. R., Tacke, S., Stegemann, L, van Bezouwen, L . S., Stuart, M. C. A., Klingauf, J., Strassert, C. A. and Besenius, P. Chem. Commun. **2015**, 51, 5253–5256.

11. Schmidbaur, H. and Schier, A. Chem. Soc. Rev. **2012**, 41, 370–412.

12. Lima, J. C. and Rodríguez, L. Chem. Soc. Rev. **2011**, 40, 5442–5456.

13. Pinto, A., Svahn, N., Lima, J. C. and Rodríguez, L. Dalton Trans. **2017**, 46, 11125–11139.

14. Aguiló, E., Gavara, R., Lima, J. C., Llorca, J. and Rodríguez, L. J. Mater. Chem. C **2013**, 1, 5538–5547.

15. Aguiló, E., Gavara, Baucells, C., Guitart, M., Lima, J. C., Llorca, J. and Rodríguez, L. Dalton Trans. **2016**, 45, 7328–7339.

16. Gavara, R., Aguiló, E., Schur, J., Llorca, J., Ott, I and Rodríguez, L. Inorg. Chim. Acta **2016**, 446, 189–197.

17. Schroeter, F., Soellner, J. and Strassner, T. Organometallics **2018**, 37, 4267–4275.

18. Aliprandi, A., Mauro, M. and De Cola, L. Nat. Chem. **2016**, 8, 10–15.

19. Carrara, S., Aliprandi, A., Hogan, C. F. and De Cola, L. J. Am. Chem. Soc. **2017**, 139, 14605–14610.

20. Fernández, E. J., Laguna, A., López de Luzuriaga, J. M., Monge, M., Montiel, M., Olmos, M. E., Pérez, J. and Rodríguez-Castillo, M. Gold Bull. **2017**, 40, 172–183.

21. González, J. J., Ortega, E., Rothemund, M., Gold, M., Vicente, C., de Haro, C., Bautista, D., Schobert, R. and Ruiz, J. Inorg. Chem. **2019**, 58, 12954–12963.

22. Fulong, C. R. P., Kim, S., Friedman, A. E. and Cook, T. R. Front. Chem. **2019**, 7, 1–13.

23. Cargnelutti, R., da Silva, F. D., Cervo, R., Schumacher, R. F. and Lang, E. S. Inorg. Chem. Commun. **2017**, 81, 51–54.

24. Chao, H. Y., Lu, W., Li, Y., Chan, M. C. W., Che, C. M., Cheung, K. K. and Zhu, N. J. Am. Chem. Soc. **2002**, 124, 14696–14706.

25. Chakraborty, S., Bhattacharjee, D. and Hussain, S. A. J. Lumin. **2014**, 145, 824–831.

26. Aguiló, E., Moro, A. J., Gavara, R., Alfonso, I., Pérez, Y., Zaccaria, F., Guerra, C. F., Malfois, M., Baucells, C., Ferrer, M., Lima, J. C. and Rodríguez, L. Inorg. Chem. **2018**, 57, 1017–1028.

27. Gavara, R., Llorca, J., Lima, J. C. and Rodríguez, L. Chem. Commun. **2013**, 49, 72–74.

28. Kilpin, K. J., Horvath, R., Jameson, G. B., Telfer, S. G., Gordon, K. C. and Crowley, J. D. Organometallics **2010**, 29, 6186–6195.

29. Arcau, J., Andermark, V., Aguiló, E., Gandioso, A., Moro, A., Cetina, M., Lima, J. C., Rissanen, K., Ott, I. and Rodríguez, L. Dalton Trans. **2014**, 43, 4426–4436.

30. Huang, T. C., Toraya, H., Blanton, T. N. and Wu, Y. J. Appl. Crystallogr. **1993**, 26, 180–184.

31. Kieffer, J. and Karkoulis, D. J. Phys. Conf. Ser. **2013**, 425.

32. Konarev, P. V., Volkov, V. V., Sokolova, A. V., Koch, M. H. J. and Svergun, D. J. Appl. Crystallogr. **2003**, 36, 1277–1282.

33. Svergun, D. I. J. Appl. Crystallogr. **1992**, 25, 495–503.

34. Svergun, D. Biophys. J. **1999**, 76, 2879–2886.

# CHAPTER 9

## AIE Gold(I) tetraphenylethene complexes

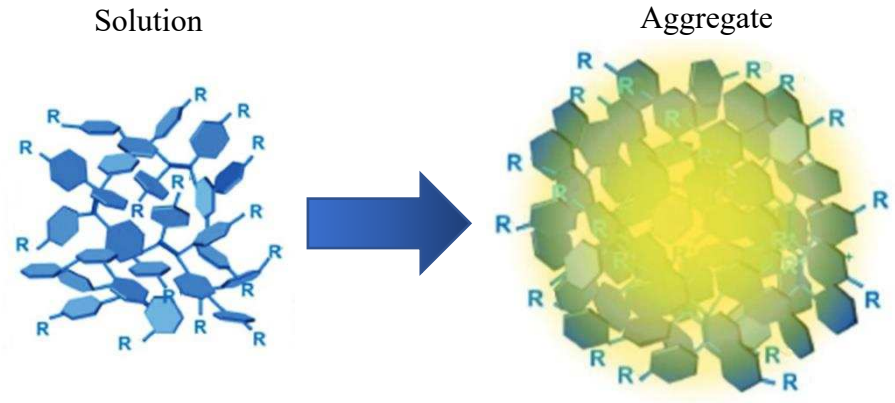


Unpublished work.

# 9. AIE GOLD(I) TETRAPHENYLETHENE COMPLEXES

## 9.1. Introduction

Traditional fluorophores with planar and strong intermolecular interactions frequently show bright emission in the monomeric state but weakened or even quenched emission in the aggregated state. On the contrary, an unusual behaviour was found for some organic molecules, in which the intensity of emission was enhanced in aggregated conditions. This is known as aggregation induced emission (AIE), and the exposure of this concept significantly changes the perception towards conventionally photophysical phenomena.[1] Due to the resulting high quantum yields and tunable emission properties, the molecules that present AIE properties have become promising candidates as biosensors, opto-electronic and energy applications among others.[2]

AIE systems were discovered by the Tang group in 2001,[3] where it was observed that propeller shaped molecules present enhanced emission in solution, in solvent mixtures, having one solvent considered as "good solvent" where the molecules are perfectly dissolved and another solvent considered as "bad solvent" that induces aggregation. AIE behaviour has been commonly observed using water as bad solvent and at high water contents. In diluted solutions, the free rotation of the common aromatic rings of organic chromophores leads to non-radiative deactivation pathways.[4] This can be suppressed when the intramolecular rotation is restricted, promoting the radiation decays, which enhances the resulting luminescence. This restriction of intramolecular motion mechanism is proposed to explain the AIE phenomenon.[5] In this way, the modifications in the stacking of the molecules can produce significant changes in the resulting emission wavelength and efficiency.

Small molecules such as hexaphenylthiazole (HPS), 2,5-bis(4-alkoxycarbonylphenyl)-1,4-diaryl-1,4-dihydropyrrolo[3,2-b]pyrrole (AAPP) or tetraphenylethene (TPE) have been widely used as AIE chromophores. In particular, TPE core represents one of the most common sources for the synthesis of compounds displaying AIE. This is in part due to the π-twist of the central C=C bond and the development of simple strategies for its functionalization.[6–9] The enhancement of the photoluminescence properties of TPE derivatives (both in the solid state, or in the aggregated form), may be significantly

different depending on the system, since the restriction of intramolecular motion represents an active dissipation factor for the non-radiative deactivation. This was previously observed in comparison with different TPE derivatives functionalized with different side chains, where the compounds containing the longest side chains displays the highest photoluminescence properties.[10]

Most of the AIE active molecules reported in the literature are based on organic molecules, while this phenomenon has been less explored for metal complexes. Apart from their well-known luminescent properties associated to the metal centres, $d^6$, $d^8$ and $d^{10}$ complexes can become triplet emitters and display strong phosphorescence emission, but they are not commonly explored regarding their possibility to aggregate. Among these metals, gold(I) can also establish aurophillic interactions that can contributed on the restriction of the intramolecular motion and promote the AIE effect.[11]

Taking this into consideration, in this chapter we have designed gold(I) complexes containing the TPE core in order to analyse the resulting AIE behaviour. The effect of the steric hindrance at the second coordination position of the gold(I) has been studied by the incorporation of different types of phosphanes suitable to promote the aggregation (Figure 1). The changes on the resulting luminescence induced by the aggregation process have been explored.

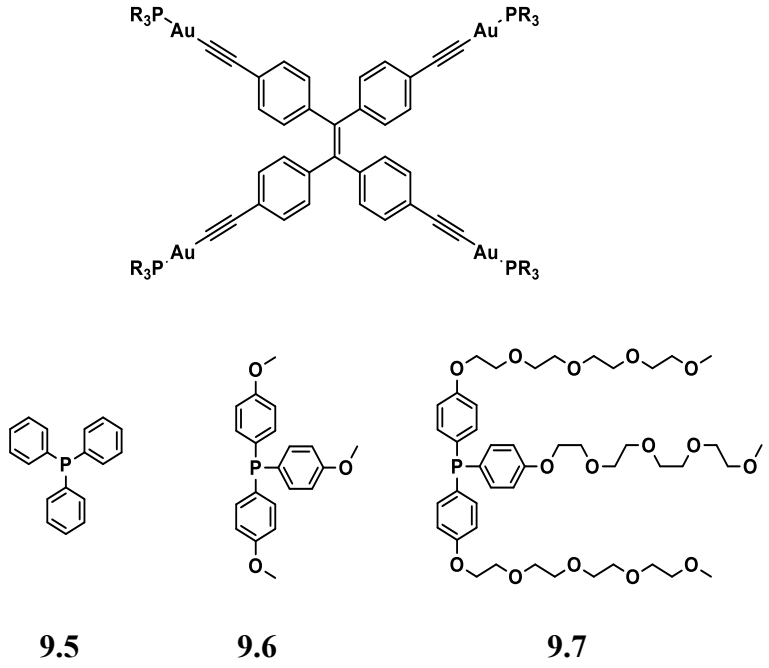


**Figure 9.1.** TPE gold(I) derivatives synthesized in this work.

## 9.2. Results and Discussion

### 9.2.1. Synthesis and Characterization

Three tetranuclear gold(I) compounds containing 1,1,2,2-tetrakis(4-ethynylphenyl)ethene (**TEPE**) chromophore and three different phosphanes ($PPh_3$ for compound **9.5**, $P(PhOMe)_3$ for compound **9.6** and $P(PhGlycol)_3$ for compound **9.7**) at the second coordination position were synthesized following the procedures described in Schemes 9.1-4. Initially, the ligand **TBPE** was obtained following a previously reported procedure[12] by the bromination reaction between tetraphenylethilene (TPE) and $Br_2$. Then, it was made react with ethynyl-(trimethyl)silane via a Sonogashira coupling with subsequent removal of the TMS-protecting group with potassium hydroxide, giving the **TEPE** ligand in a moderate yield (Scheme 9.1). $^1H$ NMR and IR spectroscopies and mass spectrometry verified the correct formation of the product by the presence of the terminal alkynyl proton at 3.09 ppm and the detection of the $[M+H^+]^+$ molecular peak at 429.17.

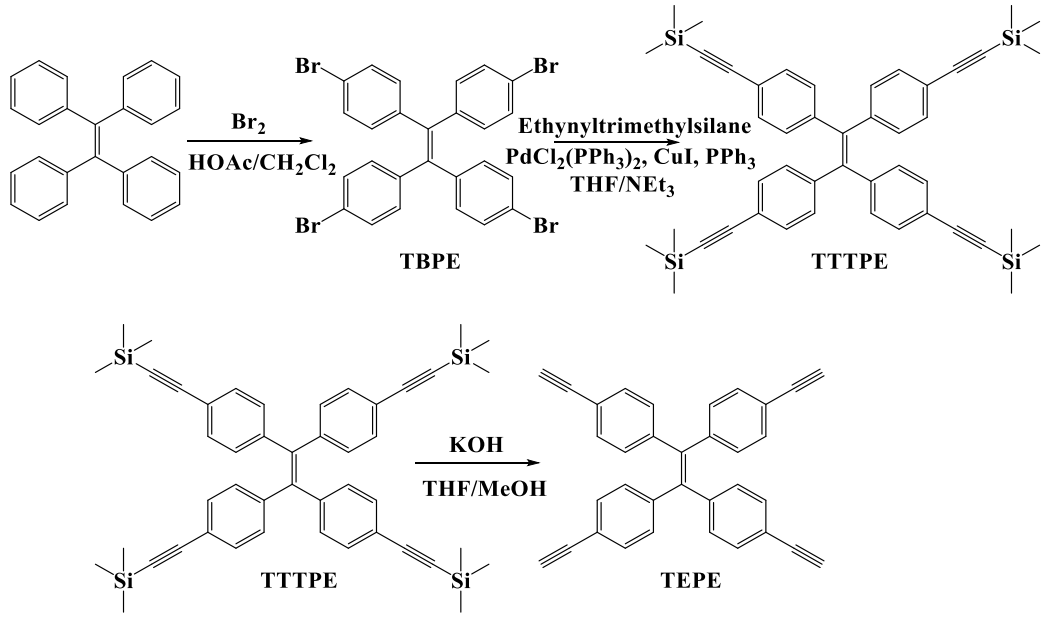


**Scheme 9.1.** Synthetic route for the synthesis of the **TEPE** ligand.

In order to promote the aggregation, we decided to coordinate as a secondary position of the gold(I) atom different kind of triphenylphosphanes bearing at the 4 position: 1) a hydrogen, 2) a methoxy group and 3) a neutral tetraethylene glycol. For the preparation of the gold(I) complex containing the phospane with tetraethylene glycol group (Scheme 9.2), tris(4-methoxyphenyl)phosphane was firstly reacted with [AuCl(tht)]. Then, the aromatic methyl ethers of **9.1** were deprotonated with $BBr_3$ followed by hydrolysis to give the phenolic gold(I) phosphane complex **9.2** in good yields. Finally, the

etherification with tetraethylene glycol monomethyl ether tosylate leds to the water-soluble gold(I) phosphane **9.3**. $^{1}H$ and $^{31}P$ NMR and IR spectroscopies together with mass spectrometry analysis verified the correct formation of the product by comparison with the reported data.[13]

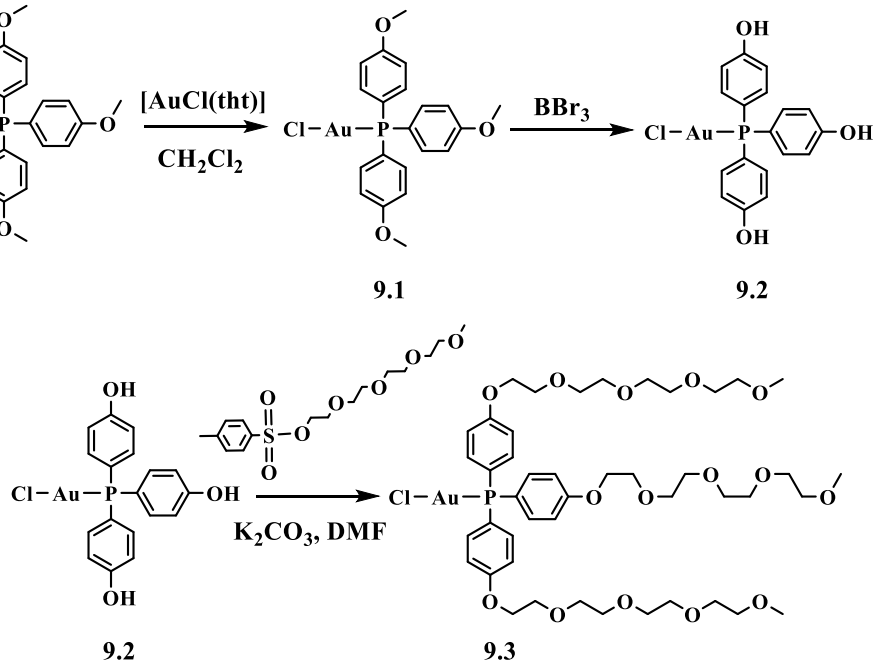


**Scheme 9.2.** Synthetic route for the preparation of **9.3**.

The reaction of **TEPE** with [AuCl(tht)] (tht = tetrahydrothiophene) in a 1:4 ratio and in the presence of sodium acetate as a base gave rise to the formation of the insoluble polymer **9.4**. The successful formation of the polymer was evidenced by the disappearance of C≡C-H vibration of the terminal alkynyl proton of **TEPE** in the corresponding IR spectra. Next, the reaction of triphenylphosphane ($PPh_3$) or tris(4-methoxyphenyl)phosphane ($P(PhOMe)_3$) allowed the formation of the desired products **9.5** and **9.6**, respectively, in good yields (Scheme 9.3).

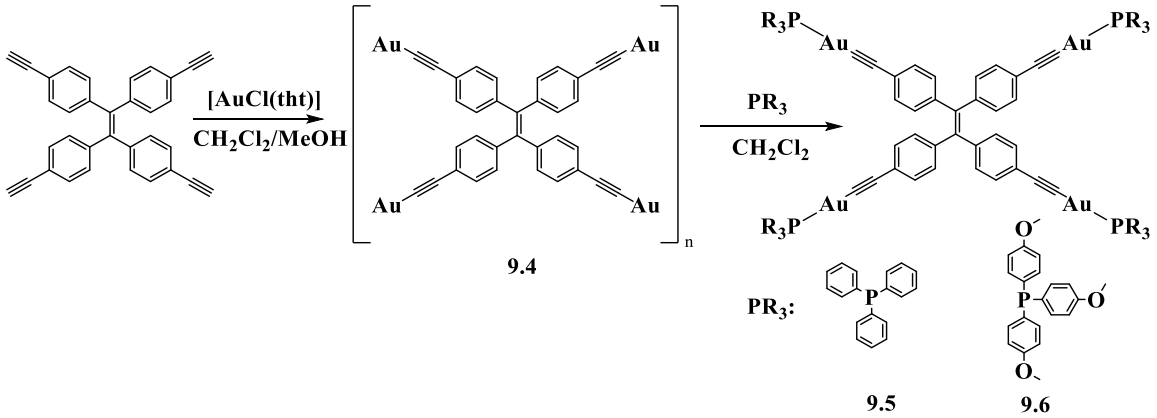


**Scheme 9.3.** Synthetic route for gold(I) complex **9.5** and **9.6**.

An alternative method was used to synthesize the gold(I) complex **9.7** where it was necessary to deprotonate firstly the terminal alkynyl protons of the **TEPE** chromophore and then making it react with the previously synthesized gold(I) chloride precursor **9.3** in a 1:4 stoichiometry (see Scheme 9.4).

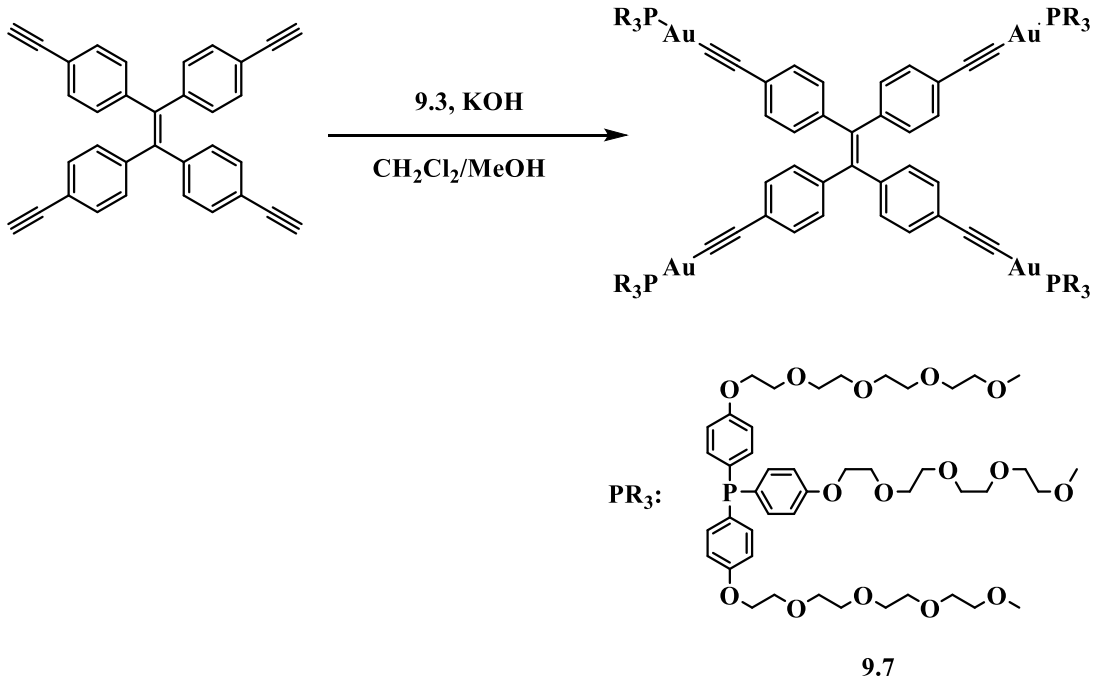


**Scheme 9.4.** Synthesis of the gold(I) complex **9.7**.

All complexes were obtained as yellow solids that are stable to the air and moisture in moderate yields (ca. 60%). Their spectroscopic data supports the proposed stoichiometry. $^{1}$H NMR spectra display the signals of both the chromophore, slightly upfield shifted due to the Au-$PR_3$ coordination, and those protons corresponding to the phosphane. Additionally, the terminal alkynyl proton at 3.09 ppm of the free ligand **TEPE** disappears providing a direct indication of the formation of the complex. $^{31}P\{^{1}H\}$ NMR spectra showed in all cases only one signal, which was ca. 50 ppm downfield shifted with respect to the free phosphane in the case of **9.5** and **9.6** and ca. 10 ppm downfield with respect to **9.3** for **9.7**, indicating the formation of only one product. The final evidence of the formation of the complexes was given by the recorded molecular peak by ESI(+) spectrometry at m/z 2261.3661 for **5** ($[M + H^+]^+$) and 1311.2441 for **6** ($[M + 2H^+]^{2+}$).

### 9.2.2. Photophysical characterization

Absorption and emission spectra of all complexes were recorded in dichloromethane at $10^{-5}$ M concentration and the results are summarized in Table 9.1.

**Table 9.1.** Absorption and emission data of gold(I) complexes **9.5-7** and the ligand precursor, **TEPE** in dichloromethane.

| **Compound** | Absorption $\lambda_{max}$ (nm) ($\varepsilon$ ($10^3$ $M^{-1}$ $cm^{-1}$)) | Emission $\lambda_{max}$ (nm) |
|---|---|---|
| **TEPE** | 274 (27.8), 347 (12.3) | 517 |
| **9.5** | 235 (120.6), 318 (70.8), 365 (34.4) | 547 |
| **9.6** | 247 (124), 318 (52.8), 365 (27.3) | 549 |
| **9.7** | 247 (126.7), 318 (54.6), 365 (29.1) | 542 |

All gold(I) complexes display three absorption bands centered at ca. 240 nm, 318 nm and 365 nm (Figure 9.1). The highest band is assigned to intraligand $\pi \rightarrow \pi^*$ transition where the phosphane is involved. The two lower absorption bands are also present in the **TEPE** precursor and are associated with different $\pi \rightarrow \pi^*$ transition of the **TEPE** where the gold(I) orbitals are involved and induces a red shift with respect to the free ligand.[14,15]

Emission spectra were recorded upon excitation of the samples at the lowest absorption band. The emission of the gold complexes is ca. 30 nm red shifted with respect to the free

**TEPE** ligand (Figure 9.2), and no significant changes were observed in the intensity of the emission when the oxygen was removed in the solution. This supports the assignment of a fluorescent intraligand $\pi \rightarrow \pi^*$ transition.

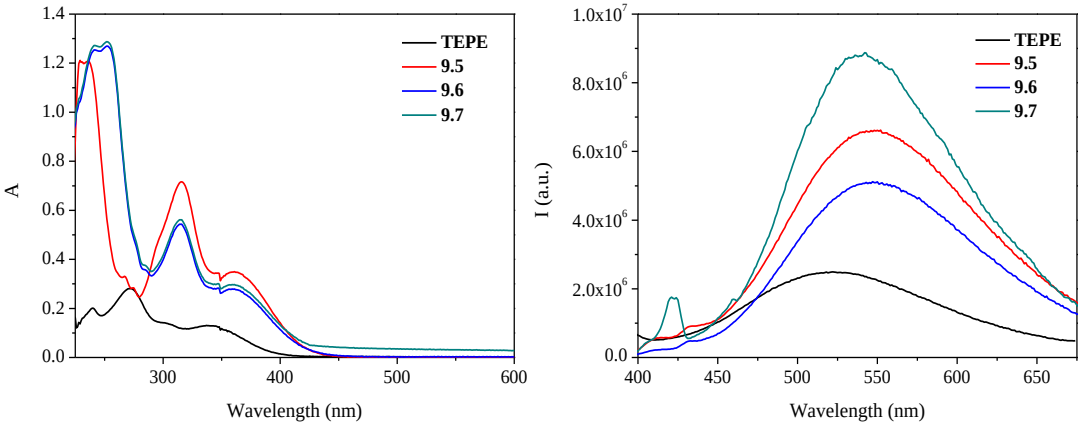


**Figure 9.2.** Absorption (left) and emission (right) spectra of **TEPE** and gold(I) complexes **9.5-7** at ca. $10^{-5}$ M.

The emission intensity of the gold(I) complexes is higher than the recorded for **TEPE** ligand with the following trend **9.7** > **9.5** > **9.6**, in agreement with the recorded fluorescent quantum yields, $\Phi_{fl}$ (Table 9.2). The emission decay times were in the order of a few nanoseconds, as expected for fluorescence emissions. The radiative and non-radiative rate constants were calculated from the fluorescence quantum yields and lifetimes. In general, the radiative rate constants do not seem to be significantly affected by the $AuPR_3$ coordination, while a decrease in the non-radiative rate constant was observed for the gold(I) complexes with respect to the **TEPE** organic counterpart, being the complex **9.7** (the one displaying highest emission intensity) the one with lower $k_{nr}$ value. This can be ascribed to the presence of bulky phophanes containing also specific groups that may be involved in additional aggregation processes (such as the glycol) and promoting the AIE behaviour. The lowest radiative constant of gold(I) complexes was calculated for **9.6** (that contains a methoxy group in the phosphane, $P(PhOMe)_3$)). This can be ascribed to the presence of this methoxy substituent that has been observed to strongly affect the radiative and non-radiative relaxation depending on the position and the number of the substituents.[16]

**Table 9.2.** Quantum yields ($\Phi_{fl}$), lifetime ($\tau_{fl}$), $k_r$ and $k_{nr}$ of **TEPE** and complexes **9.5-7** in dichloromethane.

| Compound | $\Phi_{fl}$ | $\tau_{fl}$ (ns) | $k_r$ ($ns^{-1}$) | $k_{nr}$ ($ns^{-1}$) |
|---|---|---|---|---|
| **TEPE** | 0.004 | 0.032 | 0.124 | 30.836 |
| **9.5** | 0.007 | 0.082 | 0.085 | 12.169 |
| **9.6** | 0.005 | 0.087 | 0.057 | 11.332 |
| **9.7** | 0.012 | 0.091 | 0.131 | 10.857 |

### 9.2.3. Aggregation induced emission (AIE) studies

As stated above, the twisted conformation between the aromatic rings of TEPE together with previous examples of TPE derivatives found in the literature[17–19] suggest the possibility of having aggregation induced emission (AIE) for the compounds under study. Absorption and emission spectra and quantum yields were measured in THF and in THF/water mixtures with increasing water contents in order to study the effect of the incorporation of a gold(I)-phosphane moiety in the AIE effect,. The obtained data is summarized in Table 9.3.

**Table 9.3.** Quantum yield of **TEPE** and gold(I) complexes **9.5-7** in THF and in THF/water mixtures with increasing water fractions.

| Compound | THF | 25% $H_2O$ | 50% $H_2O$ | 75% $H_2O$ | 90% $H_2O$ |
|---|---|---|---|---|---|
| **TEPE** | 0.008 | 0.01 | 0.05 | 0.13 | 0.504 |
| **9.5** | 0.017 | 0.029 | 0.034 | 0.241 | 0.239 |
| **9.6** | 0.014 | 0.020 | 0.023 | 0.150 | 0.148 |
| **9.7** | 0.013 | 0.030 | 0.040 | 0.278 | 0.285 |

A broadening of the absorption bands together with an increase of the baseline was observed for all compounds when the water contents increases, in agreement with aggregation process (Figure 9.3).[11] An increase of the emission is observed for the **TEPE** when the water fraction increases up to 90% and up to 75% for the gold(I) complexes **9.5-7**. This is supported by the quantum yields recorded in the different cases that significantly increase in the aggregated forms and are stabilized at the maximum value at these percentages of water in the solvent mixtures.

The presence of a bulky phosphane may help to block the intermolecular rotations, and, therefore the non-radiative pathways and this may be the reason for the stabilization of the maximum quantum yield values at lower water contents with respect to the **TEPE**. Nevertheless, the recorded quantum yield values of the gold complexes are lower than the recorded for the organic counterpart probably due to the ISC competitive process due to the presence of a heavy atom.

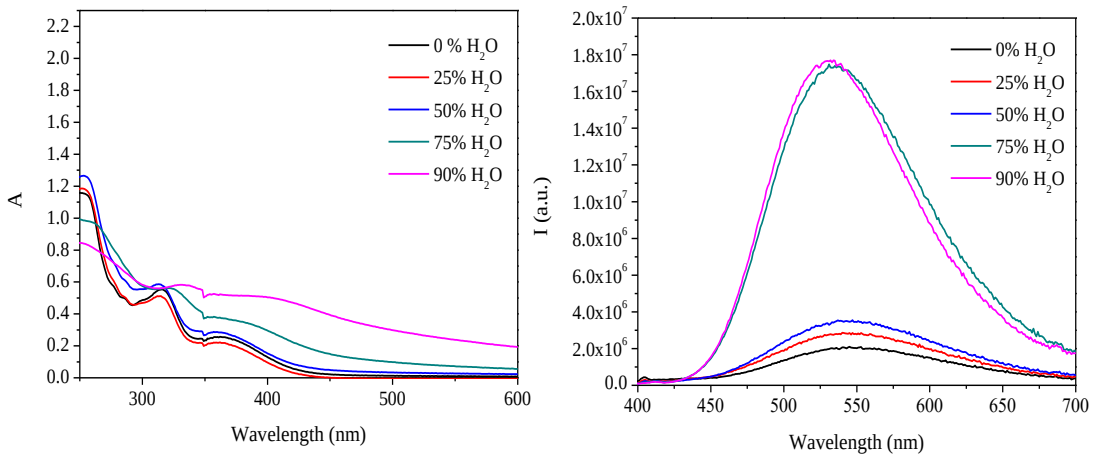


**Figure 9.3.** Emission spectra of **9.6** in THF and in THF/water mixtures with different water contents.

## 9.3. Conclusions

A series of gold(I) complexes containing the tetraphenylethene **TEPE** chromophore and three different types of phosphanes located at the second coordination position have shown AIE behaviour thanks to the presence of the $AuPR_3$ moieties that affect the resulting photophysical properties.

The incorporation of the gold(I)-phosphane groups reduces the possibility of having intermolecular rotations in the aggregates formed by the addition of water and the presence of gold(I) atom favors a faster aggregation in comparison with the **TEPE** behaviour. Additionally, the presence of the heavy atom promotes, as expected, the intersystem crossing.

## 9.4. Experimental Section

### 9.4.1. General procedures

All manipulations have been performed under prepurified $N_2$ using standard Schlenk techniques. All solvents have been distilled from appropriated drying agents. Commercial reagents 1,1,2,2-tetraphenylethylene, bromine, ethynyltrimethylsilane, copper iodine, triphenylphosphane, tris(4-methoxyphenyl)phosphane, boron tribromide, tetraethyleneglycol monoethyl ether tosylate were purchased from sigma Aldrich, and potassium carbonate and sodium acetate were purchased from Panreac. Literature methods have been used to prepare tetra(p-bromophenyl)ethane (TBPE),[12] **8.3**.[13]

### 9.4.2. Physical measurements

Infrared spectra have been recorded on a FT-IR 520 Nicolet Spectrophotometer. $^{1}H$ NMR ($\delta$(TMS) = 0.0 ppm), $^{31}P\{^{1}H\}$ NMR ($\delta$(85% $H_3PO_4$) = 0.0 ppm) spectra have been obtained on a Varian Mercury 400 and Bruker 400 (Universitat de Barcelona). ElectroSpray-Mass spectra (+) has been recorded on a Fisons VG Quatro spectrometer (Universitat de Barcelona). Absorption spectra have been recorded on a Varian Cary 100 Bio UV- spectrophotometer and emission spectra on a Horiba-Jobin-Yvon SPEX Nanolog spectrofluorimeter (Universitat de Barcelona). Luminescent quantum yields were recorded using an Absolute PL quantum yield spectrometer from Hamamatsu Photonics upon excitation the samples at 400 nm. Fluorescence lifetimes were measured via the time-correlated single-photon counting technique (TCSPC) using DeltaPro fluorescence lifetime System from Horiba upon excitation of the sample with a 390 nm nanoLED.

### 9.4.3. Synthesis and Characterization

**Synthesis of 1,1,2,2-tetrakis(4-((trimethylsilyl)phenyl)ethene (TTTPE)**

1,1,2,2-tetrakis(4-bromophenyl)ethane (0.5 g, 0.77 mmol), $PdCl_2(PPh_3)_2$ (0.054 g, 0.077 mmol) and triphenylphosphane (0.010 g, 0.038 mmol) were dissolved in a mixture of THF and triethylamine (4:1) (5 mL) under nitrogen. The solution was heated to 40 ºC for 2h, and CuI (0.01469 g, 0.077 mmol) was then added for 15 min. Trimethylsilylacetylene ( 0.66 mL, 4.63 mmol) was added and the reaction was heated to 60 ºC for 24h. Then, the temperature was increased to 85 ºC during 4h. The mixture was cooled to room temperature and evaporated to dryness. The crude product was purified by silica gel column chromatography using hexane/dichloromethane mixture (10:1) as eluent. A white solid was obtained. Yield: 70 % (386 mg).

$^1$H NMR ($CDCl_3$, ppm): 0.23 (s, 36H), 6.88 (d, J = 8.1 Hz, 8H), 7.19 (d, J = 8.1 Hz, 8H).

**Synthesis of 1,1,2,2-tetrakis(4-ethynylphenyl)ethene (TEPE)**

1,1,2,2-tetrakis(4-((trimethylsilyl)phenyl)ethene (0.2262 g, 0.32 mmol) was dissolved in THF (10 mL) into a 100 mL round-bottom flask. 10 mL methanol solution of KOH (0.059 g, 8.5 mmol) was then added. The mixture was stirred at room temperature overnight. After most of the solvent was evaporated, 20 mL of 1 M aqueous HCl solution was added and the mixture was extracted with dichloromethane three times. The organic layer was combined and washed with water, brine and then dried over sodium sulfate. After filtration and solvent evaporation, the crude product was purified by a silica gel columm chromatography using hexane/dichloromethane (8:1) mixture as eluent. TEPE was obtained as a pale yellow solid. Yield: 60 % (82 mg).

$^1$H NMR ($CDCl_3$, ppm): 3.09 (s, 4H), 6.97 (d, J = 7.9 Hz, 8H), 7.28 (d, J = 7.9 Hz, 8H). IR (KBr, $cm^{-1}$): ν(C≡C): 2156. ESI (+) m/z: 429.17 ($[M+H]^+$, calc: 429.15).

**Synthesis of $[Au_4(TEPE)]_n$ (9.4)**

Sodium acetate (0.0268 g, 0.32 mmol) and [AuCl(tht)] (0.059 g, 0.18 mmol) were added to a stirring solution of **TEPE** (0.0212 g, 0.046 mmol) in $CH_2Cl_2$/MeOH (1:1) (10 mL) under $N_2$ atmosphere at room temperature. After stirring for 30 min the resulting orange suspension was filtered, washed with $CH_2Cl_2$/MeOH (1:1) (3 x 5 mL), and dried under vacuum. Yield 80% (45 mg). IR (KBr, $cm^{-1}$): ν(C≡C): 1990.

**Synthesis of [(AuPPh$_3$)$_4$(TEPE)] (9.5)**

Solid $PPh_3$ (0.022, 0.083 mmol) was added to a stirring suspension of **9.4** (0.025 g, 0.02 mmol) in dichloromethane (10 mL) under $N_2$ atmosphere at room temperature. After stirring 1h the resulting yellow solution was concentrated to half volume and hexane (10 mL) was then added in order to favour precipitation. The resulting yellow solid was filtered and dried under vacuum. Yield 75% (34 mg).

$^{31}P\{^1H\}$ NMR ($CDCl_3$, ppm): 42.3. $^1H$ NMR ($CDCl_3$, ppm): 6.87 (d, J = 8 Hz, 8H, **TEPE**), 7.21 (d, J = 8 Hz, 8H, **TEPE**), 7.47 (m, 60H, $PPh_3$). IR (KBr, $cm^{-1}$): ν(C≡C): 2110. ESI-MS (+) m/z: 2261.3661 ($[M + H]^+$, calc: 2261.3593).

**Synthesis of [(AuPPhOMe$_3$)$_4$(TEPE)] (9.6)**

Complex **9.6** was synthesized following the same procedure than complex **9.5** but using tris(4-methoxyphenyl)phosphane (0.021 g, 0.059 mmol) instead of $PPh_3$. Yield 60% (24 mg).

$^{31}P\{^1H\}$ NMR ($CDCl_3$, ppm): 38.6. $^1H$ NMR ($CDCl_3$, ppm): 3.75 (s, 36H, OMe (phosphane)), 6.86 (d, J = 8 Hz, 8H, **TEPE**), 7.14 (d, J = 8 Hz, 8H, **TEPE**), 7.35 (m, 48H, PPh (phosphane). IR (KBr, $cm^{-1}$): ν(C≡C): 2117. ESI-MS (+) m/z: 1311.2441 ($[M + 2H]^{2+}$, calc: 1311.2486).

**Synthesis of [(AuPPhglycol$_3$)$_4$(TEPE)] (9.7)**

KOH (0.020g, 0.36 mmol) was added to a solution of **TEPE** (0.026, 0.06 mmol) in methanol (15 mL). After 30 min of stirring, a solution of **9.3** (0.273 g, 0.24 mmol) in dichloromethane (15 mL) was added. The solution was concentrated to ca. 15 mL after 24 hours of stirring at room temperature, and ether was added to precipitate a yellow solid. The product was isolated by filtration and dried under vacuum. Yield 30% (85 mg).

$^{31}P\{^1H\}$ NMR ($CDCl_3$, ppm): 38.6. $^1H$ NMR ($CDCl_3$, ppm):3.31 (s, 36H, glycol), 3.46-3.48 (m, 24H, glycol), 3.56-3.61 (m, 96H, glycol), 3.64-3.66 (m, 24H, glycol), 3.77-3.80 (m, 24H, glycol), 4.05-4.09 (m, 24H, glycol), 6.77 (d, J = 8 Hz, 8H, **TEPE**), 6.87 (d, J = , .6.87 (d, J = 7.6 Hz, 24H, PPh), 7.12 (d, J = 8 Hz, 8H, **TEPE**), 7.34 (ddd, J = 20.6 Hz, J = 8.6 Hz, J = 1.72 Hz, 24H, PPh). IR (KBr, $cm^{-1}$): ν(C≡C): 2117.

## 9.5. References


1. Li, Q. and Li, Z. Adv. Sci. **2017**, 4, 1–15.

2. Suman, G. R., Pandey, M. and Chakravarthy, A. S. J. Mater. Chem. Front. **2021**, 5, 1541–1584.

3. Luo, J., Xie, Z., Lam, J. W. Y., Cheng, L., Chen, H., Qiu, C., Kwok, H. S., Zhan, X., Liu, Y., Zhu, D. and Tang, B. Z. Chem. Commun. **2001**, 18, 1740–1741.

4. Mei, J., Hong, Y., Lam, J. W. Y., Qin, A., Tang, Y. and Tang, B. Z. Adv. Mater. **2014**, 26, 5429–5479.

5. Yuan, W. Z., Tan, Y., Gong, Y., Lu, P., Lam, J. W. Y., Shen, X. Y. Feng, C., Sung, H. H. Y., Lu, Y., Williams, I. D., Sun, J. Z. Zhang, Y. and Tang, B. Z. Adv. Mater. **2013**, 25, 2837–2843.

6. Tanaka, Y., Machida, T., Noumi, T., Sada, K. and Kokado, K. Org. Chem. Front. **2020**, 7, 2649–2656.

7. Zhou, J., Chang, Z., Jiang, Y., He, B., Du, M., Lu, P., Hong, Y., Kwok, H. S., Qin, A., Qiu, H., Zhao, Z. and Tang, B. Z. Chem. Commun. **2013**, 49, 2491–2493.

8. Wang, J., Mei, J., Hu, R., Sun, J. Z., Qin, A. and Tang, B. Z. J. Am. Chem. Soc. **2012**, 134, 9956–9966.

9. Rodrigues, A. C. B., Geisler, I. S., Klein, P., Pina, J., Neuhaus, F. J. H., Dreher, E., Lehmann, C. W., Scherf, U. and Seixas de Melo, J. S. J. Mater. Chem. C **2020**, 8, 2248–2257.

10. Rodrigues, A. C. B. and Seixas de Melo, J. S. Top. Curr. Chem. **2021**, 379, 15–53.

11. Pinto, A., Svahn, N., Lima, J. C. and Rodríguez, L. Dalton Trans. **2017**, 46, 11125–11139.

12. Wang, H., Li, B., Wu, H., Hu, T. L., Yao, Z., Zhou, W., Xiang, S. and Chen, B. J. Am. Chem. Soc. **2015**, 137, 9963–9970.

13. Kemper, B., von Gröning, M., Lewe, V., Spitzer, D., Otremba, T., Stergiou, N., Schollmeyer, D., Schmitt, E., Ravoo, B. J. and Besenius, P.. Chem. - A Eur. J. **2017**, 23, 6048–6055.

14. Xie, Y., Tu, J., Zhang, T., Wang, J., Xie, Z., Chi, Z., Peng, Q. and Li, Z. Chem. Commun. **2017**, 53, 11330–11333.

15. Chao, H. Y., Lu, W., Li, Y., Chan, M. C. W., Che, C. M., Cheung, K. K., Zhu, N. J. Am. Chem. Soc. **2002**, 124, 14696–14706.

16. Ghosh, I., Mukhopadhyay, A., Koner, A. L., Samanta, S., Nau, W. M. and Moorhy, J. N. Phys. Chem. Chem. Phys. **2014**, 16, 16436–16445.

17. Chen, X., Shen, X. Y., Guan, E., Liu, Y., Qin, A., Sun, J. Z. and Tang, B. Z. Chem. Commun. **2013**, 49, 1503–1505.

18. Jiang, G., Zeng, G., Zhu, W., Li, Y., Dong, X., Zhang, G., Fan, X., Wang, J., Wu, Y. and Tang, B. Z. Chem. Commun. **2017**, 53, 4505–4508.

19. Feng, H. T., Yuan, Y. X., Xiong, J. Bin, Zheng, Y. S. and Tang, B. Z. Chem. Soc. Rev. **2018**, 47, 7452–7476.

# CHAPTER 10

## General Conclusions

# 10. GENERAL CONCLUSIONS

In this PhD Thesis, we have successfully synthesized different series of unprecedented gold(I) complexes bearing a chromophore coordinated to the metal atom through an alkynyl moiety and different phosphanes or carbenes at the second coordination position. We have studied the luminescent properties of all the synthesized gold(I) complexes and it was compared to the emission of the parent ligands in order to analyse the effect of the coordination of a heavy atom in the emission of the chromophore. We have also investigated the applications in different research areas that include supramolecular chemistry, biology, and materials science. The luminescent properties have been also tried to be modified by applying different external stimulus.

The following conclusions are derived from the different chapters presented in this Thesis:

- In Chapter 2, the formation of aggregates induces an enhancement of the emission where Au···Au interactions play an important role in the resulting photophysical properties (mainly emission wavelength). The addition of a second metal salt and the different coordination modes affect the capacity to tune the emission colour in the solid state.
- In Chapter 3, host-guest studies were performed between a gold(I) calix[4]pyrrole derivative and tetraalkylammonium chloride salts. The receptor operates as heteroditopic or homotopic in dichloromethane and acetone solution respectively. Both receptors (ligand and gold(I) complex) bind stronger MTOACl compared to TBACl.
- In Chapter 4, an in depth photophysical characterization was performed of three different families of gold(I) derivatives containing coumarin ligands. The experimental and theoretical data shows that the emission is mainly attributed to the ligand but triplet states were also populated at room temperature in the gold(I) complexes. The compound were also able to sensitize singlet oxygen with moderate yields.

- In Chapter 5, two different types of ligands located at the second coordination position in gold(I) BTD derivatives were synthesized. The introduction of a carbene with an extended π-system allowed the possibility of having Au(I)···Au(I) contacts with mechanochromic effect. The incorporation of the compounds in polymer matrixes enhanced the emissive properties with a near unity quantum yields.
- In Chapter 6, hybrid materials were obtained by the establishment of aurophilic interactions between a gold(I) organometallic complex and gold nanoparticles. The resulting hybrid systems were characterized by SEM, DLS and SAXS techniques. The biological activity was analysed and lower $IC_{50}$ values were obtained for the hybrid materials compared to the individual counterparts suggesting the existence of a synergetic effect.
- In Chapter 7, the aggregation process was correlated with the biological properties against cancer cell line A2780 ovarian carcinoma. Additionally, other neutral and cationic gold(I) compounds with phosphanes that contain a naphtyl group ($P\{CH_2\text{-}1\text{-}NHC_{10}H_6(4\text{-}R)\}_3$, R = H, Cl, Br) have been successfully synthesized and their biological activity studied. It has been observed that the addition of an amine between the naphthyl and the phosphorous decreases the resulting biological activity.
- In Chapter 8, the addition of a hydrophilic triethylene glycol pendant arms allows the formation of an excimer of the coumarin. The micellar structure found during the characterization of the aggregates allows the possibility of using the supramolecular assemblies as hosts for the detection of three different naphthalene derivatives (used as guests).
- In Chapter 9, the AIE effect was studied for three different gold(I) complexes containing the TEPE chromophore. The incorporation of a bulky phosphane moiety reduces the possibility of having intermolecular rotation in the aggregates favouring a faster aggregation.

# APPENDIX

**Table A1.** Crystal data and structure for **5.3**.

| | |
|---|---|
| Formula | $C_{41}H_{40}AuN_2PS$ |
| Crystal size, nm | 0.250 x 0.115 x 0.057 |
| Fw | 820.74 |
| Temp., K | 296(2) |
| Wavelength, Å | 0.71073 |
| Crystal system | Triclinic |
| Space group | P-1 |
| a, Å | 8.6565(2) |
| b, Å | 19.0873(4) |
| c, Å | 23.6673(7) |
| α, º | 110.9010(10) |
| β, º | 90.025(2) |
| γ, º | 95.8040(10) |
| Volume, $Å^3$ | 3631.68(16) |
| Z | 4 |
| $D_{calc}$, mg $m^{-3}$ | 1.501 |
| Abs. coef., $mm^{-1}$ | 4.183 |
| F(000) | 1640 |
| θ range for data coll, º | 1.15 to 25.35 |
| Reflns coll./independent | 205022/13327 |
| Data/restraint/parameters | 13327/7/802 |
| GOF on $F^2$ | 1.029 |
| Final R index ($I > 2\sigma(I)$) | R1 = 0.0342,wR2 = 0.0749 |
| R index (all data) | R1 = 0.0661,wR2 = 0.0935 |
| Peak and hole, e $Å^{-3}$ | 0.589 and -1.018 |

**Table A2.** Crystal data and structure for **5.4**.

| | |
|---|---|
| Formula | $C_{53}H_{46}AuN_2PS$ |
| Crystal size, nm | 0.183 x 0.103 x 0.014 |
| Fw | 970.91 |
| Temp., K | 270(2) |
| Wavelength, Å | 0.71073 |
| Crystal system | Triclinic |
| Space group | P-1 |
| a, Å | 9.4146(2) |
| b, Å | 12.3469(3) |
| c, Å | 20.7293(6) |
| α, º | 97.6822(16) |
| β, º | 97.1348(16) |
| γ, º | 112.2059(14) |
| Volume, $Å^3$ | 2170.40(10) |
| Z | 2 |
| $D_{calc}$, mg $m^{-3}$ | 1.486 |
| Abs. coef., $mm^{-1}$ | 3.513 |
| F(000) | 976 |
| θ range for data coll, º | 1.82 to 25.35 |
| Reflns coll./independent | 126257/7925 |
| Data/restraint/parameters | 7925/54/493 |
| GOF on $F^2$ | 1.001 |
| Final R index ($I > 2\sigma(I)$) | R1 = 0.0346,wR2 = 0.0981 |
| R index (all data) | R1 = 0.0474,wR2 = 0.1131 |
| Peak and hole, e $Å^{-3}$ | 1.350 and -0.728 |

**Table A3.** Crystal data and structure for **5.6**.

| | |
|---|---|
| Formula | $C_{34}H_{39}AuN_4S$ |
| Crystal size, nm | 0.253 x 0.217 x 0.067 |
| Fw | 732.72 |
| Temp., K | 200(2) |
| Wavelength, Å | 0.71073 |
| Crystal system | Triclinic |
| Space group | P-1 |
| a, Å | 9.4798(3) |
| b, Å | 12.6101(3) |
| c, Å | 14.3603(4) |
| α, º | 97.6410(10) |
| β, º | 100.288(2) |
| γ, º | 109.9550(10) |
| Volume, $Å^3$ | 1552.35(8) |
| Z | 2 |
| $D_{calc}$, mg $m^{-3}$ | 1.568 |
| Abs. coef., $mm^{-1}$ | 4.835 |
| F(000) | 732 |
| θ range for data coll, º | 1.76 to 25.35 |
| Reflns coll./independent | 82971/5673 |
| Data/restraint/parameters | 5673/0/364 |
| GOF on $F^2$ | 1.107 |
| Final R index ($I > 2\sigma(I)$) | R1 = 0.0138,wR2 = 0.0350 |
| R index (all data) | R1 = 0.0157,wR2 = 0.0356 |
| Peak and hole, e $Å^{-3}$ | 0.323 and -0.328 |

**Table A4.** Crystal data and structure for **5.7**.

| | |
|---|---|
| Formula | $C_{42}H_{43}AuN_4S$ |
| Crystal size, nm | 0.265 x 0.215 x 0.108 |
| Fw | 848.83 |
| Temp., K | 200(2) |
| Wavelength, Å | 0.71073 |
| Crystal system | Triclinic |
| Space group | P-1 |
| a, Å | 11.1580(4) |
| b, Å | 12.2292(5) |
| c, Å | 14.6217(7) |
| α, º | 86.513(3) |
| β, º | 68.107(2) |
| γ, º | 84.983(2) |
| Volume, $Å^3$ | 1843.34(14) |
| Z | 2 |
| $D_{calc}$, mg $m^{-3}$ | 1.529 |
| Abs. coef., $mm^{-1}$ | 4.085 |
| F(000) | 852 |
| θ range for data coll, º | 3.00 to 25.35 |
| Reflns coll./independent | 62560/6749 |
| Data/restraint/parameters | 6749/0/452 |
| GOF on $F^2$ | 1.066 |
| Final R index ($I > 2\sigma(I)$) | R1 = 0.0195,wR2 = 0.0578 |
| R index (all data) | R1 = 0.0216,wR2 = 0.0590 |
| Peak and hole, e $Å^{-3}$ | 1.133 and -0.299 |

**Table A5.** Crystal data and structure for **7.1a**.

| | |
|---|---|
| Formula | $3(C_{14}H_{18}AuN_4P)$, $CH_2Cl_2$ |
| Crystal size, nm | 0.44 x 0.04 x 0.04 |
| Fw | 1495.70 |
| Temp., K | 170 |
| Wavelength, Å | 0.71073 |
| Crystal system | Orthorhombic |
| Space group | P 2c -2n |
| a, Å | 23.3244(3) |
| b, Å | 9.27650(10) |
| c, Å | 45.0709(7) |
| α, º | 90 |
| β, º | 90 |
| γ, º | 90 |
| Volume, $Å^3$ | 9751.9(2) |
| Z | 8 |
| $D_{calc}$, mg $m^{-3}$ | 2.037 |
| Abs. coef., $mm^{-1}$ | 9.258 |
| F(000) | 5712 |
| θ range for data coll, º | 1.804 to 26.370 |
| Reflns coll./independent | 77281/19153 |
| Data/restraint/parameters | 19153/768/1130 |
| GOF on $F^2$ | 1.080 |
| Final R index ($I > 2\sigma(I)$) | R1 = 0.0672,wR2 = 0.1531 |
| R index (all data) | R1 = 0.1066,wR2 = 0.1753 |
| Peak and hole, e $Å^{-3}$ | 1.657 and -2.083 |

**Table A6.** Crystal data and structure for **7.1b**.

| | |
|---|---|
| Formula | $C_{14}H_{18}Au\ N_4P$ |
| Crystal size, nm | 0.44 x 0.07 x 0.02 |
| Fw | 470.26 |
| Temp., K | 170 |
| Wavelength, Å | 0.71073 |
| Crystal system | Orthorhombic |
| Space group | F 2 -2d |
| a, Å | 21.9640(7) |
| b, Å | 41.1815(11) |
| c, Å | 6.4250(2) |
| α, º | 90 |
| β, º | 90 |
| γ, º | 90 |
| Volume, $Å^3$ | 5811.5(3) |
| Z | 16 |
| $D_{calc}$, mg $m^{-3}$ | 2.150 |
| Abs. coef., $mm^{-1}$ | 10.231 |
| F(000) | 3584 |
| θ range for data coll, º | 2.712 to 31.389 |
| Reflns coll./independent | 15857/4324 |
| Data/restraint/parameters | 4324/1/182 |
| GOF on $F^2$ | 1.020 |
| Final R index ($I > 2\sigma(I)$) | R1 = 0.0485, wR2 = 0.0963 |
| R index (all data) | R1 = 0.0724, wR2 = 0.1063 |
| Peak and hole, e $Å^{-3}$ | 2.729 and -1.317 |

**Table A7.** Crystal data and structure for **7.4**.

| | |
|---|---|
| Formula | $C_{26}H_{21}AuNP$, $CH_2Cl_2$ |
| Crystal size, nm | 0.42x 0.32 x 0.14 |
| Fw | 660.30 |
| Temp., K | 170 |
| Wavelength, Å | 0.71073 |
| Crystal system | Monoclinic |
| Space group | -P 2yn |
| a, Å | 17.7242(3) |
| b, Å | 14.0652(3) |
| c, Å | 20.1117(3) |
| α, º | 90 |
| β, º | 93.1530(10) |
| γ, º | 90 |
| Volume, $Å^3$ | 5006.15(16) |
| Z | 8 |
| $D_{calc}$, mg $m^{-3}$ | 1.752 |
| Abs. coef., $mm^{-1}$ | 6.170 |
| F(000) | 2560 |
| θ range for data coll, º | 1.768 to 31.365 |
| Reflns coll./independent | 57127/16247 |
| Data/restraint/parameters | 16247/51/618 |
| GOF on $F^2$ | 1.037 |
| Final R index ($I > 2\sigma(I)$) | R1 = 0.0519,wR2 = 0.0876 |
| R index (all data) | R1 = 0.0979,wR2 = 0.0999 |
| Peak and hole, e $Å^{-3}$ | 0.971 to -1.088 |

**Table A8.** Crystal data and structure for **7.5**.

| | |
|---|---|
| Formula | $C_{14}H_{21}AuNP$ |
| Crystal size, nm | 0.134 x 0.083 x 0.065 |
| Fw | 431.25 |
| Temp., K | 120.01(10) |
| Wavelength, Å | 1.54184 |
| Crystal system | Monoclinic |
| Space group | -P 2yn |
| a, Å | 7.18100(18) |
| b, Å | 19.7054(6) |
| c, Å | 10.4601(3) |
| α, º | 90 |
| β, º | 96.565(2) |
| γ, º | 90 |
| Volume, $Å^3$ | 1470.45(7) |
| Z | 4 |
| $D_{calc}$, mg $m^{-3}$ | 1.948 |
| Abs. coef., $mm^{-1}$ | 19.647 |
| F(000) | 824 |
| θ range for data coll, º | 4.488 to 66.713 |
| Reflns coll./independent | 4464/2586 |
| Data/restraint/parameters | 2586/0/158 |
| GOF on $F^2$ | 1.093 |
| Final R index ($I > 2\sigma(I)$) | R1 = 0.0242,wR2 = 0.0621 |
| R index (all data) | R1 = 0.0251,wR2 = 0.0629 |
| Peak and hole, e $Å^{-3}$ | 1.088 and -0.884 |

**Table A9.** Crystal data and structure for **7.13**.

| | |
|---|---|
| Formula | $C_{70}H_{70}AuCl_7N_6O_4P_2$ |
| Crystal size, nm | 0.4 x 0.34 x 0.12 |
| Fw | 1566.37 |
| Temp., K | 170 |
| Wavelength, Å | 0.71073 |
| Crystal system | Monoclinic |
| Space group | C 1 2/c 1 |
| a, Å | 20.0915(6) |
| b, Å | 14.5770(4) |
| c, Å | 24.3861(7) |
| α, º | 90 |
| β, º | 107.1290(10) |
| γ, º | 90 |
| Volume, $Å^3$ | 6825.3(3) |
| Z | 4 |
| $D_{calc}$, mg $m^{-3}$ | 1.524 |
| Abs. coef., $mm^{-1}$ | 2.530 |
| F(000) | 3168 |
| θ range for data coll, º | 1.748 to 28.282 |
| Reflns coll./independent | 16013/8486 |
| Data/restraint/parameters | 8486/150/412 |
| GOF on $F^2$ | 1.278 |
| Final R index ($I > 2\sigma(I)$) | R1 = 0.0465,wR2 = 0.1200 |
| R index (all data) | R1 = 0.0569,wR2 = 0.1244 |
| Peak and hole, e $Å^{-3}$ | 1.319 and -1.140 |

Document signat digitalment per: ANDREA PINTO I MARTINEZ

Document signat digitalment per: ANDREA PINTO I MARTINEZ

Document signat digitalment per: ANDREA PINTO I MARTINEZ